Investigation of Integrity and Effectiveness of RC Bridge Deck Rehabilitation Using CFRP Composites
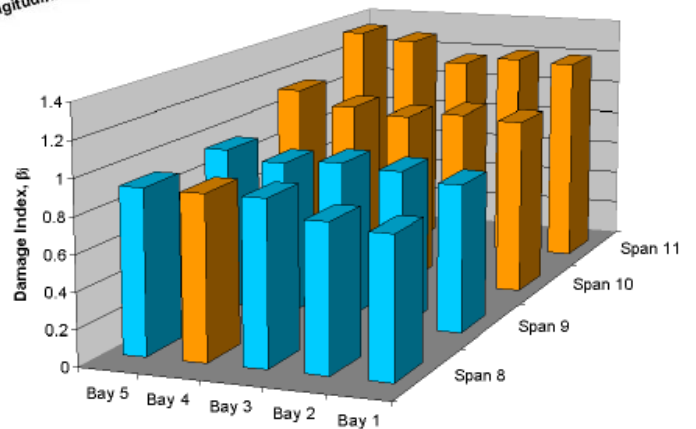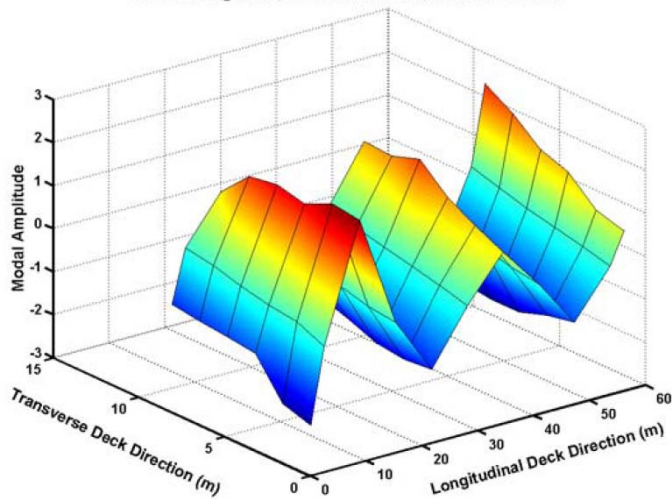
Final Report

First Bending Mode, Pre-Rehabilitation, Ambient Vibration

Investigation of Integrity and Effectiveness of RC Bridge Deck Rehabilitation Using CFRP Composites

Final Report

Report No. CA04-0112

November 2008

Prepared By:

Department of Structural Engineering
School of Engineering
University of California, San Diego
La Jolla, CA 92093-0085

Prepared For:

California Department of Transportation
Division of Engineering Services
Earthquake Engineering, MS-9
1801 30th Street
Sacramento, CA 95816

California Department of Transportation
Division of Research and Innovation, MS-83
1227 O Street
Sacramento, CA 95814

DISCLAIMER STATEMENT

STATE OF CALIFORNIA DEPARTMENT OF TRANSPORTATION
TECHNICAL REPORT DOCUMENTATION PAGE
TR0003 (REV. 10/98)

1. REPORT NUMBER CA04-0112	2. GOVERNMENT ASSOCIATION NUMBER	3. RECIPIENT'S CATALOG NUMBER
4. TITLE AND SUBTITLE Investigation of Integrity and Effectiveness of RC Bridge Deck Rehabilitation Using CFRP Composites		5. REPORT DATE November, 2008
		6. PERFORMING ORGANIZATION CODE
7. AUTHOR(S) Luke S. Lee[1], Vistasp M. Karbhari[1], Charles Sikorsky[2]		8. PERFORMING ORGANIZATION REPORT NO. SSRP-04/08
9. PERFORMING ORGANIZATION NAME AND ADDRESS [1]Department of Structural Engineering School of Engineering University of California, San Diego La Jolla, CA 92093-0085 [2]California Department of Transportation Division of Engineering Services Earthquake Engineering, MS-9 1801 30th Street Sacramento, CA 95816		10. WORK UNIT NUMBER
		11. CONTRACT OR GRANT NUMBER DRI Research Task No. 0112 Contract No. 59A0249
12. SPONSORING AGENCY AND ADDRESS California Department of Transportation Division of Research and Innovation, MS-83 1227 O Street Sacramento, CA 95814		13. TYPE OF REPORT AND PERIOD COVERED Final Report
		14. SPONSORING AGENCY CODE 913

15. SUPPLEMENTAL NOTES

This report was originally issued by UCSD in June 2004.

16. ABSTRACT

This report develops methodologies to evaluate the integrity and effectiveness of external bonding of carbon fiber reinforced polymer (CFRP) composites to the bridge deck soffit of Spans 8 and 9 of the eastbound structure of the Watson Wash Bridge. Wet lay-up and pultruded CFRP composites are applied to the deteriorated decks of the Watson Wash Bridge. A global vibration-based nondestructive evaluation procedure measuring changes in modal strain energy is used to determine stiffness changes in the bridge structure before and after application of CFRP composites. The effect of CFRP composite material variation and degradation are incorporated into a measure of the reliability index, which is related the probability of failure; failure is defined as the yield of steel reinforcement. The reliability index provides the means to combine the effects of material variation, CFRP composite degradation, and measured stiffness changes from the field to assess the service life of a FRP rehabilitated structure as shown from a series of progressive damage tests. Based upon the results of the measured system changes, effects of material variation, and effect of CFRP composite degradation, CFRP rehabilitation designs are recommended for the parallel westbound Watson Wash Bridge structure. Recommended CFRP rehabilitation designs are intended to prevent the occurrence of punching shear failure, and sustain HS20 and Permit Load demands in the longitudinal and transverse slab directions for a period greater than 25 years at a reliability level of 3.5, failure probability of 0.02%. A cost comparison between recommended CFRP rehabilitation and new bridge construction costs shows a savings of 75 to 80% with CFRP rehabilitation of the entire bridge deck area of the existing westbound Watson Wash Bridge.

17. KEY WORDS Bridge Rehabilitation, CFRP Composites, Field Evaluation, Stiffness Change, Progressive Damage, Non-Destructive Evaluation, Modal Strain Energy, Watson Wash Bridge	18. DISTRIBUTION STATEMENT No restrictions. This document is available to the public through the National Technical Information Service, Springfield, VA 22161	
19. SECURITY CLASSIFICATION (of this report) Unclassified	20. NUMBER OF PAGES 324 Pages	21. PRICE

Reproduction of completed page authorized

Investigation of Integrity and Effectiveness of RC Bridge Deck Rehabilitation Using CFRP Composites

Final Report

Abstract:

This report develops methodologies to evaluate the integrity and effectiveness of external bonding of carbon fiber reinforced polymer (CFRP) composites to the bridge deck soffit of Spans 8 and 9 of the eastbound structure of the Watson Wash Bridge. Wet lay-up and pultruded CFRP composites are applied to the deteriorated decks of the Watson Wash Bridge. A global vibration-based nondestructive evaluation procedure measuring changes in modal strain energy is used to determine stiffness changes in the bridge structure before and after application of CFRP composites. The effect of CFRP composite material variation and degradation are incorporated into a measure of the reliability index, which is related the probability of failure; failure is defined as the yield of steel reinforcement. The reliability index provides the means to combine the effects of material variation, CFRP composite degradation, and measured stiffness changes from the field to assess the service life of a FRP rehabilitated structure as shown from a series of progressive damage tests. Based upon the results of the measured system changes, effects of material variation, and effect of CFRP composite degradation, CFRP rehabilitation designs are recommended for the parallel westbound Watson Wash Bridge structure. Recommended CFRP rehabilitation designs are intended to prevent the occurrence of punching shear failure, and sustain HS20 and Permit Load demands in the longitudinal and transverse slab directions for a period greater than 25 years at a reliability level of 3.5, failure probability of 0.02%. A cost comparison between recommended CFRP rehabilitation and new bridge construction costs shows a savings of 75 to 80% with CFRP rehabilitation of the entire bridge deck area of the existing westbound Watson Wash Bridge.

.

Report No.

SSRP–2004/08

INVESTIGATION OF INTEGRITY AND EFFECTIVENESS OF RC BRIDGE DECK REHABILITATION WITH CFRP COMPOSITES

by

LUKE S. LEE

VISTASP M. KARBHARI

CHARLES SIKORSKY

Department of Structural Engineering

University of California, San Diego

La Jolla, California 92093-0085

June 2004

University of California, San Diego

Department of Structural Engineering

Structural Systems Research Project

Report No. SSRP-2004/08

Investigation of Integrity and Effectiveness of RC Bridge Deck Rehabilitated with CFRP Composites

by

Luke S. Lee

Graduate Student Researcher

Vistasp M. Karbhari

Professor of Structural Engineering

Charles Sikorsky

Senior Bridge Engineer, California Department of Transportation

Department of Structural Engineering

University of California, San Diego

La Jolla, California 92093-0085

June 2004

Technical Report Documentation Page

1. Report No. SSRP – 2004/08	2. Government Accession No.	3. Recipient's Catalog No.
4. Title and Subtitle INVESTIGATION OF INTEGRITY AND EFFECTIVENESS OR RC BRIDGE DECK REHABILITATION WITH CFRP COMPOSITES		5. Report Date June 2004
		6. Performing Organization Code
7. Author(s) Luke Lee Vistasp M. Karbhari Charles Sikorsky		8. Performing Organization Report No. SSRP – 2004/08
9. Performing Organization Name and Address Division of Structural Engineering School of Engineering University of California, San Diego La Jolla, California 92093-0085		10. Work Unit No. (TRAIS)
		11. Contract or Grant No. 59A0249
12. Sponsoring Agency Name and Address California Department of Transportation Engineering Service Center 1801 30th St., West Building MS-9 Sacramento, California 95807		13. Type of Report and Period Covered Final Report
		14. Sponsoring Agency Code

15. Supplementary Notes

Prepared in cooperation with the State of California Department of Transportation.

16. Abstract

This report develops methodologies to evaluate the integrity and effectiveness of external bonding of carbon fiber reinforced polymer (CFRP) composites to the bridge deck soffit of Spans 8 and 9 of the eastbound structure of the Watson Wash Bridge. Wet lay-up and pultruded CFRP composites are applied to the deteriorated decks of the Watson Wash Bridge. A global vibration-based nondestructive evaluation procedure measuring changes in modal strain energy is used to determine stiffness changes in the bridge structure before and after application of CFRP composites. The effect of CFRP composite material variation and degradation are incorporated into a measure of the reliability index, which is related the probability of failure; failure is defined as the yield of steel reinforcement. The reliability index provides the means to combine the effects of material variation, CFRP composite degradation, and measured stiffness changes from the field to assess the service life of a FRP rehabilitated structure as shown from a series of progressive damage tests. Based upon the results of the measured system changes, effects of material variation, and effect of CFRP composite degradation, CFRP rehabilitation designs are recommended for the parallel westbound Watson Wash Bridge structure. Recommended CFRP rehabilitation designs are intended to prevent the occurrence of punching shear failure, and sustain HS20 and Permit Load demands in the longitudinal and transverse slab directions for a period greater than 25 years at a reliability level of 3.5, failure probability of 0.02%. A cost comparison between recommended CFRP rehabilitation and new bridge construction costs shows a savings of 75 to 80% with CFRP rehabilitation of the entire bridge deck area of the existing westbound Watson Wash Bridge.

17. Key Words FRP Rehabilitation, Structural Health Monitoring, Structural Reliability, Remaining Service Life, Cost Effectiveness		18. Distribution Statement Unlimited	
19. Security Classification (of this report) Unclassified	20. Security Classification (of this page) Unclassified	21. No. of Pages 319	22. Price

Form DOT F 1700.7 (8-72)   Reproduction of completed page authorized

DISCLAIMER

The opinions, findings, and conclusions expressed in this publication are those of the authors and not necessarily those of the STATE OF CALIFORNIA.

ACKNOWLEDGEMENT

ABSTRACT

This report develops methodologies to evaluate the integrity and effectiveness of external bonding of carbon fiber reinforced polymer (CFRP) composites to the bridge deck soffit of Spans 8 and 9 of the eastbound structure of the Watson Wash Bridge. Wet lay-up and pultruded CFRP composites are applied to the deteriorated decks of the Watson Wash Bridge. A global vibration-based nondestructive evaluation procedure measuring changes in modal strain energy is used to determine stiffness changes in the bridge structure before and after application of CFRP composites. The effect of CFRP composite material variation and degradation are incorporated into a measure of the reliability index, which is related the probability of failure; failure is defined as the yield of steel reinforcement. The reliability index provides the means to combine the effects of material variation, CFRP composite degradation, and measured stiffness changes from the field to assess the service life of a FRP rehabilitated structure as shown from a series of progressive damage tests. Based upon the results of the measured system changes, effects of material variation, and effect of CFRP composite degradation, CFRP rehabilitation designs are recommended for the parallel westbound Watson Wash Bridge structure. Recommended CFRP rehabilitation designs are intended to prevent the occurrence of punching shear failure, and sustain HS20 and Permit Load demands in the longitudinal and transverse slab directions for a period greater than 25 years at a reliability level of 3.5, failure probability of 0.02%. A cost comparison between recommended CFRP rehabilitation and new bridge construction costs shows a savings of 75 to 80% with CFRP rehabilitation of the entire bridge deck area of the existing westbound Watson Wash Bridge.

EXECUTIVE SUMMARY

BACKGROUND

Deterioration and increasing functional deficiency of civil infrastructure continue to pose some of the more significant challenges to civil engineers. In the United States alone, 27.5% of bridges were structurally deficient or functionally obsolete in 2000 (ASCE 2003). Due to a lack of available resources, innovative methodologies and tools are being developed to efficiently manage the degradation and structural deficiencies present in existing infrastructure.

In order to mitigate deterioration and efficiently manage maintenance efforts on bridge structures, two methodologies are needed:

1) A methodology to extend the service life of bridge structures

2) A methodology to evaluate performance (i.e. capacity) changes of a bridge

While some researchers are engaged in developing methods of rehabilitation while others are focused on developing methodologies to monitor structures; rehabilitation and monitoring have not been integrated and applied to bridges in service. This report presents a solution to the general problem of bridge deterioration with the development and implementation of a methodology to extend the service life of reinforced concrete bridges as well as monitor the changes in performance (i.e. capacity) of that structure while in-service. The following tasks were accomplished to develop this methodology. First, a literature review of flexural strengthening and modal based non-destructive damage detection is provided. Next the specimen is described, and the strengthening plan is developed. During construction, the work was monitored visually and with a non-destructive damage detection method after construction was complete. Lastly a method is developed to evaluate remaining service life, and a cost comparison is provided comparing the cost to replace the bridge versus rehabilitation using FRP composites. We shall now briefly discuss these tasks.

To begin, a review of flexural rehabilitation of reinforced concrete structure with fibre-reinforced (FRP) composites is provided. Emphasis is placed on flexural rehabilitation of beams and slab structures and field application of FRP composites in the literature. From the prior literature reviews, the assessment of beam and slab structures focuses on the capacity increase provided by bonding of FRP composites, typically carbon fibre-reinforced (CFRP) composites, to the tension side of reinforced concrete members. While, it is generally shown in laboratory studies of beams and slabs that FRP composites are able to repair or strengthen reinforced concrete members, evaluation of the effectiveness of field applications on strengthening/repair of reinforced concrete bridge structures does not account for the effect of material degradation or quality of application in the field. The use of FRP composites for flexural strengthening of reinforced concrete bridge structures provides advantages in terms of the tailorability of the material, application while structure is in service, and the ability to increase the capacity of the bridge deck by repair of girders or slabs, to name a few. However, the issue of durability and its effect on the performance of FRP strengthened structures are unresolved. In addition, the variation of material properties of field manufactured FRP

composites is not addressed in any field applications of FRP composite. Evaluation of the effectiveness of FRP rehabilitation of existing bridges is determined with the use of load tests before and after strengthening of FRP. A significant weakness evident from the work reviewed is that the FRP bridge rehabilitation measures do not assess the performance of the structure with respect to variation and degradation in FRP composite materials nor evaluate the global rehabilitated structure to assess the change in performance of the structure with respect to time.

Next, the major components of modal testing and modal analysis applicable to bridges are reviewed to identify a means to evaluate the global response of the structure. Initially, the theoretical development of modal testing is explained, as well as methods of excitation for bridges. The methods of excitation include input-output methods and output only methods for modal testing. Input-output methods of excitation involve a contact procedure such that a forcing function is introduced to vibrate the bridge structure, such as the use of an impact hammer, drop weight, shaker, or displacement-release procedure to excite the structure. Output only methods, typically described as ambient excitation methods, are a non-contact procedure utilizing the service level conditions of the structure in order to excite the structure. Sources of "natural" vibration include vehicular traffic, wind, pedestrian traffic, ocean waves, and micro-earthquakes (Farrar and Sohn, 2001; Green, 1995; Salawu and Williams, 1995). Third, implementation of the testing procedure is described with an overview of the types of transducers available for use on modal tests. Finally, methods for extraction of modal parameters from measured frequency response functions are briefly reviewed and explained.

Dynamic testing procedure to acquire modal properties provides little value without a means to evaluate the data and provide a quantitative assessment of the structure. Next, methods for vibration based damage detection are reviewed. The purpose of this review is to evaluate damage detection methodologies to identify, locate and quantify the state of a structure for a given time. Each modal-based damage detection approach was evaluated based on the following criteria:

1. Level of damage detection desired: Level 1, Level 2, Level 3, or Level 4.

2. Demonstrated capability of the damage detection level via numerical simulation in the presence of signal noise and reduced measurements.

3. Demonstrated capability of the damage detection level via experimental validation in the laboratory in the presence of signal noise and reduced measurements

4. Validation of the damage detection algorithm to field data of large civil structures.

Based on the above criteria, the damage detection algorithm by Stubbs et al. (2000) is selected as the most suitable damage detection because of its demonstrated capability with bridges and more importantly, the ability to utilize damage detection results to evaluate the performance of the rehabilitated structure.

SERVICE LIFE EXTENSION

In this section, the development and application of the methodology to extend and monitor bridge service life is presented. First, the Watson Wash Bridge and its existing damage state are described; second, the deck slab design is evaluated with respect to Caltrans Bridge Design Specifications to determine if any reinforcement deficiencies exist with respect to HS20 (71.2 KN, 16 kips) and Permit truck (106.8 KN, 24 kips) wheel loads; and lastly, material characterization and monitoring of the structure both during construction and after are presented.

The Watson Wash Bridge is a reinforced concrete T-girder bridge located on California Interstate 40, approximately 10.3 KM (6.4 miles) east of Essex Road in the Mojave Desert. The bridge structure, constructed in 1968, consists of two parallel structures each of which is a skewed, two lane interstate bridge 226 m (741 ft) long. A visual inspection of the Watson Wash Bridge revealed a significant number of transverse cracks in the soffit of the bridge deck. The spacing of these cracks is approximately 14 cm (5.5 inches) corresponding to the average spacing of the transverse reinforcement in the deck of the bridge. Transverse reinforcement is provided in the bridge deck at 14 cm (5.5 inch) intervals. Punching shear failures on the bridge deck have resulted due to the development of transverse and longitudinal crack resulting in a concentrated deck area unable to resist the shear force demands.

The reinforced concrete deck slab design was checked using the 2004 Caltrans BDS for HS20 and Permit Truck wheel loads. Deficiencies in steel reinforcement were determined by comparing reinforcement requirements from the code analysis and reinforcement in the existing slab structure. The calculation for steel reinforcement deficiencies is based on an undamaged deck slab in 1969 versus an undamaged slab in 2004. The design of the CFRP rehabilitation applied to the bridge deck of the ratio uses a ratio of composite area to steel area, χ_{frp}. This ratio is multiplied by the steel area deficiency to determine the area of CFRP composite required for rehabilitation. The HS20 truck load of 71.2 KN (16 kips) wheel load, Permit Truck wheel load of 106.8 KN (24 kips), and punching shear prevention are the demands considered on the deck slab with Permit Truck wheel load being the governing condition. Tables 1 and 2 show the required material by method of fabrication.

Table 1: Wet Lay-up CFRP Rehabilitation Requirements

Reinforcement Direction		Permit Load
Transverse	Required CFRP	28, two layer strips
	W/ S.F.	21, three layer strips
Longitudinal	Required CFRP	4, one layer strips
	W/ S.F.	4, two layer strips

Table 2: Pultruded CFRP Rehabilitation Requirements

Reinforcement Direction	Punching Shear	Permit Load
Transverse	21 strips	29 pairs (58 strips)
Longitudinal	4 strips	5 strips

As part of the monitoring process, each bay with externally bonded FRP composites is visually inspected during construction. While visual inspection provides a subjective measure of the deck slab rehabilitation, it remains useful to identify defects and potential causes of degradation in the externally bonded CFRP composite strips. Visual inspection of the deck rehabilitation provides on-site inspection of the manufacturer's work to ensure that the CFRP composite is manufactured and applied according to design specifications. In order to quantitatively measure the change in performance of the structure before and after rehabilitation, the vibration based damage detection procedure described in Chapter 3 is employed. Vibration properties (frequencies and mode shape) of the Watson Wash Bridge are measured. A comparison of the pre and post rehabilitation mode shapes of the bridge structure is used to quantify the change in performance of the Watson Wash Bridge deck slab with CFRP composite strips applied.

While the global NDE investigates at the systems level of the rehabilitated structure, which includes the bridge deck and applied FRP composite, characterization of the state of the materials is critical to evaluate material quality and manufacturer ability to meet specified design properties. Of particular interest is the state of FRP composites applied and manufactured during the rehabilitation. Knowledge of mechanical properties of the applied CFRP allows for a direct comparison with design properties and qualification of manufacturing procedures. The pultrusion manufacturing technique is an efficient and uniform manufacturing technique producing composites of high quality in terms of uniform mechanical properties throughout the composite area. However, the wet lay-up manufacturing process is subject to defects in alignments and placement of fibers due to the manual nature of the technique, as well as exposure to changing environmental conditions including changes in temperature during manufacture and cure.

The average moduli and strength values of both wet lay-up and pultruded CFRP composites are generally greater than or equal to the design moduli of 9.42 and 20.5 msi for wet lay-up and pultruded processes, respectively, and are greater than design strength values of 128.66 ksi and 305 ksi for wet lay-up and pultruded processes, respectively. Unfortunately the variation associated with these properties remains a concern since the scatter in the data for modulus may result in specific CFRP composite locations with CFRP composite properties being below design values.

SERVICE LIFE ASSESSMENT

Determining the functionality and service life of the rehabilitated deck in Spans 8 and 9 of the Watson Wash Bridge requires a methodology that incorporates the variation in properties of the rehabilitated bridge deck and durability characterization of the bonded

composite materials. The generalized reliability index, β, a measure of the probability of failure, is applied as a measure of performance to understand the variation in material properties affecting resistance demand of the structure and second, a procedure to assess the impact of material degradation on the reliability of the structure as a function of time. Failure in the reliability analysis is defined as yield of flexural steel reinforcement, tensile strain of 0.002; the punching shear criterion, discussed in chapters 5 and 6, establishes a limit on the tensile strain developed in the bonded CFRP composite to retain aggregate interlock in the deck. The reliability analysis involves a section analysis at each instant of time where degradation occurs and thus provides strain information for concrete and FRP composite; if concrete crush, a compressive strain limit of 0.3%, or the punching shear criterion, tensile strain limit of 0.75%, are violated before steel yield, the limit criteria for the section analysis is modified to match either concrete crush or punching shear strain limit criteria and a change in failure mode is noted. It is important to note that for the FRP composite rehabilitation analysis in the deck slab of the Watson Wash Bridge, in all cases and time periods steel yield occurs first.

Next the effect of accelerated deterioration in a reinforced concrete section and degradation in CFRP composite rehabilitation is assessed on the remaining service life of the rehabilitated deck of the Watson Wash Bridge. First, an experimental procedure is implemented where a sequence of damage is introduced to the FRP rehabilitation and quantified in terms of stiffness losses in the structure. These stiffness losses are used to represent changes in a reinforced concrete deck slab over time. The measured stiffness losses are integrated into the measure of reliability index described in detail in Chapter 9 of this report. Using both the measured stiffness losses and the rate of change of reliability due to CFRP composite degradation predictions for the lower bound of remaining service life are made.

The total cost of FRP composite rehabilitation for an entire bridge structure, such as the parallel structure, for west bound traffic on Interstate 40, of the Watson Wash Bridge is estimated and compared to the cost of new bridge construction. In considering HS20 loads for service life extension of 25 years or more and maintaining the reliability index of the deck above 3.5, a cost savings of approximately 80% is observed when opting for FRP composites versus the cost of new bridge construction. The service life estimate of 25 years is conservative since the degradation in composite is modeled with the conservative assumption that the CFRP composite is fully immersed in deionized water at 23°C. To extend the life of the structure for permit load demands, a savings of approximately 75% is observed compared to new bridge construction costs.

CONCLUSIONS AND RECOMMENDATIONS

It is shown that the use of the global NDE procedure by Stubbs et al. (2000) is effective in localizing stiffness changes in the deck slab following rehabilitation with CFRP composite materials. The purpose of the global NDE procedure was to measure changes in stiffness of the deck slab following FRP composite rehabilitation.

Using the measure of the reliability index and an allowable reliability limit of 3.5, it is possible to extend the service life of an FRP rehabilitated structure in the presence of degradation in CFRP composite tensile properties for a period greater than 25 years. It is

found that the cost of FRP rehabilitation to sustain HS20 loads is approximately 20% of the cost of new bridge construction. The cost to sustain permit loads is approximately 25% of the cost of new bridge construction.

Based upon the findings of this report the following recommendations are made to ensure successful implementation of these methodologies to extend service life and monitoring developed in this report:

- Monitor the existing westbound Watson Wash Bridge structure to improve durability.

- Apply durability characterization of CFRP composite materials from exposure to other environments such as immersion in saltwater solution, alkali solution) to the performance of a FRP rehabilitated beam structure.

TABLE OF CONTENTS

LIST OF TABLES

LIST OF FIGURES

1   INTRODUCTION

1.1   Problem Statement

Deterioration and increasing functional deficiency of civil infrastructure continue to pose some of the more significant challenges to civil engineers. In the United States alone, 27.5% of bridges were structurally deficient or functionally obsolete in 2000 (ASCE 2003). The estimated cost to repair all bridge deficiencies is $9.4 billion dollars per year for 20 years (ASCE 2003).   Due to a lack of available resources, innovative methodologies and tools are being developed to efficiently manage the degradation and structural deficiencies present in existing infrastructure.

The deterioration and functional deficiencies of highway infrastructure are attributed to aging, weathering of materials (i.e. corrosion of steel), accidental damage (i.e., natural disasters), and increased traffic and industrial needs as exhibited by need for higher load ratings of structures and increasing number of lanes to accommodate traffic flow (Tajlsten, 2002; Karbhari and Seible, 2000; Meier, 2000).   However, deficiencies in structures are not restricted to the effects of aging; poor engineering judgment and inadequate design are other factors contributing to deficiencies at any time during the service life of the structure. Regardless of root cause, functional deficiencies are present in civil infrastructure and solutions to resolve these deficiencies are necessary.

In order to mitigate deterioration and efficiently manage maintenance efforts on bridge structures, two methodologies are needed:

1) A methodology to extend the service life of bridge structures

2) A methodology to monitor performance (i.e. stiffness) changes of bridge structures

While some researchers are engaged in developing methods for rehabilitation and others are focused on developing methodologies to monitor structures, rehabilitation and monitoring have not been integrated and applied to bridges in service. This report presents a solution to the general problem of bridge deterioration with the complete development and implementation of methodologies to extend the service life of reinforced concrete bridges and monitor the changes in performance (i.e. capacity) in a bridge structure.

1.2   Purpose of Report

The purpose of this report is to develop and validate methodologies to achieve the following objectives:

- Extend the service life of reinforced concrete bridge structures

- Monitor the structure to validate or confirm the efficacy of the repair / strengthening approach to extend the service life of the structure

In sections 1.2.1 thru 1.2.3 of Chapter 1, the techniques and methods employed to satisfy the objectives of this report are briefly discussed to provide the reader with an understanding of the scope of this report.

1.2.1 Service Life Extension

In order to achieve the service life extension objective, externally bonded fiber reinforced polymer (FRP) composites are used to repair and/or strengthen a bridge structure. The application of FRP composites for strengthening and rehabilitation is well documented in literature. An initial background of FRP Rehabilitation is available in Chapter 1, Section 1.3.1 of this report. A state-of-the-art literature review for flexural strengthening using externally bonded FRP composite is available in Chapter 2.

The methodology for service life extension of reinforced concrete structures includes the following components, which are developed and implemented throughout this report:

1) Design of FRP Rehabilitation
2) Manufacturing/Construction Guidelines
3) FRP Composite Materials Characterization
4) Prediction of Remaining Service Life

The prediction of remaining service life quantifies the extended life of the bridge structure with consideration for the design, quality and durability of the applied FRP composites.

1.2.2 Monitoring of Bridge Structure

Monitoring is defined as evaluating the state of damage in the bridge structure for purposes of this report. Damage is defined as a loss in stiffness. The changes in stiffness of the bridge structure are measured with the application of a global nondestructive evaluation (NDE) procedure utilizing the measured vibration properties (i.e., mode shapes and frequencies) of a structure. Furthermore, measured stiffness changes in the structure can be used in an expression to measure the probability of failure or the reliability of a structure.

Procedures for dynamic testing of structures and vibration based damage detection are components of a broader field known as structural health monitoring. A brief introduction to structural health monitoring is provided in Chapter 1, Section 1.3.2 of this report. State-of-the-art reviews for dynamic testing and vibration based damage detection are provided in Chapters 3 and 4 of this report, respectively; the objective of these literature reviews is to determine the best available techniques for dynamic testing and damage detection for given criteria.

Monitoring of the bridge structure involves the following components and actions, which are explained and applied throughout this report:

1) Dynamic Testing of Bridge Structure
2) Modal Parameter (mode shapes, frequencies) Extraction
3) Vibration Based Damage Detection
4) Prediction of Remaining Service Life

The service life assessment incorporates results from the global NDE procedure to predict the remaining life of the bridge structure and provides a quantified result in terms of time.

1.2.3 Validation of Service Life Extension and Monitoring

Experimental validation is performed with application of the service life extension and monitoring methodologies to a deteriorating bridge structure, namely the Watson Wash Bridge located on California Interstate 40. The verification process includes the following for rehabilitation and monitoring:

1) FRP Rehabilitation: design, construction, and materials characterization
2) Pre/Post FRP Rehabilitation Monitoring
3) Service Life Assessment
4) Progressive Damage
5) Cost Evaluation

The purpose of each of the above processes is to show that the rehabilitation and monitoring approaches are viable techniques for extending the service life and monitoring reinforced concrete bridge structures.

1.3 Background

In order to maximize the serviceability of civil infrastructure, two specific research areas have experienced significant developments in past decades. These are structural health monitoring of civil infrastructure (Chong et al. 2003; Yuen et al. 2004; Catbas and Aktan 2002; Sikorsky 1999) and the use of fiber reinforced polymer (FRP) composites for repair and strengthening of civil infrastructure (Teng et al. 2003; Van Den Einde et al. 2003; Bakis et al. 2002; Stallings, et al. 2000). In the following section, general introductions for FRP rehabilitation and structural health monitoring are provided. The advantages associated with FRP rehabilitation and structural health monitoring, as well as the obstacles for development of methodologies to extend service life and monitor bridge structures, respectively, are discussed.

1.3.1 FRP Rehabilitation

The degradation of civil infrastructure has prompted the development of methods for rehabilitation of existing structures. Consequently, externally bonded fiber reinforced polymer (FRP) composites are increasingly being used to strengthen and sustain performance of reinforced concrete bridge structures as evidenced by the emergence of design guidelines for FRP rehabilitation and strengthening (ACI, 2002; *fib*, 2001; TR No. 55, 2000; Tajlsten, 2002; Nanni, 2003; Arya et al., 2002). Although increasingly popular, FRP composite rehabilitation is not without its obstacles and uncertainties, which must be understood in order to develop a methodology for bridge life extension.

The application of FRP composites in civil infrastructure provides an innovative approach to rehabilitate existing reinforced concrete structures and extend service life. Advantages are realized from the characteristics of FRP composites in terms of high stiffness-to-weight ratio, high strength-to-weight ratio, corrosion resistance, ease of application, and enhanced fatigue life (Van Den Einde et al. 2003; Karbhari and Zhao 2000).

Because of its attractive qualities, the use of externally bonded FRP composites for strengthening of reinforced concrete structures, namely bridges, has attracted much interest from researchers. Literature for experimental testing and analysis of FRP applied to reinforced concrete beams and slabs is extensive; here references are provided but are by no means exhaustive (Hag-Elfasi, et al., 2004; Mosallam and Mosalam, 2003; Malek and Patel, 2003; Stallings, et al,. 2000). While rehabilitation and strengthening efforts continue, no efforts to date provide a comprehensive approach with details of design, implementation, and evaluation of a FRP composite rehabilitation on existing bridge structures. Furthermore, there is no methodology to estimate the service life extension provided by a specific FRP rehabilitation design.

Although much evidence exists supporting the effectiveness of FRP composites, issues pertaining to durability, quality, and design of FRP composites remain. One of the primary concerns involves FRP composite durability or the ability of FRP composites to sustain load over extended periods of time while exposed to harsh, changing environmental conditions (Karbhari, et al., 2003; Nanni, 2003). The lack of understanding with respect to the durability of FRP composites promotes design related uncertainty, particularly for establishing margins of safety and service life extension. The following table provides a summary of advantages and disadvantages associated with the use of FRP composites for purposes of rehabilitation.

Table 1-1. Advantages and Disadvantages for Bridge Rehabilitation w/ FRP

Advantages	Disadvantages
High strength-to-weight ratio	Unknown Durability
High stiffness-to-weight ratio	Material Variability
Corrosion Resistance	Quality Control/Quality Assurance
Ease of Construction	Design Uncertainty
Tailored Material Properties	

The unknown durability characteristics and quality control during construction present the more significant barriers to acceptance of FRP composites as a proven technology in rehabilitation of reinforced concrete structures. The unknown durability of composites directly affects the service life of the structure, since the ability of the FRP composite to sustain load in changing environments is central to the function of the rehabilitated structure. Furthermore, lack of quality control standards, the manual nature of the FRP composite manufacturing/application process, and environmental conditions during manufacturing and application contribute to variations in the material parameters of the composite. Again, the result is an uncertainty in design and unknown performance change in the existing structure.

An approach to extend the service life of bridge structures using externally bonded FRP composites requires established guidelines for design, manufacturing/construction, and monitoring. Proper design of the FRP rehabilitation emphasizes maintaining the intended function of the structure for a specified duration. Manufacturing/construction guidelines

ensure the quality of the FRP composite application in the field. Monitoring of the structure provides for a performance measure of the structure to render a decision on repair, replacement or no action.

A well-developed methodology for bridge rehabilitation using FRP composites provides a solution to the bridge deterioration problem and overcomes disadvantages often associated with the use of FRP composites for rehabilitation. The methodologies for bridge life extension and monitoring in this report remove the uncertainty associated with durability of FRP composites by predicting the remaining service life of the structure.

1.3.2 Structural Health Monitoring

Structural health monitoring is the act of evaluating the condition of a structure at a given time. A proficient structural health monitoring system is capable of determining and evaluating the serviceability of the structure, the reliability, and the remaining functionality of the structure in terms of durability (Sikorsky, 1999). Structural health monitoring requires periodic investigation during service/operation, occasional maintenance, and repair-retrofit or replacement as deemed necessary. The purpose of monitoring in this report is to assess changes in stiffness of the bridge structure and apply those measures to the reliability of the structure.

A general paradigm for structural health monitoring requires implementation of a global NDE procedure to assess the state of a new or existing structure. Those measured results act as input into a calculated performance measure and service life of the structure. If the remaining service life of the structure is acceptable, the global NDE procedure is repeated. If the service life estimate is unacceptable, then a decision to repair or replace the structure is made. Figure 1, provides a visualization of the described structural health monitoring paradigm.
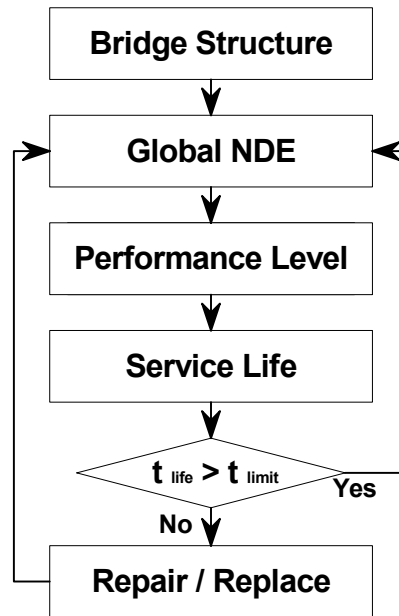
Figure 1.1. Structural Health Monitoring Paradigm

A critical component of the monitoring procedure is the methodology for global NDE, because it provides the primary interaction between the physical state of the structure and analytical methods employed in the structural health monitoring process. The robustness of a global NDE procedure is often defined in terms of levels (Rytter 1993):

Level I: Identify that damage has occurred

Level II: Identify that damage has occurred and determine the location of damage

Level III: Identify that damage has occurred, locate the damage, and estimate its severity

Level IV: Identify that damage has occurred, locate the damage, estimate its severity, and evaluate the impact of damage on the structure or estimate the remaining useful life of the structure.

For civil structures, a global NDE technique utilizing the vibration characteristics of a structure proves to be the most effective method because of the size and the impractical nature of using localized nondestructive testing (NDT) methods such as ultrasonics, piezoelectrics, and acoustic emission to examine civil structures (Sikorsky 1999; Johnson et al. 2004). Ideally, a localized NDE technique is utilized upon identification of a damage location, so as to determine the specific nature of the damage. The global nondestructive examination technique utilizing vibration properties involves the following features: 1) Dynamic testing for the acquisition of modal parameters (i.e. natural frequencies, mode shapes, and damping properties) or other features (i.e., time histories, frequency response functions, etc.) 2) A damage detection algorithm to identify damage in the structure, it's location, and severity.

The general idea of a damage detection algorithm is to use the response characteristics of a structure and evaluate the state of the structure; however, damage is typically a local occurrence, which requires higher frequency modes to detect its presence (Farrar and Doebling, 1997). From a testing perspective, the lower frequency modes, which are less sensitive to the local changes, of a civil structure are readily available and easier to access (Farrar and Doebling, 1997). Consequently, it is difficult to evaluate the reliability of a small portion of a large civil structure, thereby reducing the vibration-based damage detection problem to a statistical pattern recognition problem (Farrar et al., 2001). In addition, the presence of signal noise and incomplete measurements from real applications often result in inaccuracies and poor resolution in the damage detection techniques.

The vibration based monitoring approach is classified into three processes: experimental evaluation, analysis, and decision-making. Each of these occurrences in the monitoring process presents unique constraints. Signal noise and incomplete measurements of vibration data are constraints in the experimental evaluation component (Alampalli et al., 1997; Pothisiri and Hejlmstad 2004). Modeling errors constrain the analytical process (Sanayei et al., 2001), while the complexity of structures and lack of baseline information contribute to uncertainties in the decision-making process (Kim and Stubbs, 2002). The

following table provides a summary of the constraints associated with each action of the monitoring process.

Table 1-2. Vibration Based Monitoring Constraints

Action	Constraints
Experimental Evaluation	• Incomplete measurements • Presence of signal noise
Analysis / Modeling	• Modeling errors
Decision Making	• Complex structures • Structures without baseline measurements

A well-developed methodology for structural health monitoring is defined by a robust global NDE procedure and a means to extend the information into a usable performance measure of the structure. Thus, providing objective information for decision making (Aktan, et al., 2000) as opposed to scattered, subjective information from methods such as visual inspection (Graybeal et al., 2002).

The damage detection procedure selected for structural health monitoring of bridge structures in this report utilizes the change in modal strain energy to locate and quantify damage (Stubbs, et al., 2000). The technique is selected from a literature review (See Chapter 4) because of its proven application to reinforced concrete bridge structures in the field and its flexibility for application to an approach for estimating the remaining life of a structure.

1.4 Report Overview

The purpose of this work is to develop and validate methodologies for bridge life extension and bridge monitoring. These objectives are accomplished with the use of FRP composites for bridge rehabilitation and vibration based damage detection to monitor the structure.

To satisfy this purpose, the remainder of this report is divided into eleven chapters. In Chapter 2, an overview of flexural strengthening with externally bonded FRP composite is provided. In Chapter 3, dynamic testing of bridge structures is described in terms of theory, experimental setup, and analysis procedures. Chapter 4 contains summaries of vibration based damage detection methods; the best available method is selected based on a set of performance criteria. Chapter 5 describes the Watson Wash Bridge structure in terms of its damage state, prior monitoring work conducted on the structure, and plan for FRP rehabilitation. In Chapter 6, design and construction of the FRP strengthening measure is described. In Chapter 7, the bridge structure is monitored to evaluate changes in the structure following rehabilitation; an account of the visual inspection during FRP composite application is provided. Chapter 8 provides a characterization of field

manufactured FRP composite materials from the bridge site. In Chapter 9, the service life assessment methodology is described with estimates of the service life extension provided by the FRP composite rehabilitation. In Chapter 10, an experimental procedure simulating deterioration of the bridge deck is conducted to validate the monitoring procedure with service life estimates. Chapter 11, provides a cost comparison of FRP composite rehabilitation versus replacement of reinforced concrete bridge structures. Finally, in Chapter 12 summary and conclusions presented. Appendix A suggests a design procedure that utilizes estimates of service, durability predictions, and acceptable performance levels to develop a FRP rehabilitation design.

For illustrative purposes, a flow chart of the chapters of this report is provided in the following figure.

INTRODUCTION
(CHAPTER 1)

SERVICE LIFE EXTENSION
(OBJECTIVE ONE)

BRIDGE MONITORING
(OBJECTIVE TWO)

MODAL TESTING BACKGROUND
(CHAPTER 3)

FRP BACKGROUND/ REVIEW
(CHAPTER 2)

DAMAGE DETECTION METHODS
(CHAPTER 4)

WATSON WASH BRIDGE
(CHAPTER 5)

DESIGN AND CONSTRUCTION
(CHAPTER 6)

PRE/POST REHAB MONITORING
(CHAPTER 7)

MATERIALS CHARACTERIZATION
(CHAPTER 8)

SERVICE LIFE ASSESSMENT
(CHAPTER 9)

PROGRESSIVE DAMAGE
(CHAPTER 10)

COST EVALUATION
(CHAPTER 11)

CONCLUSIONS
(CHAPTER 12)

Figure 1.2. Report Overview Flow Chart

2 FRP COMPOSITE FLEXURAL REHABILITATION

2.1 Introduction

In the prior chapter, the objectives of this report were established, namely to develop a methodology for service life extension for reinforced concrete bridge decks and monitoring and evaluation of the structure. The methodologies for bridge deck rehabilitation and thus service life extension, focused on the application of carbon fiber reinforced polymer (CFRP) composites for flexural strengthening of a deck slab. The monitoring and evaluation objectives for a rehabilitated bridge deck introduced the topic of global nondestructive evaluation in the context of structural health monitoring.

In the upcoming chapters, an overview of flexural rehabilitation of reinforced concrete structures with fiber reinforced polymer (FRP) composites, dynamic testing of bridge structures, and damage detection using modal parameters are provided. This chapter provides an overview of flexural rehabilitation of reinforced concrete structure with FRP composites. Emphasis is placed on literature for flexural rehabilitation of beams and slab structures and if available, the use of FRP for strengthening of bridge is included.

2.2 Background

2.2.1 FRP Composites

Composite materials are materials having strong, stiff fibers – continuous or discontinuous – surrounded by a matrix material (Gay, et al., 2002). Composite materials built of fibers and polymeric resins are also known as fiber reinforced polymers (FRP) (ACI, 2002). The matrix of the composite serves to distribute the fibers and also act as the primary means of load transfer between fibers. Common fiber materials include glass, aramid, and carbon fibers. Common matrices, or resins, are epoxy, polyester, and vinyl ester resins. Typical properties of glass fiber reinforced polymers (GFRP), carbon fiber reinforced polymers (CFRP), and aramid fiber reinforced polymers (AFRP) are provided in the following table (Teng, et al., 2003).

Table 2-1. Typical Properties of GFRP, CFRP, AFRP (Teng, et al. 2003)

Unidirectional Adv. Composite Materials	Fiber Content: % by weight	Density: kg/m^3	Longitudinal Tensile Modulus: GPa	Tensile Strength: MPa
CFRP laminate (Glass/Polyester)	50-80	1600-2000	20-55	400-1800
CFRP laminate (Carbon/Epoxy)	65-75	1600-1900	120-250	1200-2250
AFRP laminate (Aramid/Epoxy)	60-70	1050-1250	40-125	1000-1800

FRP materials are lightweight, noncorrosive, and exhibit high tensile strength (ACI, 2002) and can be tailored to performance requirements via positioning, volume fraction, and/or direction of fibers in the matrix to obtain maximum efficiency (Meier, 2000; Karbhari and Seible, 2000). FRP composites are available in a variety of forms ranging from factory-made laminates to dry fibers sheets that can conform to the geometry of the structure before adding resin (ACI, 2002; Teng, et al. 2003). FRP composite materials possess important qualities, which suggest immense potential to application of civil structures. As such the replacement of externally bonded steel plates with externally bonded FRP composites has been the focus of many researchers in the past decades to repair, strengthen, and retrofit reinforced concrete structures (Bonacci and Maalej, 2000, 2001; Teng et al., 2003)

Externally bonded reinforcement initially involved the application of steel plates to the tensile face of structural components for strengthening. Flexural strengthening of existing structures with bonded steel plates was shown to be viable options as reported by Fleming and King in 1967 (ACI, 2002). However, the use of steel plates as external reinforcement presented the following disadvantages: (1) Deterioration of the bond at the steel concrete interface from steel corrosion; (2) Difficulty in handling of the plates at the construction site; (3) Increased load demand on the structure; (4) Restrictions on length of steel plates due to weight (Meier, 2000; Karbhari and Seible, 2000; Triantafillou and Plevris, 1991). In order to develop an alternative to bonding of steel plates, the use of FRP composites for strengthening reinforced concrete structures was first investigated at the Swiss Federal Laboratory for Materials Testing and Research (EMPA) where tests on RC beams strengthened with CFRP plates were conducted in 1984 (Teng, et al., 2003; Meier, 2000). In the past decades the number of researchers investigating strengthening, repair, retrofitting, or rehabilitation with FRP composites has increased significantly. In most recently reported applications for strengthening of reinforced concrete structures, the use of carbon fibers is predominant. The following table provides a qualitative assessment of fibers considering criteria that are appropriate for strengthening of reinforced concrete structures (Meier, 1995).

Table 2-2. Qualitative Comparison of Fiber Reinforcements (Meier, 1995)

Criterion	Fibre Composite Laminates made of…		
	Carbon	**Aramid**	**E-glass**
Tensile Strength	Very Good	Very Good	Very Good
Compressive Strength	Very Good	Inadequate	Good
Young's Modulus	Very Good	Good	Adequate
Long-term Behaviour	Very Good	Good	Adequate
Fatigue Behaviour	Excellent	Good	Adequate
Bulk Density	Good	Excellent	Adequate
Alkaline Resistance	Very Good	Good	Inadequate
Price	Adequate	Adequate	Very Good

Of the criteria used in the qualitative evaluation by Meier (1995), tensile strength, Young's modulus, long-term behavior, fatigue behavior, and cost are the most critical considerations when considering strengthening applications of reinforced concrete structures. The above table shows clearly that carbon fiber reinforced polymer composites most closely fulfill requirements for strengthening of existing reinforced concrete structures (Meier, 1995, 2000).

FRP composites possess the following characteristics, which provide advantages in terms of material properties and use in field applications, (1) High strength-to-weight and stiffness-to-weight ratios, (2) Enhanced fatigue life, (3) Corrosion Resistance, (4) Potential lower life cycle costs (Karbhari and Zhao, 2000; Sherwood and Soudki, 2000). In addition, the lightweight of the material and ease of application make for an attractive alternative for construction purposes. A rehabilitation strategy, such as flexural strengthening of a reinforced concrete bridge deck with CFRP composites, can be performed without interference of the intended function of the structure; i.e., no interference with traffic. Although, significant advantages are realized with FRP composites for bridge strengthening and repair, questions regarding quality and durability of FRP composites at the material level remain as well as the effect of FRP material degradation on the rehabilitated component.

2.2.2 *Manufacturing and Application*

For strengthening of bridge decks and girders, composites are generally applied in three ways as described in Table 2-3, of which wet lay-up and adhesive bonding are the most commonly used approaches (Teng, et al., 2003; Karbhari and Seible, 2000; Meier, 2000). The efficacy of any of the manufacturing/construction methods depends on the combined action of the entire system with emphasis on the integrity of the bond and interface between the composite layer and the concrete substrate (Karbhari and Zhao, 2000). In addition, the appropriate selection of materials based on stiffness and strength requirements influences the overall performance and capacity of the FRP strengthened component (Karbhari and Seible, 2000).

Table 2-3. Application Methods (Karbhari and Seible, 2000)

Procedure	Description	Time/Issues
Adhesive Bonding	Composite strip/panel/plate is prefabricated and then bonded onto the concrete substrate using an adhesive under pressure	• Very quick application • Good quality control
Wet Lay-up	Resin is applied to the concrete substrate and layers of fabric are then impregnated in-place using rollers and/or squeegees (or a pre-impregnated wet layer of fabric is squeezed on). The composite and bond are formed at the same time.	• Slower and needs more setup • Ambient cure effects • Waviness/wrinkling of fiber • Non-uniform wet-out and/or compaction
Resin Infusion	Reinforcing fabric is placed over the area under consideration and the entire area is encapsulated in a vacuum. In a variant the outer layer of fabric in contact with the bag is partially cured prior to placement in order to get a good surface.	• Far slower with need for significant setup • Ambient cure effects • Dry spots

While wet lay-up and adhesive bonding remain the predominant manufacturing/application techniques of choice, other construction techniques are being developed and considered for strengthening of FRP composite rebar. For instance, Lamanna, et al (2004) suggest mechanical attachment of FRP composites strips to the tension surface of reinforced concrete members. Mechanical attachment of FRP strips uses fasteners, which are driven through the strip and into the concrete. The purpose of the fasteners is to develop a procedure for rapid rehabilitation that removes the constraints related to preparation and curing of adhesive used to bond prefabricated FRP strips to concrete surface. Another construction technique for strengthening and repair involves the use of near-surface mounted (NSM) FRP rods. NSM FRP rods are a strengthening technique that involves the embedment of FRP rods in grooves cut into the concrete surface and bonded with an epoxy-based paste (DeLorenzis and Nanni, 2002; Taljsten, B., 2002; Alkhardaji, et al., 1999). NSM FRP rods are advantageous in cases where the strengthening system needs to be protected (i.e. in cases where impact may occur) or if the concrete surface is very uneven. The application of NSM rods typically requires a depth of 25 mm (1 inch) and involves cutting grooves into the concrete cover (Tajlsten, 2002). The methodology is only effective if all concrete dust, wet concrete, and ash are removed. In the cases where epoxy is used to mount the rods, the grooves must be completely dry prior to bonding.

2.2.3 *General Discussion*

In light of a deteriorating civil infrastructure and a lack of available resources, engineers have been required to develop innovative techniques to strengthen and extend the service life of existing structures. In this regard, the application of externally bonded fiber reinforced polymer (FRP) composites for rehabilitation of reinforced concrete (RC) bridge structures has increased.

As the application of FRP sheets for repair or strengthening continues to grow, reliable analytical methods are also required to simulate the response of strengthened or repaired concrete (Sato and Vecchio, 2003). The difference between FRP sheets and conventional steel reinforcement is substantial and must be considered when modeling the bonded interface and tension stiffening effect of the FRP composite.

FRP sheets differ from steel reinforcing bars with the following three mechanical characteristics (Sato and Vecchio, 2003):

1) FRP sheets are elastic materials, i.e. no plastic deformation occurs

2) The ratio of bond area on concrete to the cross-sectional area of FRP is much greater than steel rebar. Consequently, high localized stresses occur at cracks due to the bond stress between FRP and concrete. These localized stresses may result in brittle failure with FRP rupture before plastic deformation of the repaired section occurs.

3) FRP can peel off from the surface of the concrete. Unlike disbond of steel reinforcement from concrete, the disbond of FRP laminates occurs in a sudden, brittle manner.

Application of CFRP materials up to now has been without comprehensively documented methods for quality control and assessment. In fact, most rehabilitation applications of CFRP, be they bridge systems or other civil structures, are without a set of standardized quality assurance criteria to ensure that proper procedures and methods are adhered to during the CFRP application process. The lack of standardized quality control procedures is of serious concern for rehabilitation applications on civil structures since (1) manufacturing processes are likely to be wet lay-up or adhesive bonding, (2) fiber and resin are separate constituents rather than pre-impregnated materials and (3) application procedures take place in the field, thus being susceptible to changes in the environment (Karbhari, 2000). In order to establish a set of criteria to ensure the quality of a structural rehabilitation strategy using FRP, the focus and objectives of appropriate criteria need to be understood.

2.3 Flexural strengthening

2.3.1 *General Description*

Flexural strengthening or repair of reinforced concrete members with FRP composites is generally conducted by bonding composite materials on the tension side of bending members (Teng, et al, 2003). The design process is analogous to design of reinforced concrete sections with special considerations for FRP composite bonding (Tajlsten, 2002)

In the design or capacity evaluation of a FRP composite strengthened reinforced concrete member, the following assumptions are typically accepted in literature (Tajlsten, 2002):

- Plane sections remain plane after bending (Bernoulli's Hypothesis)

- Complete composite action between materials

- Cracked concrete retains no tensile strength

- FRP behaves linear-elastic up to failure

Figure 2.1 below provides an illustration of application of FRP composite on the tension side of reinforced concrete flexural members for flexural strengthening
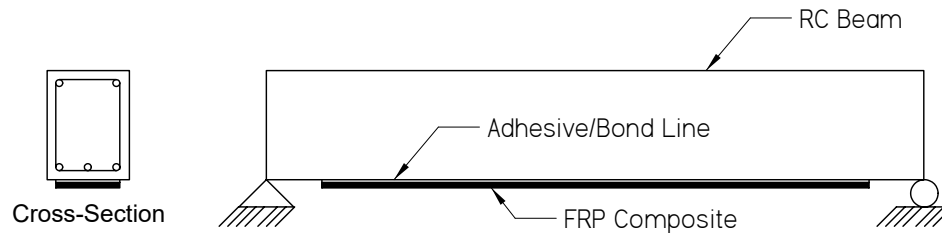
Figure 2.1. Beam Strengthened with FRP composite

Design FRP composites for flexural strengthening requires consideration for seven primary failure modes, which are controlled in the design process. The failure modes are:

1. Concrete Crushing (Tajlsten, 2002; Teng, et al. 2003)

2. Yielding of Tensile Reinforcement (Tajlsten, 2002)

3. Yielding of Compressive Reinforcement (Tajlsten, 2002)

4. FRP rupture (Tajlsten, 2002; Teng et al., 2003)

5. Shear Failure (Teng, et al., 2003)

6. Concrete Cover Separation (Tajlsten, 2002; Teng, et al., 2003)

7. Plate and Interfacial Debonding (Tajlsten, 2002; Teng, et al., 2003)

From the above list, the number of potential failure modes in flexure of FRP strengthened structures is possible. Shear failure, though not addressed in detail here, is possible if the flexural capacity of the RC member exceeds the shear capacity (Teng, et al, 2003). Yielding in the tensile reinforcement at the ultimate limit state is assumed; while yielding of steel reinforcement at the serviceability limit is not permitted (Tajlsten, 2002).

Most available literature evaluates the effectiveness of FRP composite rehabilitation based on comparisons of control specimens and specimens strengthened with FRP composites. While, the application of FRP composite on the tension side of reinforced concrete flexural members provides some measure of capacity increase relative to the pre-rehabilitated state of the structure, it is observed in literature that the term "repair" with FRP composite most often refers to restoring the intended capacity of a damaged structural component, i.e. restoring the structural member to its intended design function; whereas, "strengthening" is often referred to an increase in the load limits of the structure (i.e. upgrading the load limit of a deck slab from HS-15 to HS20-44 truck loading). In

the following sections, literature concerning the flexural strengthening of beams, slabs, and bridge structures is provided to show evidence of the effectiveness of FRP composites used to rehabilitate reinforced concrete structures, with an emphasis on bridge structures if applicable.

As shown in the following sections, available literature evaluating FRP rehabilitated structures rarely address the time dependent degradation of FRP composites when exposed to harsh changing environments. More importantly, no analytical methods are provided to assess the change in performance of FRP strengthened or repaired structures that incorporates material variability and the degradation of FRP composite materials exposed to severe environmental conditions.

2.3.2 *FRP Repair/Strengthening of Beams*

In this section, recent literature regarding the use of externally bonded FRP composites to strengthen reinforced concrete beam structures is reported.

Reed and Peterman (2004) apply CFRP composites for flexural and shear strengthening of full-scale pre-cracked, prestressed concrete beams. The beam specimens are taken from the Bridge No. 56 in Graham County, Kansas. The bridge structure is a three-span, prestressed, double-tee, bridge designed in the late 1960's for AASHTO H-15 live loading conditions. Due to overloading large shear and flexure cracks developed in the webs of the double tees. In the spring of 2000, the bridge was closed and the damaged girders were replaced. A total of three 915 mm (36 in) wide by 12.2 m (40 ft) by 585 mm deep (23 in) were tested with a pretopped 127 mm (5 in) thick flange. Specimen 1 was unstrengthened; specimen 2 was strengthened for flexure with CFRP composite; specimen 3 was strengthened for flexure and shear. The CFRP composite was designed using strain compatibility, with FRP rupture intended as the failure mode. For flexural strengthening, two layers of CFRP composite are wrapped around the bottom of the web, each layer being 305 mm (12 in) wide with a nominal thickness of 0.17 mm (0.0065 in). The CFRP shear reinforcement was designed with shear friction approach. For shear reinforcement, two layers of 150 mm (6 in) wide CFRP stirrups (fibers oriented vertically) spaced at 450 mm (18 in) on center are applied by wet lay-up.

Results show the measured moment capacity of the unstrengthened beam at 430 kN-m (317 k-ft) with failure of concrete crushing; the flexural strengthening only beam fails in horizontal shear and provides a moment capacity of 533 kN-m (393 k-ft), which is a 23.9% increase from the control specimen; the shear and flexure strengthened beam fails with FRP rupture and provides a moment capacity of 540 kN-m (398 k-ft) which is 25.6% greater than the control specimen. Relative to the H-15 capacity, the three specimen results are 25.7%, 55.8%, and 57.9% greater.

Crasto, et al. (2001) evaluated the rehabilitation of RC bridge girders with three scale tests: small-scale lab, full-scale lab, and field implementation. The authors ensured a strong bond between concrete and composite with the use of a vacuum bag to apply a uniform pressure on four layer thick unidirectional CFRP composite manufactured from graphite/epoxy prepreg (AS4C/1919). Full-scale lab tests of the rehabilitated beam showed a 30% increase in moment capacity relative to the control beam. Ultimate failure was characterized by crushing of concrete in the compression zone, preceded by

debonding of the composite. The FRP rehabilitation design from full-scale laboratory tests was applied to a precast reinforced concrete box-beam superstructure, specifically CFRP composite was applied to the box beams of the bridge deck. During the life of the rehabilitation, an acoustic tap hammer was used to monitor the bondline between composite and concrete at intervals of one, three, and ten months; while the debond area is not quantified by the authors, they qualitatively observer a slight increase in area. The field rehabilitation was evaluated one-year following application by removing an exterior strengthened beam from the bridge structure and testing in a laboratory. The test result showed the moment capacity of the strengthened beam was approximately 30% greater than the control specimen after a year of environmental exposure.

Ascione and Feo (2000) study the stresses at the composite-concrete interface, which may lead to brittle fracture of the concrete layer that supports the composite laminate. The specific topics of the problem are shear and normal stresses concentrations at the ends of the composite overlay (cut-off cross sections) and the non-uniform distributions of such stresses along the reinforced boundaries. The authors specifically address the shear and normal stresses concentrations at the ends of the composite overlay (cut-off cross-sections). The authors formulate a finite element model for studying such stresses, specifically along the beam axis. Numerical results are presented for a simply supported beam loaded in flexure, when the effects (non-uniform distribution along the strengthened boundaries) related to the out-of-plane warping of the cross-section are less relevant. Ascione and Feo, compare the results of their numerical simulation with independent experiments showing local shear stress maximum at the cut-off section and then reduce to zero.

Erki and Meier (1999) investigate the impact loading of reinforced concrete beams with externally bonded CFRP composites and steel plates. Specifically the behavior of two 8 m reinforced concrete beams externally strengthened for flexure with CFRP composites are subject to impact loading by dropping one end of the simply supported beam from heights of 0.5 m, 1.0 m, 1.5 m, and 2.0 m. It is recommended that anchoring of the beams at the ends would improve the impact resistance of CFRP strengthened beams. The beams strengthened with CFRP composites, although they performed well, did not provide the same energy absorption as beams externally strengthened with steel plates. The CFRP bonded beams show a lower maximum displacement at the center of the beam dropped from 2.0 m than beams with bonded steel plates dropped from 2.2 m.

Almusallam and Al-Salloum (2001) an analysis model to predict the nominal moment capacity of RC beams strengthened with external FRP laminates. The methodology is able to establish limits on laminate thickness in order to assure tensile failure due to steel yielding and to avoid tensile failure due to laminate rupture. Further, the methodology is developed such that for a given laminate thickness or area, the moment capacity of a beam is known. Maximum thickness of applied FRP is determined from a balanced failure of steel yield and crushing of concrete in a RC beam; while the minimum allowable thickness is the thickness of FRP laminate is determined at the maximum usable stress of the FRP or 67% of the FRP ultimate stress. The thickness relationship for moment capacity is determined from the moment equilibrium of a section and force equilibrium and is required to be within the minimum and maximum to ensure steel yield. An experimental program is followed for strengthening of a 150 mm by 200 mm

reinforced with 3phi10 mm steel rebar on the tension side, 1phi6 compression bar and phi8 steel stirrups at 100 mm center to center. The beams had a span of 2050 mm. Beams were strengthened with glass FRP and carbon FRP composites using one and two layers of either GFRP (1.3 mm) or CFRP (1.0 mm) comparing glass FRP and carbon FRP materials. It is observed that theoretical predictions for load capacity are conservative and that using four layers of GFRP composite provides the same capacity as two layers of CFRP composite.

Lau and Zhou (2001) conduct an experimental study on the performance of glass fiber composites on reinforced concrete cylinders and concrete beam specimens. Damage is simulated in a class of specimens with the introduction of a notch along the circumference of the cylinder or on the tension side of the reinforced concrete beam. In addition to ambient environment exposure, the strengthened cylinders and beams are exposed to chemical attacks with environments of water, saline water, alkaline (pH 10), and acidic solutions (pH 4) for a duration of 6 months. The authors found that the ultimate compression capacity as well as stiffness of the concrete cylinder increases with use of composite wrap technology. Effects of full immersion of plain concrete and FRP strengthened concrete beams in an acidic solution (pH 4) results in a 24.8% reduction in flexural strength; while specimens in other environments show reductions in flexural strengths within 10%.

Lamanna, et al. (2004) conducted tests on large scale beams 304.8x304.8x3657.6 mm (12 in by 12 in by 144 in) reinforced concrete beams with composite strips attached mechanically to the concrete surface. Mechanical attachment of FRP strips uses fasteners, which are driven through the strip and into the concrete. The purpose of the fasteners is to develop a procedure for rapid rehabilitation that removes the constraints related to preparation and curing of adhesive used to bond prefabricated FRP strips to concrete surface. In addition, the use of mechanical attachment also adheres to recommendations of adding mechanical anchorages at the end of strips to counter high shear stresses at the ends of bonded strips (Spadea, et al., 1998; Garden and Hollaway, 1998). It is concluded that the mechanically attached strips are just as effective as adhesively bonded FRP strip. The mechanically fastened FRP strips showed increases in yield moment over the unstrengthened control beams of up to 21.6% and increases in ultimate moment of up to 20.1%. Without predrilling, the mechanically attached strips were observed to fail by strip detachment. In general the time to mechanically attach the FRP strips is approximately 30 minutes as compared to the 4 hrs required to adhesively bond FRP strips (not considering cure time), which includes surface preparation, adhesive mixing and bonding.

2.3.3 FRP Repair/Strengthening of Slabs

In this section, a overview of literature of FRP strengthening of slabs is conducted. Currently, flexural strengthening with FRP composites to reinforced concrete slabs is design and evaluated with the same principles used in flexural strengthening of reinforced concrete beam sections.

Shahawy, (1996) et al. evaluated the flexural behavior of structurally damaged full-scale pretensioned concrete slabs with bonded CFRP composites. A total of four tests are conducted on two slabs of 4.65 m x 1.2 m x 0.3 m. One slab is a solid reinforced

concrete slab and the other is a voided slab with 14 and 5, 13 mm diameter low relaxation strands, respectively. Initially, control tests are conducted on each slab up to ultimate; the resulting cracked slabs are then repaired with the bonding of the CFRP composites to the tension surface of each slab. Four layers and three layers of CFRP composite tape are applied to the solid and voided reinforced concrete slabs. Each layer of CFRP composite tape is 0.17 mm thick, with a tensile strength of 2758 MPa (400 ksi) and tensile modulus of 141.34 GPa (20.5 msi).

For the solid RC slab, the bonding of CFRP composite recovered 90% of the ultimate moment of the precracked solid reinforced concrete slab. Failure of the control or precracked slab was inidicated by concrete crushing between the load points; whereas, the repaired solid RC slab failed by concrete crushing at midspan and minimal debonding of CFRP composite laminates.

As for the voided RC slab, the bonding of CFRP composite resisted an ultimate moment that is 178% of the precracked voided RC slab. Failure of the precracked voided slab was indicated by concrete crushing at midspan; on the other hand, failure of the repaired, voided RC slab was sudden and catastrophic with the additional reinforcement with crack propagation from one of the voides at the right bearing, which progressed longitudinally along the span toward the center. This crack development is attributed to the lack of concrete area in the compression zone of the slab due to voids.

Mosallam and Mosalam (2003) evaluate the strengthening of two-way reinforced concrete slabs by bonding carbon and glass FRP composites. The objective of their experimental and analytical program is to confirm the effectiveness of using FRP composites in repair and rehabilitation of unreinforced and reinforced concrete slabs. Each slab is 2670 x 2670 x 76 mm (105x105x3 inches) subject to a uniform pressure on the surface of the slab. Reinforced concrete slabs consisted of #3 (9.5 mm diameter) tension steel rebar at 12 in (305 mm) center to center in both slab directions. Several control specimens were tested up to 85% of ultimate, then repaired to show the viability of bonding wet lay-up FRP composites. Damaged slab specimens were repaired with two layers of 457 mm (18 inch) wide unidirectional carbon/epoxy composite strips at 18 inch (457 mm) spacing in both slab directions and an E-glass epoxy system with three unidirectional layers in both slab directions. Spacing of FRP strips was governed by the need to prevent the occurrence of shear failure in the slab. The results of the slab tests showed that repair of unreinforced concrete slabs with FRP composites provided 5 times more capacity than the unreinforced control slab. For reinforced concrete slabs, repair using FRP composites doubled the capacity of damaged two-way slabs.

Ferreira, et al. (2000), study the behavior of reinforced concrete strengthened with unidirectional composites strips on the tension side of slabs. The authors conduct a finite element analysis of composites bonded to reinforced concrete, accounting for non-linear material behavior for the concrete and for the composite strips in a shell element. The geometrical and material non-linear behavior is accounted for with use of the Ahmad shell element; the Ahmad shell element is a three-dimensional brick element degenerated to a curved shell element having nodes at the mid-surface. The element is capable of multilayer definition and is able to model laminates either of composite materials or reinforced concrete strength with composite laminates; it assumes that 'normals' to the

mid surface remain straight after deformation and the stress component normal to the shell mid-surface is constrained to be zero in the constitutive equations.

Ferreira, et al., (2000) use the shell element to model reinforced concrete with bonded CFRP composites. The developed shell element is applied to a numerical example of a simply supported slab subject to a uniform distributed load. RC slab rehabilitation is considered with glass/epoxy and carbon/epoxy composites. It is concluded from a comparison between reinforced concrete, plain concrete with bonded glass/epoxy, and plain concrete with bonded carbon/epoxy that the RC section and concrete with glass/epoxy show a similar load-displacement plot; while the concrete with CFRP composite bonded shows a greater stiffness increase than the RC section and concrete with bonded glass/epoxy.

Seim, et al. (2001) evaluate the response and efficiency resulting from the use of FRP strips for strengthening of one-way scale slabs; specifically, load capacity with externally bonded FRP and the development of shear stresses between the concrete and composite interface are investigated. In the experimental work, thirteen scaled slabs are tested. Each slab is 2290 (90 in) x 480 (19 in.) x 102 mm (4 in). Three No. 3 steel rebar provide longitudinal reinforcement in the slab and twenty No. 2 steel rebar are used in the transverse direction at 100 mm (4 in) spacing. Two slabs were used as control specimens, three slabs were strengthened with wet lay-up carbon/epoxy composites, and seven were strengthened with pultruded CFRP composite strips. One slab was strengthened with a glass fiber chopped layer that was sprayed on. For the adhesively bonded pultruded CFRP stips, slab tests variables included changes in the length of the CFRP strips, adhesive thickness, and three variations of bond completeness. For wet lay-up application, the composite covered the entire bottom surface of the slab, with variations in the number of layers and thickness of fabric.

Overall, the experimental tests of one-way scaled slabs using both prefabricated strips and fabric showed that depending on material and configuration the ultimate load capacity of the slab can be increased 3.7 times the ultimate load capacity of as-built slabs. It is noted that the failure mode of the slab changes from the conventional yield of steel to a more sudden failure with debond of FRP composite from the concrete as a result of cracking through the cover and/or rupture of the FRP composite, and/or crack growth through the outer layer of pultruded strips. The authors conclude that for pultruded CFRP only about 50% of the capacity of the strip is used, and a strain limitation of 0.65% in the adhesive. The use of wet lay-up CFRP composites covering the entire width of the slab results in a more uniform and even shear stress development. However, it is cautioned that coverage of the entire slab width causes concern for moisture retention in the concrete, which may degrade the bond at the concrete composite interface. The use of the wet lay-up CFRP composite also indicates 50-70% higher deformation levels than the prefabricated CFRP strips.

The E-glass fiber spray-up, provided an increase in load capacity of approximately 35% compared to the as-built slab, while showing significant ductility.

The effect of adhesive thickness from 1mm to 5 mm for adhesively bonded CFRP strips, is not significant to the ultimate load level of the slab; however, a 30.4% increase in maximum shear stress level was observed in the thicker adhesive layer. In spite of the

increase in shear stress level, no changes were observed in the overall response because stress levels are below critical levels in all cases.

The shortest strip length used in the analysis corresponds to the strip length required to double the yield load of the unstrengthened slab, which is 1.09 m. Longer strip lengths of 1.83 and 1.46 showed similar ultimate load levels with both slabs failing through cracking in the concrete with transition to resin rich layers of the strips at the ends; the ultimate load levels were at least 1.87 times the as-built slabs. For the 1.09 m strip lengths, the ultimate load was only 1.51 times as-built slabs; a shear dominated failure is observed in the adhesive layers at the ends of the strips with debonding of composite from concrete; this failure mode emphasizes the role of inadequate development length and the effects of stress concentrations.

Seim, et al. (2003) study the use of externally bonded CFRP composites to double the load bearing capacity of reinforced concrete slabs and restoring the load bearing capacity of slab with accidentally cut steel rebar. In this study, full-scale reinforced concrete slabs of 4500 mm x 960 mm x 203 mm; of these slabs, three were used as control specimens due to variation in longitudinal steel area; six of the slab panels were bonded with pultruded CFRP strips to double the load capacity of the slab; five of the slab panels were built with cut rebar.

For the six slab panels with bonded CFRP strips, the same quantity of pultruded CFRP strips was applied with a cross-sectional area of 240 mm^2 and a length of 3250 mm. The results showed that capacity of the CFRP strengthened slabs are twice the as-built slab capacities. The load-deflection behavior is characterized by four linear parts: first, the change in stiffness with the onset of cracking; second, yielding of steel, third, from the progression of debonding, followed by a very short nearly horizontal portion. Failure of the strengthened slabs was noted by debonding of strips at approximately 10-20% below the ultimate load level.

The objective of the cut reinforcement specimens was to evaluate the ability of the bonded CFRP composite to bridge the concentrated crack at mid-span. Debonding was observe at strain values of 0.4% near the cut location; although, the load capacity of the repaired slab was able to exceed the load capacity of as-built RC slabs.

Results of slab experiments is used to recommend a three step design procedure that involves the calculation of bending resistance, anchorage length, and reduced shear capacity. Bending resistance is determined from section analysis of the FRP strengthened section with a limit on the strain of CFRP strips at 0.65% for a distributed crack pattern and 0.4% for local corrosion or stress concentrations. Anchorage length is determined from a moment capacity diagram since the reinforcement for the slab is made up of two different materials. Shear resistance is determined from empirical relationships with a reduction factor to avoid debonding, since the phenomenon of debond close to shear cracks is considered a preliminary shear failure.

Limam, et al. (2003) conduct an experimental investigation on two 7 cm x 130 cm x 170 cm RC two-way slabs reinforced with 6 mm diameter steel rebar spaced at 20 cm in both slab directions, with a concrete cover of 17 cm. One slab is strengthened with CFRP composite strips, while the other is used as the control slab. The strengthened RC slab is designed as a three-layer plate, using the upper bound theorem of limit analysis for a

multi-layered plate to estimate the ultimate load capacity of the slab. The upper bound theorem of limit analysis involves collapse kinematic fields with discontinuities in velocity fields. Three layers represent the multi-layered plate; the bottom layer is the grid of bonded CFRP composite strips; the middle layer is the steel reinforcement; the top layer is the compressive concrete. To perform the limit analysis, failure is considered in the compressive layer, the steel layer, and the CFRP composite layer, as well as the interface between the steel layer and CFRP composite layer and mixed mechanisms. During the experiment the control slab fails at 48 KN while the CFRP strengthened slab fails at 120 KN with CFRP strip debonding and steel yielding. For this failure mechanism of the strengthened slab the limit analysis model predicts a 123 KN ultimate load.

Arduini, et al. (2004) evaluate the behavior of one-way RC slabs tested under simply supported conditions. CFRP composites were bonded to the positive and negative moment regions of the slab by manual lay-up. In all, a total of 26 specimens were tested, of which 14 focused on the positive moment region and 12 on the negative moment region. The objective of the research is to validate guidelines established by ACI 440.2R for flexural strengthening of one-way slabs, emphasizing modes of failure for variations in quantity of applied FRP composites and steel reinforcement. The tested reinforced concrete slabs are 500 cm by150 cm by 24 cm. CFRP composite sheets are applied via wet lay-up in the primary direction of the one-way slab, as opposed to two-way slabs, which behave in two directions. It is observed following tests that strengthening in the negative moment region is less effective than strengthening in the positive moment region due tot the presence of shear; the lower the existing steel reinforcement ratio, the more effective the externally bonded FRP strengthening. The load carrying capacity of one-way slabs can be increased by up to 122% compared to control slabs, where the increase is more pronounced for slabs with low steel reinforcing ratios. From agreement in their analytical approach and experimental results the authors conclude that assumptions of plane sections remain plane after loading and that perfect bond exists between concrete, steel, and FRP composite are appropriate.

Oh and Sim (2004) propose a theoretical model to predict the punching shear capacity of reinforced concrete decks with externally bonded FRP composites. The authors note the angle of the failure surface observed during punching shear failure is 35° from compression reinforcement to tension reinforcement for an un-strengthened slab. While an angle from bottom reinforcement to a bonded plate is observed at 25°C. In their model the authors utilize a standard definition for the shear strength of a plain reinforced concrete section with shear resistance from the depth of the concrete section and add components for the contribution of bottom concrete (concrete between bottom steel and bonded plate) due to the strengthening effect with bonded plates. The contribution of the bottom concrete is added due to the partial restraining effect of the bonded strengthened plate which accounts for positive characteristics such as crack control, improved structural stiffness, and the 'pseudo-dowel effect' of the strengthening material at the failure state. In addition to the bottom concrete, the authors also consider contributions from dowel action and bond-typed anchor bolts. The authors compare the analytical model with experimental data of slabs strengthened with steel plates, carbon fiber rods, GFRP laminates 8 layers thick in two directions; all slabs failed in punching shear after the yield of flexural reinforcement. The predictions between the analytical and

theoretical model did not exceed 3.7%. The largest error of 3.7% for carbon fiber rods used for strengthening, over predicted the experimental since the model assumes perfect bond between plate and concrete. A comparison between the different deck slabs shows the use of bonded GFRP laminates provided a 30% increase in load carrying capacity as opposed to unstrengthened deck slabs.

2.3.4   *FRP Repair/Strengthening of Bridge Structures in the Field*

A majority of researchers evaluate the effectiveness of an FRP composite rehabilitation with a load test on the entire structural system, rarely addressing whether or not the design was able to meet the strengthening objectives. Assessment of load capacity alone without consideration for field conditions and design provides little useful information about the effectiveness of the rehabilitation and may result in inefficient FRP composite rehabilitations in the future.   Mere determination that capacity has increased with externally bonded FRP without relating to design and to material properties of the composite fails to fully assess the quality of a FRP rehabilitation measure. A number of researchers have demonstrated the increase in capacity as a result of FRP strengthening measures in both laboratory and field conditions. Bonacci and Maalej (2000) provide a comprehensive review of strengthening with FRP; here, some recent work with externally bonded FRP is highlighted.

Alkhrdaji, et al. (1999) investigate the behavior of a full-scale bridge strengthened with FRP composite systems. The objective of the research is to assess the performance of FRP composite application to an existing bridge in order to provide necessary field verifications of design method, structural performance, and failure mode. The structure of interest is bridge J-857 on route 72 in Phelps County-Missouri. The bridge consists of three simply supported solid RC decks spanning 7.9 m (26 ft) with a deck thickness of 460 mm (18 in) and road width of 7.6 m (25 feet). The RC bridge deck is reinforced with No. 8 steel rebar at 127 mm (5 in) centers and No. 4 deformed steel rebar at 457 mm (18 in) on center in the transverse direction.

Since the bridge was scheduled for replacement, a destructive test to fail the bridge structure in the field is conducted with FRP composites applied to two of the three spans of the bridge structure. Two FRP systems were applied to two spans; these are externally bonded wet lay-up FRP sheets in one span and near-surface mounted (NSM) FRP rods in the other. NSM FRP rods are a strengthening technique that involves the embedment of FRP rods in grooves cut into the concrete surface and bonded with an epoxy-based paste. The purpose of the rehabilitation was to increase the nominal moment capacity of the bridge deck by 30% to 452.3 kN-m/m (101.7 k-ft/ft), which is the level desired for the HS20-modified truckload. Considering this strengthening requirement eight, 500 mm (20-in) wide single-ply strips were applied to the deck soffit, with strips evenly spaced over a width of 8.2 m (25 ft) for the entire length of the deck. For NSM CFRP rods, 20 rods were bonded at 375 mm (15 in) centers. The rods were embedded in 6.6 m (20 ft) long, 19 mm (0.75 inch), and 14 mm (0.5625 in) wide grooves cut onto the soffit of the bridge deck in the longitudinal slab direction.

Each of the three decks is tested to failure in a quasi-static load test.   The deck strengthened with NSM rods failed at a load of 2649 kN (596 kips) with rupture of some CFRP rods at the location of the widest crack. For wet lay-up CFRP composites, failure

was indicated by rupture and peeling of the composite at 2413 kN (543 kips). The unstrengthened deck slab failed at an ultimate load of 2053 kN (462 kips) with yielding of steel followed by concrete crushing at ultimate. Test results indicate that the measured ultimate capacity of the as-built RC slab is 46% higher than the initial prediction based on material parameters from the DOT database. Due to the high strength of the benchmark, the contribution of the FRP strengthening systems are less than the original prediction with increases of 17% and 27% for CFRP sheets and NSM CFRP rods, respectively.

Hag-Elsafi, et al. (2001) evaluated the effectiveness of FRP composites for flexural and shear strengthening of a reinforced concrete T-beam bridge with the use of load tests before and after rehabilitation. The bonded FRP laminates were used by the New York State Department of Transportation in a demonstration project to repair girders of a concrete T-beam bridge to increase their flexural and shear capacities. The cost of the rehabilitation was estimated at $300,000 in contrast to the $1.2 million required for complete structural replacement, or 25% of the cost of bridge replacement. The FRP composite was designed to compensate for a 15% loss in corroded steel, using 67% of FRP ultimate strength at steel yield. From load tests, the authors observed decreases in rebar stresses, a slight increase in concrete stresses, and improvements in transverse live load distribution. The minimal changes observed in the structure were attributed to a limited load range during testing.

Meier (2000) provides a review of composite materials used for bridge repair. Specifically evaluating the advantages of bridge repair with CFRP pultruded, wet lay-up, and post-tensioned strips. Provides discussion about the advantage and talks about research and show thte strength increase experimentally. He also includes discussion regarding CFRP composite strengthening of degraded bridge structures. A summary of some of the bridge examples by Meier are provided.

The first application of CFRP composites bonded to a bridge occurred in 1991 in the Canton of Lucerne. The Ibach Bridge is a 228 meter long continuous, multispan box beam bridge. The box section is 16 meters wide with a central and longitudinal web. During construction for installation of new traffic signals, a post-tensioning tendon in the outer web was damaged with several wires complete severed; therefore, the authorization of heavy loads across the bridge were suspended. The bridge was repaired with three CFRP strips of 5000 mm length, 2 mm thick and 150 mm wide. The repaired structure was tested with a load test from an 84-ton vehicle.

Due to the occurrence of increased traffic loads, post-strengthening of the reinforced concrete bridge deck of the Oberriet-Meningen bridge was planned and conducted in late 1996. The Oberriet-Menningen bridge is a continuous steel/concrete composite girder bridge was built in 1963 and spans the border between Switzerland and Austria. The standard load of the bridge when built was 14 tons following rehabilitation the standarad truck load is 28 tons. The rehabilitation consisted of 160 CFRP strips, each 4 m long, were laterally bonded to the bridge deck every 75 cm. Each strip is 80 mm wide and 1.2 mm thick (70% fiber volume fraction with Toray T700 fibers). The application of CFRP strips alone provided a safety factor of 1.2 for the 28 ton truckload requirement. Since a factor of 2.15 was required, an additional concrete layer, 8 cm, thick was bonded to the top of the deck.

Meier, (2000) also describes a bridge repair for the Furstenland Bridge, which is a 60 year old, reinforced concrete, box-girder bridge. Because of high chloride content in the concrete and significant corrosion of the reinforcing steel, the bottom flange of the box girder was replace; however, the torsional resistance of the girder was reduced during replacement. Two CFRP composite strips were bonded to the lower portion of each of the inside walls of the webs of the box girder. The application provided addition stiffness to the girders during construction such that bridge closure did not occur. With a total of 8000 meters of CFRP composite strips applied, the permissible load for trucks was also increase from 28 tons to 40 tons.

Stallings, et al. (2001) describe the rehabilitation of an existing seven simple span, reinforced concrete T-girder bridge structure built in 1952 on Alabama highway 110. The bridge structure was originally designed for H15-44 design loading for girders which corresponds to 63% of HS20-44 design loading currently used by Alabama DOT. Damage in the girders were observed in the form of flexural cracks spaced along the span of the bridge at approximately 170-380 mm. The objective of the repair with FRP was to mitigate the deterioration of the bridge resulting from widening of the flexural cracks due to repeated heavy traffic loading and increase the bending moment capacity by 20%. One span of the bridge was chosen for repair with CFRP composite plates applied to the bottom surface of the girder and GFRP plates applied to locations on the sides of the girder to resist flexural crack opening and add stiffness to increase stiffness of the bridge. The adhesively bonded CFRP and GFRP are 6-layer unidirectional laminates with dimensions of 267 mm by 3.09 m by 1.3 m thick for CFRP and 356 mm by 3.28 m by 1 mm thick. A vacuum bag setup was used to bond the composite to the surface of the girders.

Load tests were conducted on the structure before and after FRP application with standard ALDOT trucks with a three-axle configuration and gross vehicle weight of 346 kN. Results indicate reduction in rebar stresses after FRP repair of 4 to 12 %. Reductions in deflections are observed in the range of 2 to 12% depending on the loading configuration. In addition, dynamic tests were conducted where a truck is driven across the bridge structure; these tests indicate reductions in peak rebar stresses from 4 to 9% and reductions in peak girder deflections from 8 to 12%. The authors conclude that the CFRP composite strains are approximately equal to rebar strains.

Shahrooz and Boy (2004) repair the deck of a skewed (70-degree) three-span reinforced concrete slab bridge built in 1955. The spans of the bridge are 6.71, 8.38, and 6.71 meters, with a width of 9.75 m and slab thickness of 298 mm. The bridge structure displayed cracks on the soffit of the deck slab and had been posted because of insufficient capacity of the slab. In order to remove load limits of the structure, the bridge deck slab was strengthened with four different FRP composite systems: (1) adhesively bonded 76.2 mm wide by 1.33 mm thick CFRP composite strips at 305 mm centers; (2) adhesively bonded 127 mm wide by 4.83 mm thick CFRP composite strips at 305 mm centers; (3) one layer of 305 mm wide wet lay-up carbon fabric covering the entire northeast side of span 3; and (4) adhesively bonded 102-mm wide by4.83 mm thick carbon plates spaced at 305 mm centers with four 12.7 mm diameter anchor bolts at the ends. Results of material testing of four tensile coupons showed measured properties with a maximum 5%

coefficient of variation. Load tests were conducted on the structure before, after, and one year following the FRP composite application.

The effectiveness of the CFRP strengthening of the bridge deck is conducted before and after and one year after FRP application via load testing of the bridge structure with two standard Ohio DOT loaded dump trucks each weighing about 132 kN. It is observed from minimal decreases in deflection that flexural stiffness of the deck increases by only 1.5, 2.8, 1.8, and 1.7% for the four different CFRP designs described in the prior paragraph. The load tests following a year of service showed no change in the maximum deflection.

From an evaluation of measured strains, the concrete strain is reduced by as much as 34% following the application of CFRP composite. Similarly, after a year of service, the concrete strains in the bridge structure did not change significantly.

An analysis of the repaired deck slab is conducted with ACI guidelines for flexural strengthening with FRP composites. Based upon a maximum usable strain of 0.39%, the rating factors for the strengthened deck are computed. Before repair with CFRP, the bridge structure had operating and inventory level rating factors of 1.45 and 0.87 respectively for HS20-44 truck loading; after application of CFRP composites, the rating factors increased 22% to 1.77 and 1.06, respectively, for operating and inventory levels with the HS20-44 truck loading. With the new rating factors engineers removed the posted load limits on the bridge.

2.4   Summary

This chapter provides an overview of flexural rehabilitation of reinforced concrete structure with FRP composites. Emphasis is placed on literature for flexural rehabilitation of beams and slab structures and field application of FRP composites. From the prior literature reviews, the assessment of beam and slab structures focuses on the capacity increase provided by bonding of FRP composites, typically CFRP composites, to the tension side of reinforced concrete members. While, it is generally shown in laboratory studies of beams and slabs that FRP composites are able to repair or strengthen reinforced concrete members, the evaluation of effectiveness of field applications on strengthening/repair of reinforced concrete bridge structures do not account for the effect of material degradation or quality of application in the field. Specifically, the evaluation of FRP strengthening measures on actual bridge structures is conducted by load tests of the structure before and after FRP composite application and the durability of the FRP rehabilitated structure is determined with a load test at a later date, following service of the structure. While a load test provides an indication of the structural response to a given load, extrapolation of these results to a general model, which can predict response to any given load, is difficult, if not impossible.

The use of FRP composites for flexural strengthening of reinforced concrete bridge structures provides advantages in terms of the tailorability of the material, application while structure is in service, and the ability to increase the capacity of the bridge deck by repair of girders or slabs, to name a few. However, the issue of durability and its effect on the performance of FRP strengthened structures are unresolved. In addition, the

variation of material properties of field manufactured FRP composites is not addressed in any field applications of FRP composite.

In the following chapters, available methods to nondestructively evaluate the state of a bridge structure are summarized. Specifically, modal testing of structures to acquire the dynamic properties of a structure and the damage detection methodologies used to identify, locate, and quantify damage in a structure are addressed. The application of a validated global nondestructive evaluation procedure for bridge structures provides the means to monitor stiffness changes in a bridge structure over time and evaluate the effectiveness of FRP composite strengthening.

3   MODAL TESTING OF BRIDGE STRUCTURES

3.1   Introduction

In the prior chapter, an overview of flexural strengthening of beams, slabs, and bridge structures was provided. Evaluation of the effectiveness of FRP rehabilitation of existing bridges is determined with the use of load tests before and after strengthening of FRP. FRP bridge rehabilitation measures do not assess the performance of the structure with respect to variation and degradation in FRP composite materials nor evaluate the global rehabilitated structure from a monitoring perspective to assess the change in performance of the structure with respect to time.

In Chapter 3 of this report, the dynamic testing or modal testing of bridge structures is addressed in terms of theory, experimental procedures, and analysis techniques. Modal testing is the primary experimental procedure of a complete damage detection methodology, which serves as the tool to acquire the vibration properties (i.e., accelerations, velocities, displacements, frequency response functions, modal parameters) of a structure in order to determine and evaluate the condition and durability of the structure. The implementation of a modal testing procedure in conjunction with an analysis via a damage detection algorithm utilizing modal parameters provides a methodology for global non-destructive evaluation of civil structures. In addition, the nondestructive damage technique is applicable for evaluation of as-built and rehabilitated structures. The following are a list of reasons for the use of modal testing on civil structures, specifically its applicability to bridges.

- Determines the modal properties, which include the frequencies, mode shapes and damping properties of the bridge
- Assesses the changes in dynamic properties over a period of time to determine the changes of the mechanical properties of the bridge structure
- Quantifies the effectiveness of a rehabilitation or change to the bridge structure
- Provides a means to correlate a finite element model of the structure with the measured results from the real structure for purposes of systems identification (Maia and Silva, 1997).
- Assesses the integrity of a structure for higher loading levels due to a change of use, higher environmental loading, or an increase in allowable loading (Salawu and Williams, 1995).
- Provides a means for continuous monitoring of the structure to detect levels of degradation and locations for local inspection and repair.

This chapter highlights the major components of modal testing and modal analysis as it applies to bridges. Initially, theoretical development for modal testing is explained. Of particular importance is the development of the frequency response functions (FRF's), since the extraction of modal properties of the structure (i.e., natural frequency, damping properties, mode shapes) relies on the FRF's.

Second, methods of excitation for bridges are categorized into input-output methods and output only methods for modal testing. Input-output methods of excitation involve a contact procedure such that a forcing function is introduced to vibrate the bridge structure. Input-output techniques include the use of an impact hammer, drop weight,

shaker, or displacement-release procedure to excite the structure. Output only methods, typically described as ambient excitation methods, are a non-contact procedure utilizing the service level conditions of the structure in order to excite the structure. Sources of "natural" vibration include vehicular traffic, wind, pedestrian traffic, ocean waves, and micro-earthquakes (Farrar and Sohn, 2001; Green, 1995; Salawu and Williams, 1995). There is no single method of excitation, which is superior to all others, rather the experimenter must decide the method of excitation that is most suitable for the modal testing of a particular bridge structure and the constraints presented by the structure in the field. A comparative study on the advantages and disadvantages for the various excitation techniques is provided.

Third, implementation of the testing procedure is described with an overview of the types of transducers available for use on modal tests. Associated with the selection of sensors used for data acquisition procedures is the optimal placement of the sensors in order to minimize their quantity and ensure sufficient resolution exists to characterize the system.

Finally, methods for extraction of modal parameters from measured frequency response functions are briefly reviewed and explained. The selection of an appropriate experimental modal analysis procedure to extract the vibration properties of a structure is dependent on the type of modal test being conducted, i.e. whether an output-only procedure is specified or if forced excitation methods are employed.

3.1.1 History of Modal Testing

In the following section, a brief history of dynamic testing is provided as a precursor to the development of dynamic testing practices and procedures currently available. Dynamic testing of structures has been existent in a qualitative and intuitive manner since ancient times when man has used tools, where changes in the acoustics were observed to detect some change in the performance or quality of a tool (Farrar and Sohn, 2001). In modern times, the increasing observation of fatigue failures in structures prompted the need to monitor the behavior of structures as damage accumulated due to cyclic or repeated loadings.

Formal vibration evaluation procedures emerged during and following World War II primarily due to observations of failures in structures, which were significantly different from the expected failure mechanisms from static loading. Initially, vibration tests were simulated with the intent of evaluating the performance of a system under stress induced by vibration from a field environment (Hunter, 2001). Typical systems included gun mounts, warheads, shipping containers, and automotive or aircraft components. The objective of the first dynamic or vibration tests was to ensure the operability of the system or structure under harsh environments where systems were subject to dynamic loading in field conditions. As technology advanced with improvements and increased capacity of computers, data acquisition systems, and the enhanced performance of sensors, so too has the versatility of dynamic testing methods in providing insight into a systems survivability, evaluation of structure performance, systems identification, and reliability (Hunter, 2001).

Modal testing of structures relies heavily on the accuracy of the tools available for data acquisition and methods of excitation available to vibrate the structure. Early excitation

methods involved implementation of machines utilizing rotating eccentric weights, with electrodynamic vibration machines emerging in the 1950's. In addition, the development of electrohydraulic machines provided a method of inducing vibrations into a structure by moving a piston using fluid pressure. Information regarding the function, limitations, and capabilities of electrodynamic and electrohydraulic shakers is provided in Section 3.3.1.2 of this chapter. Improvements in electrodynamic and electrohydraulic oscillators continued through the 1960's with the introduction of high current, solid state electronics along with improvements in materials leading to stiffer, more durable armatures and test fixtures (Hunter, 2001).

Use of electrodynamic and electrohydraulic shakers is relatively straightforward, since the oscillators introduce a single frequency sinusoidal wave into the system with the amplitude of the input sine wave corresponding to the input vibration level and the amplitude of the response sine wave corresponding to the response acceleration level (Hunter, 2001). However, in order to simulate realistic conditions where multiple frequencies are excited during operation, the use of impulse excitation and ambient excitation methods developed with the general classification being input-output methods and output-only methods, respectively. Where input-output methods indicate the force or excitation level input to the structure is known and output-only methods indicate the modal parameters are extracted from the vibration response of a system from an unknown input level and source.

Associated with increased improvements in the dynamic test procedure is the development of data acquisition equipment and data processing methods. Modern data acquisition systems began with the use of accelerometers in the 1950's, with accelerometers now including integral charge amplifiers such that a majority of the signal conditioning occurs within the device (Hunter, 2001). Whereas in the past large quantities of data were used to process modal models, which are effective descriptions of linear systems, the emphasis on linear behavior for vibration response was alleviated with the use of fast Fourier transforms (FFT) and frequency domain averaging to acquire power spectra and transfer functions and therefore, modal frequencies and mode shapes.

3.2 Theoretical Basis

For a fundamental understanding of modal testing, as well as insight into the development of damage detection algorithms, the theoretical basis for modal testing and extraction of modal properties must be understood. The following section provides a theoretical overview of modal testing.

A detailed review of the development of the equations of motion (spatial model), theoretical modal analysis (modal model), and the solution to the equations of motion for a given excitation (response model) for both the single degree of freedom (SDOF) and multi degree of freedom (MDOF) systems is available in a number of structural dynamics textbooks (Ewins, 2000; Chopra, 1995; Clough and Penzien, 1975; Rao, 1995).

3.2.1 Spatial Model

There are three distinct components in the theoretical analysis for a vibrating structure. These are the spatial, modal, and response models. The spatial model is a mathematical description of the mass, stiffness, and damping of the structure by means of the equations

of motion. Developing the equations of motion for a structure typically involves utilizing Newton's 2nd law and D'Alembert's principle, which accounts for dynamic equilibrium at each time instant when inertia forces are included. Energy-based procedures involving Hamilton's principle, Lagrange's equations, or the principle of virtual work, are also available for developing the equations of motion for a structure. The generalized equation of motion for an N-degree-of-freedom system is provided below in matrix form.

$$\mathbf{m\ddot{u}} + \mathbf{c\dot{u}} + \mathbf{ku} = \mathbf{p(t)} \qquad \textbf{Eqn. 3.1}$$

where $\mathbf{m}$, $\mathbf{c}$, and $\mathbf{k}$ are the mass, damping, and stiffness matrices, respectively, with each matrix having dimensions N x N. The vector, $\mathbf{p(t)}$, describes the externally applied dynamic forces with dimension N x 1. $\mathbf{\ddot{u}}, \mathbf{\dot{u}},$ and $\mathbf{u}$ are the acceleration, velocity, and displacement response vectors of the structure each having dimension n x 1. The matrix form of the equations of motion represents N coupled, ordinary differential equations describing the spatial model of the structure.

3.2.2   Modal Model

A theoretical modal analysis is performed to describe the structure as a set of vibration modes via its natural frequencies and mode shapes. This is the modal model of the structure, which describes the structure without any external excitation or forces, i.e. free vibration. Since the natural modes characterize the response of a structure under free vibration, the mode shapes and natural frequencies for a classically damped system are evaluated by solving the following matrix eigenvalue problem for the scalar λ_n $(= \omega_n^2)$ and vector mode shape $\boldsymbol{\varphi}_n$.

$$[\mathbf{k} - \lambda_n \, \mathbf{m}] \boldsymbol{\varphi}_n = \mathbf{0} \qquad \textbf{Eqn. 3.2}$$

where λ_n, is the nth eigenvalue equal to the square of the nth natural frequency, ω_n^2; $\boldsymbol{\varphi}_n$ is the nth mode shape vector. Two possible solutions exist for the above equation, one being the trivial solution, $\boldsymbol{\varphi}_n = \mathbf{0}$, which is not useful since the result implies no motion. Nontrivial solutions occur when the following relationship is true.

$$\det |\mathbf{k} - \lambda_n \, \mathbf{m}| = 0 \qquad \textbf{Eqn. 3.3}$$

The characteristic equation evaluated from the determinate above has N real and positive roots for λ_n ($n = 1, 2,\dots, N$) from which the nth natural frequency, ω_n ($n = 1, 2,\dots, N$), is calculated. Upon evaluating the natural frequency, equation 3.2 is employed to evaluate the associated eigenvector or mode shape, $\boldsymbol{\varphi}_n$. The process of calculating natural frequencies and mode shapes assumes the structure is linear and the damping matrix, $\mathbf{c}$, is proportional to its mass, $\mathbf{m}$, and stiffness, $\mathbf{k}$, matrices (i.e. Rayleigh damping). Development of the damping matrix, $\mathbf{c}$, from individual structural elements is not a practical consideration since the damping properties of materials are not well defined, nor is the energy dissipated by friction, opening and closing of microcracks, and other similar mechanisms accounted for (Chopra, 1995). For bridge structures, the assumption of proportional damping is a valid idealization if similar damping mechanisms are distributed throughout the structure (Chopra, 1995). Proportional damping is unacceptable when the system to be analyzed consists of two or more parts with

significantly different levels of damping, i.e. a soil-structure system or structure-fluid system.

Solving the eigenvalue problem yields a set of N undamped natural frequencies, ω_n and associated mode shapes $\boldsymbol{\varphi}_n$ for $n = 1, 2, \ldots, N$. The corresponding mode shape vectors, $\boldsymbol{\varphi}_n$, are assembled into an $N \times N$ modal matrix, $\boldsymbol{\Phi}$ as shown below,

$$\boldsymbol{\Phi} = [\boldsymbol{\varphi}_1 \, \boldsymbol{\varphi}_2 \ldots \boldsymbol{\varphi}_n \ldots \boldsymbol{\varphi}_N] \qquad \textbf{Eqn. 3.4}$$

These mode shapes possess orthogonality properties with respect to the structure's physical properties such that the following $N \times N$, square, diagonal matrices result,

$$\mathbf{K} \equiv \boldsymbol{\Phi}^{\mathrm{T}} \mathbf{k} \boldsymbol{\Phi} \quad \text{and} \quad \mathbf{M} \equiv \boldsymbol{\Phi}^{\mathrm{T}} \mathbf{m} \boldsymbol{\Phi} \qquad \textbf{Eqn. 3.5}$$

where, $\mathbf{K}$, is the modal stiffness matrix with diagonal elements $K_{nn} = \boldsymbol{\varphi}_n^T \mathbf{k} \boldsymbol{\varphi}_n$ and $\mathbf{M}$, is the modal mass matrix with diagonal elements $M_{nn} = \boldsymbol{\varphi}_n^T \mathbf{m} \boldsymbol{\varphi}_n$. The assumption of proportional damping implies that the damping matrix is also orthogonal and can similarly be defined as a modal damping matrix, $\mathbf{C} \equiv \boldsymbol{\Phi}^{\mathrm{T}} \mathbf{c} \boldsymbol{\Phi}$, with diagonal elements $C_{nn} = \boldsymbol{\varphi}_n^T \mathbf{c} \boldsymbol{\varphi}_n$.

The orthogonality of modes asserts the following conditions for natural modes corresponding to different natural frequencies. When $\omega_n \neq \omega_r$,

$$K_{nr} = \phi_n^T \mathbf{k} \phi_r = 0 \quad M_{nr} = \phi_n^T \mathbf{m} \phi_r = 0 \quad C_{nr} = \phi_n^T \mathbf{c} \phi_r = 0 \qquad \textbf{Eqn. 3.6}$$

Therefore, the off-diagonal terms in the modal mass, modal stiffness, and modal damping matrices are zero. The orthogonality of modes physically implies that the work done by the nth mode inertia forces in going through the rth mode displacements is zero or that the work done by equivalent static forces associated with displacements in the nth mode in going through the rth mode displacements is zero (Chopra, 1995).

As mentioned previously, the equations of motion describing the spatial model of a structure are coupled and thus, impractical to evaluate for multi-degree of freedom systems. In order to uncouple the equations of motion, the modal model is developed by utilizing the orthogonality properties of the linear system. The displacement vector, $\mathbf{u}(t)$, is expanded into modal space such that,

$$\mathbf{u}(t) = \boldsymbol{\Phi} \mathbf{q}(t) \qquad \textbf{Eqn. 3.7}$$

where, $\mathbf{q}(t)$ is the vector of modal coordinates. The matrix transformation and orthogonality characteristics result in the conversion from the physical space to the modal space (McConnell, 2001). Substituting, equation 3.7 into equation 3.1 and premultiplying each component by $\boldsymbol{\Phi}^T$ and applying orthogonality conditions results in an uncoupled system of equations for N single degree of freedom systems in modal space.

$$\mathbf{M} \ddot{\mathbf{q}} + \mathbf{C} \dot{\mathbf{q}} + \mathbf{K} \mathbf{q} = \boldsymbol{\Phi}^{\mathrm{T}} \mathbf{p}(t) = \mathbf{P}(t) \qquad \textbf{Eqn. 3.8}$$

where, $\mathbf{M}$ is a diagonal matrix of generalized modal masses M_{nn}; $\mathbf{C}$ is a diagonal matrix with generalized damping terms, C_{nn}, for proportional damping; $\mathbf{K}$ is a diagonal matrix of

generalized modal stiffnesses, K_{nn}; $\mathbf{P}(t)$ is a column vector of the generalized modal forces $P_n(t)$, and $\mathbf{q}$ is a column vector of generalized modal coordinates, $q_n(t)$. For the case where each point has an independent excitation force, the following equation is true.

$$M_{nn}\ddot{q}_n + C_{nn}\dot{q}_n + K_{nn}q_n = \sum_{r=1}^{N}\phi_{rn}p_r(t)$$ **Eqn. 3.9**

3.2.3   *Response Model*

The response model provides a description of how a structure responds to a given excitation. For a bridge structure, the excitation source is typically a single point input or an ambient excitation involving random vibrations. In the following section, the response model for a single point excitation and for random vibrations is developed. For identification of a theoretical model of the structure, it is convenient to present the result in the frequency domain, since the output of a modal test is typically given as a function of the frequency. The response model of the structure is merely the solution of the equations of motion under a given excitation and is presented as a function of time or frequency in the form of frequency response functions (FRF's).

3.2.3.1   Single Point Excitation

For a single point excitation, where the excitation occurs at the ith location and all other forces are zero, equation 3.9 becomes,

$$M_{nn}\ddot{q}_n + C_{nn}\dot{q}_n + K_{nn}q_n = \phi_{in}p_i(t)$$ **Eqn. 3.10**

The above equation shows that the nth mode is not excited if the ith point or the location of the input is a node point, such that $\phi_{in} = 0$ (McConnell, 2001). During the modal test of a bridge structure, the location of the input excitation must be selected away from the vibration nodes of the desired mode shapes.

Methods for solving the 2nd order ordinary differential equation (ODE) given by equation 3.10 include the use of a Fourier transform to convert the equation from the time domain to the frequency domain and solving for the frequency response function. Other methods are available in standard mathematical texts such as in reference (Grossman, 2001).

One method of solving the 2nd order ODE is by the use of phasors (McConnell, 2001). Phasors provide a convenient methodology for solving time-harmonic problems in steady state without having to solve directly a differential equation. Using phasors equates time dependent terms to an exponential representation, which converts an ODE in the time domain to an algebraic equation in the frequency domain. As part of the solution process, $p_i(t)$ and $q_n(t)$ are assumed to be phasors expressed as the following exponentials,

$$p_i(t) = p_i e^{j\omega t} \textbf{ and } q_n(t) = \overline{B}_n e^{j\omega t}$$ **Eqn. 3.11**

where ω is the frequency of the excitation; $j = \sqrt{-1}$; $\overline{B}_n$ is a complex quantity containing both magnitude and phase information. Substitution of equation 3.11 into equation 3.10 results in a standard single degree of freedom, forced vibration response of

$$\bar{B}_n = \frac{\phi_{in} p_i}{K_{nn} - M_{nn}\omega^2 + jC_{nn}\omega}$$

Eqn. 3.12

The modal model for displacement at a location p is acquired by substituting equation 3.12 into equation 3.11 and subsequently substituting equation 3.11 into equation 3.8, resulting in the following,

$$u_p(t) = \sum_{n=1}^{N}\left[\frac{\phi_{pn}\phi_{in}}{K_{nn} - M_{nn}\omega^2 + jC_{nn}\omega}\right]p_i e^{j\omega t} = H_{pi}(\omega)p_i e^{j\omega t}$$

Eqn. 3.13

where $H_{pi}(\omega)$ is the receptance frequency response function (FRF) defined below,

$$H_{pi}(\omega) = \sum_{n=1}^{N}\left[\frac{\phi_{pn}\phi_{in}}{K_{nn} - M_{nn}\omega^2 + jC_{nn}\omega}\right] = \frac{U_p(\omega)}{p_i(\omega)}$$

Eqn. 3.14

where $U_p(\omega)$ is the frequency spectrum of the response $u_p(t)$ at location p and $p_i(\omega)$ is the frequency spectrum of the input time history $p_i(t)$. $H_{pi}(\omega)$ is the response a location p due to a unit excitation at the ith location which has frequency ω. If p and i are different, $H_{pi}(\omega)$ is a transfer receptance. When $p = i$, $H_{pp}(\omega)$ is a driving-point receptance. From equation 3.14, it is observed that the receptance FRF contains information regarding natural frequencies, modal damping, and mode shape.

Although the receptance FRF is convenient for displacement measurements, experimental modal analysis procedures typically measure velocity or acceleration. Therefore, if the response velocity is selected as the output quantity, the corresponding frequency domain FRF is called mobility, $Y_{pi}(\omega)$. The mobility, $Y_{pi}(\omega)$ relates the output velocity frequency spectrum, $V_p(\omega)$ for location p due to an input force frequency spectrum $p_i(\omega)$ at location i. The mobility is related to the receptance FRF by,

$$Y_{pi}(\omega) = j\omega H_{pi}(\omega) = \frac{V_p(\omega)}{p_i(\omega)}$$

Eqn. 3.15

Similarly, if the ouput quantity is the response acceleration, the corresponding FRF is called accelerance or inertance. The accelerance, $A_{pi}(\omega)$, relates the output acceleration frequency response $a_p(\omega)$ at location p to input excitation frequency spectrum $p_i(\omega)$ at location i. The accelerance is related to the mobility and the receptance by,

$$A_{pi}(\omega) = j\omega Y_{pi}(\omega) = -\omega^2 H_{pi}(\omega) = \frac{a_p(\omega)}{p_i(\omega)}$$

Eqn. 3.16

3.2.3.2   Random Vibrations

Background. Acquisition of FRFs from random vibrations to a structure requires additional formulations and parameters as opposed to a single source excitation because the excitation and response are both characterized by random processes. As part of the approach to analyze random vibrations and responses, two sets of parameters are

introduced and defined to describe random signals. The first set of parameters is classified as correlation functions, which are defined in the time domain. The second set is spectral densities, which are in the frequency domain.

Consider a typical random vibration parameter, *f(t)*, shown in Figure 3.1(a), which is assumed ergodic. An ergodic function is a type of random process, which requires a single sample to portray all the statistical properties required for its definition. The autocorrelation function, $R_{ff}(\tau)$, which is a type of correlation function, is introduced and defined as the expected or average value of the product $[f(t) \cdot f(t+\tau)]$, evaluated in the time domain. The autocorrelation function is a real and even function of time and is denoted as,

$$R_{ff}(\tau) = E\big[f(t) \cdot f(t+\tau)\big]$$ **Eqn. 3.17**

The autocorrelation function takes the form shown in Figure 3.1(b), and is used to transform the original random signal such that the requirements for evaluation via a Fourier Transform[1] is possible. The result of the Fourier transform of the autocorrelation function results in the auto- or power spectral density (PSD), $S_{ff}(\omega)$, which is a type of spectral density and is given as,

$$S_{ff}(\omega) = \tfrac{1}{2\pi} \int\limits_{-\infty}^{\infty} R_{ff}(\tau) e^{-i\omega t} d\tau$$ **Eqn. 3.18**

The auto-spectral density is a real and even function of frequency, and provides a description of the frequency function of the random signal, *f(t)*. An example plot is included in Figure 3.1(c).

| (a) Time History | (b) Autocorrelation Funciton | (c) Auto or Power Spectral Density |
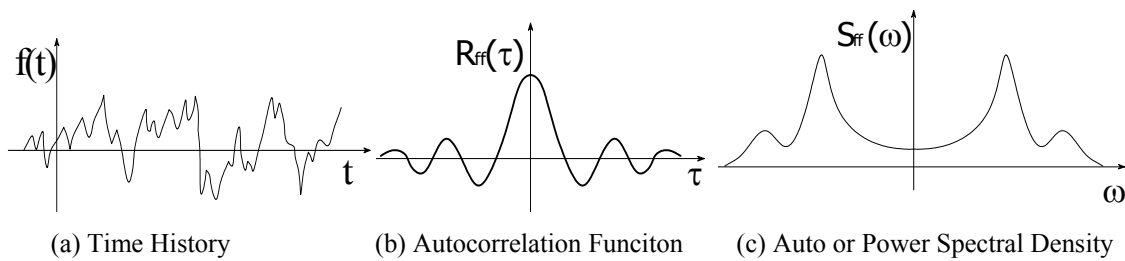
Figure 3.1. Random Signals (Ewins, 2000)

Similarly, an additional pair of correlation and spectral density functions are developed for a pair of random vibration parameters, *f(t)* and *x(t)*, to produce the cross correlation and cross spectral density functions. The cross correlation function, $R_{xf}(\tau)$, is defined as,

---

[1] The Fourier Transform decomposes or separates a waveform or function into sinusoids of different frequency which sum to the original waveform, i.e. conversion of a function from the time domain to the frequency domain. The Fourier transform of a function, *f(t)*, is given by $F(\omega) = \tfrac{1}{2\pi} \int\limits_{-\infty}^{\infty} f(t) \exp(-i\omega t) dt$.

$$R_{xf}(\tau) = E\big[x(t) \cdot f(t + \tau)\big] \qquad\qquad \textbf{Eqn. 3.19}$$

Fourier transform of the cross correlation function results in the cross spectral density (CSD),

$$S_{xf}(\omega) = \tfrac{1}{2\pi} \int\limits_{-\infty}^{\infty} R_{xf}(\tau) e^{-i\omega t} d\tau \qquad\qquad \textbf{Eqn. 3.20}$$

Cross correlation functions are real, but not always even, functions of time; while, cross spectral densities, unlike their counterpart of auto spectral densities, are usually complex functions of frequency with the following particular conjugate property,

$$S_{xf}(\omega) = S_{fx}^{*}(\omega) \qquad\qquad \textbf{Eqn. 3.21}$$

With an understanding of the correlation functions and spectral densities involved in analyzing random vibrations, the input-output relationships for systems undergoing random vibrations become the primary focus. The general mathematical process for FRF development is provided without algebraic detail for purposes of explanation in the following paragraphs.

FRF Development. Given that a force *p(t)* varying arbitrarily with time can be represented by a sequence of infinitesimally short impulses, the response of a linear dynamic system to a single impulse at time t' and magnitude $p(t')$ is provided as the following unit impulse response function (Chopra, 1995),

$$du(t) = [p(t')dt']h(t - t') \qquad\qquad \textbf{Eqn. 3.22}$$

where *du(t)* denotes the differential displacement response of the system in the time domain, *t*, and $p(t')$ is the magnitude of the impulse at time t'; $h(t - t')$ is the unit impulse response function. Subsequently the response of the system at time *t* is the sum of the responses to all impulses up to that time.

$$u(t) = \int\limits_{-\infty}^{\infty} h(t - t') p(t') dt' \qquad\qquad \textbf{Eqn. 3.23}$$

Using the above property, known as the convolution integral, an expression for the response at time *t*, *u(t)*, and the response at time $t + \tau$ is derived. Subsequently the response autocorrelation function, $R_{uu}(\tau)$ is given as,

$$R_{uu}(\tau) = E\big[u(t) \cdot u(t + \tau)\big] \qquad\qquad \textbf{Eqn. 3.24}$$

Manipulation of the above expression can result in a description of the response autocorrelation in terms of the corresponding property of the excitation, $R_{pp}(\tau)$; however the result is complicated and an unusable triple integral. Nonetheless, equation 3.24 can be transformed to the frequency domain, which results in the following convenient form,

$$S_{uu}(\omega) = \big|H(\omega)\big|^{2} S_{pp}(\omega) \qquad\qquad \textbf{Eqn. 3.25}$$

where S_{uu} is the response PSD; S_{pp} is the excitation PSD; $H(\omega)$ is the receptance FRF. Although it appears well-suited for FRF determination, the above equation does not

provide a full description of the random vibration conditions, nor could it be used to determine the FRF from measurements of excitation and response since phase information is omitted from the formulation. Therefore, a second equation, the cross correlation between the excitation and the response, is required and presented in the frequency domain form,

$$S_{pu}(\omega) = H(\omega) S_{pp}(\omega) \text{ or } S_{uu}(\omega) = H(\omega) S_{up}(\omega)$$

Eqn. 3.26

The analysis performed in this section is limited to a single excitation parameter; however, several responses can be considered by repeated application of equations 3.25 and 3.26. The analysis can be extended to a situation where several excitations are applied simultaneously, regardless of their correlation with each other. This level of analysis requires the autospectra of the individual excitations, but also the cross spectra which connect one with the others, resulting in a matrix formulation as follows,

$$[\mathbf{S}_{pu}(\omega)] = [\mathbf{H}(\omega)][\mathbf{S}_{pp}(\omega)]$$

Eqn. 3.27

here, the brackets denote matrices.

Equation 3.26 provides the basis for a method of determining a systems' FRF properties from a random vibration or ambient excitation test. A convenient formula for determining the FRF is available from estimates of the relevant spectral densities,

$$H(\omega) = \frac{S_{pu}(\omega)}{S_{pp}(\omega)}, \text{ usually identified as } H_1(\omega), \text{ or}$$

Eqn. 3.28

$$H(\omega) = \frac{S_{uu}(\omega)}{S_{up}(\omega)}, \text{ usually identified as } H_2(\omega)$$

Eqn. 3.29

The three equations, equations 3.25, 3.28, and 3.29 present a means to check the quality of calculations made using measured data.

3.3   Methods of Excitation

3.3.1   *Input-Output Methods*

The input-output method for a bridge typically involves introducing an impulse or displacement release procedure and subsequently measuring the free vibration response of the structure (Farrar and Sohn, 2001). In the following section, forced excitation methods applicable to bridge structures are examined with an emphasis on their advantages and disadvantages. In general, input-output excitation techniques are advantageous as compared to output-only methods, since they are able to suppress the effects of extraneous noise in the measured structural response (Salawu and Williams, 1995).

3.3.1.1   Impact Hammer and Drop Weight Impactor

An impact excitation requires a contact between the bridge and mass, which provides a forced-pulse excitation of the bridge (Green, 1995). The impulse hammer is usually built-up with an impactor and various tips, which help to control the frequency and force

range of the impulse (Green, 1995), see Figure 3.2. The use of the impact hammer is advantageous because of its portability and ease of operation; however, it is difficult to achieve consistent input because of the manual nature of the impact, specifically it's variability in force due to height and inconsistency of the contact point during impact.
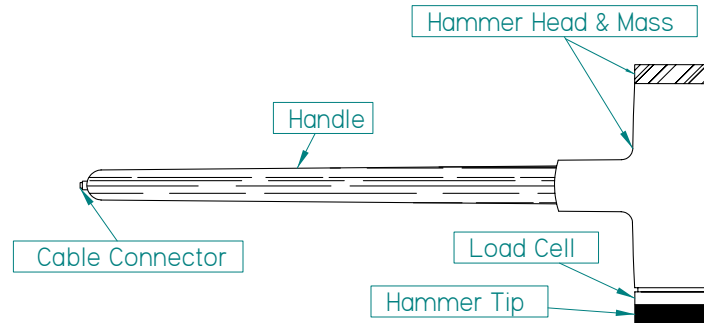
Figure 3.2. Impact Hammer

As a resolution for the inconsistencies of the input, some researchers (Farrar and Sohn, 2001; Bolton, et al., 2001b; Green 1995) implement a drop weight impactor. The drop weight device involves the use of weights, a damper, a load cell, and soft interface between the bridge and load cell, see Figure 3.3. The drop weight system uses a pulley system to raise and release the load repeatedly from the same height, thus providing a consistent excitation into the structure for accurate measurements from impact to impact. The variation of the impulse into the structure is controlled by altering the mass of the impact device and/or by changing the height of the release point for a drop weight impactor. Although impact excitation by hammer and/or drop weight is a convenient and efficient means for vibration testing of a bridge, the testing method is susceptible to input noise because of the short duration of the pulse compared to the length of recording time (Salawu and Williams, 1995).

(a) Impactor Frame   (b) Impactor Contact-point
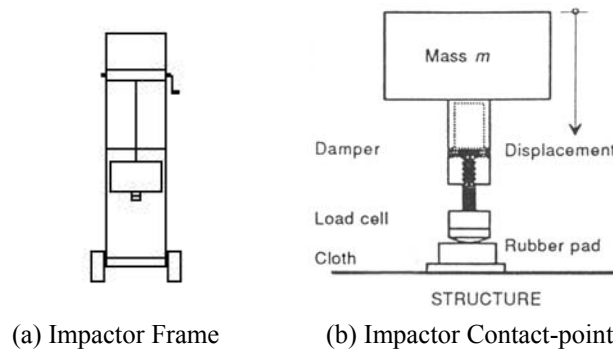
Figure 3.3. Drop Weight Impactor (Salawu and Williams, 1995)

Previously, limitations on the forced impulse excitation method are its restriction to shorter span bridges because of the potential for local damage at the point of contact, which may occur when large force levels are applied (Salawu and Williams, 1995). Green suggests limiting impact hammers to bridges with spans less than 30 meters, since greater masses are required for longer spans and the portability of the impact device becomes compromised (Green, 1995). However, Bolton, et al. have successfully

implemented a modal test procedure to examine changes in modal properties of a concrete box girder bridge with spans greater than 30 meters (Bolton, et al., 2001b).

3.3.1.2 Shaker

Another method of forced vibration testing of a bridge is through the use of shakers or vibrators, which generally stay in contact with the bridge through the testing period. Shakers are often composed of eccentric rotating masses or are electrohydraulic and are used for broadband testing, where the structure is excited with a signal containing energy over a wide range of frequencies simultaneously (Maia and Silva, 1997). Shakers are versatile in the range of forces input into the structure as well as in the type of excitation. The maximum forces can range from 5 kN to 90 kN with sinusoidal excitation, sine sweep excitation, or random excitation over the frequency range of interest (Green, 1995). The most effective excitation method with a shaker for the acquisition of modal properties is the transient type, which includes sine sweep, random burst, and triggered random excitations (Reynolds and Pavic, 2000). Once the impulse is introduced to the structures, the free vibration response is measured and modal properties are extracted.

The eccentric rotating mass shaker is a reaction type mechanical vibration machine, which generates a vibration force by using a rotating shaft carrying a mass whose center of gravity is displaced from the center of rotation of the shaft (Salawu and Williams, 1995). A constant force is applied to the structure for a given mass, rotating mass and out of balance displacement. The shaker can have more than one rotating mass, as shown in Figure 3.4, that gives the particular advantage of generating forces in more than one direction.
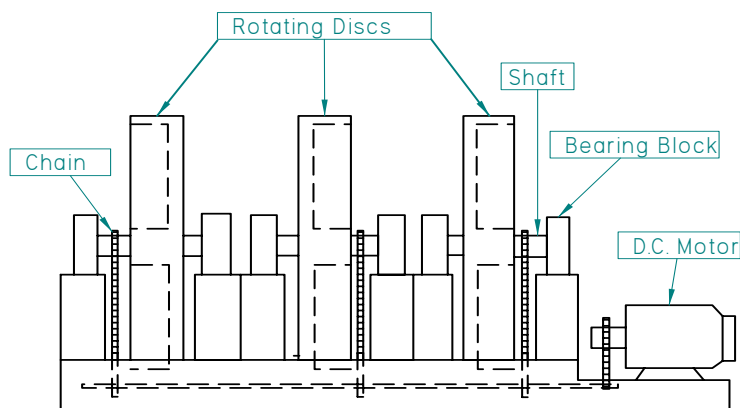
Figure 3.4. Eccentric Rotating Mass Shaker

The electrohydraulic vibrator generates forces through the countering motion induced by the high-pressure flow of liquid. The electrohydraulic shaker is built-up of a servo-controlled hydraulic actuator, which controls the motion of an attached mass. The weight of the mass can be varied to control the different levels of excitation into the structure. The electrohydraulic shakers offer the advantage of being able to excite higher modes of the structure, as well as excite the structure in bending or torsion (Salawu and Williams, 1995). Other benefits include the capability of introducing a static preload and complex waveforms to the bridge (Salawu and Williams, 1995).

Figure 3.5. Electrohydraulic Shaker[2]

Although shakers are advantageous in the types and variability of the excitation to the test bridge, disadvantages often outweigh the capabilities they present. In particular, the shaker device is often large and requires a significant amount of labor and equipment to set up and place. In addition to its being cumbersome, the devices are expensive in relation to testing with impact hammers or drop weights. Electrodynamic shakers have difficulty producing lower frequency excitation and are limited in the force levels that can be generated while servo hydraulic shakers can provide higher force levels, but have difficulties producing excitations at frequencies above 100 Hz (Farrar, et al., 1999).

3.3.1.3   Displacement-Release

The displacement-release method of excitation for modal testing requires imposing an initial, static displacement on the bridge structure by means of a cable or a large mass. The structure is released and undergoes free-vibration. This step-release is a simple form of excitation; however, the method is disadvantageous because of the safety issues associated with using large masses (Green, 1995; Salawu and Williams, 1995). Typically the response of the structure to a displacement-release excitation is governed by modes, which most closely resemble the initially deformed shape of the structure, possibly limiting the range of available modes for extraction (Salawu and Williams, 1995).
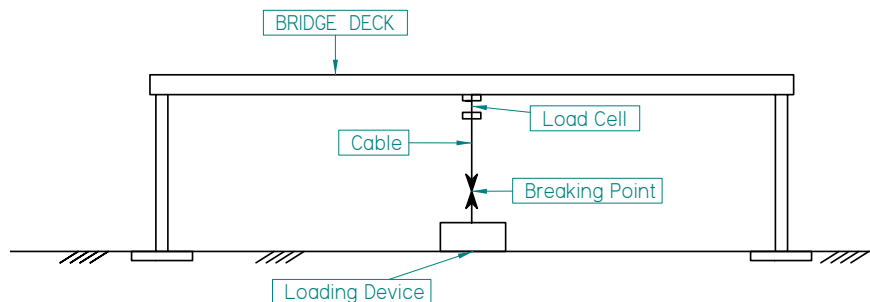
Figure 3.6. Displacement-Release of Structure (Salawu and Williams, 1995)

3.3.2   Output-Only Excitation

Ambient excitation or Output-only methods measure the response of the structure under its normal operating conditions. As compared to input-output excitation techniques, the measurement of the structural response is performed while the structure is in service (i.e., no lane closures are needed), is cost effective (essentially no cost for the excitation

---

[2] Photo available at www.hotektech.com courtesy of Hotek Technologies, Tacoma Washington.

source), and is available for the continuous monitoring of the bridge structure (Farrar and Sohn, 2001; Green, 1995; Salawu and Williams, 1995). In addition, ambient vibration testing is also applicable to long span bridges, where locations of bridge structures such as the center traffic lane or locations over water may be inaccessible for input-output excitation methods.

Sources for ambient vibration methods include vehicular traffic, wind, pedestrian traffic, ocean waves, and low seismic activity (Farrar and Sohn, 2001; Farrar et al., 1999; Green, 1995; Salawu and Williams, 1995). Several assumptions for ambient excitation test methods are necessary since the input is unknown. First, the excitation forces are assumed to be a stationary random process, having a flat frequency spectrum, thus implying that the vibration response of the bridge contains all the normal modes (Salawu and Williams, 1995). Furthermore, this eliminates concern that input-output excitation methods may have with input noise. Second, the output-only excitation methods assume that the recorded response of the structure alone is sufficient for extraction of modal parameters. While the method is certainly cost effective and implemented without disruption of traffic, ambient excitations are of unknown amplitude and often are unable to achieve high frequency excitations. Nevertheless, the development and maturation of acquisition systems and modal extraction techniques have helped to mitigate the disadvantages associated with ambient vibration techniques (Farrar and Sohn, 2001).

3.3.3 *Comparison of Excitation Techniques*

An issue with ambient vibration test methods is the ability to extract modal parameters from the response data and still attain adequate correlation to force excitation modal test methods. Farrar and James, perform a systems identification comparison on a bridge examining results from ambient excitation measurements and forced vibration testing using a hydraulic shaker (Farrar and James, 1997). The results of the ambient and forced vibration tests showed good correlation with resonant frequencies measured from the forced vibration tests found to be 1.44% to 4.37% higher in forced vibration test results; the higher frequencies from the forced vibration tests were attributed to the reduced mass of the system that resulted when bridge traffic was closed during the forced vibration tests.

A study by Bolton, et al. compares the modal parameters extracted from single-input multiple output (SIMO), using a drop weight impactor, and output-only (vehicular traffic) excitation techniques for a reinforced concrete highway bridge (Bolton, et al., 2001a). The forced excitation and ambient modal tests are conducted on a reinforced-concrete, two span bridge for purposes of comparing excitation techniques and two methods for extraction of modal properties, the first utilizing frequency domain transmissibility functions between a reference acceleration and other response accelerations. The transmissibility function is the ratio of the cross-spectrum density and the auto spectrum density. The second method, the Ibrahim time domain (ITD) technique, is a methodology for extracting modal parameters directly from decaying time or impulse response functions. The authors found good correlation between the forced and output-only testing techniques for the natural frequencies and mode shapes extracted from each test method. The following table shows a comparison of modal frequency results from the respective tests.

Table 3-1. Comparison of Modal Frequencies (Bolton, et al. 2001a)

Extraction Method	Mode				
	1 (Hz)	2 (Hz)	3 (Hz)	4 (Hz)	5 (Hz)
SIMO	10.06	12.75	14.63	16.53	21.06
Transmissibility	10.06	12.75	14.63	16.50	21.06
ITD	10.04	12.63	14.27	16.95	21.12

If the excitation techniques for the input-output and output-only test methods are shown to have good correlation, selection of the excitation method is determined based on the conditions available at the bridge and most suitable configuration for data acquisition. The following tables provide summaries of the advantages and disadvantages of the different excitation techniques available for use on the bridge structures. No single technique is superior to the others; rather it is at the discretion of the tester to select the method of excitation most suitable for the conditions in the field.

Table 3-2. Input-Output Techniques

Input-Output	Advantage	Disadvantage
Impact Hammer	▪ Cost Effective ▪ Portable ▪ Easy Operation	▪ Poor signal to noise ratio ▪ High sensitivity to nonlinearities ▪ Lack of control over frequency content
Drop Weight Impactor	▪ Mass normalized mode shapes ▪ Cost Effective ▪ Low (< 1 Hz) frequency modes with up to 20 Hz modes observed in field ▪ Can control amplitude of input	▪ Not viable for continuous monitoring ▪ Susceptible to input noise
Shaker	▪ Mass normalized mode shapes ▪ Capable of higher frequency excitations (1.5 to 100 Hz) ▪ Can apply a static preload to test structure	▪ Expensive ▪ Difficult to excite frequencies below 1 Hz ▪ Heavy weight makes it difficult to install and move
Displacement-Release	▪ Simple and effective in determining damping	▪ Response dominated by modes most resembling the deformed shape ▪ Difficult to implement ▪ Safety hazard in releasing large masses and potential damage

Table 3-3. Output-Only Techniques

Output-Only	*Advantage*	*Disadvantage*
Ambient Exicitation	• Capable of continuous monitoring • Cost-effective, excitation source is essentially free • Applicable for long span bridges	▪ Difficult to extract damping properties ▪ Uncontrolled amplitude input into the structure ▪ Limited to low frequency excitation (<1 Hz) ▪ Difficult to excite the lateral modes of a bridge, which are of interest for seismic studies

3.4 Modal Testing Procedure

Modal testing on a bridge presents unique challenges, since the testing procedure is implemented outside of a controlled laboratory environment. However, regardless of the location or obstacles existing during the test period, the goal of modal testing is to acquire sets of vibration data in the form of time histories that serve the purpose of analysis and extraction of the properties of the structure for all required modes of the bridge (Maia and Silva, 1997). The modal testing methodology includes discussion of the transducers and their placement. With the acquired time-history data, the ability to identify and separate the different modes of the structure is critical in determining the modal properties of the structure.

3.4.1 Transducers

A numerous variety of transducers are available for modal testing on a bridge structure. The response of the structure can be defined by displacement, velocity, or acceleration. The most commonly used transducer types implemented for modal testing of bridges are accelerometers, velocity, and displacement transducers. Selection of the transducer type is determined such that the mass of the transducer does not interfere with the response of the structure (Maia and Silva 1997) and the transducer provides the type of data required for structural assessment. Typically for large civil structures such as bridges, the mass of the transducer is not a concern but rather care should be used to determine the transducer does not distort the response of the structure. Transducers are desired such that the acceleration, velocity, or displacement response of the structure is measured directly for convenient use in modal parameter extraction. The following section provides an overview of sensors, which are applicable for the measurement of structural response during dynamic testing of bridge structures.

3.4.1.1 Accelerometer

Accelerometers are the most common and applicable of transducers for use during modal testing of bridge structures, since they are capable of operation over a wide range of frequencies and are easy to install (Green, 1995). There are several different types of accelerometers available for modal testing of bridge structures. Accelerometers capable of measurements of +/- 5g are available for modal testing of bridge structures and

sufficiently adequate, since the maximum accelerations observed during a modal test of a reinforced concrete bridge structure is typically 0.5g (Green, 1995).

Piezoelectric Accelerometer. The piezoelectric accelerometer is built-up of a base and case, a center post, an annular section of piezoelectric ceramic, and an annular seismic mass element, see Figure 3.7 (Maia and Silva, 1997). The base of the accelerometer is attached to the structure such that the seismic mass within the accelerometer undergoes the equivalent motion of the structure during excitation. The excitation force travels through the piezoelectric crystal, which deforms due to the excitation force. There is a change produced in the crystal proportional to the deformation that is directly related to the acceleration of the seismic mass and ultimately the response of the structure.
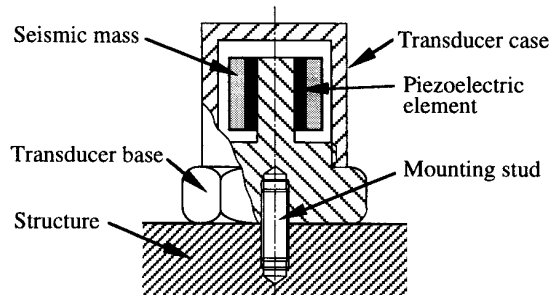
Figure 3.7. Piezoelectric Accelerometer

Piezoresistive and Capacitance Accelerometers. Other types of accelerometers available for use on bridges are piezoresistive and capacitance accelerometers. In the piezoresistive accelerometer, semiconductor flexure elements supporting a seismic mass form part of an active wheatstone bridge (Maia and Silva, 1997). As the structure displaces due to the excitation force, the wheatstone bridge becomes unbalanced and the differential output (proportional to the applied strain) relates to the measure of acceleration. Figure 3.8 displays a lay-out example of a piezoresistive accelerometer.
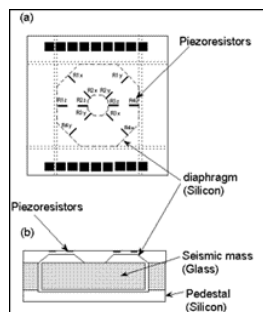
Figure 3.8. Piezoresistive Accelerometers[3]

---

[3] Figure available at www.sensorsmag.com, courtesy of Fujikura Ltd., Tokyo, Japan

Similarly, in a capacitive-type accelerometer, the measuring elements form a capacitive half-bridge versus the wheatstone bridge in the piezoresistive accelerometer. When the structure moves as a result of the excitation, the capacitive bridge becomes unbalanced, thus being able to measure the differential output relating directly to the acceleration response on the bridge. An example of a capacitance accelerometer is shown below,

Figure 3.9. Capacitance Accelerometer[4]

3.4.1.2   Velocity Transducer

A velocity transducer is built of a laser velocimeter, which is an optical system that measures the instantaneous velocity of a point (or points) on the structure. The basic laser Doppler velocimeter (LDV) operates by measuring the velocity of a point addressed by a focused laser beam using the Doppler shift between the incident light and scattered light returning to the measuring point (Stanbridge and Ewins, 1999) using an interferometer.   One advantage associated with the velocity transducer is that the transducer is a non-contact device, which is capable of measuring response of the bridge at locations that are difficult to access by the use of mirrors. However, the disadvantages associated with cost of the laser and signal processing equipment as well as time required for set-up configuration outweigh the advantages for field modal testing of bridges. A natural extension of the LDV is the scanning laser Doppler velocimeter, which incorporates a dynamic feature in the location mechanism, such that the laser beam moves from one measurement site to the next (Ewins, 2000). Ideally, the faster the scanning takes place, the shorter the measurement time. However, the speed is limited by the physical limitations inside the transducer, such as the inertia of the mirrors, which must be moved in order to bring about the desired change of direction of the beam (Ewins, 2000).

The velocity transducer is a developing technology for the response measurement of bridge structures. However, in its current state, use of a laser Doppler velocimeter for a modal test performed in the field introduces complexities in the set-up and increases cost in measuring several locations for response.

3.4.1.3   Displacement Transducer

The third type of transducer is the displacement transducer. Displacement transducers are a justifiable alternative to using accelerometers for the global response measurement

---

[4] Figure available at www.sensorsmag.com courtesy of Kistler Instruments Corporation, Amherst, NY.

of the bridge during a modal test. Unfortunately, displacement transducers require an inertial platform, which is typically unavailable or difficult to install in the field. The potentiometer is the simplest form of a displacement transducer, but is limited to low frequency vibrations and large displacement applications. An example of a potentiometer is provided in the following figure.

Figure 3.10. Potentiometer[5]

Another type of displacement transducer is the linear variable differential transformer (LVDT). The LVDT contains a free moving magnetic core connecting the magnetic flux between a surrounding primary coil and two secondary coils. When the magnetic coil moves away from its central position, the voltage in one of the secondary coils increases while the other decreases. This results in a linearly varying differential voltage output, which is utilized to determine the response of the structure. An LVDT requires the use of a push-rod in order to decouple the lateral motion and connection to the structure. Although, LVDTs may be applicable on large civil structures, its convenience is questionable because of the calibration required for each transducer location. Alternatively, laser optical range sensors are available for measuring large displacements; however, just as in the case of velocity transducers, the cost of equipment and coordination of a configuration for the measuring technique makes it an unfeasible opti0on for modal testing of bridge structures.

Figure 3.11. Linear Variable Displacement Transducer[6]

---

[5] Figure available at www.omega.com courtesy of Omega Engineering,Inc.
[6] Figure available at www.omega.com, courtesy of Omega Engineering,Inc.

3.4.2 Sensor Placement

The determination of sensor location and quantity has often been dependent on engineering judgment and experience without any formal relationships developed between the desired mode shapes and the sensor placement. A number of researchers have investigated the optimal placement of sensors for large flexible structures for the aerospace industry (Heo, et al. 1997); however, few methodologies have been proven for nondestructive evaluation and health monitoring of bridge structures, nor have the economic ramifications of using an alternative quantity and location of sensors been thoroughly investigate (Stubbs and Park, 1996). . In the following section two techniques for optimal sensor placement for modal testing of bridge structures are examined.

Sensor, or transducer, location and placement during modal testing of a bridge are a function of the cost and number of mode shapes to be acquired. Optimization of the number and placement of sensors provides a cost savings in terms of time reduction for the test set-up, data acquisition, modal analysis, and interruption of traffic (Stubbs and Park, 1996). The objective of placing sensors in multiple locations is to attain a sufficient amount of frequency response functions such that individual modes are identified from the modal test (Green, 1995). For bridge systems, the allocation of sensors for sufficient resolution of the vibration properties is a critical aspect of the modal test strategy due to the large size and restrictions on accessibility to locations of the bridge structure. Furthermore, the experimental setup time and time for data analysis increase as the number of sensors increase; consequently, the time needed to divert traffic from the bridge area increase as well as the number of FRF's required and the duration of the total test procedure (Stubbs and Park, 1996).

3.4.2.1 Sensor Optimization by Shannon's Sampling Theorem

Shannon's sampling theorem states that a signal is correctly represented by a set of samples that are assigned at with a certain periodicity, T, if it is possible to reconstruct the original signal in the time domain (Stubbs and Park, 1996). The primary concept here is that all the information contained in the original signal is also contained in sample values that are taken at equally spaced intervals. According to Shannon's sampling theorem, if a signal does not contain a component with frequency greater than or equal to f_{max}, the signal is completely determined by the set of its values at regularly spaced intervals of values of T.

$$T = \frac{1}{2 \cdot f_{max}}$$

<div align="right">**Eqn. 3.30**</div>

where the sampling rate must satisfy the inequality $f_s > 2f_{max}$ where $f_s = \frac{1}{T}$ and the minimum of this sampling rate is referred to as the Nyquist sampling rate. By extending Shannon's Sampling Method into the spatial domain from the time domain and applying the Nyquist sampling rate, Stubbs and Park develop the following rules for optimal placement of sensors (Stubbs and Park, 1996):

1. Select the highest mode to be measured.
2. Estimate $\frac{\lambda_{WL}}{2}$ for that mode, here λ_{WL} is the wavelength of the mode.

3. Place a sensor at each node of the mode.

4. Place two additional sensors within the $\frac{\lambda_{WL}}{2}$ span, with each sensor being $\frac{\lambda_{WL}}{6}$ spacing form each node.

The rules for sensor placement are applied in both the longitudinal and transverse directions of the bridge (i.e., determine the highest desired mode in the transverse direction, and follow the developed rules, repeating the method in the longitudinal direction).

3.4.2.2   Kinetic Energy Optimization Technique (EOT)

Heo, et al. derive a technique for optimal transducer placement for health monitoring of a bridge structure by maximization of the modal kinetic energy. The energy optimization technique described by Heo, et al. is a modification of Kammer's effective independence method (EIM) based on the spatial independence concept (Heo et al., 1997), which searches for sensor configurations that maximize the rank of the measured modal matrix $[\Phi_s^T \Phi_s]$, where rank indicates the number of linearly independent rows in a matrix (Strang, 1988).

Here, the principle of the Fisher information matrix, considered an "extended design matrix", is introduced, whose i^{th} row consists of independent variables for the ith data point (Atkinson and Donev, 1992). The components of the inverse Fisher information matrix are proportional to the variances of the least squares estimates of model parameters. Consequently, maximizing the Fisher information matrix minimizes the variances of the model parameters leading to an optimal design. Therefore, the Fisher information matrix (**Q**), as implemented by Heo et al., is maximized such that the covariance matrix (**Co**) between the displacement vector in the modal coordinate (**q**) and the estimated modal displacement $\left(\overline{\mathbf{q}} \right)$ is minimized:

$$Min(\mathbf{Co}) = E\left[\left(\mathbf{q} - \overline{\mathbf{q}} \right) \left(\mathbf{q} - \overline{\mathbf{q}} \right)^T \right] \qquad \textbf{Eqn. 3.31}$$

$$Max(\mathbf{Q}) = Max\left\{ \left[\Phi_s^T \Phi_S \right] \right\} \qquad \textbf{Eqn. 3.32}$$

where E indicates the expected value and $\mathbf{\Phi}_s$ represents a reduced set of the mathematical mode shapes corresponding to the target modes. In an attempt to improve the signal to noise ratio for mode shape identification of bridge structures, Heo, et al. prescribe a modified form of the EI method first by introducing the energy optimization technique (EOT).

The implementation of the procedure requires selection of an initial configuration for the sensors and the distribution of the kinetic energy is described by the definition of modal mass from the measured mode shape vectors, $\mathbf{\Phi}$.

$$\mathbf{KE} = \mathbf{\Phi}^T \mathbf{m} \mathbf{\Phi} \qquad \textbf{Eqn. 3.33}$$

Utilizing the Cholesky decomposition, the system mass matrix, **m**, is placed into upper and lower triangular Cholesky factors, with the kinetic energy now equal to,

$$\mathbf{KE} = \mathbf{\Psi}^T \mathbf{\Psi}$$
Eqn. 3.34

Where $\mathbf{\Psi} = \mathbf{U}\mathbf{\Phi}$ *and* $\mathbf{m} = \mathbf{LU}$. The matrix **L** and **U** denote the lower and upper triangular Cholesky factor. The projections of the mode shapes on the reduced sensor locations are denoted by $\overline{\mathbf{\Phi}}$ and $\overline{\mathbf{\Psi}}$. Likewise, the energy of the reduced sensor configuration is given by,

$$\overline{\mathbf{KE}} = \overline{\mathbf{\Psi}}^T \overline{\mathbf{\Psi}}$$
Eqn. 3.35

The objective of the transducer placement is to find a configuration, which maximizes the measured kinetic energy of the structure. Reduction of the number of sensors ceases when a rank deficiency of the energy matrix occurs. The problem is solved by the following iterative procedure where the eigenvalues, Λ and eigenvectors, ψ of the energy matrix are first extracted by applying the traditional algebraic eigenvalue formulation,

$$\overline{\mathbf{KE}}\psi = \psi\Lambda$$
Eqn. 3.36

Then, fractional contributions of the remaining transducers are assembled into the EOT vector:

$$\mathbf{EOT} = \sum_{i=l...m} \left[\overline{\mathbf{\Psi}}\psi\Lambda^{-\frac{1}{2}} \right]^2$$
Eqn. 3.37

The transducer location with the minimal contribution to the **EOT** vector is removed from the configuration and its contribution to the kinetic energy matrix, $\overline{\mathbf{KE}}$, is also removed. A check for rank deficiency is performed resulting in the following possible outcomes: 1) Removal of the transducer results in a rank deficiency which implies the sensor cannot be removed or 2) No rank deficiency occurs and the transducer location is removed with the process being repeated until reaching the required number of transducers.

Similar with Stubbs and Park's method for optimal transducer placement and location, Heo's method provides information regarding sensor optimization based on the premise that the data generated from the modal test is capable of being processed to evaluate the health of a bridge structure. In terms of health monitoring of structures and conducting modal tests over various intervals of time, questions pertaining to how changes in mode shapes due to accumulated damage affect sensor locations, since the optimal placement and quantity of sensors is based on a model or pre-damage measured modes shapes of the structure. Heo et al. observe that changes in mode shapes shown in bridge modal test data are not significant enough to warrant a re-optimization of sensor locations and quantity (Heo et al., 1997).

3.4.3 *Identification of Dynamic Properties*

The extraction of modal parameters from the FRFs acquired from the modal test data aims to identify, by curve fit, the constants to develop a mathematical model of the test

data. The modal analysis procedure is dependent on the curve-fit technique selected to approximate the test data and determine the coefficients for a theoretical FRF, which correlates with the test data. Many techniques are available, which predominately operate on the response characteristics of the frequency domain (Ewins, 2000).

During the modal testing process, the identification of dynamic properties is usually a self-contained analysis accompanying the data acquisition system; however, even a limited understanding of what modal analysis identification techniques are available assists in determining the type of procedure most appropriate for the extraction process. The following are a set of criteria that ought to be considered when selecting a procedure for the identification of dynamic properties from the acquired frequency response functions from the modal test.

- Experimental modal analysis techniques are divided into two groups: 1) methods applicable for frequency domain and 2) methods applicable for the time domain. Depending on the selected domain for the response of the structure, the appropriate method can be extracted. In addition to division by domain, the algorithms for identification of modal properties can be further divided into the input and output categories.

- For forced excitation techniques, a modal analysis technique, which can analyze several FRFs simultaneously, is appropriate with responses taken at various locations on the bridge, but using one excitation point (Maia and Silva, 1997). These methods are identified as single input multiple output (SIMO) techniques.

- If all the FRFs are to be analyzed simultaneously from various excitation locations and response locations, then a technique capable multi-input multi-output (MIMO) is appropriate.

For bridge structures the most fully developed method for modal testing are input-output techniques utilizing a contact excitation in the form of an impulse load via an impact hammer or drop-weight hammer. However, the application of output-only methods for large scale dynamic testing is particularly attractive, since the methods allow for continuous monitoring of the structure while still in service.

Numerous techniques for extraction of modal parameters for both input-output and output only methods are available. Experimental modal analysis measures, as aforementioned, are applied in the frequency or time domains. One computationally efficient method of modal parameter extraction for output-only vibration testing is the time domain decomposition (TDD) method (Kim, 2002). The TDD method is implemented under the premise that any vector can be spanned by its basis. Similarly, the basis of the output of a linear structural dynamic system consists of its mode shapes. An acceleration time history response of a structure is the multi-output response of a multi degree of freedom system. For a time, t, the acceleration response of the structure is approximated as,

$$\ddot{\vec{y}}(t) \approx \sum_{i=1}^{n} \ddot{\mathbf{c}}_i(t)\vec{\varphi}_i$$

Eqn. 3.38

where n, is the number of modes in the measured acceleration signals; $c_i(k)$, is the ith modal contribution factor at time, k, and $\vec{\varphi}_i$, is the ith mode shape from the measure acceleration response. Each measured time signal contains n modes within the Nyquist

frequency; however, it is difficult to decipher the exact frequency of the mode. Nonetheless, a frequency band for the ith mode is obtainable by visual inspection of power spectral density (PSD) plots for use in digital filter design. Then a digital band pass filter for the measured acceleration time history is designed to isolate each target mode of the structure. The filtered acceleration time history represents a multi-output single degree of freedom system for identification. If N samples are measured the filtered acceleration time history containing the ith mode is described by the following equation,

$$[\mathbf{Y}_i] = \vec{\varphi}_i \ddot{\mathbf{c}}_i^T$$ **Eqn. 3.39**

where, $[\mathbf{Y}_i]$ is a p x N matrix containing filtered acceleration time history information for the ith mode; p is the number of sensor locations, and N is the number of measured sample points at the time of test. Next, a p x p output energy correlation matrix, $[E_i]$, is computed from a multiplication of the filtered time history data and its transpose.

$$[\mathbf{E}_i] = [\mathbf{Y}_i][\mathbf{Y}_i]^T$$ **Eqn. 3.40**

Substituting, equation 3.39 into equation 3.40, results in,

$$[\mathbf{E}_i] = \vec{\varphi}_i \ddot{\mathbf{c}}_i^T \ddot{\mathbf{c}}_i \vec{\varphi}_i^T = \vec{\varphi}_i q_i \vec{\varphi}_i^T$$ **Eqn. 3.41**

The output energy matrix is a real semi-positive symmetric matrix, which can be decomposed into

$$[\mathbf{E}_i] = [\mathbf{U}][\mathbf{\Sigma}][\mathbf{U}]^T$$ **Eqn. 3.42**

where $[\mathbf{U}] = [\vec{\mathbf{u}}_1 ... \vec{\mathbf{u}}_p]$ is the singular vector matrix, containing p orthogonal vectors and $[\mathbf{\Sigma}] = diag[\sigma_1 ... \sigma_p]$ is a diagonal p x p matrix of singular values of $[\mathbf{E}_i]$. In the case of noise free signals, σ_1 is the only nonzero singular value, and the first column of the singular vector matrix is the mode shape. In general, the first column of the singular vector matrix is the ith undamped mode shape of the structure and singular values $\sigma_2 ... \sigma_p$ are small relative to σ_1.

The frequency result is attained via a time history result of the ith modal contribution factor. The ith modal contribution factor is calculated by multiplying both sides of equation 3.39 with the transpose of the ith mode shape.

$$\ddot{\mathbf{c}}_i^T = \frac{1}{\vec{\varphi}_i^T \vec{\varphi}_i} \vec{\varphi}_i [\mathbf{Y}_i]$$ **Eqn. 3.43**

The resulting analogy is a single output, single degree of freedom system representing the ith modal behavior of the structure. Analysis of the autospectrum of the modal contribution factor shows a single peak whose frequency location is the ith modal frequency of the structure.

The TDD technique requires the design of a digital band pass filter, which in turn requires a definition of the frequency band for which to filter the acceleration time history data. Visual inspection of autospectrums of the measured data provides the frequency range, which then allows for computation of mode shapes and frequencies. The primary computational component of the TDD does not require the discrete Fourier transform.

The technique does require the use of a singular value decomposition (SVD), but the number of analyses using a SVD is limited to the number of modes desired in the structure. Thus, for cases where is $n << p$, the method is computationally efficient and is able to extract unbiased mode shapes from closely spaced modes by adjusting the pass band range of a filter.

An example of a frequency domain modal extraction methodology is the frequency domain decomposition method, which is an extension of the classical frequency domain approach, the basic frequency domain (BFD) technique (Brincker, et al. 2000). Implementation of the FDD technique, involves computation of the power spectral density matrix, $\hat{\mathbf{G}}_{yy}(j\omega_i)$. For a lightly damped structure the response spectral density is given by,

$$\hat{\mathbf{G}}_{yy}(j\omega) = \sum_{k \in Sub(\omega)} \frac{d_k \phi_k \phi_k^T}{j\omega - \lambda_k} + \frac{\bar{d}_k \bar{\phi}_k \bar{\phi}_k^T}{j\omega - \bar{\lambda}_k} \qquad \textbf{Eqn. 3.44}$$

where, G_{yy} is the $m \times m$ PSD of the responses, m is the number of responses; λ_k, is the pole, ϕ_k is the mode shape vector, d_k, is a scalar constant, ω, denotes frequency. The complex conjugate of the pole, mode shape and scalar constant are indicated as $\bar{\lambda}_k, \bar{\phi}_k, \bar{d}_k$, respectively; j is the imaginary number.

The power spectral density matrix is then decomposed at every frequency line by SVD into a set of autospectral density functions, each of which represents a single degree of freedom system.

$$\hat{\mathbf{G}}_{yy}(j\omega_i) = \mathbf{U}_i \mathbf{S}_i \mathbf{U}_i^H \qquad \textbf{Eqn. 3.45}$$

The first vector of the singular vector matrix, $\mathbf{U}$, is an estimate of the mode shape near a peak corresponding to a mode in the spectrum plot. The natural frequency is obtained by the piece of the SDOF density function around the peak of the power spectral density (PSD).

Other examples of experimental modal analysis techniques include peak picking of the auto- and cross- powers of the measured response, which selects peaks in the spectra to acquire estimates of the resonance frequencies and subsequently operational deflection shapes are obtained (Hermans and Van der Auweraer, 1999). The natural excitation technique (NExT) essentially involves applying time domain curve-fitting algorithms to cross-correlatiom measurements made between various response measurements on an ambiently excited structure to estimate the resonant frequencies and modal damping (Farrar and James, 1997); the nonlinear least squares curve-fit approach is a general multi-degree-of-freedom curve-fit approach utilizing weight factors at each frequency point of interest and minimizing the curve fit error by differentiation (Ewins, 2000); descriptions of transmissibility functions (Bolton, et al., 2001a) and the Ibrahim Time Domain (ITD) technique (Bolton, et al. 2001a; Huang et al., 1999) were described briefly in section 3.3.3 of this chapter.

3.5 Summary

The identification of modal parameters of a bridge structure is the main objective of the modal test procedure and the first component of a complete nondestructive damage

detection technique for large civil structures. The modal test consists of the following phases, which are necessary for successful identification of modal properties of a bridge structure:

- Understanding of the theoretical basis of modal testing and development of the frequency response functions
- Selection and placement of transducers to be used on the structure for an accurate and sufficient amount of data collection
- Selection of the method of excitation considering location and available accessibility to the bridge
- Identification of dynamic properties by experimental modal analysis

Once the dynamic properties of the bridge structure (i.e., natural frequencies, damping properties and mode shapes) are identified. A system identification procedure and damage detection algorithm is implemented for completion of the nondestructive damage detection technique. It is important to emphasize that modal testing alone is not a nondestructive evaluation method but rather a tool to extract the modal parameters of a bridge structure for use as part of verification of an analysis model as in (Huang et al. 1999; Farrar and James, 1997) or in conjunction with a vibration based damage detection approach as in the damage index method approach developed by Stubbs, et al. (2000) to complete to create a global NDE procedure for bridge structures.

In the upcoming chapter, a review of vibration-based damage detection procedures is conducted. Applying vibration based damage detection methods to vibration data from modal testing completes a global NDE procedure for bridges structures. However, at question is the quality of the damage detection procedure and its applicability to bridge structures and proven application in the field. The purpose of the review of vibration-based damage detection procedures is to select a methodology with proven application to reinforced concrete bridge structures in the field and that demonstrates the potential for application to an approach for estimating the remaining life of a structure.

4   DAMAGE DETECTION METHODS

4.1   Introduction

In the prior section a review of dynamic testing of bridge structures provided insight into the methodology for acquisition of modal properties for a bridge structures. Specifically, the theory, experimental implementation, and modal analysis procedures for dynamic testing of bridge structures was discussed. The important aspect of the dynamic testing procedure was the acquisition of modal properties of a bridge structure. However, the dynamic testing procedure to acquire modal properties provides little value without a means to evaluate the data and provide a quantitative assessment of the structure.

In this chapter, methods for vibration based damage detection are reviewed. The purpose of this review is to evaluate damage detection methodologies to identify, locate and quantify the state of a structure for a given time. Following the review, the advantages and disadvantages of each vibration based damage detection approach is compared in terms of advantages and disadvantages.

4.1.1   Background

Structural health monitoring is a critical application for determining a structure's ability to provide adequate service, evaluating the necessity for maintenance, and assessing the need for repair or replacement of a component or the entire structure. A proficient structural health monitoring system is capable of determining and evaluating the serviceability of the structure, the reliability, and the remaining functionality of the structure in terms of durability (Sikorsky, 1999).   The concept of structural health monitoring is analogous to human health management as described by Aktan et al. (2000), where health management undergoes the sequence of periodic physical examination, preventive intervention, and surgery and recovery.   Similarly, structural health monitoring requires periodic investigation during service/operation, occasional maintenance, and repair-retrofit or replacement as deemed necessary by the inspection. A necessary component in the sequence of structural health monitoring activities is an efficient nondestructive evaluation (NDE) technique, which supplies an adequate amount of information to determine the functionality of the structure for its intended design objective.

The development and implementation of a structural health monitoring system utilizing the vibration characteristics of a structure is the focus of a number of researchers (Sikorsky, 1999; Aktan et al. 2000; Stubbs, et al., 2000; Salawu, 1997a; Park and Reich 1998). Common to each overview and general plan for structural health monitoring and assessment is a requirement for a robust damage detection algorithm, which is capable of identifying, locating and evaluating damage in the structure. In essence, the final goal of a structural health monitoring strategy is to determine the amount of damage a structure is able to tolerate before the damage level reaches a critical stage. Therefore, structural health monitoring is the process of implementing a damage detection strategy (Farrar, 2001) for identification and evaluation of structures.

"Monitoring" implies that an evaluation is performed on a property or aspect of the structural system over a specified duration. A damage detection algorithm for structural

systems identifies alterations of a specific property or aspect of the structure in question. For the effective use of a damage detection algorithm, the definition of damage is an important component, since this is the indicator of the performance of a structure in its current state. Farrar, et al. (1999) provide a general definition for damage as changes introduced into a system that adversely affect its current or future performance. For the purposes of a structural system, the interpretation of damage is limited to changes of the material and/or geometric properties of the structural system, including changes to the boundary conditions and system connectivity (Farrar, et al., 1999).

Vibration-based monitoring of structures is predominant and attractive in the area of structural health monitoring, since each structure possesses a unique vibration structure and the testing procedure allows for an evaluation of a large global structure in a time efficient manner. The motivation behind most vibration based damage detection strategies is the correlation of a structure's dynamic properties (i.e., natural frequencies, mode shapes, and damping properties) with the mechanical properties of a structure. Whereby, damage to a structure causes changes in the structure's stiffness, mass or energy dissipative characteristics and those alterations can be detected in variations of its dynamic properties via modal testing (Farrar, et al., 1999).

4.1.2 *Paradigm for Structural Health Monitoring*

The planning, implementation, and analysis or decision making processes involved in an overall scheme for structural health monitoring are often categorized by researchers into separate divisions to provide a general framework for the structural health monitoring process. A number of paradigms are available generalizing the activities and components of the structural health monitoring strategy. Aktan, et al. (2000) and Farrar, et al. (2001) provide two contemporary approaches to the sequence of structural health monitoring. These paradigms are valuable in providing a perspective on the diversity and breadth involved in structural health monitoring process and are reviewed briefly below.

Aktan et al. (2000) describe critical issues for the execution and acceptance of an effective structural health monitoring technique. Including a discussion of sociological and political issues related to the acceptance of a structural health monitoring strategy, the technical aspects of structural health monitoring are described as three primary components. First, the experimental arts involve experimental methods for structural identification and condition assessment of the structure. Structural identification according to Aktan et al. (1997) is defined as methods for analytically conceptualizing, modeling, designing experiments for measuring, and quantifying behavior as well as the phenomena affecting it, in order to make engineering decisions. Specifically, structural identification is related to procedures for quantifying the parameters of an analytical model given experimental information. These experimental procedures typically involve a modal analysis procedure that satisfies basic assumptions of linearity, observation, and constancy in order to provide direct quantitative information of the structure.

Second, the analytical aspects involved with condition assessment of a structure emphasize the numerical modeling of a structure, typically through a finite element analysis (FEA). According to Aktan, et al. (1998), the numerical modeling of a structure for condition assessment is to use discrete geometric models taking advantage of any heuristic knowledge base as opposed to just numerical or nonparametric models. The

analytical aspects also require the use of experimental data from modal testing so as to calibrate the model. Here the experimental and analytical components are correlated in the systems identification process by information technology such as model calibration, data integration, and parametric studies (Aktan, et al., 2000).

With the implementation of experimental and analytical procedures for system identification, components of the decision-making process are employed so as to establish clearly defined performance criteria in order to evaluate changes in the condition of the system. Condition indicators describe changes in global and local mechanical characteristics of a structure. With the premonition that changes in an index should relate to changes in the state-of-force, distribution of strain energy, and load distribution of the structure to understand the influence on overall system reliability. These condition indices are typically the final measure provided by damage detection methods, which are the primary focus of this report. Figure 4.1, provides a schematic of the generalized monitoring procedure as described by Aktan et al. (2000, 1998, 1997).

EXPERIMENTAL ARTS
Visual Inspection, Measurement
Load Testing
Modal Analysis
Instrumented Monitoring
Local & Material NDE
Direct Condition Indexes

ANALYTICAL ARTS
Visualizing
Conceptualizing
Geometric Modeling
Completeness and Reality Checks
Str-Id based condition indexes

INFORMATION TECHNOLOGY
Bridge Database
Parametric Studies
Model Calibration
Data Integration/Fusion

Heuristics

DECISION-MAKING ARTS
Synthesize Condition and Damage Indexes
Reconcile Visual and Objective Damage Indexes
Reliability Evaluation for Service and Safety
Bridge Management

Figure 4.1. Structural Health Monitoring Schematic (Aktan et al., 2000)

Aktan, et al., similar to the majority of researchers, describe an approach to structural health monitoring utilizing vibration properties of a structure in conjunction with a finite

element model for purposes of system identification and evaluation of damage. Farrar et al., provide a broader description to the implementation of structural health monitoring (1999). Farrar et al. (1999) describe the structural health monitoring strategy in four divisions: (1) operational evaluation, (2) data acquisition and cleansing, (3) feature selection, and (4) statistical model development. Depending on the structural system, its constraints, and desired level of sophistication, selection of methodologies and experimental procedures may vary for implementation of structural health monitoring.

The operational evaluation and data acquisition sections of the program require an understanding of the structure and its anticipated dynamic behavior. Specifically, a definition for damage to the system and understanding of the operational and environmental conditions limiting the data acquisition system are necessary. Subsequently, the operational evaluation customizes the structural health monitoring strategy to accommodate and/or take advantage of any unique characteristics exhibited by the structure. The operational evaluation begins to set limitations on what is monitored and how the monitoring is to take place.

During the data acquisition and cleansing, details and procedures for experimental investigation are planned and performed. Here, consideration is made in regards to the type of sensors, location of sensors, number of sensors, and defining the data acquisition/storage/transmittal hardware. Included in the data acquisition process is the normalization of data in the presence of variability during the operation and environment in order to facilitate the comparison of measured data. Data cleansing is the process of selectively choosing data to accept or reject for the feature selection process.

The feature selection process is the determination and identification of data features, which distinguish between damaged and undamaged structures (Farrar, et al., 2001). Farrar, et al., state that condensation of data is a necessity for structures where long term monitoring is desired with comparisons to several data sets. Selecting a feature of the structure for damage detection is typically application specific and may involve more than one feature, in which case a feature vector is developed to evaluate the structure. Ideally feature vectors are of low order and can be placed in a variety of combinations. For example, a feature vector may contain the first three resonant frequencies of the system, time of measurement, and a temperature reading of the system (Farrar, et al., 2001). Past experience with damaged structures and/or numerical simulation of a damaged systems response is often the basis for feature selection. Common features used in vibration based damage detection are basic modal parameters (natural frequencies and mode shape vectors), mode-shape curvature changes, dynamically measured flexibility, and updating of structural model parameters (mass, stiffness, damping).

Development of a statistical model is the final component of Farrar's monitoring paradigm. A statistical model provides information on whether changes in the features for damage detection are statistically significant (Farrar, et al., 2001). Algorithms for statistical models fall into three categories: (1) Group classification, placing features into 'undamaged' or 'damaged' categories; (2) Analysis of outliers to determine if a significant change from previously observed features occurs; (3) Regression analysis, which is the process of correlating data features with particular types, locations, or extents of damage. Figure 4.2 provides a summary and overview of the overall structural health monitoring strategy by Farrar et al.(2000).
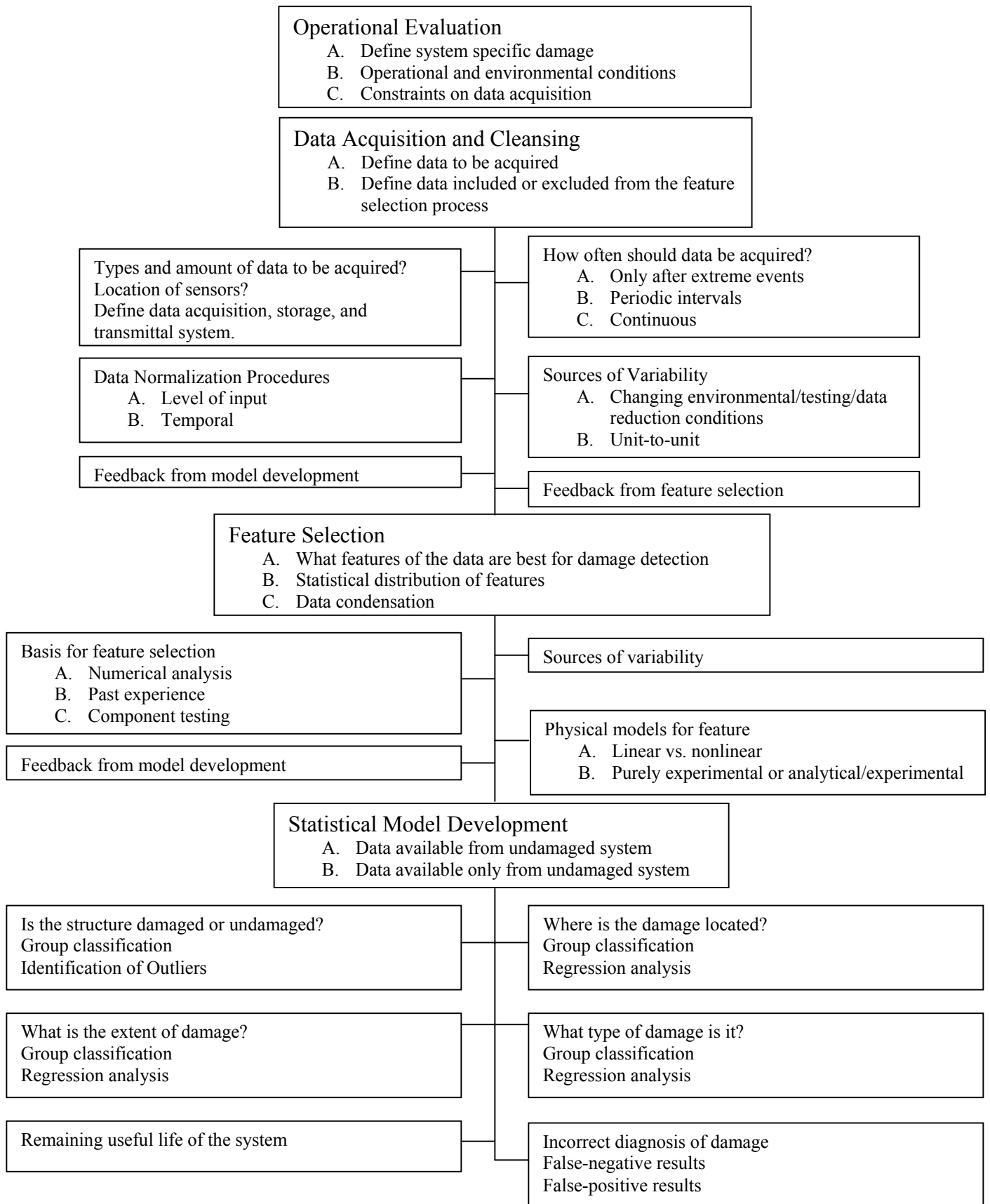
Figure 4.2. Structural Health Monitoring Paradigm (Farrar et al., 2001)

In the two paradigms presented by Farrar et al. (2001) and Aktan et al. (2000), the primary objective of the structural health monitoring process is to acquire sufficient information such that a decision regarding the most effective measure for the structure is determined, i.e. no action, repair, or replacement. The validity of an NDE methodology is predicated on the ability to identify local areas of damage in addition to translate the information to the global performance of the structure. The global performance of the structure can be defined as the residual strength of the structure, the remaining useful life in terms of time, or the probability of failure of the system. Aktan et al. (2000) suggests evaluation of the bridge reliability through the use of condition indicators or damage indices, whereas Farrar et al. (2001) recommends utilizing the damage indicators or features as part of statistical models to identify, locate, quantify and determine the remaining useful life of the structure.

Evaluation of the remaining useful life requires an integrated disciplinary approach in order to understand rates of deterioration of structural components and incorporating this information for a prediction of the performance level of the structure with respect to time. Although the potential exists for a prediction of a structures remaining useful life, the prediction is without merit unless sufficient capability to evaluate the structure in real time and provide a validation of the analytical findings is available. In the following figure a simplified schematic incorporating the experimental evaluation and sequence typical of a vibration based damage detection approach is provided,
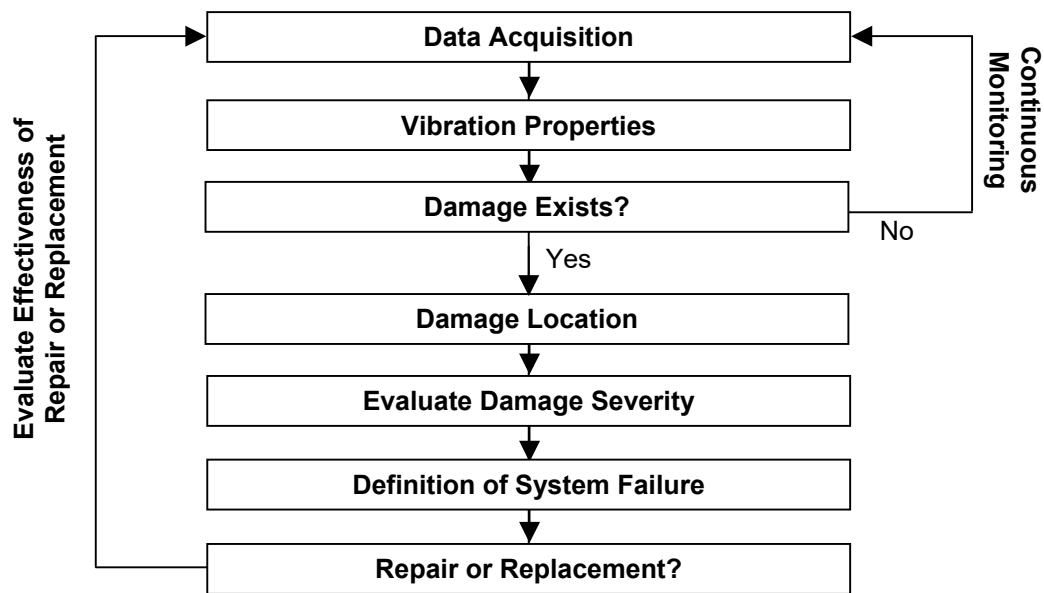
Figure 4.3. Schematic of Vibration-Based Damage Detection

The following review emphasizes damage detection algorithms specifically employing vibration properties of the structures such as accelerations, velocities, displacements, frequency response functions, etc. or derived modal parameters such as frequencies or mode shapes to characterize changes in the structural system, expressly damage.

Vibration properties are attractive for evaluation of large civil structures because of the potential in characterizing localized damaged regions from a single dynamic test of the structure. In accordance with the frameworks previously described for structural health monitoring, this report examines current literature in the area of damage detection or what is referred to by Aktan, et al. (2000) as condition indicators, or by Farrar, et al. (2001) as the feature component of the structural health monitoring paradigm. The categorization of damage detection algorithms is provided in Section 4.1.3, followed by an overview of this report in Section 4.1.4.

4.1.3 Vibration Based Nondestructive Damage Detection

For civil structures, a global NDE technique utilizing the vibration characteristics of a structure proves to be the most effective method because of the size and the impractical nature of using localized nondestructive testing (NDT) methods such as ultrasonics and acoustic emission to examine civil structures (Sikorsky, 1999). Ideally, a localized NDE technique is utilized upon identification of a damage location, so as to determine the specific nature of the damage. The global nondestructive examination technique utilizing vibration properties involves the following features: 1) Modal testing for the acquisition of modal parameters (i.e. natural frequencies, mode shapes, and damping properties) or other features (i.e., time histories, FRF's, etc.) 2) A damage detection algorithm to identify damage in the structure, it's location, and severity, 3) Prediction of system's remaining useful life, and 4) decision rules for evaluating the need for repair and/or replacement. Of particular importance is the damage detection procedure, since the accuracy of the algorithm and its effectiveness establishes the quality of the nondestructive evaluation technique.

The damage detection procedure selected to assess damage on a structural system is vital to the quality of a structural health monitoring system. Any nondestructive damage detection technique can be classified according to the following four categories (Rytter, 1993).

Level 1: Identify that damage has occurred

Level 2: Identify that damage has occurred and determine the location of damage

Level 3: Identify that damage has occurred, locate the damage, and estimate its severity

Level 4: Identify that damage has occurred, locate the damage, estimate its severity, and evaluate the impact of damage on the structure or estimate the remaining useful life of the structure.

With the classification of nondestructive damage detection methods, several challenges exist for the development of a comprehensive solution to damage detection. The general idea of a damage detection algorithm is to utilize the response characteristics of a structure and evaluate the state of the structure; however, damage is typically a local occurrence, which requires higher frequency modes to detect its presence (Farrar and Doebling, 1997). From a testing perspective, the lower frequency modes, which are less sensitive to the local changes, of a civil structure are readily available and easier to access (Farrar and Doebling, 1997). Subsequently, it is difficult to evaluate the reliability of a small portion of a large civil structure, thereby reducing the vibration-based damage

detection problem to some form of pattern recognition problem (Farrar, et al. 2001; Farrar and Doebling, 1997). In addition, the presence of signal noise and incomplete measurements from real applications often result in inaccuracies and poor resolution in the damage detection techniques.

Although not specifically addressed in this chapter, another issue of significance is the unavailability of baseline parameters of a majority of existing structures (i.e. information regarding the initial condition or undamaged state of a structure is not accessible for comparison of pre and post damaged states) (Stubbs, et al., 2000). The absence of an initial measurement becomes significant for existing deteriorating structures, since most damage detection methodologies are dependent on a comparison between the undamaged state and current state of the structure to evaluate changes to a parameter of a structure, i.e. change in stiffness. As a resolution to this problem, Stubbs and Kim provide a system identification approach to determine baseline modal parameters from as-built plans and field inspections of structures in conjunction with existing system identification approaches (Stubbs and Kim, 1996), more detail is provided in section 4.3.2 of this chapter. Often researchers rely on a theoretical finite element model to simulate the undamaged state of the structure. This is acceptable since the theoretical finite element model serves as the basis for design of the new structure. Any changes identified from the damage detection algorithm merely reflect accumulated damage, as well as the loss of capacity due to construction/design errors.

Those damage detection methods displaying the ability to perform according to their intended level of inspection in the presence of the previously mentioned constraints are considered robust and effective. For summary purposes, the oft-identified constraints impeding the damage detection procedure are listed below and arranged with respect to the stage of the structural health monitoring process as described in Section 4.1.2:

Table 4-1. Constraints in Structural Damage Detection

Occurrence	Constraints
Experimental Evaluation / Vibration Testing	• Incomplete measurements • Presence of signal noise
Analysis / Modeling	• Modeling errors
Decision Making	• Complex structures • Structures without baseline measurements

4.1.4   Chapter Overview

In the following chapter a literature review of damage detection procedures is provided examining methodologies applicable for global nondestructive damage evaluation of structures with an emphasis on those methods utilizing vibration characteristics or measurements of a structure to detect, locate, and estimate the severity of damage in the structure. Included in this report is a strategy for structural health monitoring of fiber

reinforced polymer (FRP) rehabilitated structures detailing the role of a global nondestructive damage detection methodology. Methods are categorized according to their selected feature for damage detection (i.e., frequencies, mode shapes, FRF's, etc.) or the procedures to characterize damage within the structure (i.e., optimization methods, genetic algorithms, artificial neural networks, etc.).

Past literature reviews include Doebling, et al.(1996) whom conducted an extensive literature review with brief summaries of damage detection techniques implementing changes in measured structural vibration response and their respective applications to various types of engineering structures. Salawu (1997b) specifically examines techniques using natural frequency as a parameter in structural assessment including limitations of using natural frequencies such as the influence of temperature, humidity and condition of the structure, i.e. temperature of the bridge deck soffit.

Vibration based damage detection is a broad field with both global and local methodologies for application of structures in aerospace, mechanical, and civil engineering (Farrar and Doebling, 1997). In addition to the variety of applications, a number of critical issues contributing to the success of a damage detection methodology are the steps in acquiring the modal parameters of a structure, such as excitation and measurement considerations and type and location of the sensors, as well as signal processing (Farrar and Doebling, 1997). Issues related to the acquisition of vibration properties are not addressed specifically in this review, but rather, the emphasis of this study is placed on current damage detection algorithms utilizing the quantities measured during vibration testing. Reviews addressing dynamic testing of structures for acquisition of vibration properties are available in Chapter 3 of this report.

A recurring theme amongst literature addressing damage detection algorithms is the ability of the methodology to perform in the presence of measurement noise and incomplete measurements, i.e. in the presence of signal noise or when only the first three modes of vibration of a structure are available. No comparison of damage detection methods is conducted utilizing a standard set of experimental data in this document; however, since signal noise and incomplete measurements are common occurrences in field-measured properties or during the data acquisition process a methodology validated using field-measured data is considered robust.

The amount of literature detailing a new methodology for damage detection using vibration properties has increased significantly since the early 1990's. Evidence of such growth is observed in conference proceedings of the International Modal Analysis Conference, the proceedings of SPIE-The International Society for Optical Engineering, and the International Workshop on Structural Health Monitoring. This review of damage detection methods provides an explanation in regards to the selected feature for damage detection, followed by a summary of current damage detection techniques characteristic of that feature. The following report is divided into categories according to methodology such as stiffness matrix optimization or genetic algorithms to evaluate the vibration response of a structure or according to a specific modal parameter, such as measured resonant frequencies or mode shapes. Independent of the feature selected for analysis, the damage detection methodologies identified in this report utilize a measured vibration response of the structure be it a modal parameter, time history, frequency response function, etc.

Table 4-2 provides a summary of features applied for damage detection algorithms utilizing vibration properties examined in this review.

Table 4-2. Summary of Damage Detection Categories and Methods

Category		Methodology
Modal Parameters	Natural Frequencies	• Frequency changes • Residual force optimization
	Mode Shapes	• Mode shape changes • Modal strain energy • Mode shape derivatives
Matrix Methods	Stiffness-based	• Optimization techniques • Model updating
	Flexibility-based	• Dynamically measured flexibility
Machine Learning	Genetic Algorithm	• Stiffness parameter optimization • Minimization of the objective function
	Artificial Neural Network	• Back propagation network training • Time delay neural network • Neural network systems identification with neural network damage detection
Other Techniques		• Time history analysis • Evaluation of FRFs

As part of the evaluation and comparison, the damage detection methods reviewed in this report are classified according to feature and listed with positive and negative aspects associated with health monitoring of structures and FRP rehabilitated structures.

4.2   Frequency Based Methods

The most common and earliest approaches for damage detection implement resonant frequencies of the structure to evaluate the existence of damage. Frequency based methods are developed with the implication that resonant frequency shifts occur as the structure experiences some change in its structural properties. Most damage detection methods assume that changes in the frequencies of the structure are due to damage and independent of environmental conditions. In general, changes in frequencies are unable to provide spatial information regarding damage in a structure (Farrar, et al., 2001); thus damage detection methods relying solely on changes in frequency are typically Level 1 methods.

Frequency information alone does not provide reliable results, especially because several combinations of damage in the structure can produce the same changes in the natural frequencies. Magnitude of damage is given only in a qualitative sense (Hassiotis, 2000). Resonant frequencies depend on the global properties of a system and are often

implemented in conjunction with frequency domain identification procedures to improve the level of damage detection, i.e., find the location and magnitude of stiffness degradation (Hassiotis, 2000).

For applications to large civil engineering structures the low sensitivity of frequency shifts to damage requires either very precise measurements of frequency change or large levels of damage. An exception occurs at higher modal frequencies where the modes are associated with local responses. However, the practical limitations involved with the excitation and identification of the resonant frequencies associated with these local modes, caused in part by high modal density and low participation factors, can make them difficult to identify.

In the following section, several damage detection methods utilizing resonant frequencies are investigated with an emphasis on those methods applying additional techniques to improve the level of damage detection in the structure.

4.2.1 Changes in Frequency

Bicanic and Chen (1997) present a method for damage identification using only a limited number of natural frequencies to identify, locate, and determine the extent of damage in the structure. The major premise being that any local or distributed changes in stiffness result in changes in the modal parameters. The development of the damage identification procedure involves a characteristic equation for the relative stiffness change in a structure. Although, the formulation requires that only natural frequencies be measured from pre- and post-damage states of the structure, baseline mode shapes are required to determine spatial information regarding damage. Once natural frequency measurements of the post-damage state of the structure is acquired, the change in mode shape vector is expressed as the linear combination of the original eigenvectors and frequencies, allowing for computation of the damaged mode shape vector.

$$\Delta\boldsymbol{\varphi}_i = \sum_{k=1,k\neq i}^{N} \frac{\boldsymbol{\varphi}_k^T \Delta\mathbf{K}\boldsymbol{\varphi}_i + \boldsymbol{\varphi}_k^T \Delta\mathbf{K}\Delta\boldsymbol{\varphi}_i}{\lambda_i^* - \lambda_k} \boldsymbol{\varphi}_k = \sum_{k=1,k\neq i}^{NC} C_{ik} \boldsymbol{\varphi}_k$$

$$C_{ik} = \frac{\boldsymbol{\varphi}_k^T \Delta\mathbf{K}\boldsymbol{\varphi}_i + \boldsymbol{\varphi}_k^T \Delta\mathbf{K}\Delta\boldsymbol{\varphi}_i}{\lambda_i^* - \lambda_k}$$

where, quantities denoted with superscript * refer to their respective terms for the damaged structure; C_{ik}, is the mode participation factor; N, is converted to NC to denote the number of original mode shapes available; $\mathbf{K}$ is the global system stiffness matrix; $\Delta\mathbf{K}$ is the change in the global system stiffness matrix; $\Delta\boldsymbol{\varphi} = \boldsymbol{\varphi}_i^* - \boldsymbol{\varphi}_i$, is the change in mode shape; λ_i and $\boldsymbol{\varphi}_i$ are respectively the ith eigenvalue and the corresponding mode shape for the original structure. The above expression provides an evaluation of the change in mode shapes with only post-damage natural frequencies required.

Evaluation of the mode participation factor is the critical component of this damage detection algorithm, since the change in mode shapes correspond changes in stiffness, which determines the damage state of the system. The following generalized equation is presented relating modal participation factors and scalar damage indicators. In order to

solve for scalar damage parameters, α_j, and mode participation factors, C_{ik}, numerical methods are employed (Bicanic and Chen, 1997).

$$\sum_{j=1}^{NE} a_{kji}\alpha_j + \sum_{j=1}^{NE} \sum_{l=1,l\ne i}^{NC} a_{kjl}C_{il}\alpha_j - \left(\lambda_i^* - \lambda_k\right)C_{ik} = 0$$

where α_j, is the scalar damage indicator for the jth element; NE is the number of elements in the structure; a_{kji} is the eigenmode-stiffness sensitivity coefficients, which are defined in general form as, $a_{kji} = \boldsymbol{\varphi}_k^T \mathbf{K}_j \boldsymbol{\varphi}_i$. The damage identification procedure using natural frequencies presented by Bicanic and Chen is a methodology, which if valid in field applications or real structures, would prove significantly advantageous since spatial information and severity of damage is determined with knowledge of post-damage frequencies alone, assuming the pre-damage natural frequencies of the structure and mode shapes are known. However, Bicanic and Chen show that in the presence of signal noise, the methodology performs poorly for numerical examples with noise levels of 0.5% to 2.0% showing results overestimating or underestimating damage severity, as well as resulting in false positive indications of damage.

Contursi, Williams, and Messina (1997, 1998) present a structural damage detection methodology based on changes in the natural frequencies of the structure, by reason that natural frequencies are least contaminated by measurement noise and provide good accuracy during measurement (Messina et al., 1997). The approach is based on the MDLAC developed by Messina et al. (1997, 1998). Initially a statistical evaluation program for damage location at a single site is developed then extended for multiple sites. The location of damage at a single site is determine by the damage localization assurance criteria (DLAC),

$$DLAC(j) = \frac{\left|\{\Delta\mathbf{f}\}^T \cdot \{\delta\mathbf{f}_j\}\right|^2}{\left(\{\Delta\mathbf{f}\}^T \cdot \{\Delta\mathbf{f}\}\right) \cdot \left(\{\delta\mathbf{f}\}^T \cdot \{\delta\mathbf{f}\}\right)}$$

Where, $\{\Delta\mathbf{f}\}$ is the measured frequency change vector for a structure having a single defect of unknown size or location; $\{\delta\mathbf{f}_j\}$ is the theoretical frequency change vector for damage of a known size at location j. The formulation requires that damage of a specific size at a specific location results in frequency changes which are unique to the damage scenario. Thus, when the DLAC approaches or equals a value of 1, a match between the patterns of frequency changes exist and damage in the structure is indicated by the theoretical model. A DLAC value equal to 0 implies no correlation exists between frequencies. The highest DLAC value corresponds to the predicted damage site. The DLAC criterion is a statistical measure to discriminate between patterns for potential damage sites.

Determination of the theoretical frequency change vector, $\{\delta\mathbf{f}_j\}$, requires that variations of the theoretical frequency for each damage size and location combination be evaluated for the given structure. Possible combinations of damage size and location are enormous for most civil structures and subsequently involve extensive calculations to evaluate the

damage type and location at a single location. Furthermore the DLAC becomes a reliable statistical measure when 10 to 15 modes of the structure are available (Messina, et al., 1998). Acquisition of 10 modes for large civil structures in the field is typically unfeasible and thus the damage detection methodology is susceptible to the limited number of distinct vibration modes available in large, complex structures.

Messina, et al. modify the formulation of the DLAC criterion to detect damage at multiple locations by calculating sensitivity of the frequencies according to the following equation,

$$\frac{\partial f_k}{\partial D_j} = \frac{1}{8 \cdot \pi^2 \cdot f_k^0} \cdot \frac{\left\{\boldsymbol{\varphi}_k^0\right\}^T \left[\mathbf{K}_j^0\right]\left\{\boldsymbol{\varphi}_k^0\right\}}{\left\{\boldsymbol{\varphi}_k^0\right\}^T \left[\mathbf{M}^0\right]\left\{\boldsymbol{\varphi}_k^0\right\}}$$

Where $\left\{\boldsymbol{\varphi}_k^0\right\}$ represents the kth mode shape vector, $\left[\mathbf{K}_j^0\right]$ is the stiffness matrix of the jth element within the global stiffness matrix, and $\left[\mathbf{M}^0\right]$ is the global mass matrix. The superscript zero indicates quantities for the undamaged state of the structure. Subsequently for identification of multiple damage locations, evaluating mode shapes from an analytical model is necessary since spatial information of the damage is required. A stiffness reduction factor, D_j, is incorporated into the formulation such that when D_j equals 1 no damage exists in the element and when D_j equals 0 the element is completely lost. In addition, the multiple location damage detection procedure requires an analytical model of the structure. The MDLAC by Messina et al. is provided below, assuming that corresponding reductions in natural frequencies can be written as a linear combination of the sensitivities.

$$MDLAC(\{\delta\mathbf{D}\}) = \frac{\left|\{\Delta\mathbf{f}\}^T - \left\{\delta\mathbf{f}\left(\{\delta\mathbf{D}\}\right)\right\}\right|^2}{\left(\{\Delta\mathbf{f}\}^T \cdot \{\Delta\mathbf{f}\}\right) \cdot \left(\left\{\delta\mathbf{f}\left(\{\delta\mathbf{D}\}\right)\right\}^T \cdot \left\{\delta\mathbf{f}\left(\{\delta\mathbf{D}\}\right)\right\}\right)}$$

Where, $\{\delta\mathbf{D}\}$ is a vector of changes in the stiffness reduction factor describing the combination of size and location of damage at one or more sites and $\{\delta\mathbf{f}\}$ is the vector containing the analytical predictions of frequency changes. Similar to the single location damage detection criterion, the MDLAC is obtained by searching for the vector $\{\delta\mathbf{D}\}$ maximizing the MDLAC value. Since the size of $\Delta\mathbf{f}$ is dependent on the number of modes and $\{\delta\mathbf{D}\}$ is dependent on the number of possible damage sites, the analysis becomes computationally expensive since all elements in the model are potential damage sites with varying damage sizes. The use of the MDLAC assumes that damage in an element corresponds with a homogeneous reduction of stiffness and assumes that the occurrence of damage does not change the mass of the structure. The basic underlying concept in the MDLAC is that damage at a particular location causes changes in natural frequencies larger than undamaged locations and these changes are detectable via a pattern recognition principle.

In order to alleviate some of the extensive computational aspects of the MDLAC, Messina et al. suggest limiting the search for damage to probable locations implying that some knowledge of possible damage locations need to be known before hand, further reducing the confidence in the level of damage detection capability and localization, essentially discounting any benefits provided by the frequency based technique. As previously mentioned, the methodology assumes that 10 to 15 distinct vibration modes are attainable from the vibration testing of the structure.

Numerical applications to a 2-d, 6 bay truss structure and 3-d steel frame offshore oil platform show that the methodology is able to locate damage successfully although severity estimates are unreliable. Laboratory validation is conducted on an aluminum rod test structure with a non-updated model of the finite element structure to simulate a real routine monitoring with minimum effort. Damage was simulated by reducing cross sections of the members; however, for small structure it is observed that the assumption of constant mass is no longer applicable and adversely affects the MDLAC. The method was observed to adequately locate damage from the laboratory experiment.

Hassiotis (2000) formulates an optimization algorithm on the basis that damage results in localized changes in the stiffness matrix. In order to find the magnitude of the damage, measurements of the natural frequency are used to determine a set of equations to resolve the stiffness matrix of the structure. The classical eigenvalue problem in structural dynamics, shown below, is used to find the eigenvalue sensitivities to the stiffness matrix, $\mathbf{K}$.

$$\left(\mathbf{K} - \lambda_i \mathbf{M}\right)\phi_i = \mathbf{0}$$

where $\mathbf{K}$, is the global stiffness matrix; λ_i is the eigenvalue equal to the square of the natural frequency, ω_i; $\mathbf{M}$ is the diagonal mass matrix of the structure; ϕ_i, is the eigenvector or corresponding mode shape. Application of the eigenvalue problem to evaluate the stiffness properties, typically results in an underdetermined set of equations, which is optimized using a set of optimality criterion. The damage detection algorithm presented by Hassiotis is extended from an earlier work with Jeong by employing an optimization criterion based on the impulse response measurements as provided by the Markov parameters (Hassiotis and Jeong, 1995). Markov parameters of a continuous system are the impulse response sequence of the system and obtained from the measured impulse-response of a continuous structure or from the pulse response of a discrete system.

The optimization problem is formulated as the following minimization problem for the residuals of the eigenvalue problem.,

$$\text{minimize} \ \ \tfrac{1}{2}\delta\mathbf{k}^T\mathbf{Q}\delta\mathbf{k} + \delta\mathbf{k}^T\mathbf{c}$$
$$\text{subject to} \ \ \mathbf{D}\delta\mathbf{k} = \delta\lambda \ \ \text{and} \ \ \delta\mathbf{k} \leq 0$$

where $\delta\mathbf{k}$ is a vector of element stiffness changes; $\mathbf{c}$ is a vector in linear terms of quadratic optimization; $\delta\lambda$ is a vector of changes in eigenvalue; $\mathbf{D}$, is a matrix relating changes in stiffness to changes in eigenvalues. Hassiotis introduces Markov parameters for determination of light to severe damage in any number of members in the structure whereas the previous formulation in reference (Hassiotis and Jeong, 1995) assumes the

structure has not changed significantly due to damage. $\mathbf{Q}$ is a weighting matrix in quadratic optimization, defined as $\mathbf{Q}(p,k) = \sum_{i=1}^{s}\sum_{j=1}^{l}\mathbf{T}_{k}(i,j)\mathbf{T}_{p}(i,j)$ for the optimization problem with the matrix $\mathbf{T}$ defining the Markov parameter as a relationship between the measurement locations and force input locations with the elements of the stiffness matrix.

The algorithm is applied to locate damage in a 10-story two-bay steel frame, via a numerical simulation with damage induced by decreasing stiffness in elements. The markov parameters and frequency values serve as the input data of the identification algorithm. Successful identification of damage in multiple locations is observed using 12 measured natural frequencies. However, severity estimations are unreliable. The methodology is highly dependent on the number of sensors and locations, i.e. a large number of data must be available in order to detect a large number of damage locations. Leaving the methodology susceptible to reduced measurements from the field. In addition, the problem of noise in measurements was investigated with erroneous identification of location and magnitude for noise having a coefficient of variation above 0.8%.

Ray and Tian (1999) propose a method for enhancing modal sensitivity to damage using feed back control to address the unattractive features of frequency measurements for damage detection, specifically becasue a significant amount of damage is required before a shift in modal frequencies becomes detectable (Adams, et al., 1978; Swamidas and Chen, 1995). The primary focus of the methodology by Ray and Tian is to accentuate the sensitivity of frequency shifts to damage occurring in the structure, such that modal frequencies become a viable measure for damage detection, particularly for smart structures, i.e. those capable of self-excitation, self-sensing, and closed-loop vibration control. The method reverses the control problem, instead of using a control law to make the system insensitive to changes in the system parameters; the sensitivity is magnified in a predictable manner by feedback control. As an illustration of the methodology consider the sensitivity of natural frequency, $\omega_{n} = \sqrt{\dfrac{k}{m}}$ for a single degree of freedom system to small changes in stiffness, k and mass, m,

$$\frac{\partial \omega_{n}}{\partial k} = \frac{\omega_{n}}{2k}, \ \frac{\partial \omega_{n}}{\partial m} = -\frac{\omega_{n}}{2m}$$

where ∂, denotes a change in the respective parameter. By applying feedback control, the closed-loop natural frequency is dependent on the control gain, K, resulting in a closed loop frequency, $\omega_{n_{cl}} = \sqrt{\dfrac{k+K}{m}}$. Thus the sensitivities are functions of the control gain, K,

$$\frac{\partial \omega_{n_{cl}}}{\partial k} = \frac{\omega_{n}}{2(k+K)}, \ \frac{\partial \omega_{n_{cl}}}{\partial m} = -\frac{\omega_{n_{cl}}}{2m}$$

The above sensitivity expression shows that a negative or decrease in gain, -K, enhances sensitivity to changes in stiffness, while a positive or increase in gain, +K enhances

sensitivity to changes in mass. The methodology is applied to a numerical simulation of a cantilevered beam with sensitivity of modal frequencies to damage increased by a factor of 60 for the first mode and a factor 5 for the third mode as compared to the unmodified sensitivity analysis showing a maximum frequency shift of 5% for severe damage and never exceeding 0.5% for modest damage. The method is able to detect damage; however, sensitivity to damage is dependent on the location of actuator and sensor and the mode of vibration collected.

4.3 Methods Utilizing Mode Shapes

Analyzing changes in mode shapes is another category that has received a tremendous amount of attention for purposes of damage detection. Mode shapes provide an advantage over a feature such as frequency since they are spatially defined quantities and thus identification of damage using mode shapes implies that the locations of damage are realized. However, mode shapes are difficult to measure and a large number of measurement locations may be required to accurately characterize mode shape vectors and to provide sufficient resolution for determining the damage location (Doebling, et al. 1996). Theoretically, the comparisons of mode shapes (i.e. undamaged and damaged) possess spatial information, which is useful in identifying the existence and location of damage in a structure. Predominant methods employing mode shapes compare measured mode shapes directly, or the properties of mode shapes such as curvature or modal strain energy to enhance sensitivity to damage detection and localization.

4.3.1 Mode Shape Changes

Salawu (1997c) presents a method for damage detection utilizing natural frequencies to determine the existence of damage and qualitatively determine the severity of damage globally, then employs mode shapes for identification and localization of damage. The global assessment component of Salawu's integrity index method is identified as the global integrity index, denoted GI, which is a function of natural frequency alone. Salawu assumes that mass remains constant in the formulation and changes are attributed to a reduction or increase in the global structural stiffness. The expression for the global index is provided below,

$$ GI = f(\omega) = \Sigma \left[a_r \left(\omega_{Dr} \middle/ \omega_{Or} \right) \right] $$

where, GI is the global integrity index as a function of frequency; r, is the mode number; a_r, is the weighting factor for mode, r; the subscripts D and O refer to the damaged and undamaged structures respectively. Salawu recommends using a minimum of three mode shapes for the methodology. Weighting factors a_r are structure dependent with the following effective participation factors assigned for large civil engineering structures: mode 1 – 70%; mode 2 – 20%; other modes – 10%.

If the number of available modes exceeds three, the modes most sensitive to damage are selected on the basis of the modal sensitivity value (MSV) function in the following equation.

$$MSV\left(\{\phi_A\}_r,\{\phi_B\}_r\right)=\frac{\dfrac{\left\{\Sigma\left(\phi_{Bir}\right)^2\right\}^{0.5}}{\lambda_{Br}}-\dfrac{\left\{\Sigma\left(\phi_{Air}\right)^2\right\}^{0.5}}{\lambda_{Ar}}}{\dfrac{\left\{\Sigma\left(\phi_{Air}\right)^2\right\}^{0.5}}{\lambda_{Ar}}}$$

where, the summation is from 1 to n (number of measurement points); (ϕ_{Air}) = element of the rth mode shape vector at measurement point i for data set A; and λ_{Ar} is the eigenvalue (natural frequency squared) of mode r for data set A. Subscripts A and B refer to the undamaged and damaged structures, respectively. The MSV for all modes (for a particular damage case) are normalized such that the mode showing least correlation has an MSV value of 100. Salawu states that an MSV value close to 100 is an indicator of damage; however, the effect of measurement noise and modeling errors are not considered.

Following a global evaluation of the structure based on frequencies, Salawu develops the local integrity indices (LI) in order to detect localized defects and locate damage areas. The LI index operates as a function of frequency and mode shapes as damage locator at measurement point, i. Ratios of the squares of the modal amplitudes are used to compute LI_i while the absolute difference of LI_i from unity is used to infer the damage site.

$$LI_i=\Sigma\left[a_r\left(\frac{\omega_{Dr}}{\omega_{Or}}\right)\left(\frac{(\phi_{Dir})^2}{(\phi_{Oir})^2}\right)\right]$$

where (ϕ_{Dir}) and (ϕ_{Oir}) are respectively elements of the rth mode shape vector at measurement point i for the damage and undamaged structures. The existence of damage in a structure results in $\left|LI_i-1\right|>0$ for all I; whereas $\left|LI_i-1\right|=0$ signifies no change in the structural integrity. However, values of $\left|LI_i-1\right|$ for points most likely to be the damage locations would be much greater than those for other points. Therefore, for identification of single damage locations, values of $\left|LI_i-1\right|$ are normalized such that the point with the largest values has a value of 100. If multiple damage locations are desired, the process is repeated, excluding the previously identified point(s).

Salawu (1997c) provides applications of the methodology to numerical, laboratory, and field data. The laboratory experiment was conducted on a steel I-beam with progressive levels of damage. Frequency results, as oft stated in literature, are not sensitive to damage and large changes in frequency occur only when the damage is large. The LI index is shown to adequately locate damage near the vicinity of sensors during the laboratory experiment. In addition, a reinforced concrete highway bridge was evaluated before and after repairs to the bridge with decreases in frequencies observed before and after the repair in the range of –1% to –3% indicating that the improvement to the structure was insignificant. The LI index was used to identify the locations of the repair from the sensors in close proximity. However, no indication is made to determine if the local index is at a significant level other than that the highest values are the most likely

damage locations; here a statistical model may prove useful in particular for multiple damage locations. The author does not discuss the impact of signal noise and reduced measurements; however, a field application is provided displaying the ability to identify and locate a change on a real structure. The integrity index method has not been demonstrated for damage detection on a real structure nor has the issue of baseline modal parameters been addressed.

4.3.2   Mode Shape Derivatives

Abdo and Hori (2002) provide a numerical study of structural damage detection for purposes of determining the feasibility of using changes in rotation of mode shapes of a structure. With the premise that the rotation of mode shapes will become a measurable quantity in the future, Abdo and Hori (2002) compare the changes in the displacement mode, the strain mode, and the frequency changes to identify and locate damage. Numerical simulations are conducted for the first four modes of a beam and then to a steel plate. Indicators for damage in a truss element and beam element are derived with the damage located and detected by discontinuities in the derivatives of the mode shapes. A study is performed on the feasibility of using changes in rotation of mode shapes with the assumption that rotations of modes shapes will be measured directly from the structure and not analytically derived from field measured displacement mode shapes.

It is shown that the curvature of mode shapes suffer a discontinuity at locations of damage and thus approximating the moment, M as $K\kappa^0(x_d)$, the curvature change in a beam element is evaluated as,

$$[\kappa] \approx \left(\frac{K}{K - \Delta K} - 1 \right) \left| \kappa^0(x_d) \right|$$

where, $[\kappa]$ is the amount of curvature discontinuity; $K = EI$ is the bending stiffness of the beam element; E is Young's modulus; I, is the moment of inertia; ΔK is the change in stiffness; $\kappa^0(x_d)$ is the curvature for an undamaged beam at location, x_d. The primary emphasis is to show that the derivative of the mode shape provides an improved indicator for damage compared to the displacement modes. Abdo and Hori (2002) show accurate detection and localization of damage in the plate structure using numerical simulations, by observing that localization of the rotation of mode shapes occurs at the damaged region and approximate zero values beyond the damaged location make the methodology effective and accurate. In addition, the lower modes of the structure are shown to be sufficient to detect damage at multiple locations of the plate in the numerical example.

4.3.3   Modal Strain Energy

Law et al. (2000, 1998, 1998) propose a method based on modal strain energy to detect damage at the element level with particular attention for incomplete and noisy measured modal data. Three stages are involved with the approach: (1) expansion of modal data to estimate modal parameters at unmeasured degrees of freedom; (2) localization of the damage domain using the elemental energy quotient difference to identify a group of elements forming a possible damage domain, thus reducing the problem size; (3) damage quantification based on the sensitivity of the modal frequency.

Law et al. combine the following three components in order to develop the damage detection approach. First, measured modal data is expanded to match the finite element model. Second, the modal strain energy of each element normalized with its potential energy is used to locate the damage domain. Third, the measured modal frequency changes are then employed to determine the magnitude of damage using a sensitivity-based method. Here damage is assumed to affect only the stiffness matrix, i.e., damage in a structure results in the reduction of a design parameter, such as the elastic modulus or sectional area of a member. Damping is ignored in the formulation.

Damage detection and localization of the structure is developed with the assumption that damage to the structure results in small changes modal frequencies, λ_i, and mode shape vector, Φ_i. The perturbation in the system due to damage is represented in the stiffness matrix as $\mathbf{K}^d$, the ith modal eigenvalue λ_i^d, and the ith mode shape as Φ_i^d as follows,

$$\mathbf{K}^d = \mathbf{K} + \sum_{j=1}^{L} \Delta \mathbf{K}_j = \mathbf{K} + \sum_{j=1}^{L} \alpha_j \mathbf{K}_j \quad \left(-1 < \alpha_j \leq 0\right)$$

$$\Phi_i^d = \Phi_i + \Delta \Phi_i; \quad \lambda_i^d = \lambda_i + \Delta \lambda_i$$

where, α_j is a stiffness reduction factor of the jth element of the stiffness matrix; L is the total number of elements in the system. Since the damaged and undamaged systems experience the same energy inputs, the difference in total energy of the two systems, Π_d and Π_u, respectively, is zero.

$$\Pi_d - \Pi_u = 0$$

For damage localization, the energy content within each jth element is assumed unchanged.

$$\Pi = \left(\text{Kinetic Energy}\right)_j + \left(\text{Potential Energy}\right)_j$$

The physical interpretation of the above formulation indicates that an increase in elemental modal strain energy results in a reduction in the elemental kinetic energy and thus the ratio of the modal strain energy to the kinetic energy shows increased sensitivity to damage as compared to elemental modal strain energy alone. Here this ratio is denoted as the modal strain energy coefficient (MSE) and its change between damage and undamaged states are used as an indicator for damage localization, MSECR.

$$MSECR_{ij} = \frac{\left|MSE_{ij}^d - MSE_{ij}\right|}{MSE_{ij}}$$

where $MSE_{ij} = \Phi_i^T \mathbf{K}_j \Phi_i$ and $MSE_{ij}^d = \Phi_i^{d^T} \mathbf{K}_j \Phi_i^d$ are the elemental modal strain energy of the undamaged and damaged structures assuming the stiffness matrix of the undamaged element is an adequate approximation of the damaged elemental stiffness matrix.

Here it may prove advantageous to provide a statistical model such that the user of the technique may be able to determine if the MSECR is statistically significant compared to modal strain energy ratios of the other elements. Nonetheless, the authors suggest that high values of the MSECR relative to other locations are considered indicative of a

damaged location. Furthermore, if more than one measured mode is available, the $MSECR_{ij}$ is calculated for all modes and $MSECR_j$ of the jth element is defined as the average of the summation of all $MSECR_{ij}$ normalized with respect to the maximum of $MSECR_{ij}$ for each mode as,

$$MSECR_j = \frac{1}{m}\sum_{i=1}^{m}\frac{MSECR_{ij}}{MSECR_{i,max}}$$

As a component of Law, et al.'s damage detection strategy, a mode shape expansion procedure is presented such that a limited number of measured DOF's are expanded to the full dimension of the finite element model, with the model expansion preserving the connectivity of the structure in the final expanded mode shape.

If a small change in the stiffness of the structure occurs, each perturbed mode shape is assumed as a linear combination of the original mode shapes,

$$\mathbf{\Phi}_d = \begin{bmatrix} \mathbf{\Phi}_{dc} \\ \mathbf{\Phi}_{df} \end{bmatrix} = \mathbf{\Phi}_u \mathbf{Z}$$

where $\mathbf{\Phi}_d$ and $\mathbf{\Phi}_u$ are the matrices of damaged and undamaged mode shape vectors, respectively; the subscript c denotes master DOFs of the experimental model; the subscript f indicates the number of additional DOFs to be expanded to from the measured mode shape; $\mathbf{Z}$ is a transformation matrix. The cross orthogonality of the damaged and undamaged mode shapes is expressed as follows,

$$\mathbf{\Phi}_u^T \mathbf{M} \mathbf{\Phi}_d = \mathbf{Z}$$

Therefore, when small local damage occurs, $\mathbf{Z}$, is approximately the identity matrix. The transformation matrix is obtained using the following expression,

$$\mathbf{Z} = \left(\mathbf{\Phi}_{uc}^T \mathbf{\Phi}_{uc} + \mathbf{WI}\right)^{-1}\left(\mathbf{\Phi}_{uc}^T \mathbf{\Phi}_{dc} + \mathbf{WI}\right)$$

where $\mathbf{\Phi}_{uc}$ is the measured modal matrix of the undamaged structure; $\mathbf{\Phi}_{dc}$ is the measured modal matrix of the damaged structure; $\mathbf{W}$ is the weight coefficient. If a modal analysis model is reliable and accurate, less weight is given to the analytical information by setting the weight $\mathbf{W}$ less than 1.0. Else, additional weight is given to the analytical model with values of $\mathbf{W}$ greater than 1.0.

Substituting the definition of $\mathbf{Z}$ into the modal mass relationship yields the additional expansion required to complete the damaged mode shape and thus the modal expansion of measured data,

$$\mathbf{\Phi}_{df} = \mathbf{\Phi}_{uf} \mathbf{Z}$$

Damage quantification can be expressed in the following system of equations,

$$\begin{Bmatrix} MSEC_{i1} \\ MSEC_{i2} \\ \cdots \\ MSEC_{iJ} \end{Bmatrix} = \begin{bmatrix} \beta_{11} & \beta_{12} & \cdots & \beta_{1q} \\ \beta_{21} & \beta_{22} & \cdots & \beta_{2q} \\ \cdots & \cdots & \cdots & \cdots \\ \beta_{J1} & \beta_{J2} & \cdots & \beta_{Jq} \end{bmatrix}\begin{Bmatrix} \alpha_1 \\ \alpha_2 \\ \cdots \\ \alpha_q \end{Bmatrix} \qquad \beta_{st} = -2\sum_{r=1}^{n}\Phi_i^T \mathbf{K}_s \frac{\Phi_r^T \mathbf{K}_t \Phi_i}{\lambda_r - \lambda_i}\Phi_r \quad (r \neq i)$$

where $MSEC_{ij} = \Phi_i^{d^T} \mathbf{K}_j \Phi_i^d - \Phi_i^T \mathbf{K}_j \Phi_i$ is the modal strain energy difference between the damaged and undamaged structure; q, is the number of identified damage locations, β_{st} is the element sensitivity coefficient of MSEC to damage. Solving the system of equations with expanded mode shapes provides the severity estimation of damage in the structure.

The modal strain energy method by Shi and Law is applied to a numerical simulation of a fixed-fixed beam. The methodology is able to identify damage locations accurately in the fixed-fixed beam with the MSECR value changing sequentially as a 5% and 7% signal noise are introduced. The magnitudes of damage were identified correctly with the number of analytical mode shapes greatly affecting the severity estimate, requiring 20 analytical modes in the beam application. The influence of noise in the severity estimates results in errors ranging from 0 to 30%. The methodology is experimentally applied to a two-story steel plane frame structure, with damage simulated by the loosening of semirigid joints in two locations. Both locations were identified with the first two mode shapes and mode shape expansion with 15 analytical modes, with unverified severity estimations for the loosened joints.

Stubbs et al's (2000, 1996) suggests a damage detection algorithm utilizing changes in modal strain energy. The prescribed methodology combines a modal-based damage detection algorithm analyzing the changes in the modal strain energy of the structure before and after the occurrence of damage with a procedure to estimate the systems' reliability in order to describe the performance of the structure. The damage detection algorithm alone is sufficient to describe a Level 3 global NDE technique capable of identifying, locating, and estimating severity of damage; however, the addition of the reliability analysis provides additional insight into the probability of failure of the structure and potentially into the remaining useful life of the structure. Particular attention and detail is provided to Stubbs et al's (2000) damage identification approach since it is potentially the most developed approach available for damage detection procedures with a number of publications from outside researchers evaluating the validity and applicability of the approach (Barroso and Rodriguez, 2004; Farrar and Jauregui, 1998a, 1998b; Wang and Loyd, 2000; Cornwell et al.)

The damage detection algorithm as developed and updated by Stubbs et al. (2000) detects changes in the modal strain energy to identify and locate damage where the modal parameters, specifically natural frequencies and mode shapes, are used to identify the modal stiffness properties of the as-built and existing structures. As mentioned previously, one of the difficulties associated with damage localization is that damage is typically a local phenomenon, making it difficult to determine the integrity of a small portion of the structure when only a few modal parameters are available (Stubbs, et al., 2000). To overcome this challenge, Stubbs converts the damage localization problem into a statistical pattern recognition problem where physical world data is transformed into the pattern space. Accordingly, the physical world data is depicted as the dynamic response of the structure and the pattern space represents the modal parameters of the structures. The feature space contains indicators, which are a function of pre, and post damaged modal parameters of the structure. Damage in this application is defined as a loss of stiffness.

In developing the damage index method, Stubbs prescribes the formulation with consideration for the following objectives: (1) The damage detection algorithm accurately localizes damage; (2) The damage detection algorithm uses a minimum number of modal parameters.

With damage defined as a loss of stiffness in the structure, the ith modal stiffness, K_i, for a linear undamaged structure is given by the following:

$$K_i = \Phi_i^T C \Phi_i$$

where Φ_i, is the ith modal vector and C, is the system stiffness matrix. The contribution of the jth element of the system stiffness matrix to the ith modal stiffness is given as,

$$K_{ij} = \Phi_i^T C_j \Phi_i$$

Thus, the fraction of the ith mode concentrated in the jth member (which is also called the modal sensitivity for the ith mode in the jth location) is as follows,

$$F_{ij} = \frac{K_{ij}}{K_i}$$

Similarly, the damaged structure (denoted with an asterisk) has the following modal sensitivity definition,

$$F_{ij}^* = \frac{K_{ij}^*}{K_i^*} = F_{ij}\left(1 + \sum_{k=1}^{NE} A_{ik}\alpha_k + HOT\right)$$

where, $K_{ij}^* = \Phi_i^{*T} C_j^* \Phi_i^*$ and $K_i^* = \Phi_i^{*T} C^* \Phi_i^*$; A_{ik}, is the set of coefficients associated with mode, i, at location, k; α_k, is the fraction of damage at location k in the structure; HOT, represents higher order terms.

Thus far in the development of the damage index method, no significant assumptions outside of the general framework of structural dynamics is made. By utilizing the modal strain energy, Stubbs defines a measure of sensitivity of one specific location of the structure to the total modal strain energy of the structure for an individual mode shape. This development is considered advantageous, since individual mode shapes of the structure have been identified for use in a damage detection algorithm without the need for resolving all or a large portion of mode shapes from the experimental modal analysis.

The system stiffness matrices are separated into material and geometric components as shown below,

$$C_j = E_j C_{j0}$$

$$C_j^* = E_j^* C_{j0}^*$$

where, scalars E_j and E_j^* are parameters representing material properties for the undamaged and damaged j^{th} member of the structure, respectively. The matrix C_{j0}, involves geometric quantities and possibly terms containing Poisson's ratio.

The ratio of modal sensitivities given below compares the relative modal stiffness changes of a damaged structure to an undamaged structure for a specific location.

$$\frac{F_{ij}^*}{F_{ij}} = \frac{K_i}{K_{ij}} \cdot \frac{K_{ij}^*}{K_i^*} = \left(\frac{K_{ij}^*}{K_{ij}}\right) \cdot \left(\frac{K_i}{K_i^*}\right)$$

Stubbs and Kim (1996) provide the following observations regarding the characteristics of their damage detection algorithm. 1) An equation per elemental location of the structure is available for each mode. 2) As the region of interest for the damage detection decreases in size the number of equations grows significantly. 3) A method for determining the linear coefficients A_{ik} and the higher order terms is necessary in order to proceed with the derivation.

The authors recognize that the geometry of an undamaged location is unaffected when damage occurs elsewhere in the structure. In addition, experimental test results indicate that the relative modal deformations are large after indicating the presence of damage (loss in stiffness) (Stubbs and Kim, 1996). Given the observations, the fractional change in modal strain energy, F_{ij}, in an element is assumed unchanged before and after the occurrence of damage, which is represented by the following relationship, such that $F_{ij}^* = F_{ij}$.

According to Stubbs and Kim, this approximation is valid for simultaneous structural damage at multiple locations and at a damage level up to 30% (Stubbs and Kim, 1996), implying the unchanged sensitivity assumption following the occurrence of damage and the algorithm are no longer applicable for damage scenarios where the severity exceeds 30%. Manipulation of the sensitivity relationship results in the following expression,

$$1 = \frac{F_{kj}^*}{F_{kj}} = \frac{K_{ij}^* \cdot K_i}{K_{ij} \cdot K_i^*}$$

Substituting the definitions of the undamaged and damaged stiffness relationships yields the following equation,

$$\beta_{ij} = \frac{E_j}{E_j^*} = \frac{\Phi_i^{*T} C_{jo}^* \Phi_i^*}{\Phi_i^T C_{jo} \Phi_i} \cdot \frac{K_i}{K_i^*}$$

where, β_{ij}, is the localized damage indicator relating the change in modal strain energy for element j to the ith mode. For a specific quantity of measured mode shapes, N, the damage index, β_j, is written as follows,

$$\beta_j = \frac{E_j}{E_j^*} = \frac{\displaystyle\sum_{i=1}^{N} \Phi_i^{*T} C_{jo}^* \Phi_i^* \cdot K_i}{\displaystyle\sum_{i=1}^{N} \Phi_i^T C_{jo} \Phi_i \cdot K_i^*}$$

The definition of the damage indices β_{ij} and β_j posses quantities on the right hand side, which are either available or can be approximated from experimental measurements and the geometry of the structure, C_{jo}. In addition, if the structure is discretized into a large

number of small elements, it is reasonable to assume there is no single component dominating the modal sensitivity, i.e. the modal sensitivity for the damaged and undamaged structures is small.

$$F_{ij} \ll 1 \text{ and } F_{ij}^* \ll 1$$

β_j, provides a positive and initial indicator for the existence and location of damage when $\beta_j > 1$. However, obvious difficulties in the algorithm occur if the jth member or element is located at or near a node of the ith mode, resulting in a zero in the denominator of the damage index β_j and providing a false-positive reading of damage in the structure. In order to alleviate the problem of a false-positive result, unity is added to both the numerator and denominator. Although there appears to be no rigorous formulation for the addition of unity, successful implementation of the damage index is observed (Farrar and Jauregui, 1998a, 1998b; Park, et al., 2001).

$$1 = \frac{F_{kj}^* + 1}{F_{kj} + 1} = \frac{\left(K_{ij}^* + K_i^*\right)K_i}{\left(K_{ij} + K_i\right)K_i^*}$$

Substituting the definitions for K_{ij}^* and K_{ij} results in the following indicator of damage for a single mode of the structure.

$$\beta_j = \frac{\left(\Phi_i^{*T} C_{jo}^* \Phi_i^* + \left(\frac{1}{E_j^*}\right) \sum_{k=1}^{NE} \Phi_i^{*T} E_k^* C_{ko} \Phi_i^*\right)}{\left(\Phi_i^T C_{jo} \Phi_i + \left(\frac{1}{E_j}\right) \sum_{k=1}^{NE} \Phi_i^T E_k C_{ko} \Phi_i\right)} \cdot \frac{K_i}{K_i^*}$$

$$\beta_j \approx \frac{\left(\Phi_i^{*T} C_{jo}^* \Phi_i^* + \sum_{k=1}^{NE} \Phi_i^{*T} E_k^* C_{ko} \Phi_i^*\right)}{\left(\Phi_i^T C_{jo} \Phi_i + \sum_{k=1}^{NE} \Phi_i^T E_k C_{ko} \Phi_i\right)} \cdot \frac{K_i}{K_i^*}$$

The conventional form of the damage index method when several modes are know is provided below:

$$\beta_j = \frac{\sum_{i=1}^{NM} \left\{ \left(\Phi_i^{*T} C_{jo}^* \Phi_i^* + \sum_{k=1}^{NE} \Phi_i^{*T} E_k^* C_{ko} \Phi_i^*\right) K_i \right\}}{\sum_{i=1}^{NM} \left\{ \left(\Phi_i^T C_{jo} \Phi_i + \sum_{k=1}^{NE} \Phi_i^T E_k C_{ko} \Phi_i\right) K_i^* \right\}}$$

The advantages and convenience presented by the final formulation of the damage index method in the equation above is two fold: (1) Losses in stiffness, or damage, is identified and located as a function of the pre damaged and post damaged mode shapes of the structure, Φ_i and Φ_i^*; (2) The remaining terms are available from the geometry of the structure as long as $K_i^* \approx \Phi_i^{*T} C \Phi_i^*$, implying the structure continues to behave linearly after damage occurs.

Damage Severity Estimation. The application of a set of statistical criteria for damage detection is one of the advantages that differentiate the damage index method from other global damage detection strategies. Imbedded in the damage detection algorithm is an estimate for the severity of damage in the structural element or member. A fractional change in stiffness, α_j, of an element, j, is described by the following equation,

$$\alpha_j = \frac{E_j^* - E_j}{E_j} = \frac{\Phi_i^T C_{jo} \Phi_i}{\Phi_i^{*T} C_{jo}^* \Phi_i^*} \cdot \frac{K_i^*}{K_i} = \frac{1}{\beta_j} - 1$$

where, α_j, is the fractional change in stiffness of an element, j.

Some of the limitations and characteristics of the above equation are a function of the assumptions made during the development of the damage index method. In general, the above severity estimation results in an overestimation of the severity of damage in a structure because of the assumption that the structure continues to behave linearly after the occurrence of damage, i.e. $K_i^* \approx \Phi_i^{*T} C \Phi_i^*$ when in actuality $|C| > |C^*|$ (Stubbs and Kim, 1996). Furthermore, since the damage index method assumes that the fraction of modal strain energy is equivalent before and after damage occurs, a limitation on its ability to accurately locate and identify damage exists at magnitudes greater than 30% (Stubbs and Kim, 1996). This limitation becomes a point of concern, particularly if damage scenarios exceeding losses in stiffness greater than 30% occur and are not detectable from a visual inspection of the location.

Nonetheless, if damage does not exist in the structure according to the results of the damage index method, then $\alpha_j = 0$. If damage does exist, $\alpha_j < 0$ with α_j approaching -1 as the stiffness capacity is lost (Stubbs, et al., 2000).

Kim and Stubbs (2002) return to the general problem of utilizing changes in dynamic modal parameters of structures to detect, locate, and estimate the severity of damage. In particular the modal strain energy procedure developed by Stubbs and Kim (1996) is improved for better localization and severity estimation by eliminating several assumptions and limitations imposed in the previous derivations.

Eigenvalues of the pre- and post-damage multi-degree-of-freedom structure λ_i and λ_i^* can be related in the following forms:

$$\lambda_i^* = \lambda_i + d\lambda_i = \frac{(K_i + dK_i)}{(M_i + dM_i)}$$

where K_i and M_i are the ith modal stiffness and i^{th} modal mass of the undamaged system respectively; $d\lambda_i$, dK_i, and dM_i are the change in the ith eigenvalue, the change in the ith modal stiffness, and the ith modal mass, respectively. The sensitivity matrices are similarly defined as

$$F_{ij}^* = F_{ij} + dF_{ij}$$

where F_{ij}^* and F_{ij} are the respective damaged and undamaged stiffness matrices; $F_{ij} = \dfrac{K_{ij}}{K_i}$ is the undamaged modal sensitivity expressed as the fraction of modal energy of the ith mode and the jth member; $K_{ij} = \Phi_i^T C_j \Phi_i$, is the contribution of the jth member to the ith modal stiffness, C_j is the contribution of the jth member to the system stiffness matrix, C, and Φ_i is the ith mode vector.

dF_{ij} represents the fractional change of modal energy at the jth member for the ith mode; dF_{ij} is acquired as follows,

$$dF_{ij} = \frac{K_{ij}}{K_i}\left[\frac{dK_{ij}}{K_{ij}} - \frac{dK_i}{K_i}\right]$$

where dK_{ij} represents the fractional change in K_{ij}. It is observed that $K_i \gg K_{ij}$ and thus the fraction of modal energy is reduced to the following equation,

$$dF_{ij} \cong \frac{dK_{ij}}{K_i}$$

As compared to previous formulations, the sensitivity of the modal stiffness are not assumed to remain the same for pre and post damaged structures; furthermore, the shift in the reference axis is no longer necessary to develop the damage index. The fraction of modal energy is then modified and expressed in terms of parameters representing material stiffness properties of the individual elements for the damage and undamaged structure respectively, E_j^* and E_j; geometric quantities (and possibly poisson's ratio) of the structure, C_{jo}.

$$\frac{dK_{ij}}{K_i} \cong \frac{\gamma_{ij}}{\gamma_i}\frac{dE_j}{E_j} + \frac{d\gamma_{ij}}{\gamma_i}$$

where the following quantities are defined as follows: $\gamma_{ij} = \Phi_i^T C_{j0} \Phi_i$ and $\gamma_{ij}^* = \Phi_i^{*T} C_{j0} \Phi_i^*$, $d\gamma_{ij} = \gamma_{ij}^* - \gamma_{ij}$, and $\gamma_i = \sum\limits_{k=1}^{ne} \Phi_i^T C_{k0} \Phi_i$; ne, is the number of elements. The fractional changes in modal stiffness are approximately related to the fractional changes in modal properties,

$$\frac{dK_{ij}}{K_i} \cong g_i\left(\lambda, \Phi\right) = \frac{d\lambda_i}{\lambda_i} + \frac{dM_i}{M_i}\left(1 + \frac{d\lambda_i}{\lambda_i}\right)$$

where $g_i\left(\lambda, \Phi\right)$ is the dimensionless factor representing the systematic change in modal parameters of the ith mode due to the damage.

With the sensitivities, stiffness and modal mass quantities expressed as linear relationships between damaged and undamaged states of the structure, a new damage index for nm, the number of modes, at the jth location is given by,

$$\beta_j = \frac{E_j}{E_j^*} = \frac{\sum\limits_{i=1}^{nm} \gamma_{ij}^*}{\sum\limits_{i=1}^{nm} \gamma_i \, g_i\left(\lambda, \Phi\right) + \gamma_{ij}}$$

Once damage is located, the severity is estimated from,

$$\alpha_j = \frac{dE_j}{E_j^*} = \frac{1}{\beta_j} - 1, \quad \alpha_j \geq -1$$

where damage severity is indicated as the reduction in stiffness in the jth member if $\alpha_i < 0$. The above formulation provides information in terms of location and severity of damage from changes in mode shapes of structures. The following advantages are presented by the current formulation: (1) damage can be located and sized using a few modes; (2) damage can be located and sized without solving a system of equations; and (3) damage can be located and sized in structures containing many members. A numerical simulation on a two span continuous beam is conducted to demonstrate the improvement versus the previous versions of the damage index with improvements shown in accuracy of the severity estimation and reduction of false-positive indications of damage. No examples related to field data or demonstrations on bridge structures are currently available.

4.4 Stiffness and Flexibility Based Methods

Another category of damage detection methods utilizes dynamic measurements to determine the system matrices of a structure to characterize damage in a structure. Assembly and evaluation of the system matrices provides inherent advantages of being able to locate and estimate the severity of damage by a comparison of damaged and undamaged matrices of the system. However, the problem of incomplete measurements or inability to identify all modes of the structure results in partial population of the system matrices. As with a majority of damage detection methods the realization of a stiffness reduction factor for elements of the structure are critical in terms of determining location and severity of damage. In the following section, methods utilizing system matrices are examined, in particular the stiffness matrix or flexibility matrix of the system utilizing vibration measurements of the structure.

4.4.1 Matrix Update Methods

Matrix updating procedures are a developing area for structural damage detection. In general these methods are either sensitivity-based matrix updating techniques, optimal matrix update procedures, or control-based algorithms. The data used to develop the finite element model (FEM) matrices are either the modal parameters or frequency response functions of the structure. The identification of modal parameters is mathematically derived; however, the computation becomes complicated for large and modally complex structures. Due to the inability of acquiring all modes of large structures from field vibration measurements, an approximation of the stiffness or flexibility matrices of a structure is available at best.

Optimal matrix update methods, seeking to determine system property matrices, such as the stiffness matrix using measured test data, are used extensively in FEM refinement and damage detection. Changes in the system matrices are associated with the overall health of the system, where a stiffness reduction is often associated with damage. The objective for optimization of the stiffness matrix is to adequately populate the matrix under the guide of some objective function with a constraint set defined based on preserving characteristics of the system matrix, such as symmetry, sparsity (the zero/nonzero pattern of the matrix), and positivity. Typically matrix update problems vary in terms of the iterative refinement process to converge to an approximate stiffness matrix of the system. Optimization of the stiffness matrix addresses the issue of reduced measurements for structural damage detection by completing the stiffness matrix of a system based on constraints established according to characteristics of the system matrices and satisfaction of the classical eigenvalue problem from structural dynamics. A successful matrix optimization procedure is intended as a Level 3 damage detection methodology since spatial information and damage severity information becomes available if the stiffness matrix and its subsequent changes due to damage are resolved. Matrix update methods generally vary amongst the following three considerations (Doebling, et al., 1996): (1) Objective function to be minimized; (2) Constraints placed on the problem; (3) Numerical scheme used to implement the optimization.

Abdalla, et al. (1998) propose implementing alternating projection algorithms to provide improved optimal matrix updates for damage detection purposes. In particular, the emphasis is placed on providing theoretical foundations, the formulation of the alternating projection method, and a justification of their convergence and properties. Included is a directional alternating projection damage detection algorithm, which results in enhanced convergence. Abdalla, et al, assume that the number of measured mode shapes is the same as the analytical eigenvectors, which introduces the possibility of erroneous results since accurate population of the damaged stiffness matrix requires *all* associated mode shapes and frequencies of the system.

The alternating projection method is used to solve an optimization problem with defined constraints to the optimization. The algorithm requires iterating until the intersection of all constraints is nonzero, i.e. find a matrix $\mathbf{K_d^*}$ where $\mathbf{C_1} \cap \mathbf{C_2} \cap \mathbf{C_3} \cap \ldots \cap \mathbf{C}_n \neq \mathbf{0}$. Where it is important that constraint sets $\mathbf{C}_i$, are convex, i.e. any two points (matrices) that belong to a set define a line segment that is fully contained in the set. Convexity implies that the optimization problem and feasibility problem have unique solutions. In order to preserve structural connectivity for more accurate damage detection, the following optimal matrix update problem is solved,

$$\underset{\mathbf{K_d^*}}{\text{minimize}} \left\| \mathbf{K_d^*} - \mathbf{K} \right\|$$

where, $\left\| \bullet \right\|$ denotes the Frobenius norm[+]; $\mathbf{K_d}$, is the stiffness matrix of the damaged structure and $\mathbf{K_d^*}$ is the solution matrix representing the optimally modified stiffness

---

[+] The Frobenius norm of a matrix, A is defined as follows $\left\| A \right\| = \left[\sum_{i,j} A_{ij}^2 \right]^{\frac{1}{2}} = \left[tr\left(AA^T \right) \right]^{\frac{1}{2}}$

matrix; **K** is the analytical stiffness matrix. The optimization problem is subject to the following constraints,

$$\mathbf{K}_d^* \in \mathbf{C}_1 \cap \mathbf{C}_2 \cap \mathbf{C}_3 \text{ and } \mathbf{K}_d^* \in \mathbf{C}_4$$

where, $\cap$ is the set intersection operation. $\mathbf{C}_1 = \{\mathbf{K}_d : \mathbf{K}_d \geq \mathbf{0}\}$ ensures a positive definite matrix, $\mathbf{C}_2 = \{\mathbf{K}_d : \mathbf{K}_d = \mathbf{K}_d^T\}$ introduces a constraint keeping the solution matrix symmetric, $\mathbf{C}_3 = \{\mathbf{K}_d : \mathbf{K}_d \text{ is } \mathbf{K}-\text{sparse}\}$ ensures that $\mathbf{K}_d$ is K-sparse if $\mathbf{K}_d$ has the zero/nonzero pattern of the analytical stiffness matrix. $\mathbf{C}_4 = \{\mathbf{K}_d : \mathbf{K}_d \mathbf{V}_d = \mathbf{M}\mathbf{V}_d\mathbf{\Omega}_d^2\}$ provides for a $\mathbf{K}_d^*$ such that the eigenvalue problem is satisfied, where **M** is the mass matrix, $\mathbf{V}_d$ is the measured mode shape matrix and $\mathbf{\Omega}_d$ is the measured natural frequency matrix. The fourth constraint, $\mathbf{C}_4$ does not intersect the other constraints such that flexibility is introduced in terms of satisfaction of the eigenvalue problem, since the presence of signal noise may lead to a solution that does not satisfy the eigenvalue problem. The methodology is applied to experimental data from a NASA eight bay truss with damage inflicted by the removal of truss members. The matrix optimization technique is able to able to predict damage locations; however errors in severity estimation are observed between 5% and 30%.

Escobar et al. (2001), propose a transformation matrix method for damage detection, with damage defined as a loss of stiffness. The methodology is based on the transformation matrix that reduces the global stiffness matrix of a structure to a condensed state with only the primary degrees of freedom, which correspond to the rigid body movements of the slabs on different floors of a building. The methodology is able to identify, locate, and estimate severity of damage in a structure by considering the contribution of elements to the overall performance of the structure.

The methodology assumes that an analytical stiffness matrix represents the undamaged state of the structure with the damaged global stiffness matrix acquired by a matrix update technique using the matrix of measured frequencies, Ω_d, and matrix of mode shape vectors, Φ_d by Baruch and Bar-Itzhack (1978), shown below,

$$\text{minimize } \left\| M^{-\frac{1}{2}} \left(K_d^* - K \right) M^{-\frac{1}{2}} \right\|$$

$$\textbf{subject to } K_d^* \Phi_d = M \Phi_d \Omega_d^2, \quad K_d^* = K_d^{*T}$$

where, K is the analytical stiffness matrix; K_d^* is the optimally modified stiffness matrix; M is the system mass matrix; and $\|\bullet\|$ again denotes the Frobenius norm. A closed form solution to the minimization problem is available and given below,

$$K_d^* = K - KXX^T M - MXX^T K + MXX^T KXX^T M + MX\Omega_d^2 X^T M$$

$$\text{where, } X = \Omega_d \left(\Omega_d^T M \Omega_d \right)^{-\frac{1}{2}}$$

The Baruch-Bar Itzhack formula provides a matrix update that is consistent with the measured modal data, although structural connectivity of the stiffness matrix is not ensured. Assuming the undamaged and damaged stiffness matrices of the structure are

available, the damage detection algorithm by Escobar et al. computes the transformation matrices of the structure to condense the stiffness matrices such that only those degrees of freedom associated with rigid body movements of the slabs are used for the damage identification process (Escobar, et al., 2001).   This modifies the computationally expensive procedure to a reduced set of degrees of freedoms of the structure.

The damage detection algorithm was applied to numerical simulations of a ten story office building with vibration parameters acquired from earthquake acceleration data from the Mexico City earthquake on Sept. 19, 1985.   Numerical simulations show accurate identification of damage location and severity as compared to nonlinear analyses. In addition the authors examined the effect of noise and reduced measurements on the damage detection process. As noise levels increased from 0% to 1%, 3%, and 5%, general increase in the estimated damage magnitude was also observed.   Initially 10 measurements were used to attain the stiffness matrix of the structure, analyses were conducted with reduced measurements of 50%, 70%, and 90% of the 10 mode shapes. It was found that for accurate damage location, 80% of the 10 mode shapes were required. The identified magnitudes of the damage were observed to decrease as the number of mode shapes decrease, the adjustment of the stiffness matrix is based on the difference of the undamaged stiffness matrix, consequently as fewer modes are included, the use of Baruch and Bar-Itzhack's methodology to determine the damaged stiffness matrix resulted in a result close to the original stiffness matrix.   Therefore, fewer damaged elements are identified during the damage detection process.   The damage detection algorithm presented by Escobar et al. relies on an accurate analytical model to develop the undamaged stiffness matrix and that a procedure for acquiring the stiffness matrix of a damaged structure is available

4.4.2   *Stiffness Evaluation in State Space*

Sivico, et al. (1997) present a Level 3 global damage detection methodology for civil structures with damage indicated by changes or reductions in stiffness and damping parameters of the structural elements. The damage detection algorithm utilizes the state-space representation of the time domain structural response to evaluate stiffness and damping parameters of a structure with the eigensystem realization algorithm used for systems identification, which provides a discrete state-space representation of the structure (Sivico, et al. 1997).   In addition, a method for the linear transformation to convert the arbitrary state-space representation of the structure to the physical coordinate system of the structure is necessary to implement the global damage detection methodology.

Beginning with the equations for an *n* degree of freedom (DOF) structure,

$$\mathbf{M\ddot{q}} + \mathbf{D\dot{q}} + \mathbf{Kq} = \mathbf{0}$$

Where **M**, **D**, and **K** are the mass, damping, and stiffness matrices, respectively and **q**(t) is the displacement of *n* DOF of the structure. Conversion to the state-space is facilitated by representing the displacement and velocity vectors of the structure with $\mathbf{x}_1 = \mathbf{q}$ and $\mathbf{x}_2 = \mathbf{\dot{q}}$.

$$\begin{bmatrix} \dot{\mathbf{x}}_1 \\ \dot{\mathbf{x}}_2 \end{bmatrix} = \begin{bmatrix} \mathbf{0} & \mathbf{I} \\ -\mathbf{M}^{-1}\mathbf{K} & -\mathbf{M}^{-1}\mathbf{D} \end{bmatrix} \begin{bmatrix} \mathbf{x}_1 \\ \mathbf{x}_2 \end{bmatrix} \Leftrightarrow \dot{\mathbf{x}} = \mathbf{A}\mathbf{x}$$

Sivico et al. (1997) explain the global stiffness, mass, and damping matrices are a result of individual element contributions for the undamaged system and can be expressed as follows,

$$\mathbf{M} = \sum_{i=1}^{n} \mathbf{M}_i \quad \mathbf{D} = \sum_{i=1}^{n} \mathbf{D}_i \quad \mathbf{K} = \sum_{i=1}^{n} \mathbf{K}_i$$

Where $\mathbf{M}_i$, $\mathbf{D}_i$, and $\mathbf{K}_i$ are the contributions from the ith mass, damping, and stiffness element matrices. Here, mass is assumed to be an unchanging characteristic of the structure as damage occurs. The presence of damage in the methodology is recognized by a reduction factor on the individual element contributions to the global system matrices. Damage is assumed to cause a reduction in the stiffness and/or damping contribution of an individual element, with the objective of the methodology being to evaluate the reduction factors a_i and b_i. If accurate evaluation of the reduction factors is possible, then indications of damage, locations, and severities are available from the algorithm. The equations incorporating reduction factors in the stiffness and damping matrix formulation are given below.

$$\mathbf{D}_d = \mathbf{D} + \sum_{i=1}^{d} a_i \mathbf{D}_i = \sum_{i=1}^{d} (1+a_i)\mathbf{D}_i$$

$$\mathbf{K}_d = \mathbf{K} + \sum_{i=1}^{k} b_i \mathbf{K}_i = \sum_{i=1}^{k} (1+b_i)\mathbf{K}_i$$

Where, the subscript d indicates the matrices are associated with the damaged state of the structure. Without consideration for computational costs, the damage detection methodology proposed by Sivico et al (1997), is theoretically capable of localizing and estimating damage severity at any scale depending on the level of discretization of the structure during the modeling phase. The state-space representation of the damaged structure is provided below.

$$\begin{bmatrix} \dot{\mathbf{x}}_1 \\ \dot{\mathbf{x}}_2 \end{bmatrix} = \begin{bmatrix} \mathbf{0} & \mathbf{I} \\ -\mathbf{M}^{-1}\sum_{i=1}^{k}(1+b_i)\mathbf{K}_i & -\mathbf{M}^{-1}\sum_{i=1}^{d}(1+a_i)\mathbf{D}_i \end{bmatrix} \begin{bmatrix} \mathbf{x}_1 \\ \mathbf{x}_2 \end{bmatrix} \Leftrightarrow \dot{\mathbf{x}} = \mathbf{A}_d \mathbf{x}$$

The matrices $\mathbf{A}$ and $\mathbf{A}_d$ are determined from a systems identification procedure. Matrix $\mathbf{A}$ is subtracted from matrix $\mathbf{A}_d$ to isolate the component of the stiffness directly related to the damaged state of the structure. The methodology is reduced to a comparison of the difference in stiffness and damping matrices in state-space.

$$\mathbf{A}_d - \mathbf{A} = \begin{bmatrix} \mathbf{0} & \mathbf{0} \\ -\mathbf{M}^{-1}\sum_{i=1}^{k}b_i\mathbf{K}_i & -\mathbf{M}^{-1}\sum_{i=1}^{d}a_i\mathbf{D}_i \end{bmatrix}$$

Since mass is assumed to remain constant with the occurrence of damage in the structure, the sub matrices in the lower part of $[\mathbf{A}_d - \mathbf{A}]$ can be pre-multiplied by $[-\mathbf{M}^{-1}]$, resulting in the following relationships within the matrix for stiffness and damping,

$$\tilde{\mathbf{K}} = \sum_{i=1}^{k} b_i \mathbf{K}_i \qquad\qquad \tilde{\mathbf{D}} = \sum_{i=1}^{d} a_i \mathbf{D}_i$$

Converting the summations into matrix vector equations produces the following system of equations.

$$\begin{bmatrix} K_{1_{11}} & K_{2_{11}} & \cdots & K_{n_{11}} \\ \cdots & \cdots & \cdots & \cdots \\ K_{1_{1n}} & K_{2_{1n}} & \cdots & K_{n_{1n}} \\ K_{1_{21}} & K_{2_{21}} & \cdots & K_{n_{21}} \\ \cdots & \cdots & \cdots & \cdots \\ K_{1_{2n}} & K_{2_{2n}} & \cdots & K_{n_{2n}} \\ \cdots & \cdots & \cdots & \cdots \\ K_{1_{n1}} & K_{2_{n1}} & \cdots & K_{n_{n1}} \\ \cdots & \cdots & \cdots & \cdots \\ K_{1_{nn}} & K_{2_{nn}} & \cdots & K_{n_{nn}} \end{bmatrix} \begin{bmatrix} b_1 \\ b_2 \\ \cdots \\ b_n \end{bmatrix} = \begin{bmatrix} \tilde{K}_{11} \\ \cdots \\ \tilde{K}_{1n} \\ \tilde{K}_{21} \\ \cdots \\ \tilde{K}_{2n} \\ \cdots \\ \tilde{K}_{n1} \\ \cdots \\ \tilde{K}_{nn} \end{bmatrix} \Leftrightarrow \hat{\mathbf{K}}\vec{\mathbf{b}} = \tilde{\mathbf{k}}$$

Where $\hat{\mathbf{K}}$ according to the formulation is composed of undamaged element stiffness values of the structure associated with the vector of damage reduction factors $\vec{\mathbf{b}}$. $\tilde{\mathbf{k}}$ is the known resultant for the subtraction of $\mathbf{A}$ from $\mathbf{A}_d$. Subsequently $\vec{\mathbf{b}}$ is determined from matrix operations with $\vec{\mathbf{b}} = \hat{\mathbf{K}}^{\dagger}\tilde{\mathbf{k}}$, where $\hat{\mathbf{K}}^{\dagger}$ is the pseudo inverse of the vector-matrix, $\hat{\mathbf{K}}$.

Similarly the damping reduction factors $\vec{\mathbf{a}} = \hat{\mathbf{D}}^{\dagger}\tilde{\mathbf{d}}$ are developed and evaluated. The method is capable of determining the location and severity by determination of the reduction factors $\vec{\mathbf{a}}$ and $\vec{\mathbf{b}}$. However, the system identification procedure, not described here, introduces a level of uncertainty, where any reduction factor less than 10% is not applicable, i.e. the damage detection algorithm has a minimum detectable reduction in stiffness and/or damping of 10%

The damage detection algorithm presented by Sivico, et al. (1997) details an approach utilizing the state-space representation of the structure. The transformation from state-space to the physical coordinates of the structure requires having the same amount of actuators as DOFs; or, identifying multiple single-input systems, which are combined into a multi-input state space representation. Furthermore, the algorithm requires a representation of the as-built or baseline of the structure, since a comparison of two states of the structure is necessary in order to detect and evaluate damage. Applications of the methodology are examined with numerical simulations, with any stiffness or damping reduction factors less than 10% neglected due to the uncertainty in the systems identification procedure. Damage localization and severity estimation on a simple mass-spring-damper model and three-bar truss were successful; although damage cases with stiffness or damping changes greater than 50% were simulated.

4.4.3 Dynamically Measured Flexibility

As the stiffness matrix is used for detection of damage in the system, the system's dynamically measured flexibility matrix can also be used as indicators of damage. As with the stiffness matrix development, the measurement of the flexibility matrix is approximate because of the inability to acquire all the mode shapes of a structure.

Application of the flexibility matrix presents several advantageous versus dynamically measured stiffness. First, flexibility matrices are attainable from modes and mode shapes that are determined from a mode identification procedure (Park and Reich, 1998). Second, most updating damage detection algorithms incorporate an iterative refinement process for which the fastest converging solutions are typically high eigenvalues. In stiffness-based approaches, the high eigenvalues correspond to high frequency modes, which are difficult to acquire for large civil structures; however, in flexibility based methods the high eigenvalues correspond to dominant low frequency modes of the structure, rather than unmeasured high frequency components (Park and Reich, 1998). Because the flexibility matrix demonstrates an inverse relationship to the squares of the natural frequencies, the measured flexibility matrix is more sensitive to changes in the lower frequency modes of the structure.

Park and Reich (1998) develop a flexibility-based approach using the partitioned flexibility equation in order to detect changes in substructural characteristics by identifying changes in the measured global flexibilities before and after damage. As previously mentioned, methods utilizing measured flexibility matrices are limited to approximations because of the unavailability of higher modes and thus the inability to measure the complete flexibility or stiffness matrices for a given structure. Although, no definition of damage is explicitly stated, the definition of damage implicit in the procedure by Park and Reich, and apparent in the applications, is that damage is indicated by a loss of stiffness or an increase in flexibility. The formulation by Park and Reich first provides a procedure for evaluating the global flexibility matrix of the structure from experimentally acquired modal parameters, subsequently, localized damage detection scenarios are formulated for localized flexibility of a structure in three different generalized coordinates, which are localized or substructural displacement, elemental deformation basis, and elemental strain basis.

Utilizing the theoretical concepts in structural dynamics, Park and Reich develop the equation of motion using the discrete energy functional of a linear damped structure; the equation of motion is derived taking the first variation of the energy of the system,

$$\mathbf{M}_g \ddot{\mathbf{u}}_g + \mathbf{C}_g \dot{\mathbf{u}}_g + \mathbf{K}_g \mathbf{u}_g = \mathbf{f}_g$$

where, $\mathbf{M}_g$, is the mass matrix of the assembled structure; $\mathbf{C}_g$, is the assembled damping matrix; $\mathbf{K}_g$, is the assembled stiffness matrix; $u_g, \dot{u}_g, \ddot{u}_g$, are the displacement, velocity, and acceleration vectors, respectively; $\mathbf{f}_g$, is the applied force vector.

Assembly of the global stiffness matrix, $\mathbf{K}_g$, is composed of stiffness matrices of substructures partitioned from the complete structure (Park and Reich, 1998).

The response of the structure to the applied force vector is given in the frequency domain with the frequency response function (FRF) by applying a Fourier transform to the force

and displacement components. This results in the following frequency domain output, $\overline{\mathbf{u}}_g$,

$$\overline{\mathbf{u}}_g = \mathbf{H}_g(\omega)\overline{\mathbf{f}}_g = \left(\mathbf{K}_g + j\omega\mathbf{C}_g - \omega^2\mathbf{M}_g\right)^{-1}\overline{\mathbf{f}}_g$$

where, $\mathbf{H}_g(\omega)$, the transmittance function, is called the "global" FRF. According to Park and Reich, the mass normalized "global" flexibility matrix, $\mathbf{F}_g$ is defined as follows,

$$\mathbf{F}_g = \mathbf{\Phi}\,\mathbf{\Lambda}^{-1}\mathbf{\Phi}^T,\ \mathbf{\Phi}^T\mathbf{M}_g\mathbf{\Phi} = 1,\ \mathbf{\Phi}^T\mathbf{K}_g\mathbf{\Phi} = \mathbf{\Lambda}$$

The above expressions are applicable to an analytical model and serve as a background to the development of the damage detection methodology using localized flexibilities. In actuality, the measured global flexibility matrix is significantly smaller in size relative to the analytical expression and is given below,

$$\mathbf{F}_{gm} = \mathbf{\Phi}_m\mathbf{\Lambda}_m^{-1}\mathbf{\Phi}_m^T$$

where, m, indicates the measured mode and mode shape. The global flexibilities alone are insufficient for damage localization since they are unable to model elemental changes in flexibility and the infinite number of load paths that occur in multiply-connected or continuum structures tends to "smear" elemental flexibility changes as strain energy can pass from one location to another through a number of different paths (Park and Reich). Thus the substructural flexibilities are required for accurate characterization of damage. Park and Felippa utilize a general partitioned flexibility method to establish a relationship between the global and substructural flexibilities.

The localization of damage using the global flexibility matrix, $\mathbf{F_g}$, requires resolving the localized flexibilities for the elements of the structure; these are determined by relating the global FRF, $\mathbf{H}_g(\omega)$, to the substructural FRF, $\mathbf{H}(\omega)$ via the following relationship,

$$\mathbf{H}(\omega) = \mathbf{L}\mathbf{H}_g(\omega)\mathbf{L}^T = \mathbf{L}\left(\mathbf{K}_g + j\omega\mathbf{C}_g - \omega^2\mathbf{M}_g\right)^{-1}\mathbf{L}^T$$

where, $\mathbf{L}$ is the Boolean assembly matrix relating global and substructural displacements. The combined result of the substructural FRFs and the relationship between the global FRFs and substructural FRFs leads to the following, which is used for damage detection purposes by comparing the localized flexibility of the undamaged state of the structure to its current state. For the quasistatic limit, where $\omega \to 0$, the following equation results, allowing for a calculation of the substructural flexibility, $\mathbf{F}$, by an iterative procedure.

$$\mathbf{L}\mathbf{F}_g\mathbf{L}^T = \mathbf{F}\left\{\mathbf{I} - \mathbf{B}\mathbf{F}_B^{-1}\left[\mathbf{I} - \mathbf{L}_b\mathbf{F}_L\mathbf{L}_b^T\mathbf{F}_b^{-1}\mathbf{F}_B^{-1}\right]\mathbf{B}^T\mathbf{F}\right\}$$

$$\mathbf{F} = \mathbf{K}^+,\ \ \mathbf{F}_B = (\mathbf{B}^T\mathbf{F}\mathbf{B}),\ \ \mathbf{F}_L = \left(\mathbf{L}_b^T\mathbf{F}_B^{-1}\mathbf{L}_b\right)^{-1},\ \ \mathbf{L}_b = \mathbf{B}^T\mathbf{L}$$

where the symbol (+) indicates a generalized inverse; $\mathbf{B}$, is a constraint projection matrix, $\mathbf{I}$, is the identity matrix; The above formulation is the substructural displacement based flexibility. A deformation-basis flexibility is attainable by partitioning of substructural displacements into deformational and rigid parts. The result is an equation relating global flexibility to deformation-basis substructural flexibility,

$$\mathbf{TLF}_g\mathbf{L}^T\mathbf{T}^T = \mathbf{P}_v^T\mathbf{F}_v\mathbf{P}_v$$

$$\mathbf{F}_v = \mathbf{K}_v^+, \quad \mathbf{P}_v = \mathbf{I} - \mathbf{B}_v\left[\mathbf{B}_v^T\mathbf{F}_v\mathbf{B}_v\right]^{-1}\mathbf{B}_v^T\mathbf{F}_v$$

where $\mathbf{T}$ is a matrix relating the relative rigid body deformations between two nodes; v, is used to denote the deformation-basis derivation for the respective matrices.

The final formulation is for the strain-basis flexibility, where the strain output is related to the substructural displacement. The result is a similar formulation as the displacement and deformation based substructural flexibilities.

$$\mathbf{DLF}_g\mathbf{L}^T\mathbf{D}^T = \mathbf{P}_s^T\mathbf{F}_s\mathbf{P}_s$$

$$\mathbf{F}_s = \mathbf{K}_s^+, \quad \mathbf{P}_s = \mathbf{I} - \mathbf{B}_s\left[\mathbf{B}_s^T\mathbf{F}_s\mathbf{B}_s\right]^{-1}\mathbf{B}_s^T\mathbf{F}_s$$

where $\mathbf{D}$, is the discrete strain-displacement relation matrix which can be derived from finite element shape functions; s, is used to denote the strain-based formulation of the substructural flexibility.

Application of the three damage detection methods is applied to a numerical simulation of a plane ladder using beam elements, with reductions in the bending rigidity imposed. The strain basis and deformation-basis approaches accurately identified location of damage with the strain basis providing the closest damage severity estimates. The strain-basis flexibility was applied to a beam model of a ten-story structure using three modes; the predicted damage location was verified on the real structure, but no information regarding the quantification of damage was provided. In addition the methodology was applied to the I-40 modal test data (Farrar, C.R. and Jauregui, 1998; 1998), with the correct location identified with the strain basis flexibility; however little detail is provided as to the damage scenario and the severity estimation.

4.5　Machine Learning Techniques

Machine learning is the development of computing systems, or expert systems, with learning capability (Adeli and Hung, 1995). Computational intelligence methods such as neural networks and genetic algorithms are attractive processes in the area of structural damage detection because of their effectiveness and robustness in coping with uncertainty, insufficient information, and noise (Adeli and Hung, 1995). Machine learning techniques were developed as a remedy to four major problems in expert systems: brittleness, lack of metaknowledge, knowledge acquisition, and validation (Melhem and Nagaraja, 1996).

Expert systems enable the manipulation of knowledge in a certain domain, particularly in dialogue form, by searching for answer recommendations to problems of a qualitative nature (Melhem and Nagaraja, 1996). The primary development of each system is the knowledge base employed to develop the appropriate decision rules, which are intended to simulate the expert's way of thinking. Knowledge acquisition, or the transfer of knowledge from the source of domain expertise to the knowledge base, is an art and is considered the most difficult component of machine learning techniques.

Machine learning systems are classified in the following general categories (Melhem and Nagaraja, 1996):

1. *Interactive knowledge acquisition*; programs learn new interface rules by means of user interaction

2. *Learning by being told*; adaptation of knowledge from the source and its conversion into a usable form for the learning system.

3. *Learning from examples, or inductive learning, or concept learning*; set of examples used as input and the learning system induces a higher-level concept description in the form of trees and decision rules.

4. *Learning from observations, or conceptual clustering, or concept formation*; establishment of new theories that account for given facts, requires a significant amount of inference as compared to other categories.

5. *Theory-driven learning;* involves learning general concept description with the guidance of elaborate domain theory.

6. *Learning by discovery*; problem solving procedure in which the system attempts to find and understand some regularities in its environment.

The application of machine learning techniques to structural damage detection is typically observed under the classification of inductive learning, or learning by examples. Specifically, artificial neural networks and genetic algorithms are used for the characterization of damage in vibration based damage detection of structures.

4.5.1   Artificial Neural Networks

Artificial neural networks (ANN) are a functional abstraction of the biologic neural structures of the central nervous system (Adeli, 2001). ANN's are versatile for problems that are too complex to be modeled and solved by classical mathematics and traditional processes because they are powerful pattern recognizers and classifiers. The topology of an ANN model consists of a number of simple processing elements, called nodes or neurons that are interconnected to each other. Interconnection weights that represent the information stored in the system are sued to quantify the strength of the interconnections; these weights establish the inherent abilities associated with an ANN (Hung and Kao, 2002). Before an ANN is applied, the ANN needs to learn or be trained from an existing training set consisting of pairs of input-output elements. The majority of ANNs applied to structural damage detection employ the simple error back propagation (BP) training algorithm, which is based on a gradient-descent optimizaton technique (Adeli, 2001).

The BP is an error-correcting learning procedure that generalizes the delta rule to multi-layer feed forward neural networks with hidden units between the input and output units (Adeli and Hung, 1995). The delta rule is defined as the amount of learning representing the difference between the desired and computed outputs. The multiplayer feed forward networks with hidden units are able to learn in more complicated learning domains than those lacking hidden units.

Training of a neural network, or the learning procedure, is to update the weights of the links connecting the nodes (neurons) and to minimize the average squared system error between the desired and computed outputs. This error function in the form of sum squares of errors between the actual outputs from the training set and the computed outputs is minimized iteratively. The learning, or training, rule specifies how the weights are modified in each iteration (Adeli and Hung, 1995).

ANN's operate as black box, model free, and adaptive tools to capture and learn significant structures in data. Artifical neural networks are attractive because damage detection algorithms are vulnerable to inaccuracies in the presence of imprecise or incomplete measured data (Barai and Pandey, 1995). However, damage detection methods utilizing ANNs are highly dependent on the examples used to train the network. Figure 4.4 provides a schematic of the application of structural damage detection utilizing neural networks. The measured vibration property is input into the trained network and is filtered through hidden layers resulting in output nodes, which characterize the state of damage.
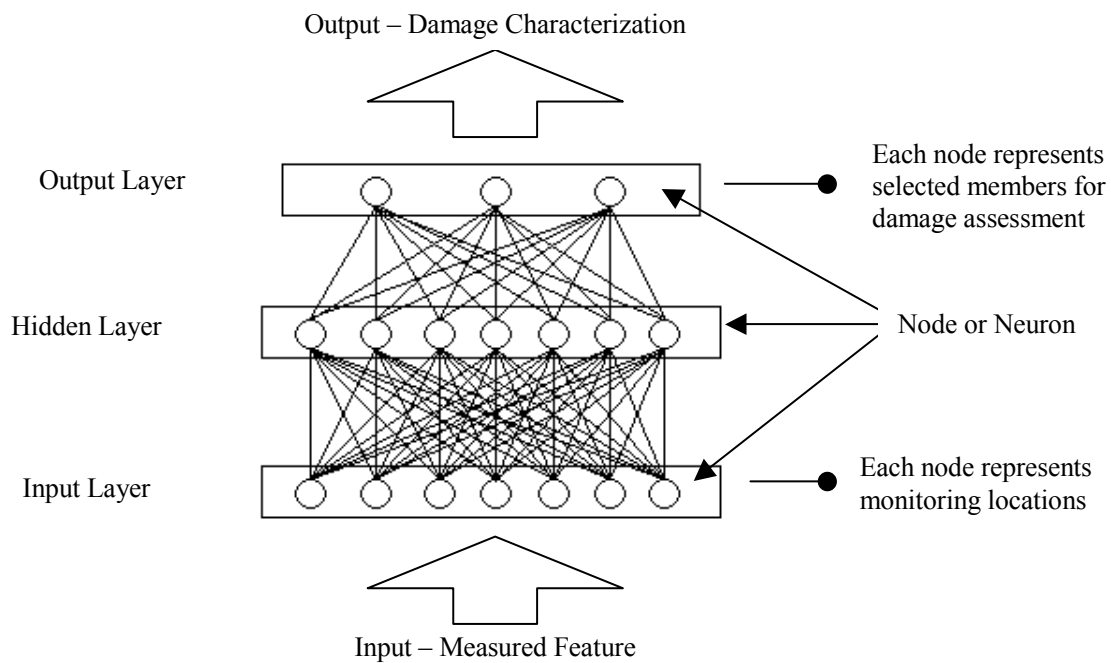
Figure 4.4. Artificial Neural Network Damage Detection

In the following section several structural damage detection methods employing ANNs are reviewed.

Zang and Imregun (2001, 2001) implement the use of neural networks with frequency response functions (FRFs) as input to the neural network to characterize damage in the structure. A specific problem addressed in the approach is that the size of FRF data, which is determined by the number of spatial response locations and the number of spectral lines, is too large for neural network applications for representative engineering problems. The direct use of such data leads to neural networks with a very large number of input nodes, which results in a large number of connections. This ultimately leads to an impractical neural network in terms of training and convergence stability. Zang and

Imregun impose a principal component analysis, which is a linear data compression technique achieving dimensionality reduction, to the FRFs for feasible application to neural networks (Zang and Imregun, 2001). The authors use a back propagation neural network with the principal components of the FRF as input to identify the existence of damage. Application of the damage detection strategy was conducted on a railway wheel with damage detected, even after a 5% random noise is introduced to the structures. The procedure was also applied to a space antenna with various modifications to the neural network for damage identification. It was observed that using too many principal components did not necessarily yield better results, since there was an increased susceptibility to signal noise. Furthermore, the extension of the methodology to damage location is more difficult, since it requires an increase in the number of input nodes and subsequently more output nodes will be required, contradicting the intent of the data FRF reduction via principal component analysis.

Barai and Pandey (1997) compare two types of neural networks for damage detection of steel truss bridge structures. One network is a traditional neural network (TNN) consisting of an input layer, output layer, and a number of hidden layers with the backpropagation method used as the training algorithm for the neural network. The other network is the time-delay neural network (TDNN), which is a class of spatiotemporal neural networks. A TDNN assumes that its output depends on its current and previous inputs. TDNN use spatial representation of temporal sequences on their input layers. In these networks the size of the input buffer is fixed, and the data entry is controlled by a time stepping arrangement. TDNN are specifically employed to deal with patterns that may vary over time and that require a period of time to be presented. The performance of the two neural networks is evaluated with an application to a numerically modeled steel truss bridge structure. With various cases representing reduction in the available input nodes, the TDNN was shown to perform better in the presence of incomplete information. The trained TNNs and TDNNs were able to identify the damaged member with reasonable estimates of the corss-sectional areas of all members.

Hung and Kao (2002) develop an ANN based nondestructive damage detection approach with two primary components. The first is a system identification approach using a neural systems identification network (NSIN) to acquire the undamaged and damaged states of the structure. The inputs into the NSIN are relative displacement, velocity, and acceleration and external excitations. The outputs of the NSIN are relative displacements, velocities and accelerations. Accordingly, the approximation by the NSIN in a discrete linear system is analogous to identifying the mass, damping, and stiffness coefficients in the equation of motion. However, determining the systems dynamic characteristics from the optimal weight of the approximating neural network is arduous because of the non-uniqueness of the optimal weights, and also since the values of the network weights are not directly related to the system's physical properties. Therefore, Hung and Kao develop the partial derivative form of the ANN, such that the NSIN results in partial derivatives of the outputs.

The second component is the ANN or neural damage detection network (NDDN) used to identify the location and extent of the structural damage. The NDDN is trained to recognize the partial derivatives of the outputs with respect to the inputs of NSINs that identify the structure in undamaged as well as various damaged states by assuming that

some a priori information about the system is available. The output of the NSIN is used as the input to the NDDN.

Numerical simulation of the approach is conducted using a single degree of freedom structure and a 5 story shear building to demonstrate the feasibility of the approach. With damage in the applications defined as a decrease in stiffness or damping. The application to the 5-story shear building shows good correlation between the predicted stiffness loss and location as compared to the numerically simulated damage. The methodology is also observed to be able to detect damage scenarios for which it has not been specifically trained.

4.5.2   *Genetic Algorithms*

Genetic algorithms (GA) have been introduced for solution of optimization problems as an effective means for exploring a large complex space in an adaptive way, with general rules following biological evolution mechanisms of reproduction, crossover, and mutation (Adeli and Hung, 1995). GA is a search method based on Darwin's theory of evolution and survival of the fittest. Darwin's theory of natural selection is that "…any being, if it vary slightly in any manner profitable to itself…will have a better chance of surviving" (Chou, and Ghaboussi, 2001). Solution of an optimization problem by GA requires five components (Adeli and Hung, 1995):

(1) *Encoding.* This is the process where the decision variables of the optimization problem are assigned in a string of binary digits (1's and 0's) called a chromosome, i.e. if there are *m* decision variables and each decision variable is encoded in an *n*-digit binary number, then a chromosome is a string of $n \times m$ binary digits.

(2) *Evaluation or objective function*. The objective function evaluates the given decision variables and return a value. The value of the chromosome's objective function determines the fitness of that chromosome. The fitness value establishes the probability that a chromosome will be selected as a parent and reproduces, i.e. generate new chromosomes.

(3) *Initialization of the population.* An appropriate initialization methodology for the chromosome population is selected depending on the application. Typically, initialization of the chromosome population is a random process.

(4) *A set of operators to perform evolution between two consecutive chromosome populations*. GA simulates the process of natural selection for parent selection, selecting chromosomes to create a new generation, where the fittest members reproduce most often. Following the parent selection, the crossover process is applied to recombine two chromosomes and generate two new chromosomes when a random value associated to this pair is greater than a predefined crossover rate. The crossover operation is followed by a one-point mutation, which alters one bit in the string (chromosome) when a random value between 0 and 1, associated to that bit is greater than the predefined mutation rate.

(5) Working parameters. The working parameters are a set of predefined parameters, which guide the GA, such as the length of the decision variable encoded as a binary string, the number of chromosomes generated and operated in each generation, the crossover rate, mutation rate, and the stopping criterion. The crossover and mutation rates are assigned as real numbers between 0 and 1. The stopping criterion is a predefined number such as the number of iterations or a tolerance value for the objective function.

A flow chart of the genetic search procedure is shown in the figure below (Mares and Surace, 1996) followed by a review of several damage detection methodologies using GA as the search algorithm for optimization of the defined objective function.
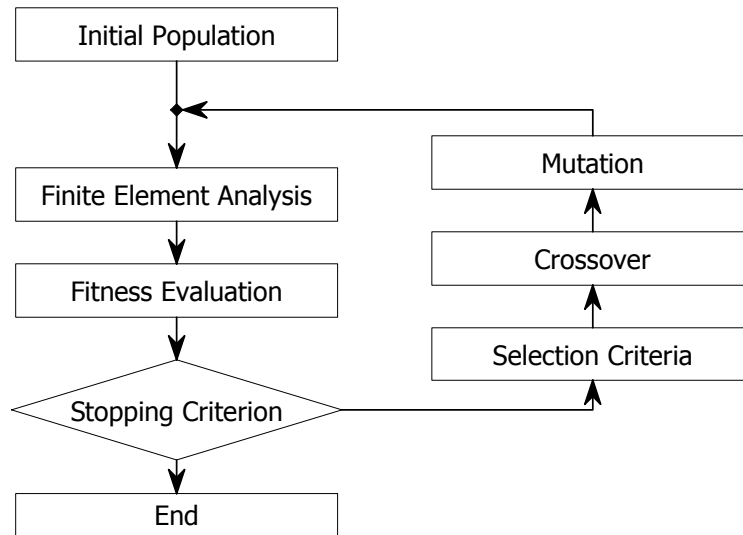
Figure 4.5. Flowchart of Optimization by Genetic Algorithm

Chou and Ghaboussi (2001) utilize static displacement measurements for structural damage detection posed as an optimization problem solving for unknown stiffness variables of the structure. GA is employed here so as to find the best-fit solution of the unknown stiffness parameters. The optimization problem for single and multiple loading conditions is shown below,

$$\mathbf{As} = \mathbf{p} \cdot \mathbf{a} \qquad \begin{bmatrix} \mathbf{A}_1 \\ \mathbf{A}_2 \\ \vdots \\ \mathbf{A}_{nlc} \end{bmatrix} \mathbf{s} = \begin{Bmatrix} (\mathbf{p}-\mathbf{a})_1 \\ (\mathbf{p}-\mathbf{a})_2 \\ \vdots \\ (\mathbf{p}-\mathbf{a})_{nlc} \end{Bmatrix}$$

where $\mathbf{A}$ is the matrix of element force components; $\mathbf{p}$ is the load vector; $\mathbf{a}$ is the element force component times a known stiffness variable. The above formulation cannot be solved directly since the number of unknowns is greater than the number of equations. Also, matrix $\mathbf{A}$ cannot be fully populated due to insufficient number of measured displacements. Chou and Ghaboussi propose two methods implementing GA to evaluate

the unknown stiffness parameters of the structure. The first method uses the different between measured displacements and the computed displacements is minimized using GA; the fitness function is shown below,

$$f = \left[\sum_j \prod_i \left(1 + \left| \frac{u_{ij} - u_{ij}^m}{u_{ij}^m} \right| \right)^{p_1} \right]^{-p_2}$$

where the superscript m, denotes the measured response; u_{ij} is the displacement at the ith degree of freedom under the jth load condition, and it is computed from the finite element model; u_{ij}^m is the corresponding measured displacement; p_1 and p_2 are used to magnify differences among the strings; Chou and Ghaboussi select $p_1 = p_2 = 2$.

The second method was developed to avoid solving the system of equation in finite element analyses needed for the fitness evaluation in the first method. Here, the unmeasured displacement and material properties are encoded in GA strings and allow the correct values of the unmeasured displacements evolve during the process of GA. The entire displacement vector becomes available, both measured and unmeasured displacements decoded from the GA. The displacement vector is used to determine a residual force vector **R**,

$$\mathbf{R} = \mathbf{Ku} \text{-} \mathbf{p}$$

which is used to determine the fitness function shown below.

$$f = \left[\sum_j \prod_i \left(1 + \left| \frac{u_{ij} - u_{ij}^m}{u_{ij}^m} \right| \right)^{p_1} \left(1 + \frac{|R_{ij}|}{\|p_j\|_2} \right)^{p_2} \right]^{-p_3}$$

where R_{ij} is the computed residual force at the ith degree of freedom in the jth load condition; $\|p_j\|_2$ is the Euclidean norm of the jth load; ; p_1, p_2, and p_3, are used to magnify differences among the strings; Chou and Ghaboussi select $p_1 = p_2 = p_3 = 2$.

Application of the method is conducted for numerically simulated damage on a plane truss structure. The application shows the ability to identify and detect damage, with the second proposed methodology shown to be more robust when multiple damage locations occur. A second application is provided for numerically simulated damage on a plane truss bridge structure. The effect of noise on the methodologies affects the severity estimation of damage by increasing the scatter; however, the damage location is still correctly identified.

Mares and Surace (1996) formulate an objective function for GA using stiffness reduction factors as parameters. The objective function incorporates a residual forces vector, which is formulated considering the stiffness of the damaged structure as opposed to the stiffness of the undamaged structure. The residual force is determined as a sum of three parts: 1) the identification error, **e**; 2) the residue vector associated with the structural damage **R′**; 3) vector associated with an inaccurate mathematical model of the undamaged structure, **f**.

$$\mathbf{R}^{err} = \left[\left(\mathbf{K} + \Delta\mathbf{K} \right) - \hat{\lambda}_d \mathbf{M} \right] \hat{\mathbf{\Phi}}_d$$

$$= \left[\left(\mathbf{K}_d + \sum_{i=1}^{m} \alpha_i \mathbf{K}_i + \Delta\mathbf{K} \right) - \hat{\lambda}_d \mathbf{M} \right] \hat{\mathbf{\Phi}}_d$$

$$= \left[\mathbf{K}_d - \hat{\lambda}_d \mathbf{M} \right] \hat{\mathbf{\Phi}}_d + \sum_{i=1}^{m} \alpha_i \mathbf{K}_i \hat{\mathbf{\Phi}}_d + \Delta\mathbf{K}\hat{\mathbf{\Phi}}_d = \mathbf{e} + \mathbf{R}' + \mathbf{f}$$

where, $\mathbf{R}^{err}$, is the residual force in terms of the identification, damage, and modeling; $\mathbf{K}$ is the original stiffness matrix; $\Delta\mathbf{K}$ is the error in the original stiffness matrix; $\mathbf{M}$, is the system mass matrix; $\hat{\lambda}_d$ and $\hat{\mathbf{\Phi}}_d$ are the eigenvalue and eigenvector including the identification error; α_i are the stiffness reduction factors. Mares and Surace question the assumption of the traditional method of residual force vectors that the residual forces can be applied to detect damage as long as the uncertainties of the identification error is not large. As part of the optimization problem using GA, the objective function is defined considering the residual force term differentiating the errors in modeling, damage, and identification. The objective function to be maximized is provided below,

$$J_{obj}\left(\beta_1^*, ..., \beta_i^*, ... \right) = \frac{c_1}{\sum_{j=1}^{r} \mathbf{R}_j^* \left(\beta_1^*, ..., \beta_i^*, ... \right)^T \mathbf{R}_j^* \left(\beta_1^*, ..., \beta_i^*, ... \right) + c_2}$$

where c_1, represents a constant used to control the value of the objective function; c_2 represents a constraint used to build a well defined function for the ideal case; represents the number of modes taken into consideration; $\mathbf{R}_j^*$ is the generalized residual force for each mode j, given by

$$\mathbf{R}_j^* = \sum_{i=1}^{m} \beta_i^* \mathbf{K}_i \mathbf{\Phi}_{dj} - \lambda_{dj} \mathbf{M} \mathbf{\Phi}_{dj} = \mathbf{K}^* \mathbf{\Phi}_{dj} - \lambda_{dj} \mathbf{M} \mathbf{\Phi}_{dj}$$

β_i^* are a set of parameters that are allowed to evolve during the GA optimization procedure. If the model is absent of initial errors and the identified eigenvalues and eigenvectors are not affected by experimental errors, when each of the structural parameters β_i^* has the same values as the counterpart in its set of parameters β_i from the damaged case, the generalized residual force becomes zero and the objective function is maximize. A numerical simulation of a five bay truss structure and cantilever beam is conducted to evaluate the methodology in the presence of noise and reduced measurements. The best results for damage detection and quantification require a minimum of 10 modes for the truss and 8 modes, with the damage detection procedure compromised with a decrease in the number of the modes. Introduction of noise at 5% reduces the precision of damage detection although location is identified.

Hao and Xia (2002) present a structural damage detection approach minimizing the objective function using a genetic algorithm with real number encoding. The objective function of the algorithm compares changes of the measured modal parameters, namely frequencies and mode shapes, from the undamaged and damaged structure with those of the analytical model before and after updating. Versatility is achieved in the methodology since a precise model of the structure is not necessary. The damage detection strategy compares the measured vibration data before and after damage and

updates a finite element model of the structure such that its changes in vibration properties are approximately equal to changes observed in the measured vibration data due to structural damage. The objective function of the GA is to minimize,

$$J = \left\| W \left\{ \Delta V^A \left(\{\alpha\} \right) - \Delta V^E \right\} \right\|^2$$

$$= \left\{ \Delta V^A \left(\{\alpha\} \right) - \Delta V^E \right\}^{\mathrm{T}} \mathbf{W}^2 \left\{ \Delta V^A \left(\{\alpha\} \right) - \Delta V^E \right\}$$

where, $\|\bullet\|$ denotes the Frobenius norm; $\mathbf{W}$ is a diagonal positive definite matrix of the weight for each term; ΔV represents changes in the vibration data; $\{\alpha\}$ is a vector of stiffness reduction factors; the superscripts A and E represent the analytical and experimental data, respectively. Modifications to the objective function are conducted in terms of the modal parameter used. Hao and Xia implement the objective functions for frequency measurements, mode shapes, and a combination of frequencies and mode shapes for purposes of damage detection. The goal is to estimate the stiffness reduction factor for each element, $\{\alpha\}$, so that the objective function is minimized; however, in GA the aim is to always increase the fitness so the minimization problem is converted into a maximization problem by defining the fitness as a large number subtracted by the initial objective function.

The damage detection method is applied to a laboratory tested aluminum cantilever beam and frame. Damage was introduced to the structure by a saw cut at one location for a severe damage case, with successful identification of damage location; however, false-positive indications of damage were observed due to measurement noise and nonlinearity. Although not addressed by the authors, the stiffness reduction factor tends to underestimate the severity of the damaged element showing an stiffness reduction of approximately 50% while the section was weakened 93.75%. In the frame examples, multiple damage locations are introduced to the structure. The combined use of frequency and mode shape measurements provide for damage localization; however, the methodology is highly dependent on the weights per contribution of the frequency and mode shape measurements. The methodology is unable to accurately estimate damage severity in the structure.

4.6 Other Methods

4.6.1 Time History Analysis

Fugate, et al. (2001) present a damage detection methodology implementing statistical process control methods to vibration-based damage detection methods. Development of a statistical model is effective in analyzing extracted features to determine if a statistically significant change in the behavior of the structure has occurred. Here statistical process control (SPC) is applied to vibration measurements by determining the distribution with associated mean, μ, and variance, σ^2, of acceleration measurements. The idea being that as the structure is damaged the mean, the variance, or both may change. The implementation of SPC provides a framework for monitoring future acceleration measurements and for identifying new data that is inconsistent with past

data. The damage detection strategy requires the use of quality control charts to monitor the mean, the variance or some other function of the acceleration measurements.

Assuming the mean and standard deviation are known, a control chart is constructed with a line at the mean, μ, and two more lines with representing the upper and lower control limits, $\mu + k\sigma$ and $\mu - k\sigma$, respectively. The number k is selected such that when the structure is in good condition a large percentage of observations lie within the control limits. However, in practice acceleration measurements are typically autocorrelated, thus the implementation of an autoregressive[+] model (AR) to the time history data is implemented in order to develop control charts from the residuals of the fitted AR model. If the fitted AR model is approximately correct, the residuals from the fit are sufficiently uncorrelated with no systematic pattern.

For autocorrelated data, an X-bar control chart is appropriate to determine if any significant changes in the structure have occurred. The X-bar control chart requires the formation of subgroups of size, n; the sample mean within each subgroup is then calculated and charted. The centerline of this control chart is the mean, μ, with the standard deviation of the charted values equal to $\sigma / \sqrt{n}$. The control limits are placed at $\mu \pm k\sigma / \sqrt{n}$.

The vibration damage detection problem is presented in the context of statistical pattern recognition to evaluate the occurrence of some change in the structure (Fugate, et al., 2001). However, the methodology presented is limited to evaluating whether or not a change in the behavior of the structure has occurred. Whether or not that change in the vibration properties is due to damage or other change in the structure and environment (i.e., change in mass, boundary condition, weather, etc.) is indiscernible. The location of damage is not identified nor the severity of damage determined. The appeal in SPC is realized in long term health monitoring; as the feature of interest is selected, future observations can be monitored to see if the feature distribution has exhibited any significant change to warrant an inspection. The methodology is applied to a laboratory tested reinforced concrete column with outliers occurring as the structure is damaged.

4.6.2 *Frequency Response Function based Damage Detection*

As part of the frequency response function (FRF) curvature method utilizing modal parameters, Sampaio et al. (1999), provide the definition of damage as a change in stiffness, where damage is generally measured from changes to one of its dynamic properties of mass, stiffness, or damping. Sampaio et al, assume damage to be a first order approximation such that the mass of the structure remains unchanged and thus is a negligible dynamic property of the structure. In addition, changes to damping characteristics of the structure from damage are also ignored. The assumptions specified

---

[+] Autoregressive (AR) models are used to model a stationary time series. The current value of the time series is a linear combination of the p most recent past values of itself plus an error term , which incorporates everything new in the series at time t that is not explained by the past values. In simple terms, AR models utilize the statistical properties of the past behavior of a variable at some time, t, to predict its behavior in the future.

for the FRF curvature method are intended to observe the structural behavior through the stiffness parameters of the FRF's.

The FRF curvature method presented by Sampaio, et al. is an extension of the mode shape curvature method by Pandy, et al. (1991) to all frequencies in the measurement range, i.e. using FRF data instead of limiting observations to mode shapes. A central difference approximation is applied to determine the curvature for each frequency by the following equation,

$$\alpha''(\omega)_{i,j} = \frac{\alpha(\omega)_{i+1,j} - 2\alpha(\omega)_{i,j} + \alpha(\omega)_{i-1,j}}{h^2}$$

Where, $\alpha_{i,j}$, is the receptance FRF measured at location i for a force input at location j and h is the distance between measured points $i+1$ and $i-1$. The absolute difference between the FRF curvature of the damage and undamaged structure at location i along the chosen frequency range is calculated, for an applied force at point j, by

$$\Delta\alpha''_{i,j} = \sum_{\omega}\left|\alpha''_d(\omega)_{i,j} - \alpha''(\omega)_{i,j}\right|$$

For several force location cases, the FRF curvature differences are summed directly.

$$S_i = \sum_{j}\Delta\alpha''_{i,j}$$

The FRF curvature method proposed by Sampaio et al., utilizes the mode shape curvature method combined with a summation approach for multiple force locations. There are no significant differences between the FRF curvature method and mode shape curvature method in terms of method of formulation. The primary advantage of the FRF curvature method is that once the FRF's are evaluated via a Fourier transform from the time history response record, individual modes are not required to determine the presence of damage in the system. However, the authors observe a decrease in reliability of detecting damage and estimating damage severity as the range of frequencies is increased in the damage detection process.

Several laboratory-controlled examples are used to generate data and provide a comparison at a simplified level to mode shape based methods for damage detection. In accordance with the work performed by Farrar and Jaruegui (1998a, 1998b) on the I-40 bridge over the Rio Grande, an analysis is performed on the bridge deck data. In summary the FRF method was unable to detect damage, for the first three damage levels, although damage was identified for the most severe damage scenario.

4.7   Monitoring of FRP Rehabilitated Structures

4.7.1   *Strategy for Health Monitoring of FRP Rehabilitated Bridge Systems*

Health monitoring of FRP rehabilitated bridge structures requires three levels of interrogation, the materials level, components level, and systems level. The materials level of investigation involves standardized tests of composite materials used for quality assurance and durability estimation by means of tension tests, test for interlaminar shear strength by short beam method, three point bending for flexural properties, moisture

absorption, and determination of glass transition temperature with materials exposed to various environmental conditions. The components level inspection assesses defects and their respective effects to the rehabilitation and influence on the performance of the rehabilitated bridge structure. Here local NDE methods are employed such as ultrasonic testing, thermography, and shearography in conjunction with a visual inspection and acoustic impact or "tap" testing of the FRP rehabilitation. At the systems level, a global NDE procedure is utilized to evaluate the overall structural capacity and identify local damage areas for the components level inspection. The objective of the systems level inspection is three fold,

1) Evaluate the global structure to determine the current performance level of the structure and effectiveness of rehabilitation

2) Identify locations and estimate severity of damage for purposes of further interrogation using local NDE techniques

3) Validate global system performance prediction. Where the prediction is based upon results of the components and materials level investigation.

The systems level phase of the health monitoring strategy is essential in incorporating the impact of materials degradation and defects to the performance of the FRP rehabilitated bridge structure and determining the existing state of the bridge relative to predictions.

Unfortunately, most proposed damage detection strategies rarely display these three stages of validation and few contain field applications reflecting the intended level of nondestructive evaluation (i.e., Level 1, 2, 3, or 4). In Table 4-3, the advantages and disadvantages of features for damage detection reviewed in this report are described. These global NDE algorithms are developed with the intent to identify changes in a system regardless of improvement or degradation. Since degradation is a more critical aspect to the safety of structures, the severity of damage is typically estimated by defining damage as a loss in stiffness with the inherent assumption that damage affecting the performance of a structure is realized by losses in stiffness.

Table 4-3. Advantages and Disadvantages of Damage Detection Strategies

Technique	Advantages	Disadvantages
Frequencies	• Capable of damage identification • Simplest derived modal parameter	• No spatial information provided by frequency measurements • Qualitative damage severity estimation • Low sensitivity to damage
Mode Shapes	• Contains spatially related information, thus damage location is readily available	• Large number of measurement locations required to accurately characterize mode shapes
Matrix Update Methods (Matrix Optimization)	• Resolving system matrix provides damage location and severity	• Most precise solution is an approximation since all modes of a structure cannot be measured
Artificial Neural Networks	• Able to solve complex problems difficult to model and explain by classical mathematics • Flexibility available in feature used for damage detection	• Uncertainty in assigning weights to connections between layers • Training of networks requires prior knowledge of damage mechanisms in the system • Potential convergence instability with large quantities of data
Genetic Algorithms	• Capable of solving large complex problems for optimal solutions • Optimization begins from a population unlike traditional methods which initiate from a single point • Operates in the presence of uncertainty and insufficient information	• Dependent on validity of the objective function • Appropriate size of population, crossover rate, and mutation rate not clearly defined for structural problems

4.7.2   Damage Detection Summaries

In the following section, the damage detection methods reviewed in this report are compared in tabular form with an investigation into the positive and negative aspects displayed during the validation portion of each method, (i.e., if consideration for signal noise or reduced measurements exists, use of field measured data, classification level of the global damage detection procedure, etc.).

Although, no specific damage detection procedure displays a significant advantage over their respective counterparts, it is observed that those methods utilizing mode shapes are the most developed in terms of displaying the ability to identify, locate, and estimate the severity of damage. In particular, the method by Stubbs, et al. (2000, 1996) is arguably the most developed methodology available for damage detection with several field applications verified and third party reviews conducted on the quality of the methodology (Barroso and Rodriguez, 2004; Farrar and Jauregui, 1998a, 1998b; Wang et al., 2000). In

addition, it is the only reviewed methodology, which applies a statistical model to determine if its condition indicator or damage index is significant, in addition to relating the quantified damage to the reliability or probability of failure of the system. However, given its applications and advantages, the minimum required amount of measurements and effect of signal noise is not addressed; nor has the application of the system reliability evaluation procedure been validated on real structures.

It is important to note, a number of methodologies that have been reviewed in this chapter demonstrate the ability to identify, locate, and estimate the severity of damage in structures using numerical simulations. However, the absence of field validations detracts from their performance due to signal noise thus limiting their potential for damage detection of FRP rehabilitated bridge structures. Machine learning techniques continue to receive a significant amount of research in the area of structural damage detection also showing ability to identify, locate, and estimate damage severity; however, training of the network or quantity of input information necessary for GA and ANN are still unresolved issues with no methods demonstrating robustness with field measured data.

Table 4-4. Frequency Based Damage Detection Methodologies

Method	Positive Aspects	Negative Aspects
Bicanic and Chen (1997)	• Back calculation of mode shapes • Frequencies only for damage localization	• Unable to identify or locate damage with signal noise levels of 0.5% and 2.0% • No validation with field structure • No examination with reduced measurements
Contursi, Williams, and Messina (1997, 1997, 1998, 1998)	• Capable of damage identification and localization with frequencies alone	• Requires 10 to 15 modes for accurate damage detection • Computationally expensive • No examination of signal noise • No validation with field structure
Hassiotis (2000) Hassiotis and Jeong (1995)	• Only frequencies required to evaluate stiffness matrix of the system • Capable of damage identification and localization • Able to identify damage with 0.8% signal noise	• Unable to determine damage severity of structure • Stiffness matrix remains incomplete • Dependent on the number of sensors and sensor locations (i.e., requires large amount of data for improved accuracy) • No validation with real structures
Ray and Tian (1999)	• Increased frequency sensitivity to damage by change in control gain • Capable of damage identification	• Tailored to smart structures, not applicable to existing structures • Sensitivity to damage dependent on vicinity of sensor and actuator • No validation with real structures

Table 4-5. Damage Detection Utilizing Mode Shapes

Method	Positive Aspects	Negative Aspects
Law, Shi, and Zhang (2000, 1998, 1998)	- Capable of identifying, locating, and quantifying damage - Contains modal expansion procedure addressing reduced measurements - Able to expand additional modes from 2-3 experimentally measured modes	- Presence of signal noise results in severity estimate errors from 0% to 30%. - No field evaluation on bridge structure
Stubbs et al. (2000) Stubbs and Park (1996)	- Capable of identifying, locating, and quantifying damage - Applies statistical model (hypothesis testing) to differentiate between damaged and undamaged areas - Damage characterization using individual mode shapes - Field application and verification of methodology on reinforced concrete bridge structures - Procedure for acquiring baseline modal properties of existing structure - Method for evaluation of system reliability - Most developed and applied damage detection procedure	- Dependent on experimentally calibrated numerical model - Valid only for damage severity levels up to 30% - Effect of signal noise or not explicitly addressed - No definition of required minimum number of mode shapes for accurate damage characterization
Kim and Stubbs (2002)	- Capable of identifying, locating, and quantifying damage - Able to use individual mode shapes - Damage located and sized without need to solve system of equations - Improved approximation of damage severity compared to previous method	- No field validation studies - Presence of signal noise not addressed - No definition as to minimum number of mode shapes for accurate damage characterization

Table 4-6. System Matrix Based Damage Detection Methodologies

Method	Positive Aspects	Negative Aspects
Abdalla et al. (1998)	• Capable of identifying and locating damage	• Unreliable severity estimations with errors between 5% and 30% • Presence of signal noise not addressed • Susceptible to inaccuracies with reduced measurements • No field validation studies
Escobar et al. (2001)	• Transformation to rigid body modes reduces computational costs • Capable of identifying, locating, and quantifying damage	• Increases in signal noise results in increase of severity estimate • Accurate damage detection requires a minimum of 8 modes • Decrease in damage severity estimate with decrease in number of measured modes • Assumes stiffness matrix of structure is readily available from analytical model • No field evaluation studies
Sivico et al. (1997)	• Capable of identifying, locating, and quantifying damage • Evaluates changes in damping	• Computationally expensive • Minimum detectable reduction in stiffness and/or damping is 10% • Number of actuators or multiple single input systems must be same as degrees of freedom in problem • No field evaluation studies
Park and Reich	• Capable of damage identification, localization and quantification • Flexibility determined directly from modal identification procedure, no addition computation necessary • Identification and localization of damage using field data • High eigenvalues in flexibility base methods correspond to dominate, measureable low frequency modes • Greater sensitivity to damage	• Does not address the effects of signal noise and reduced measurements • No severity validation provided from field data application

Table 4-7. Damage Detection Utilizing Artificial Neural Networks

Method	Positive Aspects	Negative Aspects
Zang and Imgruen (2001, 2001)	• Capable of identifying and locating damage • Damage localization in the presence of 5% signal noise • FRF data reduction to reduce computational costs	• Unable to estimate damage severity • Increasing the number of principal components in analysis does not improve results because of increased susceptibility to signal noise
Barai and Pandey (1997)	• Capable of damage identification • TDNN procedure capable of identification with incomplete information • Application to numerically simulated steel bridge	• Incapable of damage localization or severity estimation
Hung and Kao (2002)	• Use neural network for system identification approach to acquire characteristics of undamaged and damaged states of structure • Capable of damage identification and localization • Able to detect damage scenarios for which specific training has not been implemented	• Systems identification requires displacement, velocity, and acceleration in addition to quantification of input source • In capable of severity estimation • Signal noise and reduce measurements not addressed

Table 4-8. Damage Detection Utilizing Genetic Algorithms

Method	Positive Aspects	Negative Aspects
Chou and Ghaboussi (2001)	• Capable of damage identification and localization • Does not require solving system of equations in finite element method • Uses measured displacements without the need for additional processing	• Increase in signal noise increase scatter of severity estimation • No application to real structures
Mares and Surace (1996)	• Capable of damage identification, localization and quantification • Successful damage identification and localization in 5% signal noise	• Damage severity estimation requires 8-10 modes of structure • No application to real structures
Hao and Xia (2002)	• Flexibility in terms of accuracy of FEM • Capable of damage identification, localization, and quantification	• Signal noise in measurements results in false-positive indications • Underestimates damage severity • Weighting factors for contribution of frequencies and mode shape measurements not clearly defined

Table 4-9. Other Damage Detection Methodologies

Method	Positive Aspects	Negative Aspects
Fugate et al., (Time History Analysis) (2001)	• Uses time history data to determine damage presence, requires no additional processing • Statistics used as indicators of change to structure	• Incapable of damage localization or severity estimation • Does not detect damage, rather identifies only a change in the structural behavior
Sampaio, et al. (1999)	• Uses FRF data directly from structure's dynamic test	• Decrease in reliability of damage identification, localization and severity estimation as range of frequencies is increased • Low sensitivity to damage

4.8   Summary

In the this chapter an overview of current damage detection algorithms is presented in the context of health monitoring of structural systems. Damage detection methods examining changes in modal parameters, specifically natural frequencies and mode shapes are presented. In addition optimization methods for the stiffness matrix of the structure are investigated with a methodology for dynamically measured flexibility matrix also reviewed. Due to the complexity of large civil structures and susceptibility of measured modal data to signal noise, damage detection algorithms in the form of optimization problems and decision-making programs have evolved employing machine learning techniques, namely genetic algorithms and artificial neural networks. Other available methods include examination of time histories and frequency response functions, which avoid the need for experimental modal analysis to extract modal parameters from vibration test data. The shear volume of damage detection algorithms makes it difficult to include all literature addressing damage detection of structural systems using vibration properties.

Depending on the vibration properties and tools available for structural health monitoring, appropriate damage detection is critical to the level and quality of evaluation conducted on the structure. Important considerations when selecting damage detection methodologies are the following:

1. Level of damage detection desired: Level 1, Level 2, Level 3, or Level 4. Currently no damage detection methodologies have been observed in literature, which incorporate a strategy for evaluation of the remaining useful life of the structure.

2. Demonstrated capability of the damage detection level via numerical simulation in the presence of signal noise and reduced measurements.

3. Demonstrated capability of the damage detection level via experimental validation in the laboratory in the presence of signal noise and reduced measurements

4. Validation of the damage detection algorithm to field data of large civil structures.

Based on the above criteria and an evaluation of the advantages and disadvantages of the reviewed techniques, the damage detection algorithm by Stubbs et al. (2000) is selected as the most suitable damage detection because of its demonstrated capability with bridges and more importantly, the authors suggest the applicability of the measured changes in the structure to a means to evaluate its performance.

In the following chapter, the Watson Wash Bridge structure is introduced and the state of the structure is characterized. Specifically, the development of longitudinal and transverse cracking patterns is evaluated and an analysis of the deck slab is conducted to determine if any reinforcement deficiencies exist.

5   WATSON WASH BRIDGE

5.1   INTRODUCTION

In Chapters 2 thru 4, reviews of FRP composite rehabilitation, dynamic testing of bridges, and vibration based damage detection detailed the state-of-the-art. The review of vibration based damage detection methods in Chapter 4 was also used to select a proven methodology for monitoring bridge structures. A global NDE procedure is necessary to assess the condition of the bridge prior to FRP composite rehabilitation, as well as to continuously monitor the structure during service. The damage index algorithm and its severity estimation proved to be the best available technique based upon the following criteria: (1) Level of NDE Technique (i.e. Level I, II, III, or IV); (2) Proven application to bridge structures; (3) adaptability of the approach to bridge reliability.

In Chapter 5, the development and application of methodologies for bridge life extension and monitoring begins. A representative reinforced concrete T-girder bridge structure, the Watson Wash Bridge, is used to demonstrate methodologies for bridge life extension and monitoring. Prior to application of methodologies for bridge life extension and monitoring, the need to perform such actions must be established with characterization of the existing state of the structure by visual inspection and analysis. Therefore the objective of Chapter 5 is to establish the need for bridge life extension and monitoring of the Watson Wash Bridge.

The objective of Chapter 5 is accomplished with the following five tasks: first, the Watson Wash Bridge and its existing damage state are described to provide background regarding the state of the structure; second, the deck slab design is evaluated with respect to Caltrans Bridge Design Specifications to determine if any reinforcement deficiencies exist with respect to HS20 (71.2 KN, 16 kips) and Permit truck (106.8 KN, 24 kips) wheel loads; third, an analysis of the deck slab is conducted to calculate the minimum reinforcement required to prevent the occurrence of punching shear failure; fourth, prior monitoring activities of the structure are reviewed; fifth, the rationale for FRP composite rehabilitation of the Watson Wash Bridge deck is expressed.

5.2   Watson Wash Bridge

The Watson Wash Bridge is a reinforced concrete T-girder bridge located on California Interstate 40, approximately 10.3 KM (6.4 miles) east of Essex Road in the Mojave Desert. Figure 5.1 shows a map identifying the location of the bridge structure. Figure 5.2 shows a photograph of the bridge structure.

Figure 5.1. Map of Watson Wash Bridge Location

Figure 5.2. Watson Wash Bridge

Figure 5.3 provides an overview of the spans and bays of the bridge structure. The superstructure consists of a cast-in-place reinforced-concrete deck and girder structural system with sixteen 12.8 m (42 ft) central spans and two shorter spans of 10.52 m (34.5 ft) at each abutment. The 15.6 cm (6-1/8 inches) thick deck spans transversely across six girders at 2.13 m (7 ft) centers. The bridge is built of 18 spans and five bays within each span. The bridge is composed of five frames connected with shear transfer hinges. All monitoring and rehabilitation activities are conducted in the center frame, Frame S-3, composed of spans 8 through 12 (Figure 5.3).
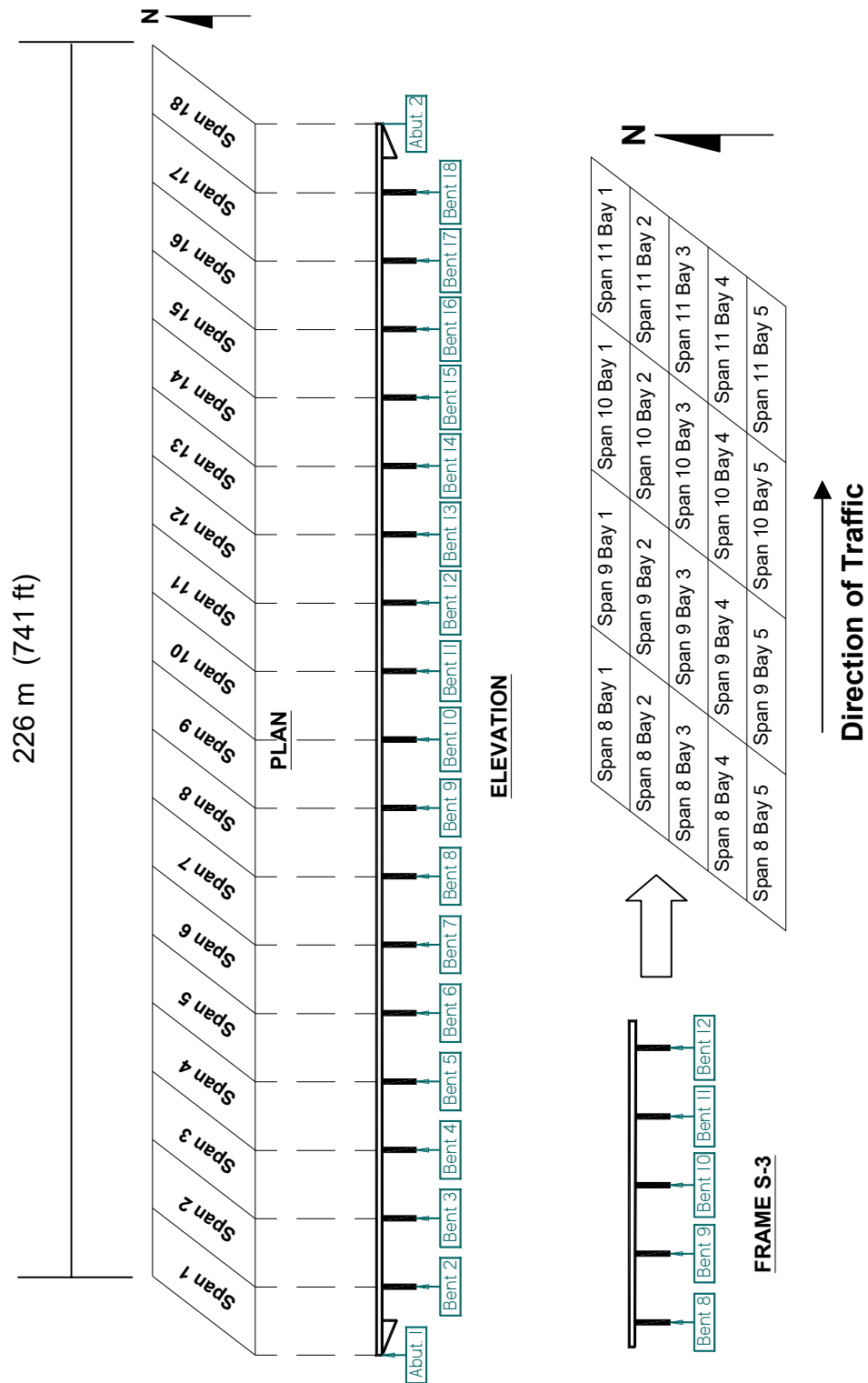
Figure 5.3. Overview of Watson Wash Bridge and Frame S-3
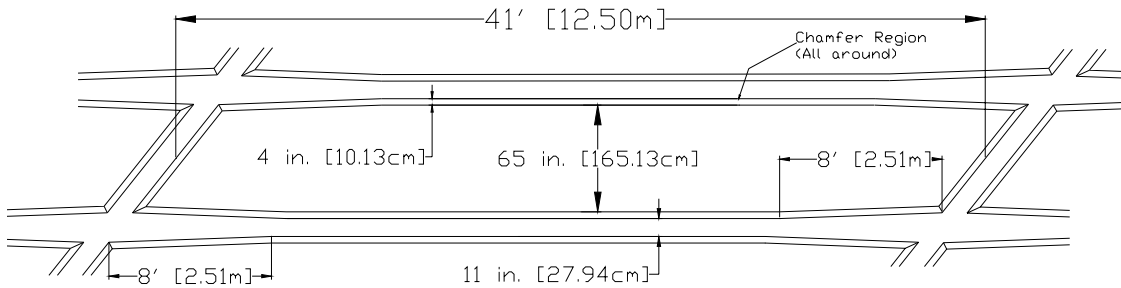
Figure 5.4. Typical Interior Bay of Watson Wash Bridge
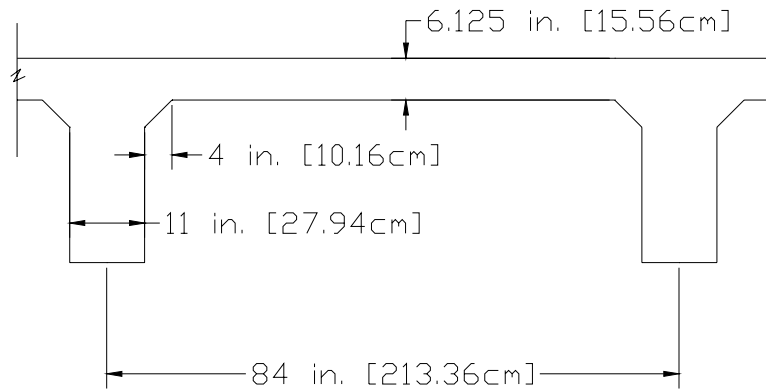
Figure 5.5. Typical Cross-Section of Bay

The T-girders are 0.76 m (2.5 ft) deep from top of the deck to the base of the girder, with a girder width of 28 cm (11 inches). The girders are tapered from 28 cm (11 inches) to 61 cm (24 inches) at the face of the bents. The effective slab width is 185.4 cm (6 ft. 1 inch).

5.2.1 Damage Characterization

Transverse reinforcement is provided in the bridge deck at approximately 12.7 to 15.24 cm in the form of No. 5 rebar (d_{bar} =15.875 mm). While six No. 5 rebar (d_{bar} =15.875 mm), evenly spaced in approximately the center four feet between girders, are prescribed at a spacing of approximately 24.38 cm (9.6 inches). This results in a longitudinal-to-transverse reinforcement ratio of approximately 50%.

A visual inspection of the Watson Wash Bridge reveals a significant number of transverse cracks in the soffit of the bridge deck. The spacing of these cracks is approximately 14 cm (5.5 inches) corresponding to the average spacing of the transverse reinforcement in the deck of the bridge. Figure 5.4 shows transverse cracking on the bridge deck soffit.

Significant amounts of transverse and longitudinal cracking exist near the center of Bay 4 of Frame S-3 which corresponds to the right wheel load of east bound traffic on the right lane of I-40 of the Watson Wash Bridge. The evenly spaced cracking in both directions

on the bridge soffit indicates the potential for punching shear failure exists. In Bay 4 of Span 8, Caltrans maintenance crews repaired a punching shear failure occurrence.

Longitudinal and transverse cracking behavior of the deck slab is a result of a lack of steel reinforcement and corrosion caused by aging, increased load demands, or combination thereof. Efflorescence on the bottom soffit of the Watson Wash Bridge decks shows signs of rust indicating corrosion of steel. Furthermore, the bridge design is based upon the code in place as of 1969; where, for instance, the existing girder depth of 0.76 m (2.5 ft) fails to meet the current Caltrans BDS (2004) minimum requirement of 0.83 m (2.73 ft) for a 12.5 m (42 ft) span.

Figure 5.6. Transverse Cracking on Bridge Deck Soffit with Efflorescence

Punching shear failures on the bridge deck are caused by the development of transverse and longitudinal crack resulting in a deck area unable to resist the shear force demands from the HS20 and Permit wheel load. Development of transverse cracks in the deck is the first stage of the deterioration process. Parallel transverse cracks on the bridge effectively reduce the bridge deck slab into a series of reinforced concrete beams normal to the direction of traffic. Consequently, longitudinal cracks begin to form creating the potential for punching shear failure in the bridge deck. Figure 5.7 provides an illustration of the cracking patterns leading to punching shear failure.

(a) Formation of Transverse Cracks   (b) Longitudinal Cracking   (c) Punching Shear Failure
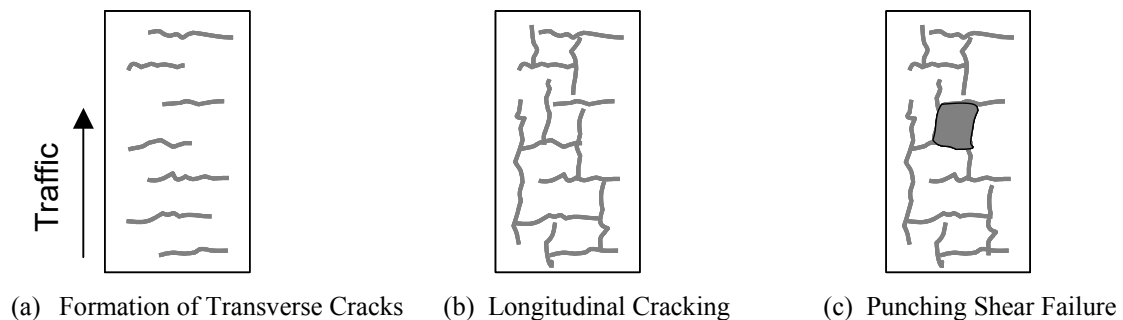
Figure 5.7. Flexural Cracking Patterns Leading to Punching Shear

5.3   Deck Slab Design

Design of the deck slab utilizing current code requirements provides a means to measure any reinforcement deficiencies with respect to current load conditions, namely the HS20 (71.2 KN, 16 kips) and permit truck (106.8 KN, 24 kips) wheel loads. The permit truck wheel load is considered since these trucks are known to traverse the bridge structure. In this section, deck slab design in accordance with Caltrans Bridge Design Specifications of 2004 is conducted. Updating the flexural reinforcement requirements for the Watson Wash Bridge deck slab to current Caltrans Bridge Design Specifications (BDS) assists in determining if any steel reinforcement deficiencies exist in the structure. The following calculations determine the flexural reinforcement requirements for a reinforced concrete deck of a T-girder bridge. For this deck slab design, units are first given in the FPS system per Caltrans BDS design procedure followed by SI units in parentheses.

5.3.1   Material Properties

The following material properties are used for the transverse deck slab design.

5.3.1.1   Concrete Compressive Strength, f'_c

$f'_c = 3,600$ psi (24.82 MPa)………………………per BDS Section 8.2

5.3.1.2   Concrete Modulus of Elasticity, E

$$E_c = w_c^{1.5} \cdot 33\sqrt{f'_c}$$ …………………………per BDS Section 8.7.1
$$E_c = 150^{1.5} \cdot 33\sqrt{3600} = 3,637 \text{ ksi (25.08 MPa)}$$

Concrete compressive strength and modulus are assumed at 3,600 psi (24.82 MPa) and 3,637 ksi (25.08 MPa), respectively.

5.3.1.3   Steel Properties

The steel reinforcement is based on a yield strength, f_y, of 60,000 psi (413.7 MPa) per BDS section 8.3.3 with a Young's modulus of 29,000 ksi (200 GPa) per BDS section 8.7.1.

5.3.2   Slab Geometry

The slab thickness, t_s, and longitudinal girder center-to-center spacing is 6-1/8 inches (15.56 cm) and 7 feet (2.13 m), respectively. Since the deck slab is built monolithic with its girders, the transverse distance between girders is defined as the clear span, or 73 inches (1.85 m) per Section 3.24.1.2 (a).

5.3.3   Load Criteria

5.3.3.1   Dead Load

The dead load is the sum of contributions from reinforced concrete and wearing surface on the bridge deck.

$$w_{DL} = t_s \times w_c + surface \qquad \textbf{Eqn. 5.1}$$

where, w_{DL}, is the dead load distributed load; t_s, thickness of the slab; w_c, normal weight concrete, 150 pcf (2.40 g/cc); *surface,* wearing surface on the top of the deck, 25 psf (1.2 KPa).

$$w_{DL} = \frac{6.125}{12} \cdot 150 + 25 = 101.56 \text{ psf (4.86 KPa)} \qquad \textbf{Eqn. 5.2}$$

The dead load moment is calculated by modeling a one foot (0.305 m) wide transverse segment of the slab. A continuity factor of 0.8, for moment redistribution, is applied for slabs, which are continuous over three or more supports, per BDS section 3.24.3.1.

$$M_{DL} = (0.8)\frac{w_{DL} \cdot S_{span}^2}{8} \qquad \textbf{Eqn. 5.3}$$

where, M_{DL}, is the dead load moment per foot width; S_{span}, is the clear span of the slab, 73 inches or 6.083 ft (1.85 m).

$$M_{DL} = (0.8)\frac{101.563 \cdot (6.083)^2}{8} = 375.85 \ \tfrac{lb\text{-}ft}{ft} \ \text{(1.68 KN-m/m)} \qquad \textbf{Eqn. 5.4}$$

5.3.3.2   Live Load

HS 20-44. The live load moment is calculated using the live load moment equation in section 3.24.3.1 of the Caltrans BDS. Live load moment is provided per foot width of the slab.

$$M_{LL} = \left(\frac{S_{span}+2}{32}\right) \cdot P \qquad \textbf{Eqn. 5.5}$$

where, M_{LL}, is the live load moment per foot width; S_{span}, is the clear span in feet, $6\tfrac{1}{12}$ feet (1.85 m); P, equal to 16 kips (71.2 KN) for transverse slabs (per Section 3.7.4)

$$M_{LL} = \left(\frac{6\tfrac{1}{12}+2}{32}\right) \cdot 16 = 4.04 \ \tfrac{kip\text{-}ft}{ft} \ \text{(18.1 KN-m/m)} \qquad \textbf{Eqn. 5.6}$$

For the live load moment an impact factor for trucks oscillating up and down while traveling across the bridge is required per BDS section 3.8.2.1 in addition to the continuity factor.

$$M_{LL} = (1.3)(0.8)4.04 = 4{,}203 \ \tfrac{lb\text{-}ft}{ft} \ \text{(18.84 KN-m/m)} \qquad \textbf{Eqn. 5.7}$$

The total moment demand for the HS 20-44 load condition is as follows.

$$M_{HS20} = 4{,}203 + 375.85 = 4{,}578.85 \ \tfrac{lb\text{-}ft}{ft} \ \text{(20.52 KN-m/m)} \quad \textbf{Eqn. 5.8}$$

Permit Truck Wheel Load. For a permit truck wheel load, P is equal to 24 kips, giving the following live load moment demand.

$$M_{LL} = \left(\frac{S+2}{32}\right) \cdot P = \left(\frac{6\frac{1}{12}+2}{32}\right) \cdot 24 = 6.06 \, \tfrac{\text{kip-ft}}{\text{ft}} \quad (27.16 \text{ KN-m/m}) \quad \textbf{Eqn. 5.9}$$

Applying the impact and continuity factors, the live load moment demand for a permit truck results in the following.

$$M_{LL} = (1.3)(0.8)6.06 = 6,305.35 \, \tfrac{\text{lb-ft}}{\text{ft}} \quad (28.26 \text{ KN-m/m}) \qquad \textbf{Eqn. 5.10}$$

The total moment demand for the permit truck load condition is given below.

$$M_{Total} = 6305.35 + 375.85 = 6,680.85 \, \tfrac{\text{lb-ft}}{\text{ft}} \quad (29.95 \text{ KN-m/m}) \qquad \textbf{Eqn. 5.11}$$

5.3.4 Reinforcement Requirements

The required area of steel reinforcement is determined according to Service Load Design per BDS section 8.14.1.3. According to BDS section 8.15.2.1 the allowable stresses for the extreme compression fiber, $f_c = 0.4 f'_c$, for transversely reinforced deck slabs is 1,440 psi (9.93 MPa). The allowable stress in the steel reinforcement, f_s, for transversely reinforced deck slabs is 20,000 psi (137.89 MPa) per BDS section 8.15.2.2.

5.3.4.1 Existing Steel Distribution

The existing transverse steel reinforcement in the transverse deck slabs of Watson Wash Bridge are #5 rebar spaced at approximately 5.5 inches (14 cm) center to center. The longitudinal reinforcement consists of #5 rebar at a spacing of 9.6 inches (24.4 cm) center-to-center.

5.3.4.2 Existing Distribution Reinforcement Percentage

The existing ratio of distribution reinforcement is computed as follows. The area of transverse reinforcement per foot of the slab is 0.62 in^2 (4 cm^2). For the longitudinal distribution, the area per foot of slab is approximately 0.31 in^2 (2 cm^2), resulting in a reinforcement distribution ratio of 50 percent.

5.3.4.3 Required Steel Reinforcement for HS 20 Load

5.3.4.3.1 Transverse Steel Reinforcement Requirements

$$M_{HS20} = A_{sreq} f_s jd \rightarrow A_{sreq} \geq \frac{M_{HS20}}{f_s jd} \qquad \textbf{Eqn. 5.12}$$

where, M_{HS20}, is the total moment demand for the HS20 load condition as calculated in Section 5.3.3; A_{sreq}, is the required area of steel reinforcement to satisfy service conditions; f_s, is the allowable stress in the steel reinforcement; jd, is the lever arm of the section.

$$A_{sreq} \geq \frac{(4{,}578.85 \, \tfrac{\text{lb-ft}}{\text{ft}})(12 \, \tfrac{in}{ft})}{(20{,}000 \, \text{psi})(0.85)(6.125'' - 1'' - \tfrac{5}{8}'' \cdot \tfrac{1}{2})} = 0.67 \, \tfrac{in^2}{ft} \quad (14.2 \text{ cm}^2/\text{m}) \qquad \textbf{Eqn. 5.13}$$

5.3.4.3.2 Longitudinal Steel Reinforcement Requirements

The longitudinal steel reinforcement is determined using a longitudinal to transverse reinforcement area ratio per section Caltrans BDS 3.24.10.2.

$$\frac{A_{slong}}{A_{strans}} = \frac{220}{\sqrt{S_{span}}} \leq 67\,\% \qquad \textbf{Eqn. 5.14}$$

where, S_{span}, is the span length in feet.

A span length of 6.083 ft (1.85 m) results in a required longitudinal reinforcement ratio of 89%, therefore a reinforcement ratio must be selected that is less than the 67% allowable.

Matching the existing reinforcement distribution percentage of 50% in the Watson Wash Bridge deck slab results in the following steel requirement for the longitudinal reinforcement

$$A_{slong} = A_{stran}(0.5) = 0.67\,\tfrac{in^2}{ft}\cdot 0.5 = 0.34\,\tfrac{in^2}{ft}\,(7.2\text{ cm}^2/\text{m}) \qquad \textbf{Eqn. 5.15}$$

5.3.4.4   Required Steel Reinforcement for Permit Truck Load

5.3.4.4.1 Transverse Steel Reinforcement Requirements

$$M_{Permit} = A_{sreq}f_s jd \rightarrow A_{sreq} \geq \frac{M_{Permit}}{f_s jd} \qquad \textbf{Eqn. 5.16}$$

where, M_{Permit}, is the total moment demand for the Permit load condition as calculated in Section 5.3.3; A_{sreq}, is the required area of steel reinforcement to satisfy service conditions; f_s, is the allowable stress in the steel reinforcement; d, is the distance from the top of the slab to the center of steel reinforcement

$$A_{sreq} \geq \frac{(6680.85\,\tfrac{lb\text{-}ft}{ft})(12\,\tfrac{in}{ft})}{(20{,}000\text{ psi})(0.85)(6.125'' - 1'' - \tfrac{5}{8}''\cdot\tfrac{1}{2})} = 0.98\,\tfrac{in^2}{ft}\,(20.74\text{ cm}^2/\text{m}) \;\; \textbf{Eqn. 5.17}$$

5.3.4.4.2 Longitudinal Steel Reinforcement Requirements

As in the calculations with the HS20 loading, a span length of $6\tfrac{1}{12}$ feet (1.85 m) gives a percentage distribution of 89%. Matching the existing 50% reinforcement ratio in the Watson Wash Bridge deck results in the following steel requirement for the longitudinal reinforcement

$$A_{slong} = A_{stran}(0.5) = 0.98\,\tfrac{in^2}{ft}\cdot 0.5 = 0.49\,\tfrac{in^2}{ft}\,(10.37\text{ cm}^2/\text{m}) \qquad \textbf{Eqn. 5.18}$$

5.3.5   Shear Capacity

According to the current Caltrans BDS section 3.24.4, slabs designed for bending moment in article 3.24.3 of the BDS shall be considered satisfactory in shear.

5.4   Punching Shear Analysis

The potential for punching shear is evaluated based upon the existing crack formations in the deck slab. HS20 (71.2 KN, 16 kips) and Permit truck (106.8 KN, 24 kips) load conditions are considered to evaluate the possibility of punching shear failure in the bridge deck. Here, units and equations are given in the SI system followed by FPS.

5.4.1   Loading Conditions

For the punching shear analysis the shear load is defined as $V_u = (1.3)P$ where 1.3 is the impact factor and P is equal to 71.2 KN (16 kips) for the HS20 load condition and 106.8 KN (24 kips) for the permit load (Caltrans 2004). The loading area is taken as a 50.8 cm (20 inches) x 20.3 cm (8 inches) rectangle for both load conditions (Caltrans 2004).

$$V_u = 1.3 \cdot 71.2 = 92.6 \text{ KN (20.8 kips)   HS 20 Load Condition} \qquad \textbf{Eqn. 5.19}$$

$$V_u = 1.3 \cdot 106.8 = 138.8 \text{ KN (31.2 kips)   Permit Load Condition} \qquad \textbf{Eqn. 5.20}$$

5.4.2   Punching Shear Model

A two directional punching shear model typically assumes a 45° failure cone (MacGregor 1997) from the perimeter of the loading area with a nominal punching shear perimeter, p_s, defined along the slab centerline, as shown in Figure 5.8.

$$p_s = 2(663.6 + 358.8) = 2044.8 \text{ mm (80.5 inches)} \qquad \textbf{Eqn. 5.21}$$
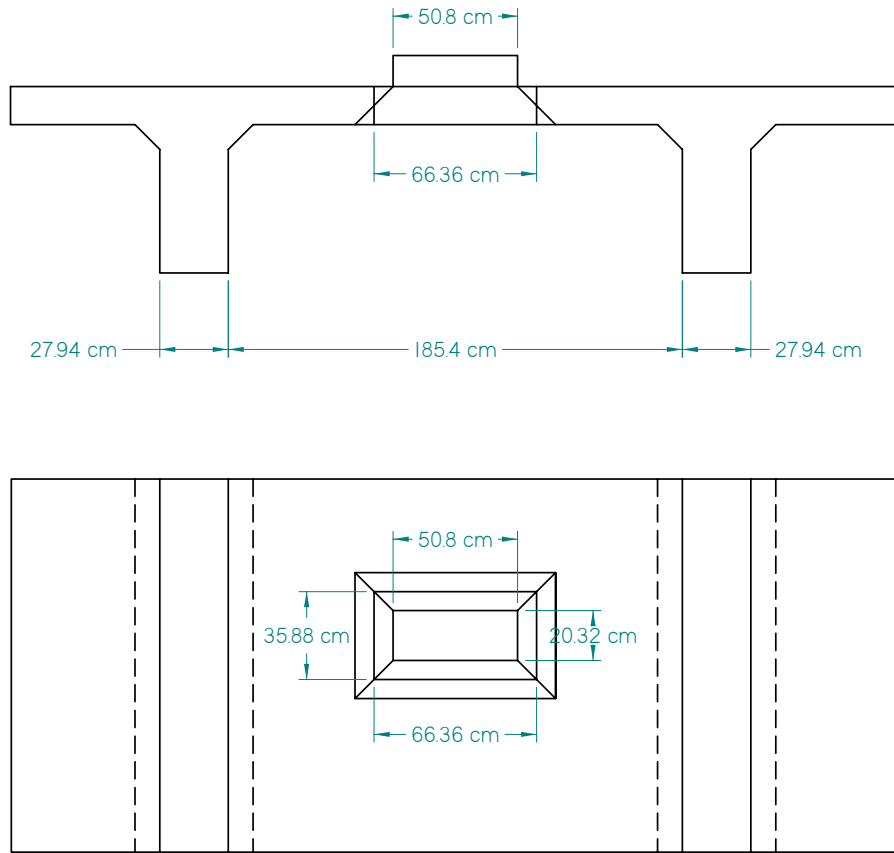
Figure 5.8. Punching Shear Model

The punching shear capacity with the nominal punching shear perimeter is given below.

$$V_n = 0.332\sqrt{f_c'} \cdot p_s \cdot d$$
$$p_s = 2044.8 \ mm \ (80.5 \ in.)$$
$$d = 155.58 \ mm - 25.4 \ mm - \frac{15.875 \ mm}{2}$$
$$= 122.24 \ mm \ (4.8125 \ in.)$$

Eqn. 5.22

$$V_n = 0.166\sqrt{24.82 MPa} \cdot 2044.8 \cdot 122.24 = 206.71 \ KN \ (46.47 \ kips) \quad \textbf{Eqn. 5.23}$$

Assuming a punching shear perimeter defined by the flexural crack patterns (both transverse and longitudinal) and reinforcement spacing (both transverse and longitudinal) over two crack/reinforcement spacings as

$$p_s = 2(2 \cdot 243.8 + 2 \cdot 139.7) = 1534 \ mm \ (60.4 \ inches) \quad \textbf{Eqn. 5.24}$$

The punching shear capacity with the perimeter defined by two crack/reinforcement spacings reduces to,

$$V_n = 0.166\sqrt{24.82 MPa} \cdot 1534 \cdot 122.24 = 155.07 \ KN \ (34.86 \ kips) \quad \textbf{Eqn. 5.25}$$

In the event that the flexural cracks should open such that load transfer efficiency in concrete is reduced, the concrete shear capacity reduces to $1\sqrt{f_c'}$, thus resulting in the following punching shear capacity over two crack/reinforcement spacings.

$$V_n = 0.083\sqrt{24.82 MPa} \cdot 1534 \cdot 122.24 = 77.54 \; KN \; \text{(17.43 kips)} \qquad \textbf{Eqn. 5.26}$$

In addition it is possible that an incident, such as impact due to tire puncture, may cause the entire load to be transferred into one crack/reinforcement spacing.

$$p_s = 2(243.8 + 139.7) = 767 \text{ mm (30.2 in.)} \qquad \textbf{Eqn. 5.27}$$

$$V_n = 0.166\sqrt{24.82 MPa} \cdot 767 \cdot 122.24 = 77.54 \; KN \; \text{(17.43 kips)} \qquad \textbf{Eqn. 5.28}$$

$$V_n = 77.54 \text{ KN (17.43 kips)} < V_u = 92.52 \text{ KN (20.8 kips)} \quad \textbf{Eqn. 5.29}$$

Does not satisfy either load condition

From the above analyses it is shown a situation can occur where the nominal concrete shear capacity is less than the ultimate shear load, i.e. $V_n < V_u$. In order to prevent punching shear failure due to complete load transfer into one crack/reinforcement spacing, aggregate interlock needs to be maintained.

5.5   Additional Steel Requirements

The deck design and punching shear analyses provide an evaluation of the existing state of the structure. A deficiency in steel reinforcement area is determined by calculating the steel reinforcement requirements per 2004 Caltrans BDS and steel reinforcement currently existing in the deck slab of the Watson Wash Bridge. In addition, due to the existing damage state of the deck, the potential for punching shear failure is evaluated and the additional reinforcement necessary to prevent its occurrence is determined.

5.5.1   Deck Slab Reinforcement Deficiencies

5.5.1.1   Transverse Reinforcement

The following table summarizes the reinforcement requirements for the Watson Wash Bridge deck slab in the transverse direction for both HS 20 and Permit Truck load conditions. The difference in area between the design requirements and steel currently present in the bridge indicates any deficiencies in steel reinforcement. An equivalent amount of rebar to adequately restore the capacity of the bridge is calculated in terms of equivalent number of No.5 rebar.

Table 5-1. Transverse Reinforcement Requirements

Load Condtion	A_{sreq} cm^2/m (in^2/ft)	Existing Steel cm^2/m (in^2/ft)	Deficiency cm^2/m (in^2/ft)	Equiv. No. 5 Rebar (per m of slab) (per ft of slab)
HS 20	14.2 (0.67)	13.12 (0.62)	1.06 (0.05)	0.53 rebar (0.16 rebar)
Permit Truck	20.74 (0.98)	13.12 (0.62)	7.62 (0.36)	3.81 rebar (1.16 rebar)

5.5.1.2 Longitudinal Reinforcement

In the Watson Wash Bridge deck, the ratio of longitudinal reinforcement to transverse reinforcement is 50%. The following table summarizes the results for the longitudinal reinforcement requirements in the deck slab for the Watson Wash Bridge. Similarly, the deficiencies are computed in terms of steel reinforcement area per m width of deck slab. The number of additional steel is also given in terms of No. 5 rebar (d_{bar} = 15.875 mm) to compare with the reinforcement size in the existing deck slab.

Table 5-2. Longitudinal Reinforcement Requirements

Load Condition	A_{sreq} cm²/m (in²/ft)	Existing Steel cm²/m (in²/ft)	Deficiency cm²/m (in²/ft)	Equiv. No. 5 Rebar (per m of slab) (per ft of slab)
HS 20	7.20 (0.34)	6.56 (0.31)	0.64 (0.03)	0.33 rebar (0.10 rebar)
Permit Truck	10.37 (0.49)	6.56 (0.31)	3.81 (0.18)	1.90 rebar (0.58 rebar)

5.5.2 Punching Shear Criteria

5.5.2.1 Steel Requirement

In order to avoid sequential crack opening, first in the transverse slab directions and subsequently in the longitudinal deck slab directions the spacing of the longitudinal deck slab bottom reinforcement should have the same distribution as the existing transverse reinforcement. The existing bottom transverse reinforcement is at a spacing of approximately 13.97 cm (5.5 inches), while the current longitudinal rebar spacing is 24.38 cm (9.6 inches). In order to have the equivalent spacing, the additional reinforcement necessary is as follows:

$$\text{Additional Rebar Necessary} = \frac{S_{total}}{s} - N_{steel} \qquad \textbf{Eqn. 5.30}$$

where, S_{total}, is the distance between the end reinforcement bars; s, is the new spacing desired between rebar; N_{steel}, is the number of existing steel rebar

$$\text{i.e., } \frac{121.92 \text{ cm}}{13.97 \frac{\text{cm}}{\text{No. 5 rebar}}} - 6 \text{ No. 5 rebar} = 2.73 \text{ No. 5 rebars} \qquad \textbf{Eqn. 5.31}$$

Steel reinforcement area equivalent to 2.73 No. 5 rebar (d_{bar} = 15.875 mm) in the longitudinal slab direction provides matching spacing for both longitudinal and transverse reinforcement in the Watson Wash Bridge deck slab. The additional longitudinal reinforcement mitigates development of transverse cracks on the deck slab and thus preventing the occurrence of punching shear behavior.

5.5.2.2 Strain Limitation

Another criteria for the punching shear design is the maintaining of soffit crack widths to maintain load transfer capability. It has been observed that high load transfer efficiency

is available with aggregate interlock for crack widths up to 2.5 mm (Jensen and Hansen 2003). Crack widths are limited to 1 mm or less to maintain aggregate interlock and also because AASHTO guidelines limit crack widths to 1 mm or less to avoid spalling and limit water penetration (AASHTO 1993). This requirement ensures that sufficient aggregate interlock will exist to maintain load transfer in the deck slab. By determining the minimum allowable strain the rehabilitation can be designed to effectively control the soffit crack widths. The following is the strain limit criteria based upon the spacing of the cracks in the transverse slab direction such that nominal concrete shear capacity is assumed.

$$\varepsilon_{\lim} = \frac{1 \text{ mm}}{25.4 \text{ }^{mm}\!/_{in}} \cdot \frac{1}{5.5 \text{ inches}} = 0.0072 \text{ }^{mm}_{mm} \approx 0.0075 \text{ }^{mm}_{mm} \qquad \textbf{Eqn. 5.32}$$

The strain limitation is a rehabilitation design requirement to ensure that sufficient aggregate interlock exists. Accordingly, if the soffit crack widths are controlled within the 1 mm crack width, the deck slab is able to sustain the required shear demands.

5.5.2.3 Spacing Constraints

The rehabilitation scheme must be developed such that punching shear cones of 38.1 cm (15 in) in diameter do not form, which requires that spacing between the longitudinal rehabilitation measures does not exceed 30.48 cm (12 in).

5.6 Prior NDE of Watson Wash Bridge

In May of 1999 and September of 2000, modal tests were conducted on the eastbound structure of the Watson Wash Bridge for the purpose of assessing the effectiveness of repair methods proposed by the Office of Structure Maintenance and Investigations (OSM&I) (Stubbs et al. 2001). Vibration characteristics (i.e. frequencies and mode shapes) of the structure were acquired via modal testing of the superstructure before and after repairs. In accordance with the global NDE procedure described by Stubbs et al. (2000), changes in frequency of each frame of the Watson Wash Bridge are noted with relative changes of mass and stiffness of the structure. Furthermore damage is identified, located, and quantified from the changes in measured mode shapes of the structure using the damage index method (Stubbs et al. 2000). The frequency, stiffness, and mass changes for Frame S-3 are presented in the following tables.

Table 5-3. Measured Frequencies of Frame S-3

	Test 1 (May 17, 1999)	Test 2 (Sept. 15, 2000)	Relative Change $\left(\frac{\omega_2}{\omega_1} - 1\right) \cdot 100$
Mode 1	5.59 Hz	5.44 Hz	-2.68%
Mode 2	6.97 Hz	6.31 Hz	-9.47%

Table 5-4. Effective Stiffness Properties of Frame S-3

	Girder Modulus GPa (ksi)	Deck and Bent Modulus GPa (ksi)	Mass Density g/cm^3 (lbs-s^2/ft^4)
Before Repair (1999)	17.81 (2,583)	17.81 (2,583)	2.42 (4.7)
After Repair (2000)	17.83 (2,586)	17.83 (2,586)	2.71 (5.26)
Percent Change (%)	0.12%	0.12%	11.91%

Utilizing extracted modes from the Watson Wash Bridge structure, effects of repairs and/or changes of the structure were assessed. More importantly, the nondestructive evaluation methodology proposed in (Stubbs et al., 2000) was effectively demonstrated on the Watson Wash Bridge as a practical technology to evaluate damage or repairs in a structure. In the vibration based damage detection assessment of the Watson Wash Bridge it was determined that the application of a 1-inch asphaltic concrete overlay increased the dead load of the deck while no changes in stiffness were observed (Stubbs et al., 2001).

From damage localization results, damage or losses in stiffness were observed in the bridge decks of all five frames of the Watson Wash Bridge structure. The indicated damage locations were visually correlated with locations of the bridge structure where major repairs were made or where there was evidence of sealant leaking due to cracking within the deck.

5.7   Need for FRP Rehabilitation

Externally bonded reinforcement initially involved the application of steel plates to the tensile face of structural components for flexural strengthening of bridge decks. However, the use of steel plates as external reinforcement presented the following disadvantages: (1) deterioration of the bond at the steel concrete interface from steel corrosion; (2) Difficulty in handling of the plates at the construction site; (3) Increased load demand on the structure (Triantafillou and Plevris, 1991). In order to overcome disadvantages associated with the external bonding of steel plates, fiber reinforced polymer (CFRP) composites were introduced as a material innovation for civil infrastructure.

The Watson Wash Bridge is a deteriorating structure showing evidence for punching shear failure. The deck slab of the bridge structure requires rehabilitation to halt the deterioration and cracking in the bridge deck. A rehabilitation approach is necessary, which can satisfy the following criteria:

1)   Prevent the occurrence of punching shear failure

2)   Construction without obstructing service (i.e., no lane closures)

3)   Rapid Rehabilitation

4)   Extend service life of the structure without adding significant dead load

FRP composites possess the following characteristics, which provide advantages in terms of material properties and use for strengthening of the deteriorating bridge deck: (1) High strength-to-weight and stiffness-to-weight ratios, (2) Enhanced fatigue life, (3) Corrosion Resistance, (4) Potential lower life cycle costs (Karbhari and Zhao, 2000; Sherwood and Soudki, 2000). In addition, the lightweight of the material and ease of application make for an attractive alternative for construction purposes. A rehabilitation strategy, such as flexural strengthening of a reinforced concrete bridge deck with CFRP composites, can be performed without interference of the intended function of the structure; i.e., no interference with traffic.

Although the use of FRP composites for rehabilitation of bridge decks is not new, past demonstration projects have been inconclusive due to inappropriate design or poor construction practices. The Byron Road Bridge Rehabilitation Project (Sikorsky et al., 2002) demonstrated the ability to extend service life with FRP rehabilitation, as well as identify, localize, and quantify the effects of repair and damage in the structure over an extended period of time. However, little capability was developed in terms of understanding and predicting the remaining service life of a FRP rehabilitated structure due primarily to changes in the design reinforcement pattern made by on-site DWR engineers. The changes in reinforcement pattern effectively resulted in changes of design where deficiencies and susceptibility to punching shear failure continued to exist. Therefore, deterioration of the structure as caused by degradation in FRP, deck, girder, or combination thereof was not identified.

The selection of FRP composites is appropriate for service life extension of the Watson Wash Bridge Deck since the use of the advanced material presents an efficient means to overcome the drawbacks of externally bonded steel plates. The need to use FRP composite is evident for purposes of demonstration and validation for bridge life extension, since past application for bridge life extension and monitoring has not been conclusive. Specifically, the amount of service life extension for the bridge structure with FRP rehabilitation is unknown and the cost effectiveness of FRP rehabilitation is also unclear. In addition, FRP composites for strengthening of the Watson Wash Bridge Deck may be utilized to satisfy common criteria related to repair and maintenance of bridges: stop or slow deterioration of bridge deck, closure of the structure during maintenance, conduct rapid maintenance, and extend the useful life of the structure.

5.8   Summary

The objective of Chapter 5 is to demonstrate the need for rehabilitation of the Watson Wash Bridge by conducting five tasks.

The first task involved a visual inspection of the structure, where the crack formations on the soffit of the bridge deck are noted. Deterioration of the Watson Wash Bridge deck slab is attributed to deterioration and lack of reinforcement to accommodate existing load demands.

A design of a reinforced concrete deck slab is conducted with the 2004 Caltrans BDS for HS20 and Permit Truck wheel loads. Deficiencies in steel reinforcement are determined

by comparing reinforcement requirements from the code analysis and reinforcement in the existing slab structure. The calculation for steel reinforcement deficiencies is based on an undamaged deck slab in 1969 versus an undamaged slab in 2004.

The immediate need for rehabilitation and strengthening is evidenced by the existing pattern of transverse and longitudinal cracks, which indicate the potential for punching shear failure. An analysis for prevention of punching shear failure establishes criteria to retain aggregate interlock in the deck slab by maintaining soffit crack widths to 1 mm and matching reinforcement spacing in both the longitudinal and transverse slab directions.

Prior monitoring of the structure is reviewed to show applicability of the global NDE procedure to assess changes in the deck slab of the Watson Wash Bridge. Frequency and stiffness changes due to the addition of a surface overlay on the Watson Wash Bridge deck is evaluated in the prior monitoring application of the structure. It is concluded that the surface overlay increases the mass of the structure and does not provide any significant stiffness increases.

The need for FRP composite rehabilitation is expressed in terms of selecting a rehabilitation approach with the following qualities: prevent punching shear failure, rapid construction, rehabilitation without traffic obstruction, conduct rapid rehabilitation, and extend the useful life of the structure.

In the upcoming chapter, the design and construction of the FRP rehabilitation is detailed with the intent of extending service life of the structure by increasing the load carrying capacity or at minimum preventing the occurrence of punching shear failure in the deck. Later chapters incorporate the use of vibration based monitoring approach with FRP composite durability characteristics to assess the remaining service life of the structures

6   FRP DESIGN AND CONSTRUCTION

6.1   INTRODUCTION

Previously, Chapter 5 provided an introduction to the Watson Wash Bridge with a description of its geometry, damage state, and the prior monitoring activities on the structure. It was concluded that the deck slab of the bridge structure was deteriorating and, thus, susceptible to punching shear failure. Transverse cracking, longitudinal cracking, and efflorescence provided evidence of deterioration in the deck slab. Furthermore, analysis was conducted comparing the existing deck slab to a design of the deck slab with available bridge design specifications; steel reinforcement deficiencies were calculated for HS20 and Permit Truck wheel loads. In addition, the additional reinforcement necessary to prevent the occurrence of punching shear failure in the cracked deck was calculated. The need for FRP composite rehabilitation was expressed in terms of the advantages inherent in using composites for repair and prevention of punching shear failure.

In Chapter 6, emphasis is placed on the objective of bridge life extension. The objective of this chapter is to detail design methodology, final design, and construction of FRP composites to extend the life of a reinforced concrete bridge deck. The following tasks are accomplished to achieve the objective of this chapter: first, an overview of the design methodology is provided; second, a summary of the reinforcement deficiencies in the deck slab of the Watson Wash Bridge is recounted from Chapter 5; third, materials and their properties are discussed and selected; fourth, the FRP composite design procedure is detailed and a summary of the rehabilitation of the Watson Wash Bridge Deck is provided; sixth, construction guidelines for manufacturing and application of the FRP composites to the Watson Wash Bridge deck are given.

6.2   Design Methodology

Design of the FRP rehabilitation to prevent the occurrence of flexural cracks or to support an increase in load demands is based upon a deficiency in existing reinforcement to support the given demands. The use of FRP composites provides a means to introduce additional reinforcement on a RC section and thereby increase the load capacity of the structure, or in the case of punching shear failure, prevent the pattern of flexural cracking that leads to punching shear failure.

The FRP rehabilitation design approach presented in this section is based upon a measured deficiency in reinforcement as a result of changing load conditions, a developing failure pattern in the structure, or both. An FRP composite equivalent to steel reinforcement in terms of stiffness and area is determined assuming the same force is likely to develop in an externally bonded FRP composite area and a steel reinforcement area. Here, consideration is made for material parameters and limiting conditions, (i.e. ultimate tensile strength, yield strength, strain limit) in the reinforcing and FRP composite materials. A ratio between the area of FRP composite and steel reinforcement is developed based on the stiffness and strength parameters, where the required FRP composite necessary to rehabilitate a deficient structure is determined from a deficiency in steel reinforcement. Then, based upon the geometric constraints between the structure

geometry and geometry of available composite materials, spacing and placement of FRP composite is determined with the number of FRP composite strips, as in the number of steel rebar in a RC section. Figure 6.1, provides an illustration of the primary components in this preliminary design methodology.

DETERIORATING RC STRUCTURE - Visual Inspection - Code Comparison	REINFORCEMENT DEFICIENCY - Loading Conditions - Failure Patterns
FRP-to-STEEL EQUIVALENT - Material Parameters - Reinforcement Area Ratio	MATERIALS SELECTION - Fiber and Matrix Selection - FRP Composite Design Values
REQUIRED FRP COMPOSITE AREA - FRP composite Area per unit width	No. of STRIPS AND/OR LAYERS - Available geometry of Section - Construction Requirements

Figure 6.1. FRP Rehabilitation Design Methodology

6.2.1 FRP-to-Steel Reinforcement Equivalent

The FRP composite-to-steel area ratio is used to evaluate the required area of composite from the calculated steel reinforcement deficiencies. The equations below show the computation for the FRP to steel ratio, assuming equivalent forces are developed in the steel and composite at ultimate with a predefined strain limit for the FRP composite.

The primary assumption in the design approach is that the force developed in the steel is the same as the composite at ultimate. By establishing equilibrium between the force in FRP composite, T_{frp}, and the force in the steel rebar, T_s, the ratio of composite to steel reinforcement for an RC section, η_{frp}, is determined.

$$T_{frp} = T_s \qquad \textbf{Eqn. 6.1}$$

The force in the composite and steel is equal to the product of the limiting stress and cross-sectional area.

$$A_{frp} \times \min\{E_{frp}\varepsilon_{\lim}, f_u\} = A_s \times \min\{E_s\varepsilon_{\lim}, f_y\} \qquad \textbf{Eqn. 6.2}$$

where, min{}, denotes the minimum value of the set. By rearranging and introducing χ_{frp}, the ratio of composite area to steel area is set equal to the ratio of force in steel to force in composite.

$$\chi_{frp} = \frac{A_{frp}}{A_s} = \frac{\min\{E_s\varepsilon_{\lim}, f_y\}}{\min\{E_{frp}\varepsilon_{\lim}, f_u\}} \qquad \textbf{Eqn. 6.3}$$

- 124 -

where, subscripts *frp* and *s*, are used to denote FRP composite and steel reinforcement, respectively; A is the cross-sectional area; E, is the modulus of elasticity; ε_{lim}, is the allowable strain limit; f_y, is the yield stress of the steel reinforcement, and f_u is the ultimate stress of the FRP composite; χ_{frp}, is the FRP to steel reinforcement ratio.

χ_{frp} is calculated by the ratio of forces. From a known deficiency in steel reinforcement, the required area of FRP composite is determined to rehabilitate a structure or component.

6.2.2 *Required FRP Composite*

Since FRP composite strips are available in different geometries depending on material manufacturer, the appropriate number of FRP composite strips and/or layers to be applied is dependent on the cross-sectional area of a single FRP composite strip. In addition consideration is necessary from a spacing perspective to distribute the externally bonded FRP composite reinforcement uniformly to the surface of the RC structure. The FRP composite area required is calculated by multiplication of χ_{frp} to the required additional steel area.

$$A_{frp\_req} = \chi_{frp} A_{s\_req} \qquad \textbf{Eqn. 6.4}$$

where, A_{s_req}, is the required steel reinforcement area per unit width; A_{frp_req}, is the required area of FRP composites per unit width. The number of FRP strips is determined by dividing the required FRP composite area, A_{frp_req}, by the area of a single FRP composite strip. The area of a single composite strip is dependent on manufacturing technique (i.e., wet lay-up of fabric allows for variation in thickness, by adding or subtracting the number of layers) and manufacturer specifications (i.e., a prefabricated FRP strips is available in a fixed cross-sectional geometry unless a sufficient supply is purchased). If reinforcement deficiencies are computed per unit width of the structure, the total number of strips is determined by multiplication with the width of the structural member, as in the following equation.

$$N_{total} = \frac{A_{frp\_req}}{n \cdot A_{frp\_one}} L_s \qquad \textbf{Eqn. 6.5}$$

where, A_{frp_req}, is the required area of FRP composites per unit width; A_{frp_one}, is the nominal cross-sectional area of a FRP strip; n, is the number of layers in the FRP composite; L_s is the distance spanned by the applied FRP composite; N_{total}, is the total number of FRP composite strips required to rehabilitate the structural member for a given deficiency.

6.3 Application of Design Methodology

The preliminary design approached outlined in Section 6.2 is applied to a representative deficient structure in need of rehabilitation, namely the Watson Wash Bridge Deck, to illustrate the details of this preliminary design approach. Specifically, spans 8 and 9 of Frame S-3 are rehabilitated with FRP composites.

The objectives for strengthening of the Watson Wash Bridge deck are to eliminate the occurrence of punching shear failure by constraining transverse and longitudinal flexural

cracks in the slab and increase the flexural capacity of the deck slab to support the HS20-44 design wheel load, 71.2 KN (16 kips) and Permit Truck wheel load, 106.8 KN (24 kips). The Permit Truck wheel load is included in the design criteria because trucks of this load have been known to traverse the structure.

6.3.1   Reinforcement Deficiencies

In Chapter 4, a comparison of the existing bridge deck reinforcement with the Caltrans BDS (Caltrans 2004) is conducted for both the HS20-44 design wheel load, 71.2 KN (16 kips), and permit truck wheel load, 106.8 KN (24 kips), conditions. The service moment demands for the design truck and permit truck are 20.53 KN-m/m (4.58 kip-ft/ft) and 29.94 KN-m/m (6.68 kip-ft/ft), respectively. In addition an analysis for punching shear failure was conducted considering a strain limit in the composite of 0.75% at ultimate to maintain soffit crack widths to ensure aggregate interlock in the deck slab. Table 6-1 provides a summary of the additional steel reinforcement required in terms of No. 5 rebar (d_{bar} = 15.875 mm) per length of slab to satisfy code service level requirements for the design wheel load, permit truck wheel load, and the punching shear criteria. The length (longitudinal direction) and width (transverse direction) of the deck slabs are 12.5 m (41 ft) and 1.85 m (73 inches), respectively as seen in Figure 6.2.
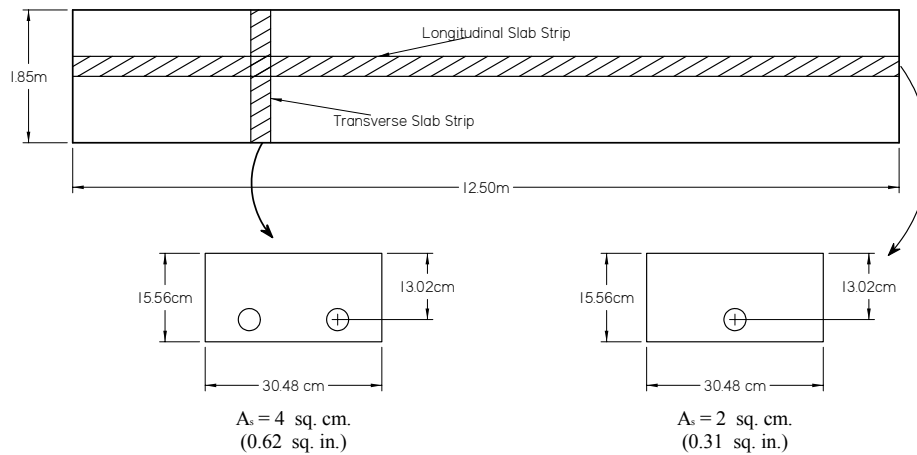
Figure 6.2. Geometry of a Single Bay

Table 6-1. Summary of Reinforcement Deficiencies

Reinforcement Direction	Load Condition		
	HS20-44 Truck rebar/m (rebar/ft)	Permit Truck rebar/m (rebar/ft)	Punching Shear rebar/m (rebar/ft)
Transverse	0.53 (0.16)	3.81 (1.16)	--
Longitudinal	0.33 (0.10)	1.90 (0.58)	1.48 (0.45)

Only the longitudinal steel reinforcement deficiency is computed for the punching shear criterion, since the emphasis for this criterion is the need to prevent the occurrence and growth of transverse cracks that result due to a lack of longitudinal reinforcement. Multiplying the values of the Table 6-1 by the cross-sectional area of a No. 5 rebar, 2 cm^2 (0.31 in^2), results in the required area of steel reinforcement.

Table 6-2. Summary of Reinforcement Deficiencies

Reinforcement Direction	Load Condition		
	HS20-44 Truck cm2/m (in2 / ft)	Permit Truck cm2/m (in2 / ft)	Punching Shear cm2/m (in2 / ft)
Transverse	1.06 (0.050)	7.62 (0.360)	--
Longitudinal	0.66 (0.031)	3.81 (0.180)	2.94 (0.139)

The transverse reinforcement for punching shear is determined considering the reinforcement spacing required to prevent the development of punching shear cones. For a punching shear rehabilitation a maximum spacing of 60.96 cm (24 inches) on center is prescribed to provide additional reinforcement per crack spacing in addition to the steel reinforcement existing in the deck slab. Of the three loading conditions, the governing condition is the permit truck wheel load, with punching shear being the next critical limit.

Spacing of FRP composite strips for rehabilitation is governed by requirements from the punching shear criterion. The FRP composite strips are to be placed at a spacing no greater than 38.1 cm (15 inches) to provide the necessary reinforcement per crack spacing in addition to the longitudinal steel reinforcement to prevent the occurrence of punching shear failure.

6.3.2   *Materials for Bridge Deck Rehabilitation*

As part of the experimental component of this research, FRP composites for rehabilitation of a deficient RC bridge structure are constructed via, both, wet lay-up application of FRP composites and adhesive bonding of prefabricated FRP strips. Both wet lay-up and adhesive bonding construction methods are used for comparison purposes.

6.3.2.1   Wet Lay-up FRP System

As part of the rehabilitation design, the constituent materials selected for the FRP application are carbon fibers with an epoxy resin matrix. Carbon FRP composites are used for the rehabilitation since they show better overall characteristics when considering tensile strength, tensile modulus, long-term behavior, fatigue behavior and cost (Meier 1995). The following carbon fabric and resin system are prescribed for the Watson Wash Bridge deck rehabilitation for wet lay-up manufactured CFRP composites.

6.3.2.1.1 Carbon Fabric

The wet lay-up CFRP composites are built up with a carbon fabric consisting of a 600 gsm (18 oz/sq. yd), 24 k tow, unidirectional woven carbon fabric[1], incorporating T700 carbon fibers. The nominal fabric characteristics and fiber mechanical properties are provided in Table 6-3.

Table 6-3. Fabric Dimensions and Carbon Fiber Properties

Fabric Dimensions		Fiber Properties			
Thickness mm (in)	Width mm (in)	Tensile Strength GPa (ksi)	Tensile Modulus GPa (msi)	Elongation %	Density g/cm3 (lb/ft3)
1.02 (0.040)	152.4 (6)	4.96 (720)	231.66 (33.6)	2.1%	1.79 (111.75)

6.3.2.1.2 Epoxy Resin

The resin system used to impregnate the carbon fabric is two-component epoxy resin[2], mixed at a ratio of 2 parts resin and 1 part hardener. The epoxy resin system is advertised as a long pot life epoxy resin system with a gel time of ~60 minutes at 23°C (73°F).

6.3.2.2   Prefabricated CFRP Strips

The prefabricated CFRP composite strips incorporate carbon fiber and an epoxy resin system compatible with the pultrusion manufacturing process. Two different prefabricated CFRP composite strip systems are applied to the bridge structure for purposes of comparison in terms of overall performance.

6.3.2.2.1 System 1 Prefabricated CFRP Strips[3]

The system 1 strips are the primary prefabricated CFRP strips applied to the bridge and have a nominal width of 50.8 mm (2 in) and thickness of 1.27 mm (0.050 in). According to the specifications data sheet provided by the supplier the system 1 CFRP strips provide a minimum glass transition temperature of 110°C (230°F). The mechanical properties, per material specification, indicate a tensile strength of 2.1 GPa (305 ksi) and tensile modulus of 141.34 GPa (20.5 msi); however, it is noted that a nominal fiber volume fraction is specified at 0.6, which results in a modulus of 140.4 GPa (20.36 msi) using the

---

[1] Carbon fabric was provided by Structural Composite Construction Inc. (SCCI) and is designated as C-2 Fabric System.
[2] Epoxy resin was provided by SCCI and is designated as FM-1 resin system.
[3] System was provided by SCCI and has the designation CS-02.

rule of mixtures while assuming a matrix modulus of 3.45 GPa (0.5 msi) and no voids[4].
Table 6-4 provides a summary of the pultruded strip properties as provided by the
manufacturer. In order to bond the pultruded strips to the bridge deck a two-component
epoxy adhesive, identified as System 1 Adhesive[5], mixed at a 1 to 1 ratio by volume is
used. Specifications of the epoxy adhesive system indicate a pot life of approximately 30
minutes at 23°C (73°F).

6.3.2.2.2 System 2 Prefabricated CFRP Strips[6]

For purposes of comparison, one bay of the bridge was rehabilitated with System 2
prefabricated CFRP strips, which have a nominal width of 50.8 mm (2 in) and thickness
of 1.19 mm (0.047 in). According to the specifications data sheet provided by the
manufacturer, the System 2 prefabricated CFRP strips provide a minimum temperature
resistance of 150°C (300°F). Tensile strength and modulus of elasticity are specified at
2.4 GPa (348 ksi) and 155.1 GPa (22.5 msi), respectively with a minimum fiber volume
fraction of 0.68. Table 6-4 provides a summary of the pultruded CFRP strip properties as
provided by the manufacturer. Accordingly, the System 2 Epoxy Adhesive is a two-
component epoxy adhesive mixed at a ratio of 3 parts A to 1 part B by volume with a pot
life of 70 minutes at 23°C (73°F) and is used to bond the System 2 prefabricated CFRP
strips.

Table 6-4. Manufacturer Properties of Prefabricated Strips

Type	Geometry		Composite Properties			
	Thickness mm (in)	Width mm (in)	Tensile Strength GPa (ksi)	Tensile Modulus GPa (msi)	Strain at Failure %	Fiber Volume Fraction %
System 1	1.27 (0.050)	50.8 (2)	2.1 (305)	141.3 (20.5)	1.2 %	60%
System 2	1.19 (0.047)	50.8 (2)	2.4 (348)	155.1 (22.5)	1.9 %	68%

6.3.3   Design Values of CFRP Composite Rehabilitation

In order to implement the preliminary design procedure, design values of the CFRP
composite materials are necessary. Since material parameters such as tensile modulus
and ultimate strength of composite materials depend on manufacturing process,
representative material properties are needed for both the wet lay-up and prefabricated
CFRP composites, prior to design.

---

[4] The nominal tensile modulus specified for SCCI pultruded strips is overestimated compared to a
theoretical evaluation with the provided nominal volume fraction of 0.6, a high matrix modulus of 0.5 msi,
and the rule of mixtures $E_1 = E_f V_f + E_m V_m = 33.6 \times 0.6 + 0.5 \times 0.4 = 20.36$ msi .

[5] System 1 Epoxy Adhesive is provided by SCCI and has the designation BG-02.
[6] System 2 was provided by Sika and is designated as Sika CarboDur prefabricated strips.

6.3.3.1 Theoretical Mechanical Properties

As a preliminary measure, theoretical values for the tensile modulus and tensile strength of a CFRP composite are calculated using the rule of mixtures and Hooke's law. A fiber volume fraction range of 20% to 50% is specified for a hand lay-up process (Astrom 1997); nominal fiber volume fractions for the pultruded strips are provided in Table 6-4 at 60% for System 1 strips and 68% for System 2 strips. Since, carbon fiber properties are provided only for the System 1 prefabricated strips (T700 fibers), the theoretical calculations for both prefabricated strips are conducted using the carbon fiber properties in Table 6-3.

This calculation of theoretical values for CFRP composite mechanical properties conservatively neglects resin properties since its contribution is low in a fiber-dominated case. Using the nominal modulus of the carbon fiber given in Table 6-3, as 231.7 GPa (33.6 msi), a range of theoretical values for modulus and strength properties of the wet lay-up CFRP composites is presented in the following table. In addition, the tensile strength is approximated considering the strain-to-failure of the composite as provided by the manufacturer, a strain-to-failure of 0.75% per punching shear design criteria, and Hooke's law for purposes of comparison.

Table 6-5. Theoretical Modulus and Strength Values

Fiber Volume Fraction (%)	Tensile Modulus GPa (msi)	Tensile Strength GPa (ksi)	Approximated Strength GPa (ksi)		
			0.75 % Strain	1.2 % Strain	1.9% Strain
20	46.33 (6.72)	0.99 (144.0)	0.35 (50.40)	0.56 (80.64)	0.88 (127.68)
35	81.08 (11.76)	1.74 (252.0)	0.68 (88.20)	0.97 (141.12)	1.54 (223.44)
50	115.83 (16.80)	2.48 (360.0)	0.87 (126.00)	1.39 (201.60)	2.20 (319.20)
60	139.00 (20.16)	2.98 (432.0)	1.04 (151.20)	1.67 (241.92)	2.64 (383.04)
68	157.55 (22.85)	3.38 (489.6)	1.18 (171.36)	1.89 (274.18)	2.99 (434.11)

The above table provides an indication of the expected properties of CFRP composites based upon manufacturing process and ultimate failure strain. For processes, such as wet lay-up, which yield low fiber volume fractions, specific guidelines are necessary to ensure that the manufacturing process is consistent and does not negatively impact the design.

6.3.3.2 Wet Lay-up CFRP Design Values

The modulus and strength values for design of the bridge deck rehabilitation with wet lay-up manufactured CFRP composites are based on material test results obtained from field-manufactured specimens prior to initiation of application activity on the rehabilitation project. Composite panels of 1-layer, 2-layer, and 3-layer specimens were manufactured and tested over a 48-hour period to determine typical field values for modulus and strength of composites.

Table 6-6. Tested Tensile Modulus and Tensile Strength

Lay-up Design	Measured Thickness mm (in)	Tested Modulus GPa (ksi)	Tested Strength GPa (ksi)
1-Layer	1.16 (0.0453)	65.16 (9450.32)	0.719 (104.25)
2-Layer	2.02 (0.0797)	64.92 (9415.40)	0.887 (128.66)
3-Layer	3.11 (0.1223)	60.18 (8727.80)	0.746 (108.19)

The preliminary manufactured panels adhered to the same design and manufacturing guidelines, to be described in Chapter 6, during construction of the rehabilitation. The preliminary wet lay-up composite panels show a steadily decreasing modulus with increasing number of layers, which indicates an ineffective compaction process with the aluminum roller, in addition to an inability to align the fibers correctly with the increasing number of layers for the composite strips. From the preliminary field fabricated panel results, guidelines for the manufacturing process were modified with an emphasis on the compaction of the material with an aluminum roller, and alignment of composite layers during the application process.

The 2-layer modulus and strength values of 64.92 GPa (9415.4 ksi) and 0.887 GPa (128.66 ksi), respectively are selected for preliminary design of the wet lay-up manufactured CFRP rehabilitation without consideration for material allowables. A characteristic value, i.e., mean minus three times standard deviation, is not used since the design value is significantly decreased and is overly conservative as will be seen in section 7.6. During the design process, a safety factor of 1.2 was included for the transverse strips and 1.56 for longitudinal strips for rehabilitation designs at locations span 8, bay 5 (S8B5) and S9B5. Safety factors are applied to provide increase the level of rehabilitation compared to location S8B3 and S9B3; however, it is noted that as in other safety factors the level of safety that is provided is unknown. Including a safety factor increases the number of layers necessary for the rehabilitation.

6.3.3.3   Prefabricated CFRP Design Values

The modulus and strength values used for design of prefabricated CFRP composites are determined from the more conservative of manufacturer supplied data and third party testing[7] of material to be applied on the Watson Wash Bridge. Manufacturer supplied information is shown in Table 6-4. Third party testing results of System 1 prefabricated strips are given in the following table.

Table 6-7. Tested Properties of System 1 Prefabricated Strips

Material	Width mm (in)	Thickness mm (in)	Strength GPa (ksi)	Modulus GPa (msi)
System 1	12.7 (0.498)	1.27 (0.050)	3.08 (446)	151.69 (22.0)

Since third party testing results in properties greater than the manufacturer specified properties, the design modulus and strength values for the System 1 prefabricated CFRP strips are taken as 141.34 GPa (20.5 msi) and 2.10 GPa(305 ksi). Design values for System 2 CFRP composites are also taken as 141.34 GPa (20.5 msi) and 2.10 GPa (305 ksi).

6.4   Rehabilitation Design

Utilizing the computed steel reinforcement deficiencies as reported in Section 4.5, an equivalent CFRP design is determined for wet lay-up manufactured and pultruded CFRP composites. Table 6-7 summarizes the locations on the bridge, by span and bay, to be rehabilitated and the manufacturing method of the applied CFRP strips and Figure 6.3 illustrates the rehabilitated locations on Frame S-3 of the Watson Wash Bridge. All CFRP composites bonded to the Watson Wash Bridge are unidirectional composites, where "transverse reinforcement" implies the fibers are oriented perpendicular to the direction of traffic and "longitudinal reinforcement" indicates fibers are oriented parallel to the direction of traffic.

Table 6-8. Manufacturing Technique by Location

Span Number	Bay Number				
	1	2	3	4	5
8	System 1	System 1	Wet Lay-up	Caltrans Repair	Wet Lay-up
9	System 1	System 1	Wet Lay-up	System 2	Wet Lay-up

---

[7] Third party testing on System 1 prefabricated strips was conducted by Composite Materials Research Group

Figure 6.3. CFRP Composite Rehabilitated Locations

The bays within a span are numbered from north to south. As an example Table 6-8 indicates that in S9B3, the CFRP applied at this location is manufactured via wet lay-up. Location S8B4, is not rehabilitated using CFRP strips, rather the Caltrans repair for punching shear failure, which is to replace the concrete in the region of the punching shear failure, is left intact for purposes of comparison. Figure 6.4 shows the punching shear repair in location S8B4.

Figure 6.4. Caltrans Repair at Location S8B4

6.4.1 CFRP-to-Steel Reinforcement Ratio

The CFRP composite to steel ratio is used to evaluate the required area of composite from the calculated steel reinforcement deficiencies. The equations below show the computation for the CFRP to steel ratio, assuming equivalent forces are developed in the steel and composite at ultimate and a limiting strain of 0.75% per the punching shear criterion, which is maintain soffit crack widths in order to ensure shear capacity in the deck slab.

By establishing equilibrium between the force in FRP composite, T_{frp}, and the force in the steel rebar, T_s, the ratio of composite to steel, χ_{frp}, is determined.

$$T_{frp} = T_s \qquad \textbf{Eqn. 6.6}$$

The force in the composite and steel is equal to the following.

$$A_{frp} \times \min\left\{E_{frp}\varepsilon_{\lim}, f_u\right\} = A_s \times \min\left\{E_s\varepsilon_{\lim}, f_y\right\} \qquad \textbf{Eqn. 6.7}$$

- 133 -

where min{} indicates the minimum value of the set. By rearranging and introducing χ_{frp}, the ratio of composite area to steel area is equivalent to the ratio of force in steel to force in composite.

$$\chi_{frp} = \frac{A_{frp}}{A_s} = \frac{\min\{E_s \varepsilon_{\lim}, f_y\}}{\min\{E_{frp} \varepsilon_{\lim}, f_u\}} \qquad \textbf{Eqn. 6.8}$$

6.4.2 Required CFRP Composite

The CFRP composite area required is calculated by multiplication of the ratio χ_{frp} to the required additional steel area.

$$A_{frp\_req} = \chi_{frp} A_{s\_req} \qquad \textbf{Eqn. 6.9}$$

The number of strips is determined by dividing the required CFRP composite area by the area of a single composite strip. Since the reinforcement deficiencies are computed per meter of slab, the total number of strips is determined by multiplication with the longitudinal or transverse slab length.

$$N_{total} = \frac{A_{frp\_req}}{n \cdot A_{frp\_one}} L_{slab} \qquad \textbf{Eqn. 6.10}$$

where, A_{frp_req}, is the required area of FRP composites per meter of slab span; A_{s_req}, is the required steel reinforcement area per meter of slab span; A_{frp_one}, is the nominal cross-sectional area of a 1-layer FRP strip; n, is the number of layers in the composite; L_{slab} is the distance spanned by the applied FRP composite; N_{total}, is the total number of CFRP strips required to rehabilitate the slab.

Table 6-9 provides a detailed example of the design calculations for wet lay-up and pultruded CFRP composite strips considering the steel deficiencies from Table 6-1 for the Permit Truck wheel load.

The design calculations in Table 6-9 for the permit truck wheel load indicate that a minimum of 26.10 strips or 27 transverse strips are required to strengthen the deck slab with wet lay-up manufactured CFRP. A minimum of 3.87 strips or 4 wet lay-up longitudinal CFRP strips is required. For the pultruded CFRP strips, 57.54 strips or 58 CFRP transverse strips and 4.27 strips or 5 longitudinal composite strips. Spacing of the rehabilitation is determined considering equal distribution of the CFRP strips throughout the area of the slab and the punching shear criterion.

Table 6-9. CFRP Rehabilitation Design for Permit Load

Manufacturing Process	Wet Lay-up		Pultruded	
CFRP Strip Direction	Trans.	Long.	Trans.	Long.
L_{slab} m (ft)	12.50 (41)	1.85 (6.08)	12.50 41	1.85 (6.08)
No. 5 Bars required, rebar/m (rebar/ft)	3.81 (1.16)	1.90 (0.58)	3.81 (1.16)	1.90 (0.58)
A_{s_req} , cm^2/m (in^2/ft)	7.62 (0.36)	3.81 (0.18)	7.62 (0.36)	3.81 (0.18)
E_s, GPa (msi)	200 (29.0)	200 (29.0)	200 (29.0)	200 (29.0)
f_y , MPa (ksi)	413.69 (60.0)	413.69 (60.0)	413.69 (60.0)	413.69 (60.0)
$\min\left\{E_s\varepsilon_{\lim},f_y\right\}$, MPa (ksi)	413.69 (60.0)	413.69 (60.0)	413.69 (60.0)	413.69 (60.0)
E_{frp}, GPa (msi)	64.92 (9.42)	64.92 (9.42)	141.34 (20.5)	141.34 (20.5)
f_u, GPa (ksi)	0.887 (128.66)	0.887 (128.66)	2.1 (304.0)	2.1 (304.0)
$\min\left\{E_{frp}\varepsilon_{\lim},f_u\right\}$, MPa (ksi)	486.90 (70.6)	486.90 (70.6)	1060.05 (153.8)	1060.05 (153.8)
$\chi_{frp}=\dfrac{A_{frp}}{A_s}=\dfrac{\min\left\{E_s\varepsilon_{\lim},f_y\right\}}{\min\left\{E_{frp}\varepsilon_{\lim},f_u\right\}}$	0.85	0.85	0.39	0.39
$A_{frp\_req}=\chi_{frp}A_{s\_req}$, cm^2/m (in^2/ft)	6.48 (0.306)	3.24 (0.153)	2.96 (0.140)	1.48 (0.070)
n, number of layers	2	1	1	1
A_{frp_one} , cm^2/strip (in^2/strip)	3.10 (0.48)	1.55 (0.24)	0.65 (0.10)	0.65 (0.10)
$N_{total}=\dfrac{A_{frp\_req}}{n\cdot A_{frp\_one}}L_{slab}$	26.10	3.87	57.54	4.27
# of Strips Required	**27**	**4**	**58**	**5**

6.5 Design Summary

6.5.1 Wet Lay-up Manufactured CFRP Design

The material properties for the wet lay-up CFRP composite used in design are 64.92 GPa (9,415.40 ksi) for modulus and 0.887 GPa (128.66 ksi) for strength of the composite. Since, locations S8B5 and S9B5 correspond to the right lane of the bridge road, heavier traffic loads are experienced at those locations on the bridge deck. Therefore, for wet lay-up CFRP strips in locations S8B5 and S9B5, a nominal safety factor is applied to the CFRP rehabilitation design resulting in the placement of additional material to provide an increased level of safety as compared to locations S8B3 and S9B3.

A summary of design parameters and applications is provided in Table 6-10 for the different locations of the bridge structure. All CFRP composites applied to the Watson Wash Bridge are unidirectional composites used as "transverse reinforcement" meaning the fibers are oriented perpendicular to the direction of traffic and "longitudinal reinforcement" indicates fibers are oriented parallel to the direction of traffic. For purposes of comparison, locations S8B3 and S9B3 are rehabilitated for the Permit Truck load condition, with levels of safety available from design assumptions, resulting in 28-two layer strips for transverse reinforcement and 4-one layer strips for longitudinal reinforcement. Locations S8B5 and S9B5 employ a rehabilitation design for the Permit Truck load, with a nominal safety factor 1.2 applied resulting in 21-three layer strips for transverse reinforcement and a safety factor of 1.56 applied, resulting in 4-two layer strips for the longitudinal reinforcement.

Table 6-10. Wet Lay-up CFRP Rehabilitation Requirements

Reinforcement Direction		Permit Load
Transverse	Required CFRP	28, two layer strips
	W/ S.F. of 1.2	21, three layer strips
Longitudinal	Required CFRP	4, one layer strips
	W/ S.F. of 1.56	4, two layer strips

Spacing of the CFRP rehabilitation is governed by the punching shear criterion as reported earlier in section 4.5.2. CFRP strips are placed such that punching shear perimeters are unable to develop, which translates into a nominal spacing of 60.96 cm (24 inches) center-to-center (c-to-c) for the transverse CFRP wet lay-up strips. The longitudinal CFRP wet lay-up strips are applied with consideration for the existing longitudinal steel reinforcement in the deck slab and thus placed at 22.86 cm (9 inches) c-to-c. The 22.86 cm (9 inches) c-to-c minimizes the overlap between composite and longitudinal steel reinforcement in the bridge slab. The spacing dimensions of the transverse and longitudinal reinforcement at the locations for the wet lay-up CFRP are provided in the following figure.
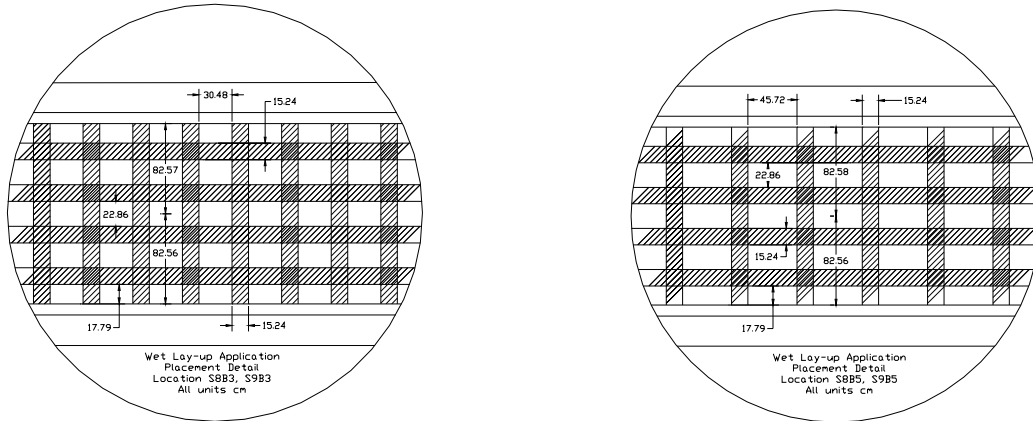
(a) CFRP Spacing for locations S8B5 and S9B5   (b) CFRP Spacing for locations S8B3 and S9B3

Figure 6.5. Placement of Wet Lay-up CFRP

Table 6-11 provides a summary of the rehabilitation design using wet lay-up manufactured CFRP by location. For purposes of comparison, locations S8B3 and S9B3 are rehabilitated for the Permit Truck load condition. Locations S8B5 and S9B5 employ the Permit Truck load rehabilitation, with a nominal safety factor of 1.2 applied for transverse strips and a safety factor of 1.56 applied for longitudinal CFRP strips. Figure 6.7 identifies rehabilitation location by design requirement.

Table 6-11. Wet Lay-up Rehabilitation Design and Spacing

Location (Span – Bay)	Transverse Reinforcement		Longitudinal Reinforcement	
	Quantity	C-to-C Spacing cm (inches)	Quantity	C-to-C Spacing cm (inches)
8-3	28, 2-layer strips	45.72 (18)	4, 1-layer strips	22.86 (9)
8-5	21, 3-layer strips	60.96 (24)	4, 2-layer strips	22.86 (9)
9-3	28, 2-layer strips	45.72 (18)	4, 1-layer strips	22.86 (9)
9-5	21, 3-layer strips	60.96 (24)	4, 2-layer strips	22.86 (9)

Spacing of the CFRP rehabilitation is governed by the punching shear criterion. CFRP strips are placed such that punching shear perimeters are unable to develop, which translates into a maximum spacing of 60.96 cm (24 inches) center-to-center (c-to-c) for the transverse CFRP wet lay-up strips. A c-to-c spacing of 45.72 cm (18 inches) is used for transverse CFRP strips in S8B3 and S9B3 for a uniform distribution of rehabilitation over the slab area, resulting in 28 strips as opposed to the required 27 strips. For locations S8B5 and S9B5, 21 transverse CFRP strips are placed 60.96 cm (24 inches) c-to-c. The longitudinal CFRP wet lay-up strips are applied with consideration for the existing longitudinal steel reinforcement in the deck slab and thus placed at 22.86 cm (9 inches) c-to-c. The longitudinal composite strip spacing is placed to alternate between

the existing steel reinforcement spacing and the externally bonded CFRP wet lay-up strips.

6.5.2 Prefabricated CFRP Strip Design Summary

Material properties for the design of the pultruded CFRP are 141.34 GPa (20.5 msi) and 2.10 GPa (305 ksi) for modulus and strength, respectively. Locations S8B1, S8B2, S9B1, and S9B2 are designated for repair using System 1 prefabricated strips, while System 2 prefabricated strips are applied in location S9B4. The rehabilitation design in locations S8B1, S9B1 and S9B4 utilize the punching shear condition as the governing load condition while locations S8B2 and S9B2 are rehabilitated for the Permit Truck wheel load without any safety margins.

The rehabilitation design using pultruded CFRP composite strips is summarized with locations S8B1 and S9B1, and S9B4 requiring 21 transverse strips and 4 longitudinal strips; where System 1 prefabricated strips are bonded to locations S8B1 and S9B1, and System 2 prefabricated strips are bonded to S9B4. Locations S8B2 and S9B2 are designed with consideration for the Permit Truck Load, requiring 58 transverse strips bonded to the deck in adjacent pairs (i.e. 29 pairs, bonded side by side with no gaps), and 5 longitudinal strips.

Table 6-12. Pultruded CFRP Rehabilitation Requirements

Reinforcement Direction	Punching Shear	Permit Load
Transverse	21 strips	29 pairs (58 strips)
Longitudinal	4 strips	5 strips

As with the wet lay-up manufactured CFRP composites, the spacing of the unidirectional composites is governed by the punching shear criterion resulting in a nominal spacing of 60.96 cm (24 inches) c-to-c. Similarly, the longitudinal CFRP strips are bonded to the bridge deck soffit such that the bonded pultruded strips alternate between existing steel reinforcement. The spacing of the longitudinal and transverse strips for both the punching shear and permit load requirements is shown in Figure 6.6.
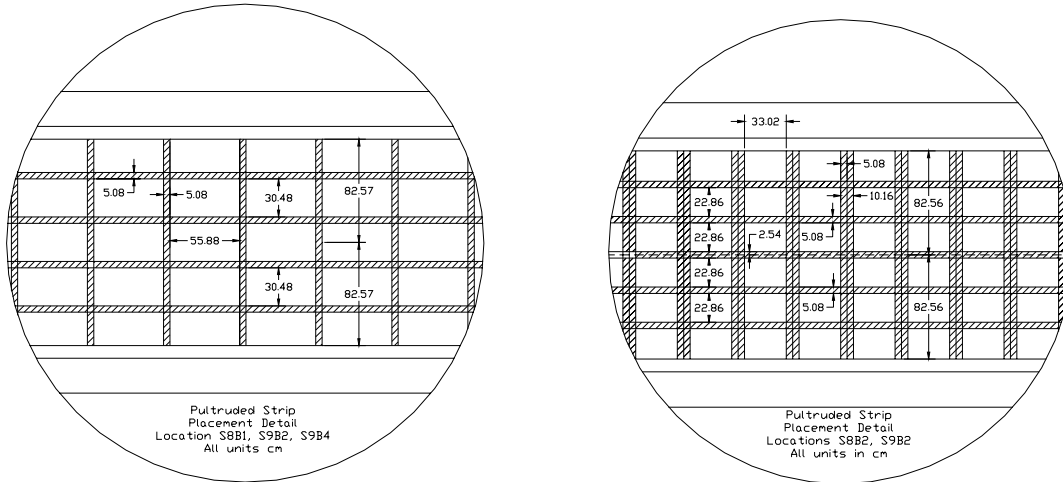
(a) CFRP Spacing at S8B1, S9B1, and S9B4   (b) CFRP Spacing at S8B2 and S9B2

Figure 6.6. Placement of Pultruded CFRP Strips

The rehabilitation design in locations S8B1, S9B1 and S9B4 utilize the punching shear condition as the governing load condition, while locations S8B2 and S9B2 are rehabilitated for the Permit Truck Load Condition. Locations S8B2 and S9B2 are strengthened with 29 pairs of transverse strips and 5 longitudinal strips. A transverse strip pair is two 50.8 mm (2 inches) wide CFRP pultruded strips applied adjacent to each other, which is effectively a 101.6 mm (4 inches) wide single strip of CFRP. Locations S8B1 and S9B1 are strengthened to prevent punching shear failure and thus have 21 transverse strips and 4 longitudinal strips.   Table 6-13 provides a summary of the rehabilitation design using pultruded CFRP strips with respect to location

Table 6-13. Pultruded Rehabilitation Design and Spacing

Location (Span – Bay)	Transverse Reinforcement		Longitudinal Reinforcement	
	Quantity	C-to-C Spacing cm (inches)	Quantity	C-to-C Spacing cm (inches)
8-1	21 strips	60.96 (24)	4 strips	35.56 (14)
8-2	29 pairs	43.18 (17)	5 strips	27.94 (11)
9-1	21 strips	60.96 (24)	4 strips	35.56 (14)
9-2	29 pairs	43.18 (17)	5 strips	27.94 (11)
9-4	21 strips	60.96 (24)	4 strips	35.56 (14)

Spacing of transverse CFRP strips is governed by the punching shear criterion resulting in a maximum spacing of 60.96 cm (24 inches) c-to-c in locations S8B1, S9B1 and S9B4. Transverse strip pairs in locations S8B2 and S9B2 are placed 43.18 cm (17 inches) c-to-c for purposes of placement and uniform distribution over the slab area. Longitudinal CFRP strips are bonded to the bridge deck soffit such that the overlap between the pultruded strips and existing steel reinforcement is minimized. For locations S8B1, S9B1, and S9B4 a spacing of 35.56 cm (14 inches) c-to-c is used, while locations S8B2 and S9B2 are placed at 27.94 cm (11 inches) c-to-c.

Figure 6.7 shows the rehabilitated locations of Frame S-3 by design requirement.

Figure 6.7. Design Requirement for Rehabilitated Locations

6.6 FRP Rehabilitation Construction Guidelines

6.6.1 Surface Preparation

Since the efficacy of the method depends on the integrity of the bond of the FRP to the concrete substrate it is essential that the surfaces are adequately prepared. All unsound material and surface efflorescence must be removed and the surface rebuilt if necessary. Sandblasting is needed to expose aggregate. Details for surface preparation including specifications are listed in ACI 440 guidelines (2002) and NCHRP 514 construction guidelines (Mirmiran et al. 2004) and must be followed.

6.6.2 Wet Lay-up CFRP Composites

The wet lay-up procedure was used for locations span 8 bay 3 (S8B3), S9B3, S8B5, and S9B5. The two component epoxy resin was stored in a refrigerator on site prior to mixing due to the extremely high temperatures prevalent at the time of rehabilitation (32.2°C – 46.1°C). Mixing was performed using a mechanical mixer incorporating shearing action and once mixed, the resin was poured in the nip region of a mechanical impregnator, as seen in Figure 6.9. The distance between the rollers of the impregnator was set at 1 mm and the fabric was allowed to move through the impregnator before being wound on a cardboard roller for final application. The impregnated mate was unrolled and placed in position by one applicator (Figure 6.8), while a second used an aluminum roller to remove excess resin and air voids. The entire length is checked for defects during and after placement.

Figure 6.8. Wet Lay-up Construction

Figure 6.9. Impregnator for Wet Lay-up CFRP

6.6.3   *Adhesively Bonded Prefabricated CFRP Composite*

Adhesive bonding of prefabricated CFRP composite strips was used for locations S8B1, S8B2, S9B1, S9B2, and S9B4. Prior to placement, the prefabricated CFRP composite strips were precut to precise dimensions for each location, inspected for splits at cut ends, and attempted dry (i.e., without application of adhesive). The two component epoxy adhesive is mixed using a mechanical mixer incorporating shearing action and once mixed, the adhesive is applied to the surface of the deck slab and the prefabricated strip, as shown in Figure 6.10. The thickness of the bondline between concrete surface and prefabricated strips is not to exceed 3 mm for longitudinal strips and 5 mm for transverse strips. The prefabricated CFRP strips are bonded by applying pressure in a continuous manner from one end of the pultruded strip to the opposite end in the fiber direction, as shown in Figure 6.11. Uniform pressure is applied on the CFRP strip using a polyurethane roller and excess adhesive is removed using a squeegee edge.

Figure 6.10. Mixing and Application of Adhesive

Figure 6.11. Pultruded Strip Construction

6.7 Summary

Extending the service life of a structure requires understanding the cause of deterioration and selecting the measure best suited to restore functionality to the structure. In the case of the Watson Wash Bridge, transverse and longitudinal cracking in the deck slab provides evidence of deterioration in the structure. CFRP composites are selected as the means to prevent the occurrence of punching shear failure and increase the strength of the deck slab.

The objective of Chapter 6 is to detail the design methodology for FRP composite rehabilitation. Design values are determined from tension tests of specimens representative of wet lay-up and pultrusion composite processing techniques. Design of the CFRP rehabilitation uses a ratio of composite area to steel area, χ_{frp}; the ratio is multiplied by steel area deficiency to determine the area of CFRP composite required for rehabilitation. The HS20 truck load of 71.2 KN(16 kips) wheel load, Permit Truck wheel load of 106.8 KN (24 kips), and punching shear prevention are the primary demands on the deck slab with Permit Truck wheel load being the governing condition and the punching shear criterion, second.

In addition to design of the CFRP rehabilitation, the quality of construction and application are important factors in extending the life of the structure. Accordingly construction guidelines are established for surface preparation, material preparation and mixing, and application.

The next chapter initiates the monitoring phase of the Watson Wash Bridge rehabilitation, with a visual inspection of the CFRP composite rehabilitation and application of the global NDE procedure to evaluate stiffness changes in the deck

7 STRUCTURAL HEALTH MONITORING

7.1 Introduction

Chapter 6 provided an account of the bridge life extension procedure using CFRP composites. Specifically, the design of the FRP rehabilitation and construction guidelines was detailed. The rehabilitation design was based on the deficiency of the existing steel reinforcement and a ratio of CFRP composite cross-section area to steel reinforcement cross-section area. Guidelines for construction and application of the CFRP composite strips to the soffit of the bride deck were also described in order to instruct the fabricator.

With the completed FRP composite rehabilitation, evaluation of the CFRP composite in terms of manufacturing quality of material and its effect on the structure are necessary. Chapter 7 provides a field evaluation of the CFRP composite rehabilitation. The objective of this chapter is to monitor the bridge structure after rehabilitation with CFRP composites. In order to accomplish this objective two tasks within the scope of structural health monitoring are conducted:

1) Visual inspection of the applied FRP composites

2) Global NDE using modal parameters to quantify stiffness changes in the deck slab

As part of the monitoring process, each bay with externally bonded FRP composites is visually inspected. While visual inspection provides a subjective measure of the deck slab rehabilitation, it remains useful to identify defects and potential causes of degradation in the externally bonded CFRP composite strips. Visual inspection of the deck rehabilitation provides on-site inspection of the fabricator's work to ensure that the CFRP composite is manufactured and applied according to design specifications.

The T-girder bridge structure is monitored at 1 month, 12 months, and 20 months after rehabilitation CFRP composites. Vibration properties (frequencies and mode shape) of the Watson Wash Bridge are measured at each time and fractional stiffness changes are measured in the bridge deck structure.

7.2 Visual Inspection

7.2.1 Visual Inspection of Wet Lay-up CFRP

In the following section, field observations of the wet lay-up manufactured CFRP placed on the Watson Wash Bridge are provided; deviations in the prescribed procedure and changes or modifications to the design are noted. Observations are provided with respect to each bay with wet lay-up CFRP composites manufactured and applied to the deck soffit. Information from the inspection procedure includes the following:

1) Duration Required to Complete Manufacturing and Application of Composites

2) Observations During Manufacturing and Application

3) Material Samples Manufactured

4) Summary of CFRP Composite Strips on the Bridge Deck

5) Locations Identified as Potential Regions of Defect Growth

7.2.1.1 Location 9-3, Date: September 2-3, 2001

Duration: Manufacture and application of wet lay-up CFRP was initiated at 8:00 AM on September 2, 2001. The completion of span 9, bay 3 exceeded the expected time to completion of one workday, primarily due to rejections of several longitudinal and transverse strips during manufacture, details are provided below. The first day of activity concluded at approximately 2:30 PM, Sept. 2, 2001.

Manufacture and application of wet lay-up CFRP continued the following day at 8:20 AM on September 3, 2001 with completion of the CFRP rehabilitation on location 9-3 at 11:44 AM, September 3, 2001.

Observations During Manufacture and Application: As prescribed during the application process the longitudinal strips were first applied in their entirety followed by one layer of all transverse strips. The second layer of transverse strips was completed on day 2 of the application. During the first day of application, one longitudinal strip was rejected because its length was 60.96 cm (2 ft) short of the required length. In addition, several transverse strips were rejected because of applicator inability to keep fabric aligned with chalk markings during placement and excessive handling resulting in severe fiber waviness and displacement of edge tows. Rejected samples were considered unusable and discarded appropriately.

For the 21st transverse strip from the west end of location 9-3, primer was placed in the wrong location and reapplied in the correct location. In addition, numerous epoxy stains from resin dripping and handprints resulted from the wet lay-up application on the webs of the girders and adjacent bents. For subsequent applications, a plastic lining attached to the chamfer was required to ensure cleanliness of the work.

Since completion of location 9-3 did not occur during one workday, material application ceased following the first layer of transverse strips. Continuation of the application on the second day of the application required cleaning and priming surfaces of the first layer of strips prior to application of the second layer.

Material Samples Manufactured: Per material sample requirements, 3-1 layer and 3-2 layer sample panels were fabricated in Span 9 adjacent to Bay 3 prior to material application, with 3-1 layer and 3-2 layer sample panels manufactured at the end of the workday. Since two workdays were required to complete the bay, 3-1 layer and 3-2 layer panels were fabricated at the beginning and end of the second workday. The total number of sample panels manufactured for location 9-3 was 12-1 layer panels and 12-2 layer panels.

At Completion: In accordance with design requirements, the completed location 9-3 is built up of 28-2 layer transverse strips spaced at 45.72 cm (18 in) c-to-c and 4-1 layer longitudinal strips spaced at 22.86 cm (9 in) c-to-c. No modifications to the rehabilitation design in terms of quantity and spacing of reinforcement was observed.

Figure 7.1. Location 9-3 Completed

Locations Identified for Visual Inspection[1]:

- At the East end of the 3rd longitudinal strip, the strip shows misalignment between the 27th transverse strip and bent wall.

- A potential location for continuous monitoring is observed at the overlap between the 1st longitudinal strip and 24th transverse strip, where a gap at edge of the transverse strip appears to exist.

- On the 3rd transverse strip, the overlaps on the 2nd and 3rd longitudinal strips show indications of a gap at the free edge of the transverse strip.

7.2.1.2   Location 8-3, Date: September 4, 2001

Duration: Manufacture and application of wet lay-up CFRP initiated at 10:32 AM on September 4, 2001 following preparation activities. Manufacture and application of wet lay-up CFRP to span 8, bay 3 was completed at approximately 5:00 PM.

Observations During Manufacture and Application: As prescribed during the application process the four 1-layer longitudinal strips were first applied in their entirety, followed by one layer of all transverse strips. The second layer of transverse strips is then applied.

Although the manufacture and application process of the applicators was improved as compared to the work conducted on location 9-3, several transverse strip applications were rejected due to excessive handling and fraying of fibers.

Material Samples Manufactured: Per material sample requirements, 3-1 layer and 3-2 layer sample panels were fabricated in Span 8 adjacent to Bay 3 prior to material application, with 3-1 layer and 3-2 layer sample panels manufactured at the end of the

---

[1] For locations identified for visual inspection, transverse strips are numbered starting from 1 at the West end of the bay and numbered consecutively towards the East end of the bay. Longitudinal strips are number from 1 thru 4, left-to-right, facing west towards Barstow (i.e. facing opposite the direction of traffic). This note applies for both wet lay-up CFRP and pultruded CFRP strips.

workday. The total number of sample panels manufactured for location 8-3 was 6-1 layer panels and 6-2 layer panels.

At Completion: In accordance with design requirements, the completed location 8-3 is built up of 28-2 layer transverse strips spaced at 45.72 (18 in) c-to-c and 4-1 layer longitudinal strips spaced at 22.86 cm (9 in) c-to-c. No modifications to the rehabilitation design in terms of quantity and spacing of reinforcement was observed.

Figure 7.2. Location 8-3 Completed

Locations Identified for Visual Inspection:
- Between the 2nd and 3rd transverse strips, a crack traversing the entire width of the bay is identified at location 8-3.
- At the overlap of the 20th transverse strip, a gap is seen adjacent to the 1st longitudinal strip.

7.2.1.3 Location 8-5, Date: September 6, 2001

Duration: Manufacture and application of wet lay-up CFRP initiated at 6:53 AM on September 4, 2001 following preparation activities. Manufacture and application of wet lay-up CFRP to span 8, bay 5 was completed at approximately 2:08 PM.

Observations During Manufacture and Application: As prescribed during the application process one layer of the four longitudinal strips were first applied in their entirety followed by one layer of all transverse strips. The second layer of longitudinal strips were applied, such that an alternating sequence between longitudinal and transverse strips occurs with the objective being to mitigate the occurrence of air gaps at the overlap between longitudinal and transverse strips. Following the second layer of longitudinal strips, the remaining two layers of transverse strips were applied with all the second layers being completed first, then followed by the third layers of the transverse strips.

Material Samples Manufactured: Per material sample requirements, 3-1 layer, 3-2 layer, and 3-3 layer sample panels were fabricated in Span 8 adjacent to Bay 5 prior to

material application, with 3-1 layer, 3-2 layer, and 3-3 layer sample panels manufactured at the end of the workday. The total number of sample panels manufactured for location 8-5 was 6-1 layer panels, 6-2 layer panels, and 6-3 layer panels.

At Completion: In accordance with design requirements, the completed location 8-5 is built up of 21-3 layer transverse strips spaced at 60.96 cm (24 in) c-to-c and 4-2 layer longitudinal strips spaced at 22.86 cm (9 in) c-to-c. No modifications to the rehabilitation design in terms of quantity and spacing of reinforcement was observed.

Figure 7.3. Location 8-5 Completed

Locations Identified for Visual Inspection:

- On the 16th transverse strip, the overlaps at the 1st and 2nd longitudinal strips are observed and noted for their appearance as a potential void. In addition, at the 16th transverse strip, at the end nearest the 4th longitudinal strip, the end of the composite extends approximately 0.64 cm (0.25 in) off the edge of the slab.

- The region between the 10th transverse strip and the 2nd and 3rd longitudinal strips shows what appears to be an edge gap.

7.2.1.4 Location 9-5, Date: September 8, 2001

Duration: Manufacture and application of wet lay-up CFRP initiated at approximately 7:23 AM on September 8, 2001 following preparation activities. Manufacturing and application of wet lay-up CFRP to span 9, bay 5 was concluded and completed at approximately 12:00 Noon.

Observations During Manufacture and Application: As prescribed during the application process one layer of the four longitudinal strips were first applied in their entirety followed by one layer of all transverse strips. The second layer of longitudinal strips was then applied in their entirety, identical with location 8-5. Following the second layer of longitudinal strips, the remaining two layers of transverse strips were applied

with all the second layers being completed first, then followed by the third layers of the transverse strips.

Material Samples Manufactured: Per material sample requirements, 3-1 layer, 3-2 layer, and 3-3 layer sample panels were fabricated in Span 8 adjacent to Bay 5 prior to material application, with 3-1 layer, 3-2 layer, and 3-3 layer sample panels manufactured at the end of the workday. The total number of sample panels manufactured for location 8-5 was 6-1 layer panels, 6-2 layer panels, and 6-3 layer panels.

At Completion: In accordance with design requirements, the completed location 9-5 is built up of 21-3 layer transverse strips spaced at 60.96 (24 in) c-to-c and 4-2 layer longitudinal strips spaced at 22.86 cm (9 in) c-to-c. No modifications to the rehabilitation design in terms of quantity and spacing of reinforcement was observed.

Figure 7.4. Location 9-5 Completed

Locations Identified for Visual Inspection:
- On the 15th transverse strip, a gap adjacent to the overlap with the 1st longitudinal strip is observed as a potential void.
- Between the 11th and 12th transverse strips, a transverse crack is observed traversing across the entire width of the bay.

7.2.2 *Visual Inspection of Pultruded CFRP Strips*

In the following section, field observations of the pultruded CFRP placed on the Watson Wash Bridge are provided, including any deviations in the prescribed procedure and changes or modifications to the design. Since the pultruded CFRP composites are manufactured in a controlled laboratory environment prior to bonding, visual inspection of each bay primarily focuses on the adhesive layer, which bonds the composite to the concrete surface. As in the prior section, each visual inspection is conducted per bay with the following information provided:

1) Duration Required to Complete Application of CFRP Composite Strips

2) Observations During Manufacturing and Application

3) Locations Identified as Potential Regions of Defect Growth

Material samples are not specified from each bay of the application since the CFRP composites are pultruded in controlled laboratory conditions and their mechanical properties are uniform. In order to evaluate the pultruded CFRP composite properties, representative samples are cut from the pultruded CFRP composite rolls and tested. Those results are provided in Chapter 8 of this report.

7.2.2.1 Location 9-1, SCCI Pultruded Strips, Date: October 3, 2001

Duration: Application commenced at 8:00 AM on October 3, 2001. The time of finish is unavailable and not provided by the applicator; however, the location 9-1 was completed in its entirety during the workday of October 3, 2001.

Observations and Completion: As prescribed for the application for location 9-1, 4 longitudinal SCCI pultruded CFRP strips are first applied to the soffit of the bridge deck at 35.56 cm (14 in) c-to-c, followed by 21 transverse strips at 60.96 (24 in) c-to-c. During the first day of application several transverse strips were rejected since the strips were not flush with the edges of the bay. Location 9-1 is rehabilitated to prevent the occurrence of punching shear failure in the bridge deck.

During the application it was observed, the consistency of the adhesive became increasingly fluid as the day progressed. Therefore, strips were continuously observed for sagging to determine whether scaffolding would be required to hold composite strips in place. No scaffolding was necessary during the first day of work.

A cavity approximately 22.86 cm (9 in.) in diameter was filled with epoxy adhesive in order to maintain a continuous bondline for the pultruded strips. A picture of the filled hole is provided below.

At Completion: In accordance with design requirements bay 9-1 is repaired to prevent the occurrence of punching shear failure. Four longitudinal CFRP composite strips at 35.56 cm (14 in) c-to-c and 21 transverse CFRP composite strips at 60.96 cm (24 in) c-to-c are applied.

Figure 7.5. Location 9-1 Completed

Locations Identified for Visual Inspection:
- The cavity shown in Figure 7.6, is a location requiring monitoring since the 3rd longitudinal strip experiences a change in bond thickness at that location.

Figure 7.6. Cavity in Bay 9-1 Filled with Epoxy Adhesive

7.2.3   Location 8-1, SCCI Pultruded Strips, Date: October 8, 2001

Duration: Specific start and end times of the application are unavailable; however, the entire application of pultruded CFRP strips to location 8-1 was completed in one workday on October 8, 2001.

Observations During Application: As prescribed for the application for location 8-1, 4 longitudinal SCCI pultruded CFRP strips are first applied to the soffit of the bridge deck at 35.56 cm (14 in) c-to-c, followed by 21 transverse strips at 60.96 cm (24 in) c-to-c. In accordance with design requirements, bay 8-1 is repaired to prevent the occurrence of punching shear failure.

Prior to application of the strips, a modification to the location of the 3rd transverse strip, from the west side of bay 8-1, was displaced 7.62 cm (3 in) such that the edge-to-edge distance between the 2nd and 3rd transverse strips is 60.96 cm (24 in) and the edge to edge distance between the 3rd and 4th transverse strips is 48.26 cm (19 in). The modification was conducted in order to avoid an overlay at the end of a transverse strip and the end of a longitudinal strip.

Locations Identified for Visual Inspection:
- There exists a transverse crack extending the entire width of the bay between the 13th and 14th transverse strips.
- The 8th transverse strip appears to have an increasing bond line from the 4th longitudinal strip to the nearest girder.
- The 19th transverse strip appears to show a deficiency in the epoxy adhesive between the 2nd and 3rd longitudinal strips.

Figure 7.7. Location 8-1 Completed

7.2.4   *Location 8-2, SCCI Pultruded Strips, Date: October 9, 2001*

Duration: Specific start and end times of the application are unavailable; however, the entire application of pultruded CFRP strips to location 8-2 was completed in one workday on October 9, 2001.

Observations During Application: As prescribed for the application for location 8-2, 5 longitudinal SCCI pultruded CFRP strips are first applied to the soffit of the bridge deck at 27.94 cm (11 inches) c-to-c, followed by 29 transverse pair assemblies (2 strips per pair) at 43.18 cm (17 inches c-to-c). The CFRP composite applied is designed to strengthen the deck slab for permit truck wheel loads.

Locations Identified for Visual Inspection:

- An air gap approximately with 6.4 mm (¼ inch) diameter, of unknown depth, appears in the bondline of the 27th pair assembly, adjacent to the first longitudinal strip.

Figure 7.8. Location 8-2 Completed

7.2.5   Location 9-2, SCCI Pultruded Strips, Date: October 10, 2001

Duration: Specific start and end times of the application are unavailable; however, the entire application of pultruded CFRP strips to location 9-2 was completed in one workday on October 10, 2001.

Observations During Application: As prescribed for the application for location 9-2, 5 longitudinal SCCI pultruded CFRP strips are first applied to the soffit of the bridge deck at 27.94 cm (11 inches) c-to-c, followed by 29 transverse pair assemblies (2 strips per pair) at 43.18 cm (17 inches) c-to-c. The CFRP composite applied is designed to strengthen the deck slab for permit truck wheel loads.

Locations Identified for Visual Inspection:

- An air gap, approximately 6.4 mm (¼ inch) in diameter, with unknown depth, occurs at the 21st pair assemble adjacent to the 1st longitudinal strip.

Figure 7.9. Location 9-2 Completed

7.2.6 Location 9-4, SIKA Pultruded Strips, Date: October 11, 2001

Duration: Specific start and end times of the application are unavailable; however, the entire application of pultruded CFRP strips to location 9-4 was completed in one workday on October 11, 2001.

Observations During Application: As prescribed for the application for location 8-1, 4 longitudinal Sika Carbodur strips are first applied to the soffit of the bridge deck at 35.56 cm (14 inches) c-to-c, followed by 21 transverse strips at 60.96 cm (24 inches) c-to-c.

During the application, it is observed that the SIKA epoxy adhesive remained consistent throughout the workday. The SIKA adhesive compared to the SCCI adhesive possesses a grainy texture possibly due to the addition of a filler, which was more manageable during the field application.

Locations Identified for Visual Inspection:
- A crack extending the width of the bay is observed between the 5th and 6th transverse strips.

Figure 7.10. Location 9-4 Completed

7.3   Vibration Based Global NDE

Summaries of modal testing and vibration based damage detection techniques are provided in Chapters 3 and 4 of this report. Here, a brief review of the components of the global NDE procedure as it applies to the evaluation of the Watson Wash Bridge deck rehabilitation is conducted.

The global NDE procedure for the Watson Wash Bridge utilizes three primary processes to collect and analyze information from the bridge structure. These processes are as follows:

1) Dynamic Testing of the Structure

2) Modal Parameter Extraction

3) Damage Detection Algorithm

This section details procedures and results for monitoring of the Watson Wash Bridge Structure after FRP rehabilitation (1 month), 1 year after FRP rehabilitation (12 months), and prior to demolition of the bridge structure (20 months). The monitoring of the bridge structure requires the following steps: (1) Test Setup; (2) Data Acquisition and Analysis; (3) Damage Identification, Localization; and Quantification. The objective of this section is to illustrate the application of a structural health monitoring methodology to assess changes in the global structure due to FRP rehabilitation and monitor changes in performance over time.

7.3.1   Dynamic Testing

Dynamic testing and modal analysis serves to acquire a vibration signature (i.e. mode shapes) of the bridge structure at instants of time. The changes in measured modal parameters are used to determine the changes in a structure as the components of the superstructure weaken or deteriorate as a result of fatigue, interfacial failure mechanisms, or material deterioration over time. The modal testing and analysis is the experimental

phase of monitoring a civil structure to acquire the appropriate input into a damage detection algorithm.

Four output-only modal tests were conducted on the Watson Wash bridge structure in July 2001 (before rehabilitation), November 2001 (after FRP rehabilitation), October 2002 (12 months following FRP rehabilitation), and in June of 2003 prior to demolition (20 months after FRP rehabilitation). The four tests were conducted to determine if application of a structural health monitoring approach is capable of detecting changes in structural performance; a vibration based NDE procedure is used to identify, locate, and quantify the extent of changes in the RC bridge deck as a result of FRP rehabilitation.

7.3.1.1 Test Setup

The objective of the modal test is to implement an experimental procedure to acquire acceleration time histories at different points and directions of a structure, in order to ascertain the modal model through experimental modal analysis.

7.3.1.2 Excitation Method

During each of the modal tests, normal traffic over the bridge structure was used as the source of ambient excitation. The ambient excitation using normal traffic was selected for the following reasons:

> (1) Use of ambient excitation does not require closure of the bridge structure or interruption to bridge service

> (2) Use of normal traffic excitation illustrates potential for autonomous health monitoring of large scale bridge structures

7.3.1.3 Sensors

Standard capacitive accelerometers were used for the data acquisition procedure of the modal test, since accelerometers are able to operate over a wide range of frequencies and are typically easy to install. Accelerometers were mounted onto the soffit of the RC bridge structure using aluminum mounting plates attached to the structure. Figure 7.11 below shows a mounted accelerometer on the Watson Wash Bridge.

Figure 7.11. Accelerometer Attached to Watson Wash Bridge Structure

7.3.1.4 Sensor Locations

An important component of the modal testing process is the location of sensors and the spacing of sensors on the bridge deck. The spacing of sensors and number of sensor locations impacts the modal test procedure logistically, since, a limited number of sensors are available, and the number of patches or setups covering the spatial area of the deck compounds the time to complete a single test. Analytically, the sensor locations are critical since the resolution of the mode shape influences the accuracy of the damage detection results, where increasing the distribution of sensors over the bridge deck increases the likelihood of identifying, localizing, and quantifying the area of change or damage in an area of the structure.

For the modal tests of the Watson Wash Bridge Structure a sensor grid of six lines in the longitudinal deck directions and 11 lines in the transverse deck direction is used. Effectively, the longitudinal and transverse lines represent the row and column numbers of a matrix, respectively. For girder lines 1, 2, 5, and 6, accelerometers are attached at the hinges, at bent locations, and at mid span of Spans 8, 9, 10, and 11. For girder lines 3 and 4 sensors are applied at hinges and midspan, sensors are not applied at the bent locations. Therefore, sensor lines 1, 2, 5, and 6 contain 11 sensors each, while sensor lines 3 and 4 are composed of 6 sensors locations. The total number of sensor locations is 56. Accelerometer locations are shown in Figure 7.12. All sensors are bonded to the soffit of longitudinal girders in the bridge structure.

GIRDER LINES - Sensor Locations
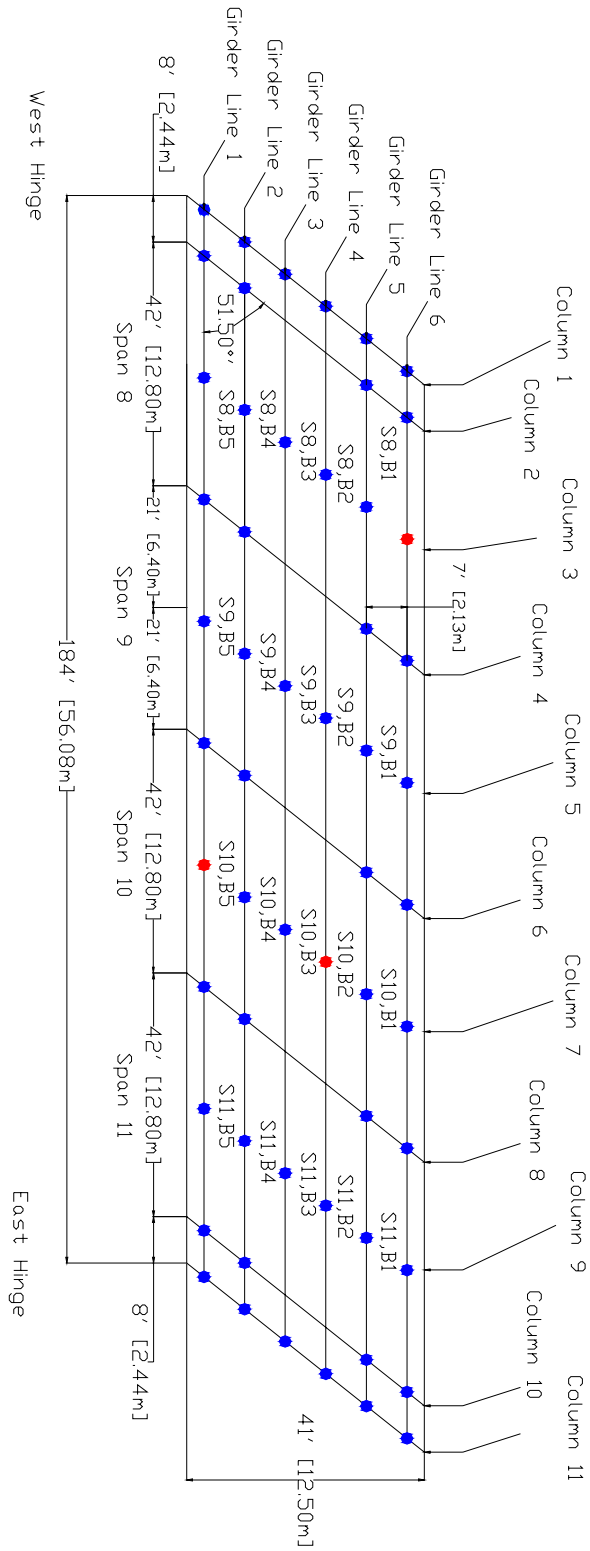
Figure 7.12. Diagram of Accelerometer Locations

In Figure 7.12, a blue circle indicates an accelerometer location; a red circle represents a reference sensor location where the accelerometer is stationary between sensor setups and is used to join multiple data sets into a single data set during the multi-setup modal test. Sensors are placed along the line of the girders at midspan since the primary regions of interest are bays or deck slabs between girders. It is desired to assess the performance of each bay, or the slab between girders, as components, which assemble the deck area of the bridge structure. In essence the deck slab between bents 8, 9, 10, and 11 are divided into 20 elements, with each element representing an area of the deck slab between girders. As shown in Figure 7.12 each deck slab location is identified by span and bay number, i.e. span 8, bay 3 is denoted S8, B3.

7.3.2   *Experimental Modal Analysis*

As normal traffic traverses the bridge structure, acceleration data is recorded at 200 samples/sec at each sensor for a total duration of approximately 1 minute per sensor configuration/setup. The sampling rate of 200Hz corresponds to a Nyquist frequency of 100 Hz or half the sampling frequency.

7.3.2.1   Time Domain Decomposition

A procedure for output-only experimental modal analysis in the time domain referred to as time domain decomposition (TDD) (Kim 2002) is implemented under the premise that any vector can be spanned by its basis. Similarly, the basis of the output of a linear structural dynamic system consists of its mode shapes. An acceleration time history response of a structure is the multi-output response of a multi degree of freedom system. For a time, t, the acceleration response of the structure is approximated as,

$$\ddot{\overline{y}}(t) \approx \sum_{i=1}^{n} \ddot{c}_i(t)\varphi_i \qquad \textbf{Eqn. 7.1}$$

Where n, is the number of modes in the measured acceleration signals; $c_i(t)$, is the ith modal contribution factor at time, t, and φ_i, is the ith mode shape vector from the measure acceleration response. Each measured time signal contains n modes within the Nyquist frequency; however, it is difficult to decipher the exact frequency of the mode. Nonetheless, a frequency band for the ith mode is obtainable by visual inspection of power spectral density (PSD) plots for use in digital filter design. Then a digital band pass filter for the measured acceleration time history is designed to isolate each target mode of the structure. The filtered acceleration time history represents a multi-output single degree of freedom system for identification. If N samples are measured the filtered acceleration time history containing the ith mode is described by the following equation.

$$[\mathbf{Y}_i] = \varphi_i \ddot{c}_i^T \qquad \textbf{Eqn. 7.2}$$

Where, $[\mathbf{Y}_i]$ is a $p \times N$ matrix containing filtered acceleration time history information for the ith mode; p is the number of sensor locations, and N is the number of measured sample points at the time of test. Next, a $p \times p$ output energy correlation matrix, $[\mathbf{E}_i]$, is computed from a multiplication of the filtered time history data and its transpose.

$$[\mathbf{E}_i] = [\mathbf{Y}_i][\mathbf{Y}_i]^T \qquad \textbf{Eqn. 7.3}$$

Substituting, equation 7.2 into equation 7.3, results in,

$$[\mathbf{E}_i] = \vec{\varphi}_i \ddot{\mathbf{c}}_i^T \ddot{\mathbf{c}}_i \vec{\varphi}_i^T = \vec{\varphi}_i q_i \vec{\varphi}_i^T \qquad \textbf{Eqn. 7.4}$$

The output energy matrix is a real semi-positive symmetric matrix, which can be decomposed into

$$[\mathbf{E}_i] = [\mathbf{U}][\mathbf{\Sigma}][\mathbf{U}]^T \qquad \textbf{Eqn. 7.5}$$

Where $[\mathbf{U}] = [\vec{\mathbf{u}}_1 ... \vec{\mathbf{u}}_p]$ is the singular vector matrix, containing p orthogonal vectors and $[\mathbf{\Sigma}] = diag[\sigma_1 ... \sigma_p]$ is a diagonal $p \ x \ p$ matrix of singular values of $[\mathbf{E}_i]$. In the case of noise free signals, σ_1 is the only nonzero singular value, and the first column of the singular vector matrix is the mode shape. In general, the first column of the singular vector matrix is the ith undamped mode shape of the structure and singular values $\sigma_2 ... \sigma_p$ are small relative to σ_1.

The frequency result is attained via a time history result of the ith modal contribution factor. ith modal contribution factor is calculated by multiplying both sides of equation 7.2 with the transpose of the ith mode shape.

$$\ddot{\mathbf{c}}_i^T = \frac{1}{\vec{\varphi}_i^T \vec{\varphi}_i} \vec{\varphi}_i [\mathbf{Y}_i] \qquad \textbf{Eqn. 7.6}$$

The result is analogous to a single output, single degree of freedom system representing the ith modal behavior of the structure. Analysis of the autospectrum of the modal contribution factor shows a single peak whose frequency location is the ith modal frequency of the structure.

The TDD technique requires the design of a digital band pass filter, which in turn requires a definition of the frequency band for which to filter the acceleration time history data. Visual inspection of autospectrums of the measured data provides the frequency range, which then allows for computation of mode shapes and frequencies. The primary computational component of the TDD does not require the discrete Fourier transform. The technique does require the use of a singular value decomposition (SVD), but the number of analyses using a SVD is limited to the number of modes desired in the structure. Thus, for cases where $n << p$, the method is computationally efficient and is able to extract unbiased mode shapes from closely spaced modes by adjusting the pass band range of a filter.

7.3.2.2   Considerations for Implementation

The TDD methodology is extended during the vibration testing of the Watson Wash Bridge by using a simple patching procedure based upon normalizing the partial mode shape to a single reference sensor location. For each setup of sensor locations the modal amplitudes for each location are acquired then incrementally joined with respect to the reference location. For 56 sensor locations of Frame S-3, five setups are used to resolve the entire mode shape of the structure.

The frequency results per setup from each modal test are averaged together to gain an indication of the frequency of the entire structure. Use of the TDD allows for a real time

evaluation of the frequencies and mode shapes with a simple programming language, such as the one available in Matlab, thus providing an immediate indication as to the quality and consistency of the data. The efficiency with which the TDD technique computes mode shapes and frequencies of the test provides a check of each partial mode shape and is advantageous for testing of large structures, as opposed to collecting data and merely examining acceleration time history plots, where such data quality assessments are subject to operator judgment.

However, patching of partial mode shapes of a large structure is not without its limitations or assumptions. The reference sensor locations must be selected away from vibration nodes, so as to avoid normalization by zero or a number near zero; this implies that prior knowledge of mode shapes is necessary prior to placing sensors. The application of the TDD technique for a single setup is applicable to damage detection algorithms since the mode shape extracted does not require the normalization process to join partial mode shapes.

7.3.2.3 Summary of Output-Only Modal Tests

Output only modal tests of Frame S-3 of the Watson Wash Bridge were conducted at four instants of time. Table 7-1 is a summary of the output only modal tests conducted.

Table 7-1. Summary of Output Only Modal Tests

Test Date	Test ID	Description
July 2001	Pre01	Pre FRP Rehabilitation
November 2001	Post01	Post FRP Rehabilitation
October 2002	Year02	12 Months After Rehabilitation
June 2003	Demo03	20 months After Rehabilitation

For each of the output only modal tests, it is desired to extract modal parameters to include a vibration based global nondestructive evaluation procedure to detect the occurrence of stiffness changes in the structure. With modal parameters acquired at each instant of time and a vibration based NDE procedure as in (Stubbs et al. 2000) it is possible to measure changes in the performance of the deck slab. Modal parameters act as the input into a vibration based NDE technique to provide estimates of increases in stiffness of the deck slab from bay to bay as well as provide indications of the degradation that occurs in the structure over time, while the CFRP rehabilitated bridge deck remains in service.

7.3.3 Data Analysis

7.3.3.1 Acceleration Time History

The modal parameters of the ambient vibration tests on Frame S-3 of the Watson Wash Bridge are extracted using the TDD technique. Acceleration time histories are recorded from all sensor locations of the bridge structure.
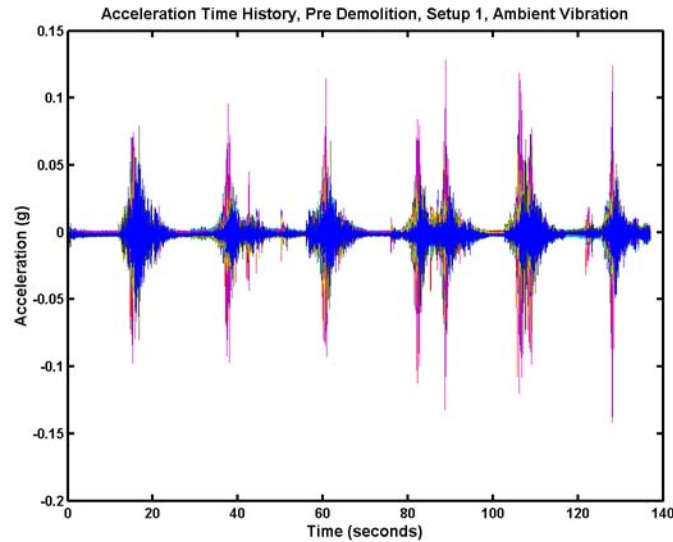
Figure 7.13. Measured Acceleration Time History

A sample acceleration time history is provided in Figure 7.13. Figure 7.13 shows acceleration versus time for a single setup from ambient vibration data collected prior to demolition of the Watson Wash Bridge structure.

7.3.3.2 Selection of Frequency Bands

From the acceleration time history, the power spectral density plots are generated to determine the frequency bands that act as input into the TDD technique. Selection of frequency bands is based on peaks observed from PSD plots.

The frequency bands are ranges input into the TDD to filter acceleration time history data in order to isolate a response of the structure. The frequency ranges are used as input into a low pass filter such as a Butterworth filter (Lathi, 2002) to isolate a single frequency within a visually identified range. For each of the ambient vibration tests the same band of frequencies are used since frequencies do not exceed the band range during the monitoring period of the structure, as it will be shown in section 7.3.3.3. In addition it is well-documented in literature that frequencies are insensitive to damage or changes in large bridge structures (Salawu, 1997b; Farrar, et al. 2001)
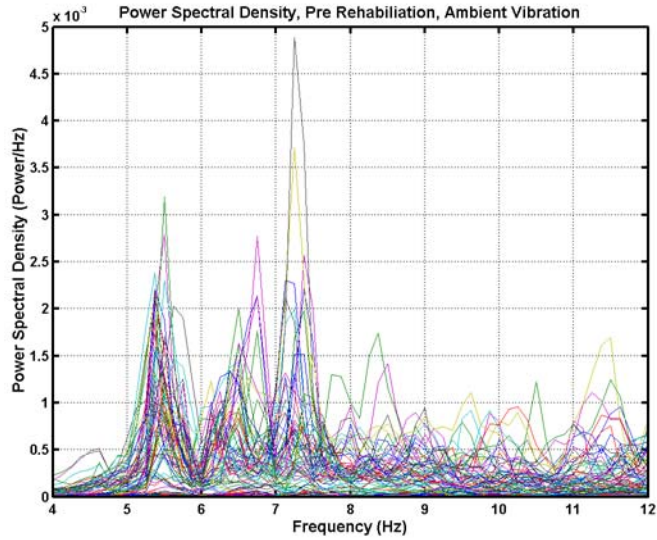
Figure 7.14. Power Spectral Density of All Signals, July 2001

In Figure 7.14, peaks in the PSD plots are observed between 5 and 6 Hz, 6 and 7 Hz, and between 7 and 8 Hz prior to rehabilitation of the bridge structure. A closer examination of the PSD plot reveals that a number of frequency bands contain peaks which may correspond to vibration modes of the bridge structure. Therefore, a wide array of frequency bands is used as input into the experimental modal analysis procedure for each time period. For each ambient modal vibration test, the same array of frequency bands is used to extract mode shapes from the recorded time history data of the bridge. The upper and lower bounds of the frequency bands used in the modal extraction procedure are shown in Table 7-2.

Table 7-2. Frequency Bands Used in TDD Method

Frequency Band	Lower Bound (Hz)	Upper Bound (Hz)
1	5.2	5.8
2	6.0	6.6
3	6.9	7.4
4	7.0	7.6
5	8.2	8.6
6	8.6	9.2
7	9.0	9.4
8	9.5	10.0
9	11.0	11.8
10	11.6	12.4

Figure 7.15 shows the PSD plot for acceleration time history data recorded after FRP rehabilitation of the bridge deck. It is noted that besides the peak observed between 5 and 6 Hz, the PSD plot does not indicate any consistency among sensors for vibration modes in the frequency ranges specified in Table 7-2. Similar observation are made for Figure 7.16 and Figure 7.17, which are PSD plots for modal tests 1 year after FRP rehabilitation and prior to demolition, respectively. The frequency bands specified in Table 7-2 are applied when extracting the mode shapes from the measured acceleration time history of the bridge structure. While the PSD plots potentially indicate that only one vibration mode between 5 and 6 Hz is detected consistently in all data sets, mode shapes are validated between modal tests with the use of the modal assurance criteria (MAC) values (Ewins, 2000).
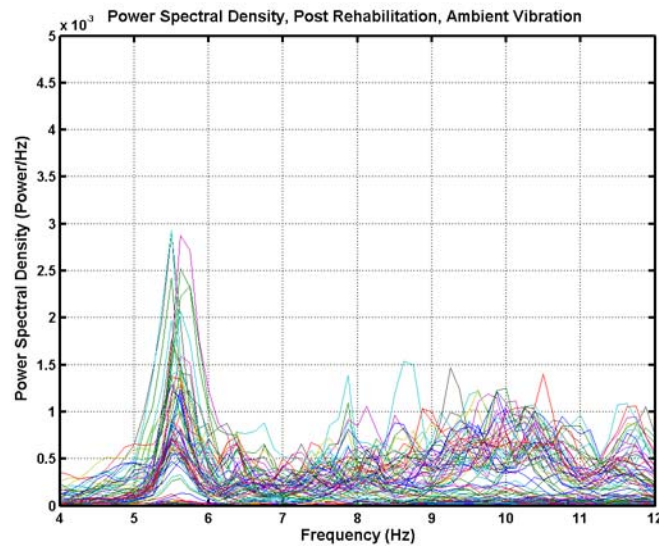
Figure 7.15. Power Spectral Density of All Signals, November 2001
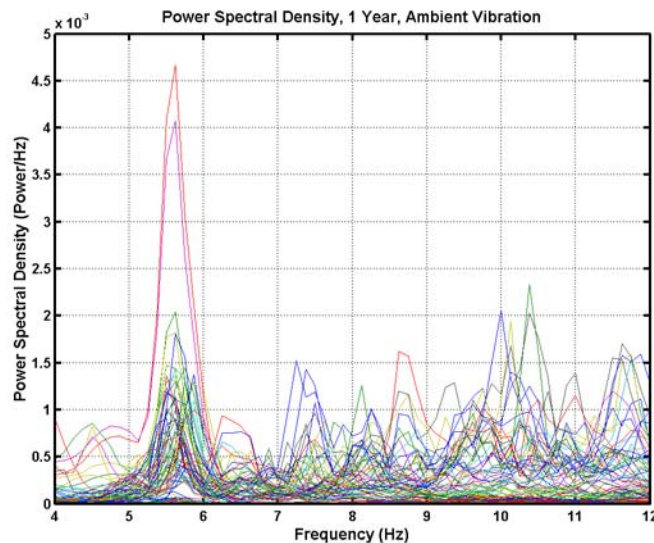
Figure 7.16. Power Spectral Density of All Signals, October 2002
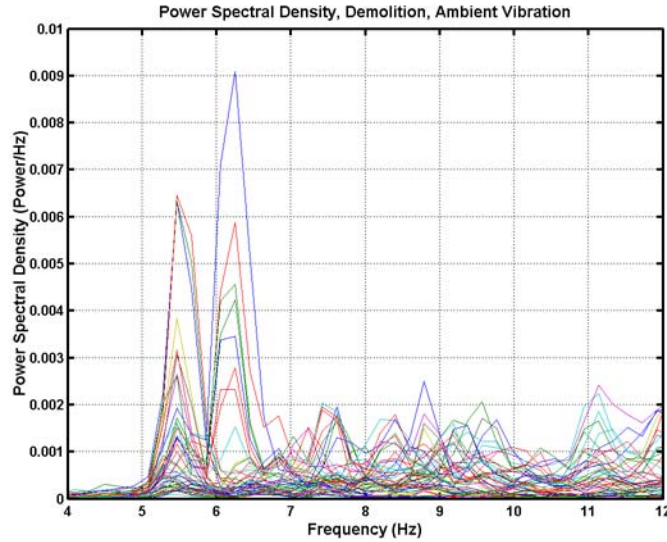
Figure 7.17. Power Spectral Density of All Signals, June 2003

7.3.3.3 Extracted Mode Shapes

From the PSD plots provided in the previous sections, the frequency bands were determined. Applying the TDD technique a vibration mode shape for a given frequency band can be extracted using the TDD technique; however, the mode shape must be verified. Verification is determined utilizing the modal assurance criterion, to determine if correlation between mode shapes of different sets exists. If a mode shape is correlated for all tests from July 2001 thru June 2003, then it is accepted.

7.3.3.3.1 Modal Assurance Criterion

A common method used to compare any two sets of vibration mode shapes is the modal assurance criterion (MAC). The MAC value indicates the correlation between two sets of mode shapes (Ewins, 2000). The MAC value between the qth mode of the first data set A and r[th] mode of second data set B is defined as follows:

$$MAC\left(\{\boldsymbol{\phi}_A\}_q, \{\boldsymbol{\phi}_B\}_r\right) = \frac{\left|\{\boldsymbol{\phi}_A\}_q^T \{\boldsymbol{\phi}_B\}_r\right|^2}{\left(\{\boldsymbol{\phi}_A\}_q^T \{\boldsymbol{\phi}_A\}_q\right)\left(\{\boldsymbol{\phi}_B\}_r^T \{\boldsymbol{\phi}_B\}_r\right)} \qquad \textbf{Eqn. 7.7}$$

where $\{\boldsymbol{\phi}_A\}_q$ is the mode shape vector for mode q of data set A and $\{\boldsymbol{\phi}_B\}_r$ is the mode shape vector for mode r of data set B. A MAC value close to 1 indicates that the two modes are well correlated and a value close to 0 is indicative of uncorrelated modes.

Table 7-3 thru Table 7-5 show the MAC values for mode shape results from the frequency bands identified in Table 7-2. The mode shape sets from Post Rehabilitation (November 2001), 1 Year after Rehabilitation (October 2002), and before demolition (June 2003) are compared to the Pre Rehabilitation (July 2001).

- 165 -

Table 7-3. MAC Values, July 2001 vs November 2001

	1	2	3	4	5	6	7	8	9	10
1	0.9245	0.0581	0.0062	0.0475	0.0219	0.0374	0.0122	0.0007	0.0047	0.0051
2	0.0206	0.0040	0.1254	0.0673	0.0083	0.0552	0.0315	0.0705	0.0991	0.1169
3	0.0034	0.0109	0.0101	0.1569	0.0012	0.0098	0.0215	0.0000	0.0349	0.0257
4	0.0061	0.0202	0.0060	0.1733	0.0145	0.0245	0.0049	0.0001	0.0399	0.0270
5	0.1871	0.0441	0.0130	0.0173	0.0242	0.0923	0.1172	0.0177	0.0458	0.0525
6	0.0012	0.0006	0.0011	0.0001	0.0081	0.0286	0.0130	0.0733	0.0810	0.1480
7	0.0478	0.0052	0.0716	0.0148	0.0017	0.1823	0.0006	0.0010	0.1181	0.0671
8	0.0069	0.0004	0.0024	0.0018	0.0002	0.0318	0.0994	0.0009	0.0011	0.0019
9	0.0187	0.0011	0.0049	0.0039	0.0018	0.0015	0.0000	0.0031	0.0648	0.0835
10	0.0016	0.0006	0.0214	0.0244	0.0000	0.0584	0.0137	0.0349	0.0001	0.0001

Table 7-4. MAC Values, July 2001 vs. October 2002

	1	2	3	4	5	6	7	8	9	10
1	0.9140	0.1636	0.0857	0.0394	0.0525	0.0013	0.0079	0.0348	0.0099	0.0060
2	0.0050	0.0094	0.0050	0.0049	0.0064	0.0342	0.0219	0.0582	0.0005	0.0027
3	0.0843	0.0159	0.0001	0.1193	0.0039	0.0078	0.0598	0.0010	0.0107	0.0016
4	0.0403	0.0239	0.0012	0.1616	0.0002	0.0053	0.0680	0.0022	0.0187	0.0019
5	0.0666	0.3548	0.0015	0.0106	0.0170	0.0008	0.0177	0.0142	0.0001	0.0018
6	0.0142	0.0016	0.0039	0.0031	0.0003	0.0281	0.0227	0.0511	0.0001	0.0005
7	0.0612	0.0981	0.0001	0.0010	0.0016	0.1117	0.1253	0.0349	0.0223	0.0003
8	0.0040	0.0050	0.0001	0.0044	0.0265	0.0023	0.0001	0.2382	0.0654	0.0320
9	0.0064	0.0008	0.0001	0.0021	0.0000	0.0087	0.0266	0.0122	0.0028	0.0113
10	0.0177	0.0004	0.0039	0.0015	0.0007	0.0037	0.0160	0.0005	0.0006	0.0002

Table 7-5. MAC Values, July 2001 vs. June 2003

	1	2	3	4	5	6	7	8	9	10
1	0.9563	0.0616	0.0117	0.0012	0.1196	0.0429	0.0028	0.0005	0.0012	0.0203
2	0.0321	0.1768	0.0003	0.0010	0.0308	0.0019	0.0732	0.0114	0.0216	0.0622
3	0.0066	0.0752	0.4497	0.6591	0.0117	0.0375	0.0525	0.0131	0.0046	0.0000
4	0.0101	0.0835	0.4389	0.6709	0.0215	0.0219	0.0961	0.0160	0.0095	0.0003
5	0.1983	0.0066	0.0060	0.0031	0.0029	0.0643	0.0267	0.0231	0.0527	0.0127
6	0.0006	0.0725	0.0176	0.0393	0.0000	0.0078	0.2427	0.2287	0.0995	0.0012
7	0.0698	0.2038	0.0396	0.0867	0.0481	0.0066	0.0412	0.2048	0.0274	0.0203
8	0.0040	0.0054	0.0178	0.0207	0.0340	0.0113	0.1922	0.1283	0.0049	0.0006
9	0.0286	0.0050	0.0092	0.0037	0.0025	0.0024	0.0021	0.0041	0.1236	0.5522
10	0.0026	0.0424	0.0109	0.0097	0.0450	0.0309	0.0062	0.0112	0.0003	0.0203

From the preceding tables it is observed that one mode of vibration between the 5 and 6 Hz frequency band is correlated from the ambient vibration output-only mode tests. The corresponding MAC values from Table 7-3 thru Table 7-5 are 0.9245, 0.9140, and 0.9563, respectively. It is concluded that from the ambient vibration output-only tests one mode of vibration is consistently identified from each modal test.

7.3.3.3.2 Mode Shapes

The identified mode from the MAC values is the first bending mode of Frame S-3 of the Watson Wash Bridge structure. Table 7-6 shows the modal amplitudes at each sensor location of the bridge structure for PRE, POST, 1YR, and DEMO ambient vibration tests on the bridge structure. Locations are denoted by girder line number (row number) and column number as shown in Figure 7.12 (i.e. 410 indicates line 4, column number 10, and ID 205 indicates girder line 2, column number 5).

Table 7-6. Modal Amplitudes of First Bending Mode

ID	PRE	POST	1 YR	DEMO	ID	PRE	POST	1YR	DEMO
101	-1.8282	-0.0002	-1.8751	-1.9782	401	-1.1010	-0.7600	-1.3390	-1.1552
102	-0.0766	0.0002	-0.0713	-0.1068	402	0.0000	0.0000	0.0000	0.0000
103	2.6298	1.9926	2.8337	2.5806	403	2.1282	1.5506	2.0224	2.0398
104	0.0390	0.0577	0.0326	0.0372	404	0.0000	0.0000	0.0000	0.0000
105	-1.2853	-0.9589	-1.3173	-1.3915	405	-1.4430	-1.1475	-1.3971	-1.4899
106	-0.0208	-0.0266	-0.0310	-0.0178	406	0.0000	0.0000	0.0000	0.0000
107	1.0000	1.0000	1.0000	1.0000	407	1.8245	1.3837	1.2351	1.7823
108	0.0261	0.01208	0.0315	0.0301	408	0.0000	0.0000	0.0000	0.0000
109	-1.0839	-1.0613	-1.1513	-1.3119	409	-1.8854	-1.8710	-2.4311	-1.9783
110	-0.0038	-0.0053	-0.0141	0.0138	410	0.0000	0.0000	0.0000	0.0000
111	0.7435	1.1057	0.7161	1.2883	411	1.2996	1.2696	0.9320	1.6124
201	-1.7701	-0.9699	-1.8317	-1.8604	501	-1.1752	-0.6181	-1.2203	-1.4474
202	0.0630	0.0090	0.4804	-0.0836	502	0.0228	0.0175	-0.0219	-0.0297
203	2.5707	1.9410	2.6580	2.7597	503	1.8716	1.0480	1.7816	1.8740
204	-0.0295	-0.0044	0.0351	0.0350	504	0.1685	-0.0162	0.0308	0.0243
205	-1.4894	-0.9782	-1.4392	-1.5244	505	-1.3715	-1.0239	-1.2278	-1.3103
206	0.0094	0.0037	-0.0073	-0.0083	506	0.0056	0.0170	-0.0012	-0.0010
207	1.1662	1.0363	1.1450	1.2390	507	1.4529	1.3136	0.9826	1.2964
208	-0.0171	-0.0313	0.0180	0.0217	508	-0.0119	-0.0253	0.0122	0.0143
209	-1.3680	-1.6514	-1.2432	-1.5795	509	-1.9485	-2.1776	-2.6573	-2.9420
210	0.0128	0.0169	-0.0134	-0.0213	510	0.0266	0.0532	-0.0169	-0.0394
211	0.7648	1.1392	0.7396	1.3779	511	1.6726	1.3970	1.1405	1.4540
301	-1.0426	-0.8256	-1.3478	-1.6645	601	-1.2458	-0.5959	-1.1917	-1.3090
302	0.0000	0.0000	0.0000	0.0000	602	-0.0112	0.0092	0.0080	-0.0012

Table 7-6. (Cont'd) Modal Amplitudes of First Bending Mode

ID	PRE	POST	1 YR	DEMO	ID	PRE	POST	1YR	DEMO
303	2.1249	1.7932	2.1801	2.1254	603	1.0638	0.9162	0.5406	0.7424
304	0.0000	0.0000	0.0000	0.0000	604	0.0018	-0.0289	-0.0101	0.0003
305	-1.5483	-1.0761	-1.5245	-1.5635	605	-1.2734	-0.9623	-1.1503	-1.1047
306	0.0000	0.0000	0.0000	0.0000	606	0.0380	0.0205	0.0452	0.0352
307	1.3813	1.2367	1.1606	1.4309	607	1.3408	1.2531	0.8745	1.1663
308	0.0000	0.0000	0.0000	0.0000	608	-0.0476	-0.0307	-0.0672	-0.0544
309	-1.7466	-1.8609	-1.4084	-1.4035	609	-1.8229	-2.2222	-2.6921	-3.0269
310	0.0000	0.0000	0.0000	0.0000	610	0.0763	0.0465	0.0261	0.0757
311	1.2126	1.2305	0.8804	1.5580	611	1.9336	1.4386	1.2040	2.2904

Plotting the surface of the first vibration modes from the modal tests shows the first bending mode of vibration of the bridge structure in Figure 7.18 thru Figure 7.21. The identified mode shapes of the structure are used as input parameters for the vibration based damage detection procedure to determine if increases or decreases in stiffness can be detected and if stiffness changes can be related to the wheel load capacity of the deck slab over time.
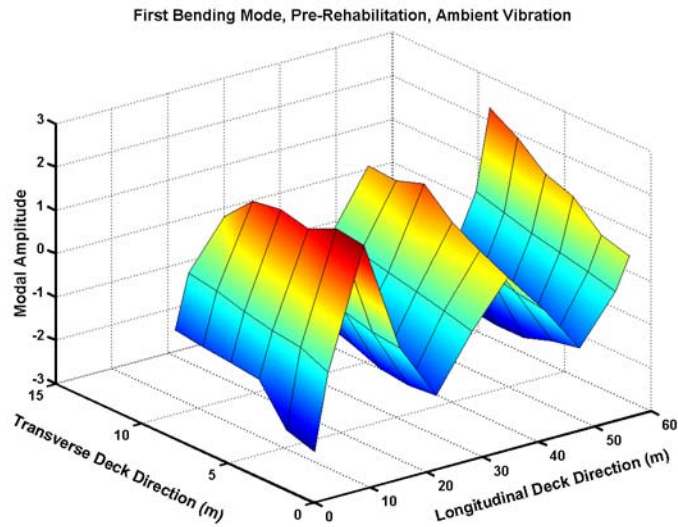
Figure 7.18. First Bending Mode, PRE, July 2001

First Bending Mode, Post-Rehabilitation, Ambient Vibration
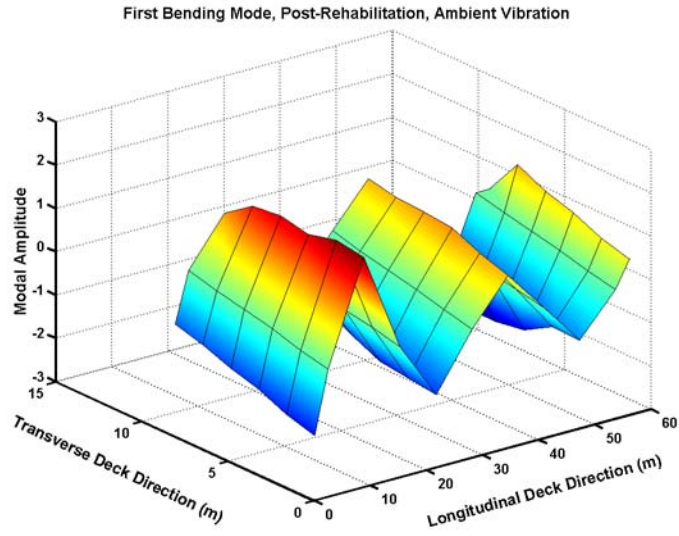
Figure 7.19. First Bending Mode, POST, November 2001

First Bending Mode, 1 Year after Rehabilitation, Ambient Vibration
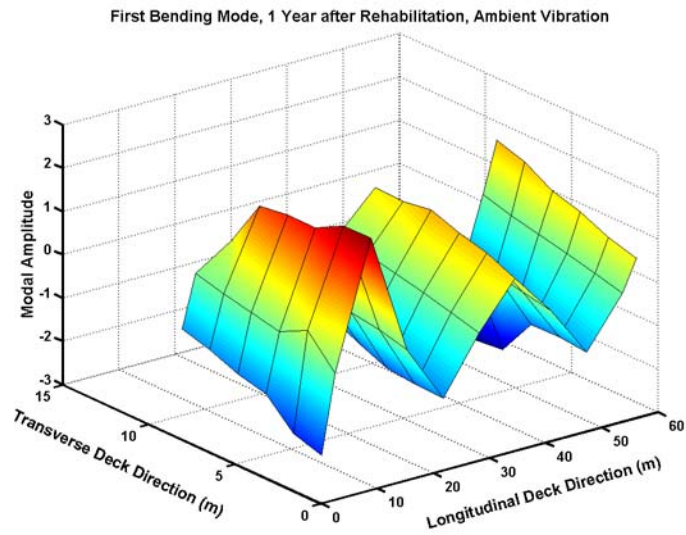
Figure 7.20. First Bending Mode, 1 YR, October 2002

First Bending Mode, Pre Demolition, Ambient Vibration
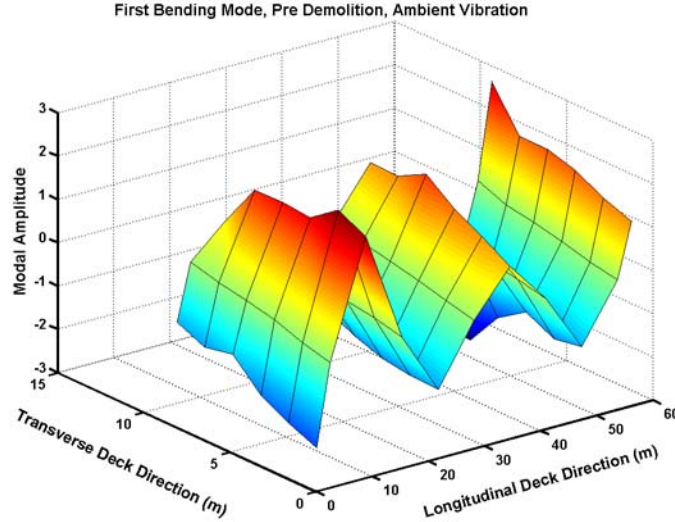
Figure 7.21. First Bending Mode, DEMO, June 2003

7.3.4   Vibration Based Nondestructive Evaluation

7.3.4.1   Background

Output only modal testing and experimental modal analysis represents the data collection component of the structural health monitoring process. The nondestructive evaluation process requires the use of a vibration based NDE technique to identify stiffness changes in a structure. For the purposes of this analysis, the damage index method by Stubbs, et al. (2000) is applied. The damage index is denoted by the following formulation.

$$\beta_j = \frac{k_j}{k_j^*} = \frac{1}{2}\left[\frac{\Phi_i^{*T}C_{j0}\Phi_i^*}{\Phi_i^{*T}C^*\Phi_i^*}\cdot\frac{\Phi_i^T C \Phi_i}{\Phi_i^T C_{j0}\Phi_i}+1\right]$$ **Eqn. 7.8**

where k_j, and k_j^* are scalar parameters representing the material stiffness properties of the undamaged and damaged j^{th} member of the structure, C_{j0} is a matrix of geometric quantities (and possibly terms containing Poissson's ratio), C and C^* are the system stiffness matrices for the undamaged and damaged structure, Φ_i and Φ_i^* are the respective undamaged and damaged i^{th} modal vectors. If β_j is greater than one, damage may exist; if β_j is less than one and greater than zero, a stiffness increase may have occurred.

The severity estimation in terms of fractional stiffness loss or increase, α_j, is given for each potentially changed element, j, by the following equation.

$$\alpha_j = \frac{k_j^* - k_j}{k_j} = \frac{1}{\beta_j}-1$$ **Eqn. 7.9**

where β_j is the damage index shown in eqn. 11.8. All other variables are defined previously.

7.3.4.2 <u>Implementation</u>

With the identified mode shapes from output-only modal tests, the damage detection algorithm is implemented. In order to locate stiffness changes in the bridge deck a beam element formulation is applied to the damage detection model (Stubbs et al 1997). For the beam element formulation the damage index, β_j:

$$\beta_j = \frac{EI_j}{EI_j^*} = \frac{1}{2} \left[\frac{\int_{x_j}^{x_j + \Delta x_j} \{\phi_i'''^*(x)\}^2 dx}{\int_{x_j}^{x_j + \Delta x_j} \{\phi_i''(x)\}^2 dx} \cdot \frac{\int_0^L \{\phi_i''(x)\}^2 dx}{\int_0^L \{\phi_i'''^*(x)\}^2 dx} + 1 \right]$$ **Eqn. 7.10**

where, ϕ_i'' and $\phi_i'''^*$, are the undamaged and damaged i^{th} modal curvature, x_j is the initial coordinate of element j; Δx_j is the length of element j. The vibration based damage detection procedure compares two sets of mode shapes of a structure to identify and locate changes in stiffness of the structure. If $\beta_j > 1$, indicates a stiffness loss in element j; $\beta_j < 1$ indicates a stiffness increase in element j; and $\beta_j = 1$ indicates no stiffness change in element j. The procedure is applied according to the following steps:

1. Calculate mode shape curvatures using a cubic spline curve fit of the mode shape and numerical derivatives (computations are conducted using commercial programming languages such as in Matlab).

2. Calculate the damage index, β_j, for each element, j.

3. The fractional stiffness change, α_j, (loss or gain) is determined. If $\alpha_j > 0$, then an increase in stiffness has occurred; if $\alpha_j < 0$, then a loss in stiffness is deemed to have occurred.

7.3.4.3 <u>Frequency Results</u>

As a qualitative indicator of changes in Frame S-3 of the Watson Wash Bridge, the measured first bending mode frequencies are provided from dynamic tests conducted between May 1999 and June 2003, prior to demolition of the Watson Wash Bridge. A summary of first bending mode frequency results for Frame S-3 are shown in the following table:

Table 7-7. Frame S-3 Mode 1 Frequency Results

Date:	May-99	Sep-00	Jul-01	Nov-01	Jun-03
Mode 1 (Hz)	5.59	5.44	5.438	5.563	5.547

The dynamic testing of the Watson Wash Bridge began on May 1999, with an initial characterization of the vibration properties of the structure prior to a maintenance action of applying a surface overlay to the road surface. Following the maintenance action, a

subsequent dynamic test was conducted in September of 2000, the surface overlay on the deck of the structure is shown to increase the mass of the bridge deck without any significant stiffening of the structure, resulting in a 2.68% reduction in the mode 1 frequency of Frame S-3.

Approximately 289 days following the September 2000 dynamic tests, in July 2001, a modal test is conducted prior to rehabilitation of the bridge decks of Spans 8 and 9 using CFRP composites. No significant change in frequency is observed between the September 2000 and July 2001 dynamic testing results.

The rehabilitation of Spans 8 and 9 was conducted from September 2–8, 2001 for wet lay-up manufactured CFRP and from October 3-11, 2001 for the pultruded CFRP composites, without any obstruction to bridge traffic. In November of 2001, another modal test was conducted following the rehabilitation to acquire the vibration properties of the structure following rehabilitation with FRP. A 2.30% increase in frequency is observed relative to the first mode frequency measured in July of 2001.

Approximately 1476 days later, in June 2003, prior to the demolition of the Watson Wash Bridge, a first mode frequency decrease of 0.29% is observed.

A preliminary evaluation of mode 1 frequencies provides indications as to the change in structural performance relative to two distinct maintenance actions. First, the asphalt overlay applied to the structure in May 1999, increases the mass of the structure while providing negligible changes in the stiffness. On the other hand, the mode 1 frequencies indicate that rehabilitation of approximately two spans of Frame S-3 (2 of 4 spans, or 9 of 20 bays) with CFRP composites contributes to an increase in the stiffness of the frame. A summary of the maintenance measures and first mode frequency results is illustrated in the following figure.
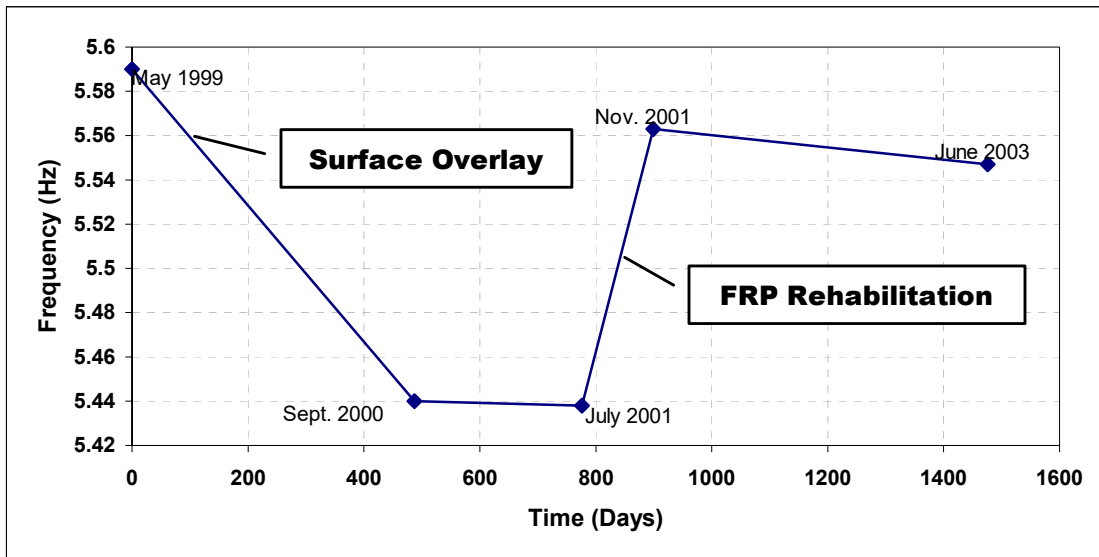
Figure 7.22. First Mode Frequency Results

An independent evaluation of the Watson Wash Bridge Structure of Frame S-3 showed that a mass density increase of 11.9% occurs following the application of the asphalt overlay from 2.42 g/cc (4.7 lb-s^2/ft^4) to 2.71 g/cc (5.26 lb-s^2/ft^4) (Stubbs et al, 2001) between May 1999 and September 2000. The mass density increase correlates with the experimentally measured frequency decrease since no stiffness increase is observed with the addition of the asphalt surface overlay.

Following the rehabilitation of Spans 8 and 9 of the Watson Wash Bridge, a frequency increase is observed between July 2001 and November 2001. The change in frequency suggests that the FRP rehabilitation provided an increase in stiffness of the structure since an inconsequential amount of dead load is introduced to the structure with CFRP composites bonded to the deck soffit.

The frequency decline between November of 2001 to June of 2003, may be attributed to one or more of the following conditions:

- Environmental degradation of the CFRP due to exposure in the Mojave Desert climate
- Stiffness increase of the deck slabs results in greater load transfer to the girders, subsequently causing the deterioration in the girders of the structure
- Continued deterioration of the unrehabilitated spans of Frame S-3.

The measured change in frequency provides only a qualitative indication of change in stiffness of the structure following rehabilitation. In order to quantify improvements in the deck slab of spans 8 and 9, stiffness changes are determined with measured mode shapes in the following section.

7.3.4.4   Damage Indicator Results

The damage indicator results are used to identify locations where increases or decreases in stiffness have occurred during normal service operation of the structure. For the monitoring of Spans 8, 9, 10, and 11 of the Watson Wash Bridge, the structure is divided into 20 elements. Each element represents an area of the deck slab between girders and bents of the span; Figure 7.23 shows the elements representing the deck slab of the bridge. One element represents a single bay of the Watson Wash Bridge. Of these elements, those that are rehabilitated with CFRP composites are denoted with the color blue; locations that are not rehabilitated are denoted in the color orange. Each element is identified by its span and bay location, i.e. span 9, bay 5 is element S9B5.
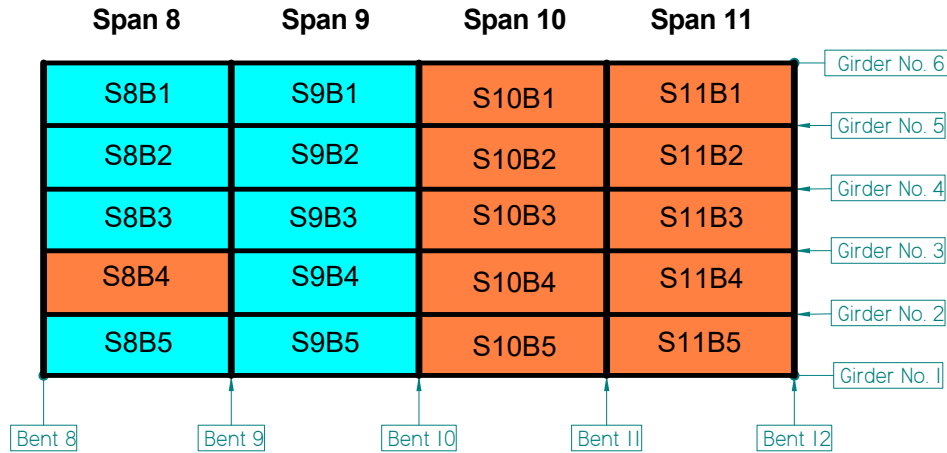
Figure 7.23. Element Division for Monitoring of Bridge Deck

Figure 7.24 shows damage index results from equation 8.10, comparing mode shapes measured before and after rehabilitation of spans 8 and 9 with CFRP composites. A damage index, β_j, value less than one indicates that stiffness has increased in a location or element; a β_j value greater than one indicates that a decrease in stiffness in a location has occurred. In Figure 7.24, damage index values less than one are measured in spans 8 and 9 as expected since CFRP composite rehabilitations are constructed in those locations. A damage index value less than one in S8B4, an unrehabilitated location, is attributed to the stiffening effects in adjacent locations. In the unrehabilitated locations of spans 10 and 11, damage index values greater than one are observed, indicating stiffness losses in the region.
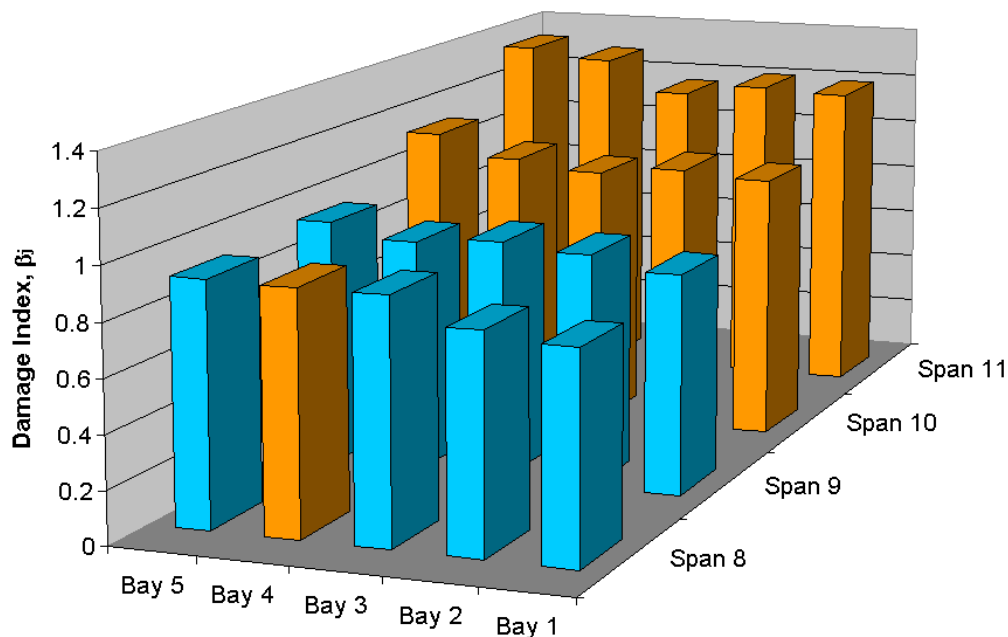
Figure 7.24. Damage Indices After CFRP Construction

Figure 7.25 shows damage index results comparing mode shapes measured before and 12 months after rehabilitation. In bays 3, 4, and 5 of spans 8 thru 12, a uniform distribution of damage index values is observed, which suggest that stiffness redistribution occurs in those locations in the right lane of traffic where heavier truck loads are observed. Bays 3 and 5 of spans 8 and 9 correspond to regions surrounding the unrehabilitated location of S8B4, as well as wet lay-up manufactured CFRP composites.

In bays 1 and 2 of spans 8 thru 12, the damage index results show a similar pattern as compared to Figure 7.24. The rehabilitated locations S8B1, S8B2, S9B1, and S9B2 continue to show damage index values less than one, indicating the stiffness increase is maintained at 12 months. S8B1, S8B2, S9B1 and S9B2 are rehabilitated using pultruded CFRP composites.
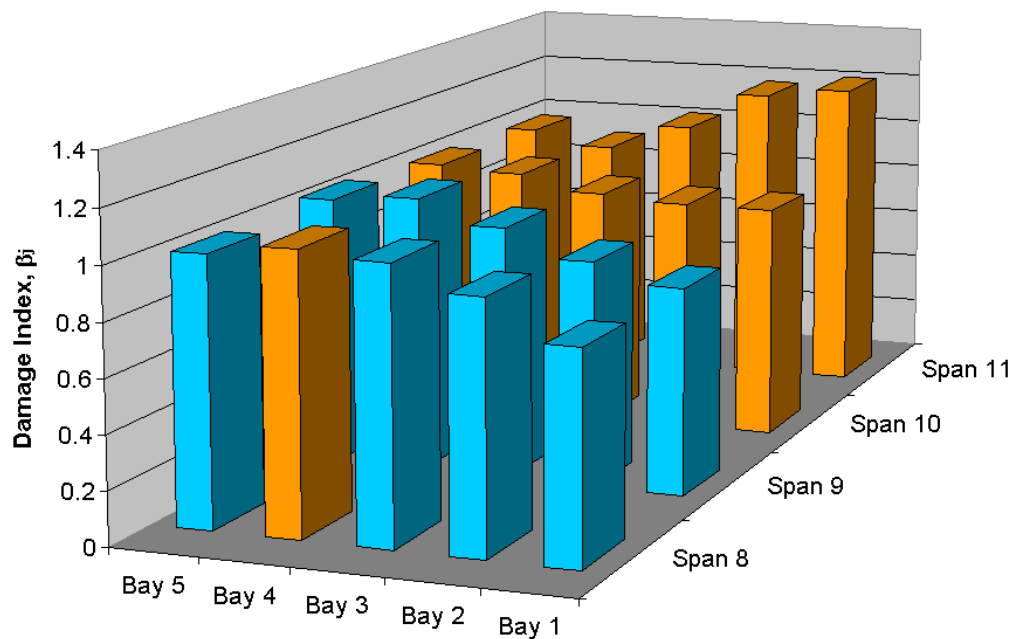
Figure 7.25. Damage Indices 12 Months After FRP Construction

Figure 7.26 shows damage index results comparing mode shapes measured before and 20 months after rehabilitation. Bays 3, 4 and 5 of spans 8 thru 12 show similar results as compared to Figure 7.25. Furthermore, bays 1 and 2 of spans 8 thru 12 also show similar damage index results. At twenty months, damage index results in spans 10 and 11, compared to Figure 7.24 indicate stiffness increases have occurred although no rehabilitation measures were conducted in the regions.
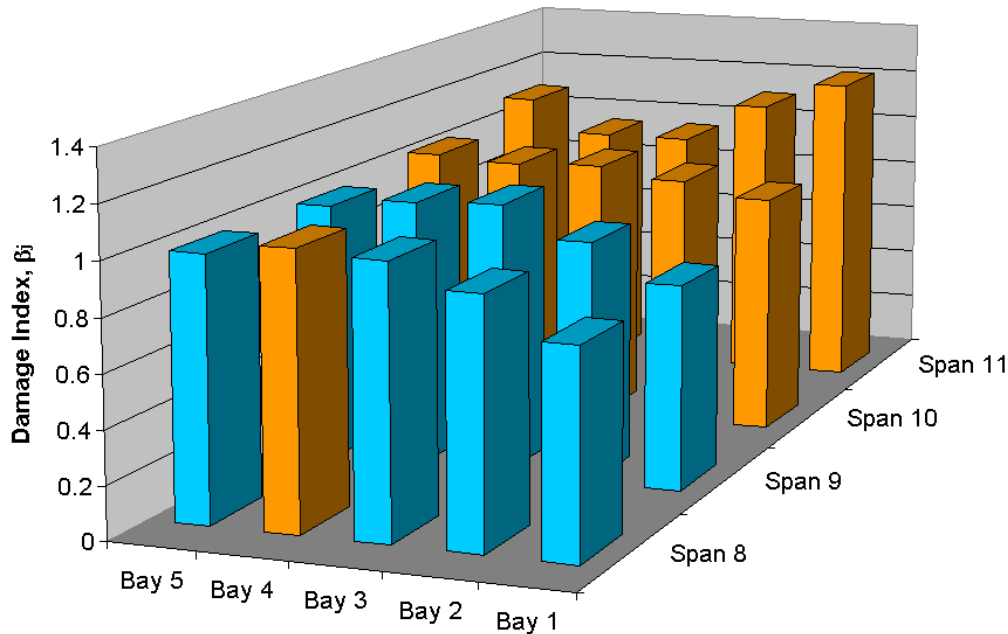
Figure 7.26. Damage Indices 20 Months After FRP Construction

7.3.4.5 Computed Stiffness Changes

Implementing equation 8.9, fractional stiffness losses, α_j, are computed from computed damage indices for each location. Table 7-8, Table 7-9, and Table 7-10 show fractional stiffness losses measured in each element after, 12 months after, and 20 months after CFRP composite bonding to spans 8 and 9 of the Watson Wash Bridge.

Table 7-8. Stiffness Changes after Rehabilitation

Span No.	Fractional Stiffness Change by Location				
	Bay 5	Bay 4	Bay 3	Bay 2	Bay 1
Span 8	9.77%	10.43%	10.46%	23.71%	28.77%
Span 9	7.27%	13.72%	10.65%	13.47%	20.41%
Span 10	-10.35%	-3.24%	0.22%	-3.03%	-1.01%
Span 11	-25.24%	-23.14%	-14.82%	-18.00%	-16.98%

Table 7-8 shows an average stiffness increase of 16.63% in span 8 and 13.10% in span 9. In spans 10 and 11, average stiffness losses of –3.48% and –19.64% are calculated, respectively. All bays of span 8 show increases in stiffness with the greatest increase occurring in location S8B1 at 28.77%. The lowest stiffness increase is observed in S8B5 at 9.77%. It is important to note that location S8B4 is unrehabiltiated and its stiffness increase is attributed to the stiffening provided by adjacent bays of the bridge structure. In span 9, the highest stiffness increase occurs in S9B1 opposite S8B1. The lowest

stiffness increase of span 9 is measured in S9B5 at 7.27%. The stiffening of spans 8 and 9 result in measured stiffness losses in spans 10 and 11.

Table 7-9. Stiffness Changes 12 Months After Rehabilitation

Span No.	Fractional Stiffness Change by Location				
	Bay 5	Bay 4	Bay 3	Bay 2	Bay 1
Span 8	0.08%	-4.00%	-1.82%	8.07%	28.58%
Span 9	-1.92%	-4.32%	4.34%	17.27%	28.09%
Span 10	1.05%	2.89%	9.47%	12.11%	12.26%
Span 11	2.25%	8.42%	-2.64%	-15.48%	-18.09%

Table 7-9 shows stiffness changes 12 months after rehabilitation with CFRP composites. Average stiffness increases of 6.18% and 8.7% are calculated for spans 8 and 9, respectively. In bays 3, 4, and 5 of spans 8 and 9 the effect of the CFRP rehabilitation is reduced. More specifically, a redistribution of stiffness is observed in bays 3, 4, and 5 of all spans that correspond to the right wheel load of traffic and with rehabilitation locations influenced by the unrehabilitated state of S8B4. As deterioration in span 8 and span 9 occurs a stiffening effect is observed in spans 10 and 11 for bays 3, 4, and 5. The pultruded CFRP composites applied in bays 1 and 2 of spans 8 and 9 continue to show increases in stiffness as compared to wet lay-up constructed CFRP composites.

Table 7-10. Stiffness Changes 20 months After Rehabilitation

Span No.	Fractional Stiffness Change by Location				
	Bay 5	Bay 4	Bay 3	Bay 2	Bay 1
Span 8	1.48%	-2.67%	-0.93%	8.70%	29.72%
Span 9	2.27%	-1.20%	-2.73%	9.95%	29.47%
Span 10	-1.39%	0.33%	-0.76%	3.14%	9.34%
Span 11	-8.70%	4.03%	4.02%	-10.67%	-18.46%

Table 7-10 shows stiffness changes 20 months after rehabilitation with CFRP composites. Average stiffness increases of 7.26% and 7.55% are calculated for spans 8 and 9, respectively. The stiffness changes are similar to the those measured 12 months after rehabilitation, where the stiffness distributions occur in bays 3, 4, and 5 of spans 8 thru 12. These locations correspond to the right lane of traffic on the Watson Wash Bridge where heavier truck traffic is observed and the wet lay-up constructed CFRP composites exist in spans 8 and 9.

Figure 7.27 and Figure 7.28 illustrate stiffness changes in spans 8 and 9 after rehabilitation with CFRP composites. As observed previously, a decrease in stiffness occurs in locations adjacent to S8B4 at 12 months and 20 months after rehabilitation.
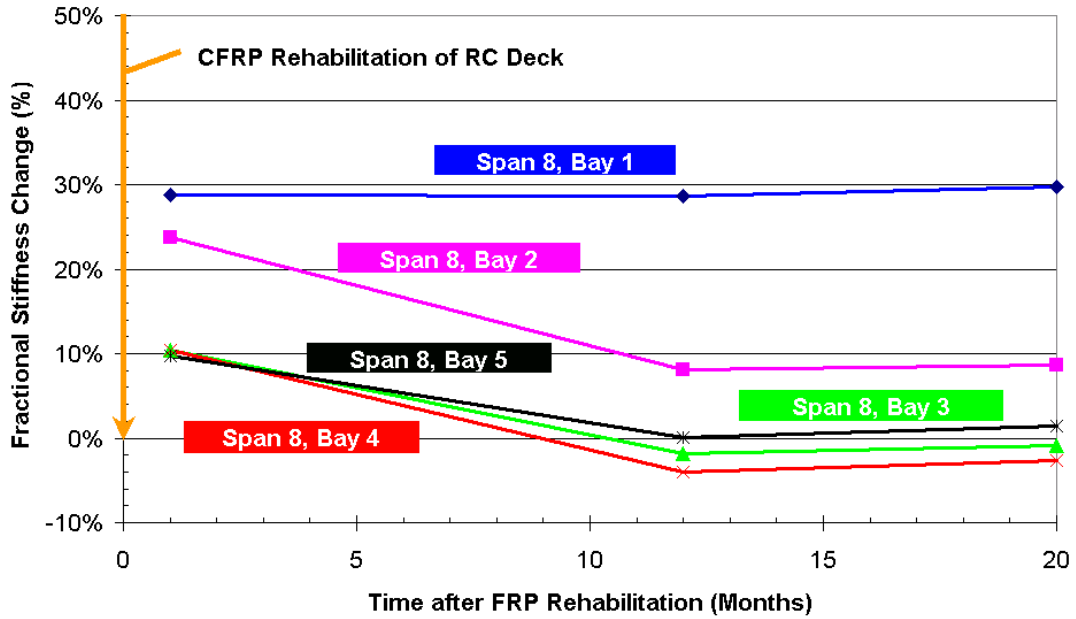
Figure 7.27. Stiffness Changes in Span 8 After Rehabilitation
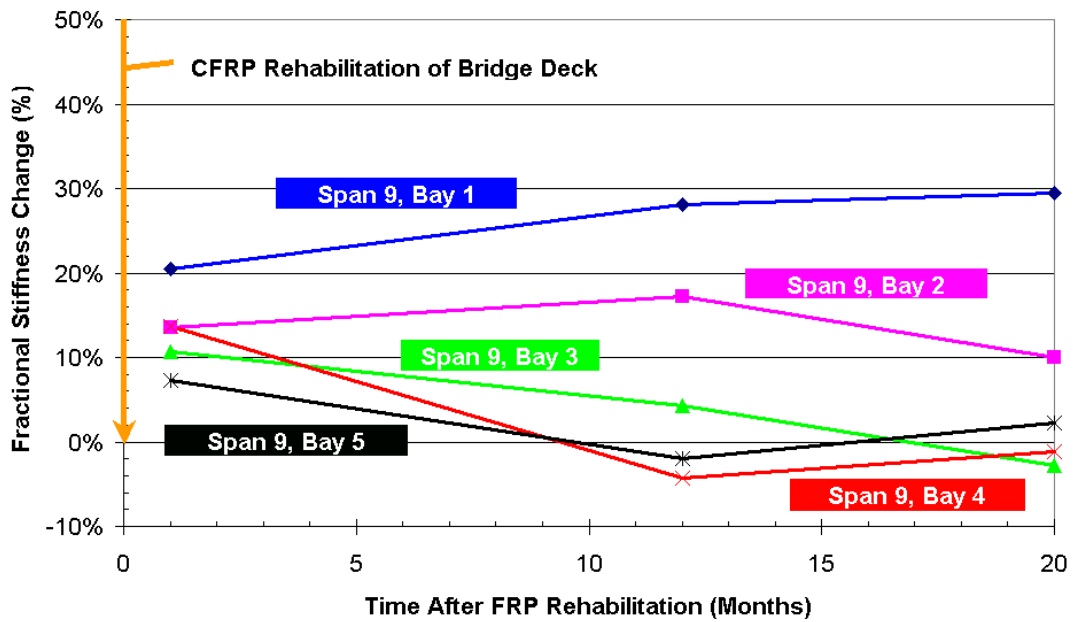
Figure 7.28. Stiffness Changes in Span 9 After Rehabilitation

7.4 Summary

By employing visual inspection and a vibration based damage detection procedure an assessment of the FRP composite bonded to the deck soffit of spans 8 and 9 of the Watson Wash Bridge is conducted.

The visual inspection of the bonded CFRP composite rehabilitation provides observations during manufacture and application of wet lay-up and pultruded CFRP composites strips. Locations of defects and cracks are identified which may continue to grow and ultimately lead to disbond of the CFRP composite rehabilitation. The visual inspection process is inherently subjective and results in a nonintegrated evaluation of the composite, bond, and reinforced concrete.

In order to evaluate the integrity of the FRP composite rehabilitation as an entire system which includes composite, bond, and the reinforced concrete structure, a vibration based global NDE procedure is implemented. Dynamic testing of Frame S-3 is performed to determine vibration properties, namely frequencies and mode shapes. The measured frequencies of Frame S-3 are used to provide a qualitative overview of changes in the structure as a result of maintenance action. Changes in modal strain energy are used to measure fractional stiffness changes 1 month, 12 months, and 20 months after rehabilitation with CFRP composites.

In Chapter 8 of this report, mechanical properties of field manufactured or wet lay-up manufactured CFRP composites and pultruded CFRP composites are investigated. Investigation of the quality and consistency of the field manufactured CFRP composite strips and bonded prefabricated CFRP composite provides insight into the performance of the fabricator and evaluates the quality of the CFRP composite rehabilitation at the materials level.

8   MATERIALS CHARACTERIZATION

8.1   Introduction

In the preceding chapter, Frame S-3 of the Watson Wash Bridge was assessed via visual inspection and a vibration based global NDE procedure. The visual inspection of rehabilitated spans 8 and 9 presented observations from the construction process and identified potential defects. The vibration based global NDE procedure by Stubbs et al. (2000) was used to estimate stiffness changes in the rehabilitated bays of spans 8 and 9.

The visual inspection and global NDE of the FRP rehabilitation evaluates the state of the entire rehabilitated system and is unable to characterize the quality of FRP composite, bond, or bridge deck separately. Of particular interest is the state of FRP composites applied and fabricated during the rehabilitation. Knowledge of mechanical properties of the applied CFRP allows for a direct comparison with design properties and qualification of manufacturing procedures. This chapter characterizes mechanical properties of the FRP composites applied to the bridge deck soffit of the Watson Wash Bridge, including characterization of epoxy resin and adhesives.

8.2   Material Samples

Samples of wet lay-up manufactured for and prefabricated strips bonded for the rehabilitation of the Watson Wash Bridge deck. Wet lay-up manufactured CFRP composites consist of 1-layer, 2-layer, and 3-layer CFRP composites. While prefabricated CFRP composite strip samples are taken from strips used during rehabilitation.

8.2.1   Selected Samples

8.2.1.1   Pultruded CFRP

With consideration for the composite manufacturing techniques, material samples from the applied CFRP composites are collected. For prefabricated CFRP composite, samples are taken at random from the pultruded strip rolls used during the rehabilitation. A total of 60 tensile specimens are tested for pultruded strips of which 30 are system 1 prefabricated CFRP specimens and 30 are system 2 prefabricated CFRP specimens. During material testing, two specimen from System 1 were excluded from this analysis due to slipping at the grips. Results for system 1 are composed of 28 samples. Figure 8.1 is a picture of a pultruded CFRP strip roll at the Watson Wash Bridge.

Figure 8.1. Pultruded CFRP Composite Roll

8.2.1.2 Wet Lay-up CFRP

The manual nature of the wet lay-up construction process results in an increased potential for variation of mechanical properties of the composites. In addition, properties of the wet lay-up composites may vary from day-to-day, location-to-location, and within a single day at beginning of manufacturing and at the end of the workday. The following paragraph summarizes the sampling requirements for wet lay-up CFRP composites.

Samples of wet lay-up manufactured CFRP are required at the beginning and end of each workday, where workday is defined as a day in which wet lay-up manufactured CFRP composites are manufactured. At the beginning of the workday three unidirectional CFRP composite panels, 15.24 cm (6 inches) wide by 45.72 cm (18 inches) long, of one-layer thickness and three CFRP composite panels, 15.24 cm (6 inches) wide by 45.72 cm (18 inches) long, of two-layer thickness are manufactured. The same number and thickness of panels are required at the end of the workday. For locations where three-layer CFRP composites are specified (Locations 8-5, 9-5), three, three-layer CFRP composite panels are also manufactured at the beginning and at the end of the workday.

A total of five workdays were required to complete manufacturing and application of wet lay-up CFRP composites on four bays. In all, 30 one-layer thick, 30 two-layer thick, and 12 three-layer thick CFRP composite panels were fabricated. Of these, one panel of each thickness type is selected from the beginning and end of each workday, which results in 10 one-layer, 10 two-layer and 4 three-layer CFRP panels equally divided between the beginning and end of workdays. Five 0° unidirectional tensile specimens 25.4 mm x 254 mm (1″ x 10″) are cut from the selected panels according to ASTM D3039 specifications. The following table summarizes the number of tested tension specimens by workday.

Table 8-1. Summary of Wet Lay-up CFRP Composite Samples

Date	Location	Tensile Specimen		
		1-Layer	2-Layer	3-Layer
Sept. 2, 2001	9-3	10	10	N/A
Sept. 3, 2001	9-3	10	10	N/A
Sept. 4, 2001	8-3	10	10	N/A
Sept. 6, 2001	8-5	10	10	10
Sept. 8, 2001	9-5	9	10	8
Totals:		49	50	18

The remainder of this chapter presents the mechanical properties of the representative CFRP samples from the deck rehabilitation of Spans 8 and 9 of the Watson Wash Bridge. While minimal characterization of pultruded CFRP composites is required, the wet lay-up manufactured composites call for in-depth analysis because greater variation is expected from the manufacturing process.

8.3   Pultruded CFRP Composites

Material characterization of pultruded CFRP composites is conducted from 28 samples from System 1 pultruded strips and 30 samples from system 2 pultruded strips acquired during the rehabilitation procedure.

8.3.1   Mechanical Properties

Table 8-2 and Table 8-3 show statistical characteristics of the System 1 and System 2 pultruded CFRP composite specimen, respectively. In addition, histograms of tensile modulus and tensile strength data for the pultruded CFRP strips are provided in Figure 8.2 thru Figure 8.5. All tests were conducted pursuant to ASTM D3039 with coupons 25.4 cm long by 12.7 mm wide.

Table 8-2. Mechanical Properties of System 1 CFRP

	Thickness mm (in)	Tensile Modulus GPa (ksi)	Tensile Strength MPa (ksi)	% of Assumed Design Values	
				Modulus = 141.34 GPa	Strength = 2100 MPa
Average	1.268 (0.0499)	139.71 (20263.79)	2503.46 (363.10)	98.85%	119.21%
St. Dev.	0.0116 (0.0005)	12.86 (1864.48)	289.74 (42.02)	--	--
COV	0.91%	9.20%	11.57%	--	--
Maximum	1.296 (0.0510)	178.94 (25953.05)	2861.06 (414.96)	126.60%	136.24%
Minimum	1.250 (0.0492)	123.52 (17915.06)	1863.55 (270.28)	87.39%	88.74%
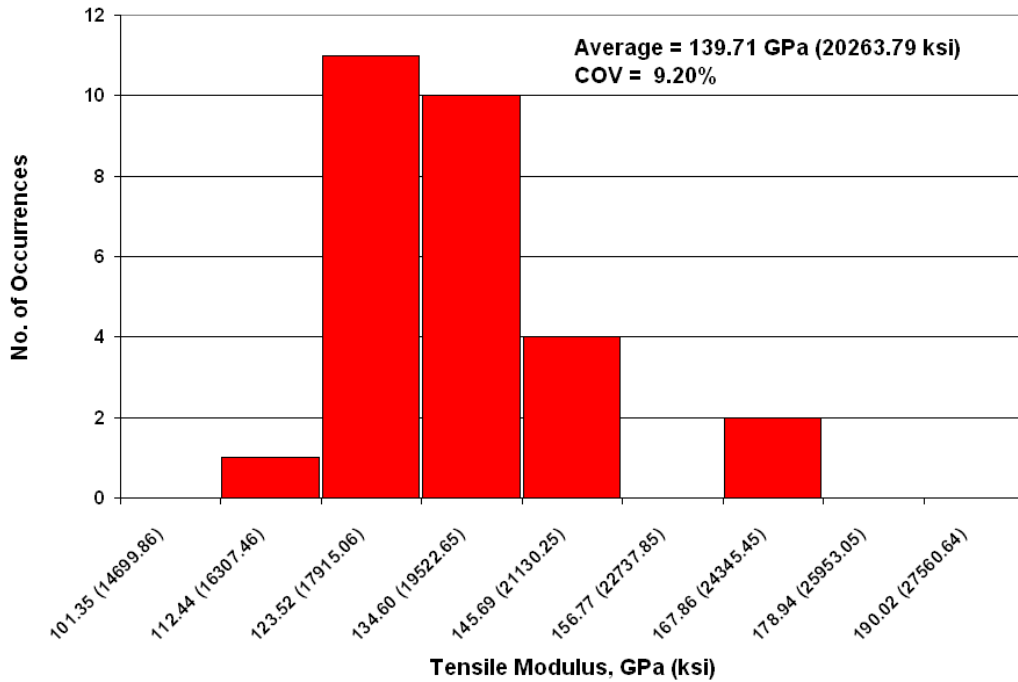
Figure 8.2. Histogram of Tensile Modulus Distribution for System 1 CFRP
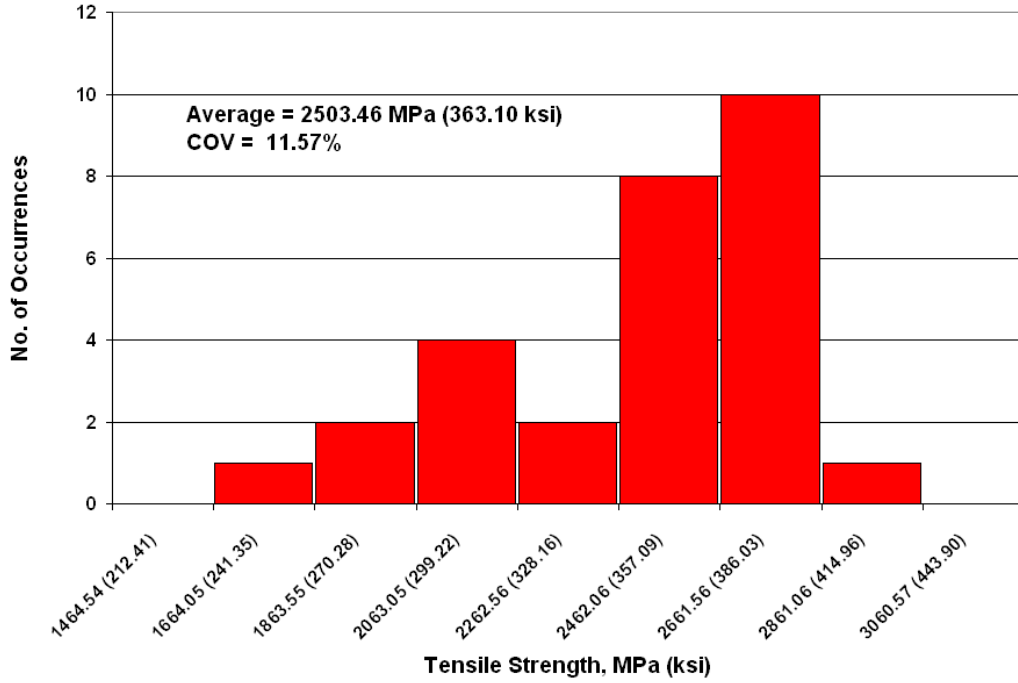
Figure 8.3. Histogram of Tensile Strength Distribution for System 1 CFRP

Table 8-3. Mechanical Properties of System 2 CFRP

	Thickness mm (in)	Tensile Modulus GPa (ksi)	Tensile Strength MPa (ksi)	% of Assumed Design Values	
				Modulus = 141.34 GPa	Strength = 2100 MPa
Average	1.313 (0.0517)	166.18 (24102.46)	2522.03 (365.79)	117.58%	120.10%
St. Dev.	0.0142 (0.0006)	12.33 (1787.90)	273.70 (39.70)	--	--
COV	10.8%	7.42%	10.85%	--	--
Maximum	1.334 (0.0525)	196.67 (28524.56)	2901.05 (420.76)	139.15%	138.15%
Minimum	1.282 (0.0505)	150.75 (21864.43)	1982.93 (287.60)	106.66%	94.43%
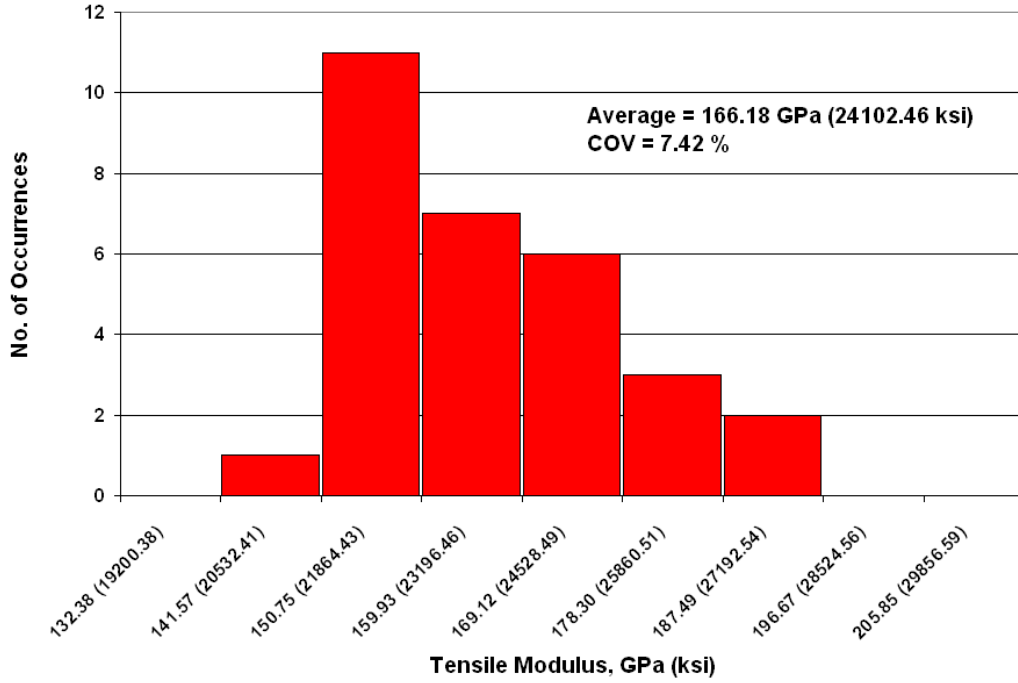
Figure 8.4. Histogram of Tensile Modulus Distribution for System 2 CFRP
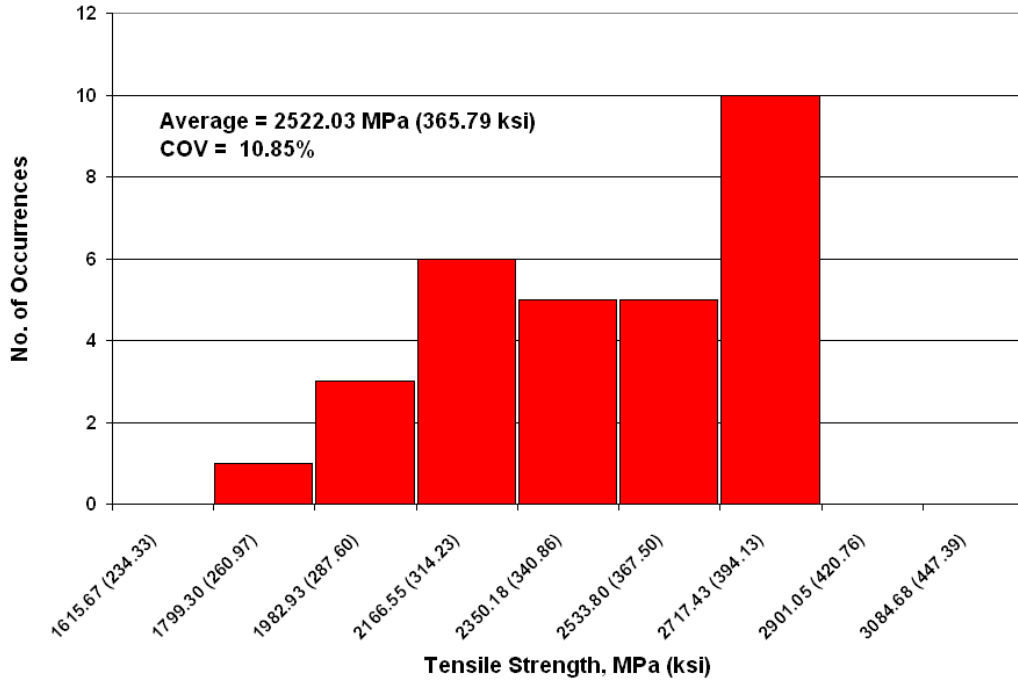
Figure 8.5. Histogram of Tensile Strength Distribution for System 2 CFRP

8.3.2 Discussion of Results

CFRP composite rehabilitation shows an average Young's modulus for System 1 pultruded strips at 139.71 GPa (20.26 msi), which is 1.15% less than the design modulus of 141.34 GPa (20.50 msi) with 17 of the tested specimen less than the design value. Tensile strength of the SYSTEM 1 Pultruded composites is measured at 2.50 GPa (363.10 ksi) which is 19.05% greater that the design strength value.

The System 2 pultruded CFRP strips show a measured modulus of 166.18 GPa (24.10 msi), which is approximately 17.58% greater than the design modulus of 141.34 GPa (20.5 msi). The measured tensile strength of the System 2 pultruded composites shows a strength value of 2.52 GPa (365.79 ksi), which is 19.93% greater than design tensile strength of 2.10 GPa (305 ksi).

8.3.2.1 Comparison to Manufacturer Specified Properties

The tested System 2 prefabricated specimens show an average tensile modulus of 166.18 GPa (24.10 msi), which is 6.99% greater then the manufacturer specified modulus of 155.32 GPa (22.5 msi). Measured strength of the System 2 strips at 2.52 GPa (365.79 ksi) is 5.0% greater than manufacturer specified properties of 2.4 GPa (348.0 ksi).

For System 1 prefabricated strips, the measured tensile modulus and tensile strength are 1.15% less than and 19.05% greater than the manufacturer tensile modulus and strength, respectively. This suggests that the System 1 prefabricated CFRP strips do not consistently achieve the specified properties.

8.4 Wet Lay-up CFRP Composites

8.4.1 Mechanical Properties by Number of Layers

8.4.1.1 One Layer CFRP Composites

Table 8-4 lists the statistical characteristics of 1-layer thick CFRP specimen tested pursuant to ASTM D3039. Histograms of the tensile strength and tensile modulus are shown in Figure 8.6 and Figure 8.7, respectively.

Table 8-4. Tensile Properties of 1 Layer CFRP Composite

	Thickness mm (in)	Tensile Modulus GPa (ksi)	Tensile Strength MPa (ksi)	% of Assumed Design Values	
				Modulus = 64.92 GPa	Strength = 889 MPa
Average	1.10 (0.0434)	70.37 (10205.65)	1043.74 (151.38)	108.39%	117.41%
St. Dev.	0.05 (0.0019)	9.44 (1369.66)	125.98 (18.27)	--	--
COV	4.41%	13.42%	12.07%	--	--
Maximum	1.17 (0.0462)	94.18 (13659.23)	1308.48 (189.78)	145.07%	147.19%
Minimum	1.00 (0.0395)	50.24 (7286.37)	806.04 (116.91)	77.38%	90.67%
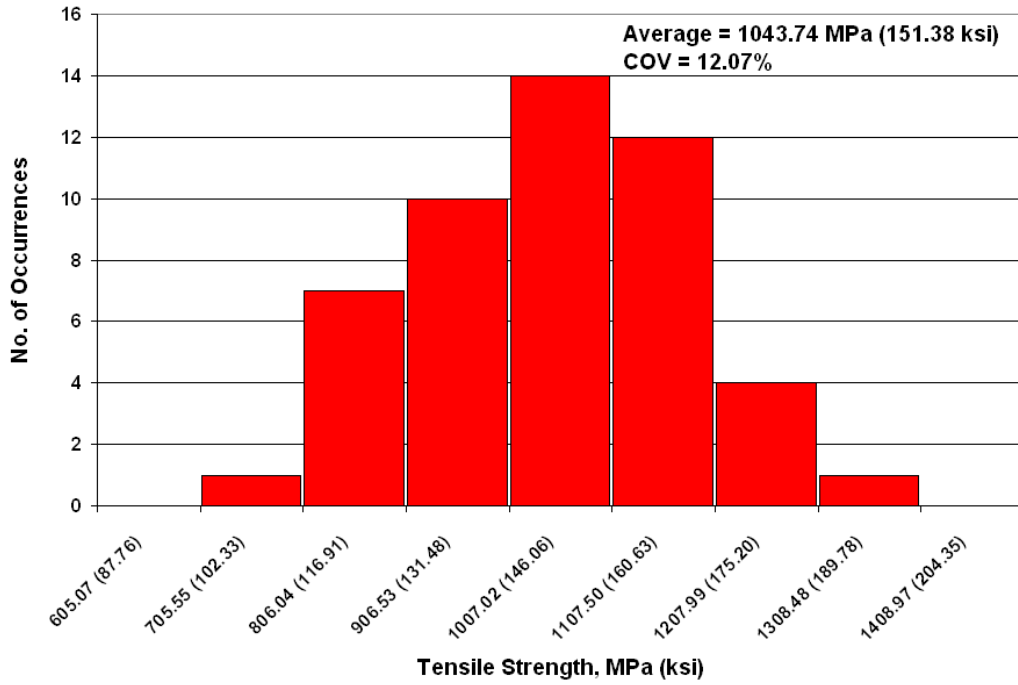
Figure 8.6. Histogram of Tensile Strength Distribution for 1-Layer CFRP
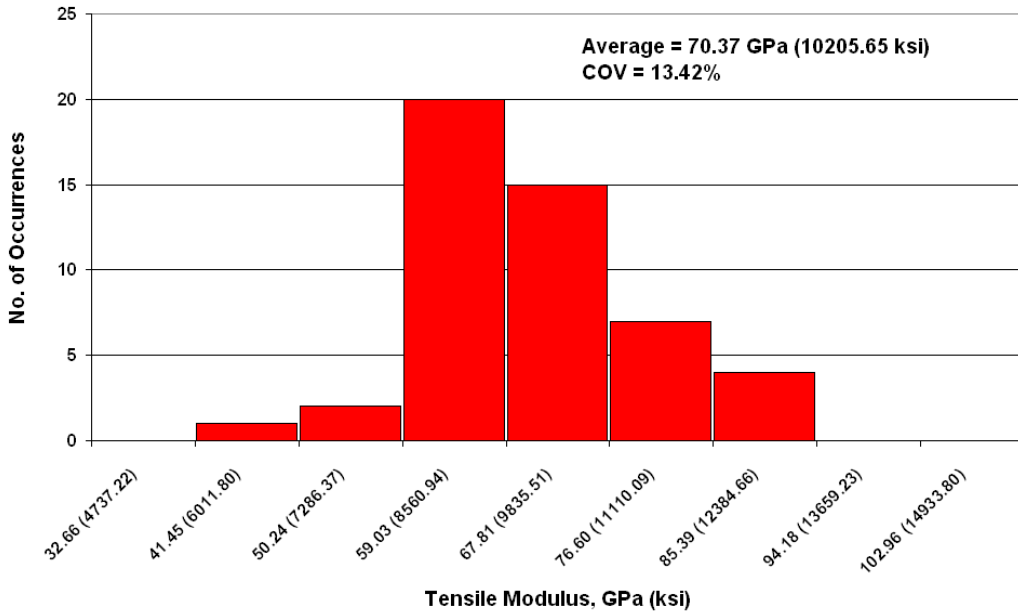
Figure 8.7. Histogram of Tensile Modulus Distribution for 1-Layer CFRP

8.4.1.2 Two Layer CFRP Composites

Table 8-5 lists the statistical characteristics of 2-layer thick CFRP specimen   tested pursuant to ASTM D3039. Figure 8.8 and Figure 8.9 are histograms of tensile modulus and tensile strength.

Table 8-5. Tensile Properties of 2 Layer CFRP Composite

	Thickness mm (in)	Tensile Modulus GPa (ksi)	Tensile Strength (MPa) (ksi)	% of Assumed Design Values	
				Modulus = 64.92 GPa	Strength = 889 MPa
Average	1.88 (0.0739)	78.96 (11451.92)	1100.58 (159.63)	121.62%	123.80%
St. Dev.	0.06 (0.0022)	7.20 (1044.75)	133.86 (19.42)	--	--
COV	3.00%	9.12%	12.16%	--	--
Maximum	1.99 (0.0782)	100.09 (14516.45)	1396.69 (202.57)	154.17%	157.11%
Minimum	1.76 (0.0693)	62.02 (8995.46)	782.05 (113.43)	95.54%	87.97%
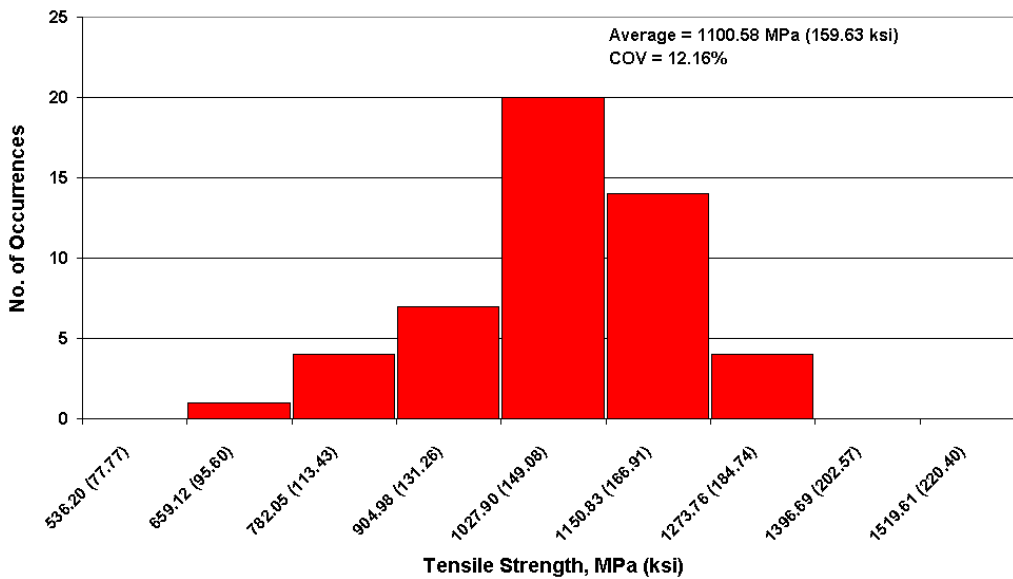
Figure 8.8. Histogram of Tensile Strength Distribution for 2-layer CFRP
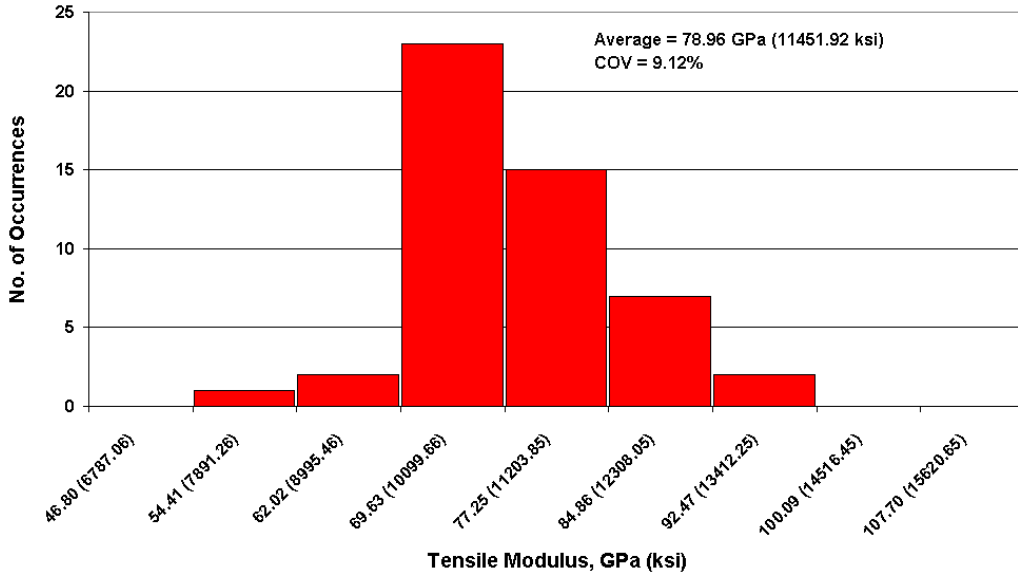
Figure 8.9. Histogram of Tensile Modulus Distribution 2-Layer CFRP

8.4.1.3   Three Layer CFRP Composites

Table 8-6 lists the statistical characteristics of 3-layer thick CFRP specimen   tested pursuant to ASTM D3039..   Figure 8.10 and Figure 8.11 are histograms of tensile strength and tensile modulus.

Table 8-6. Tensile Properties of 3 Layer CFRP Composite

	Thickness mm (in)	Tensile Modulus GPa (ksi)	Tensile Strength (MPa) (ksi)	% of Assumed Design Values	
				Modulus = 64.92 GPa	Strength = 889 MPa
Average	2.75 (0.1083)	78.68 (11411.74)	1031.03 (149.54)	121.20%	115.98%
St. Dev.	0.13 (0.0050)	5.39 (782.29)	124.73 (18.09)	--	--
COV	4.59%	6.86%	12.10%	--	--
Maximum	3.01 (0.1183)	89.71 (13010.62)	1153.56 (167.31)	138.18%	129.76%
Minimum	2.47 (0.0973)	69.96 (10147.21)	696.34 (101.00)	107.77%	78.33%
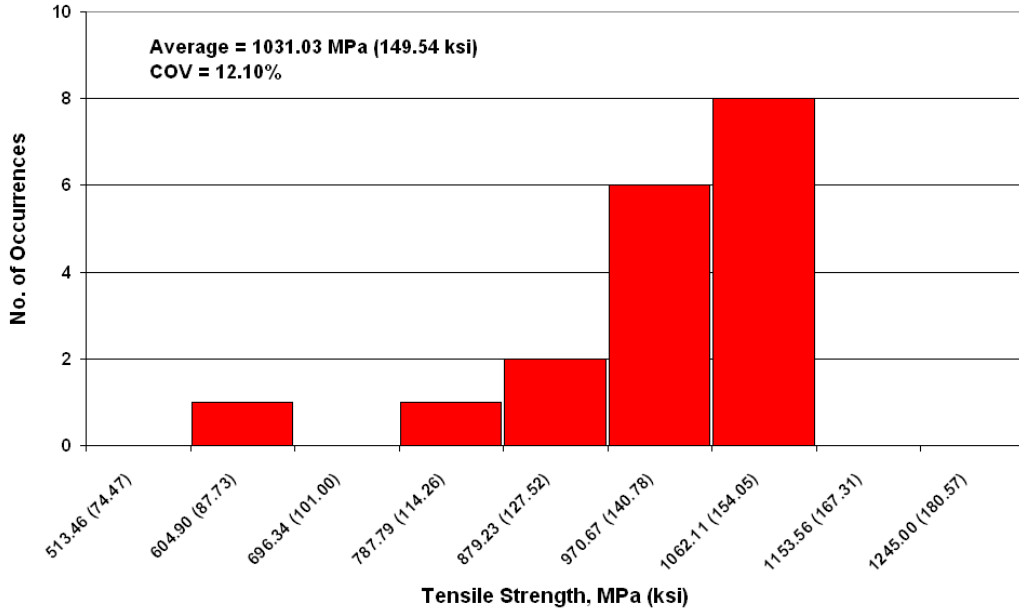
Figure 8.10. Histogram of Tensile Strength Distribution for 3-layer CFRP
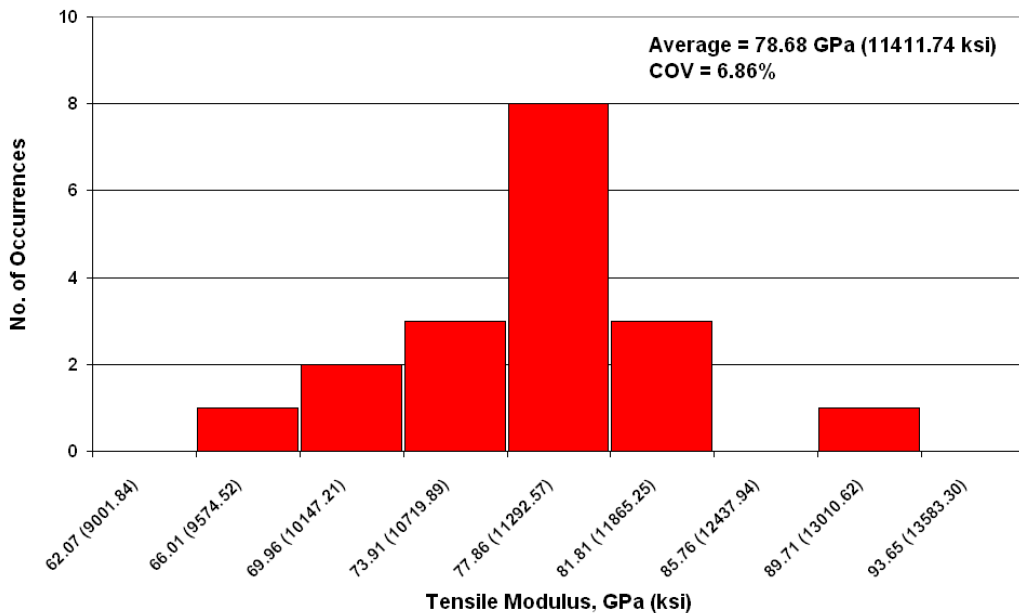
Figure 8.11. Histogram of Tensile Modulus Distribution for 3-Layer CFRP

8.4.1.4   Scatter in Field Manufactured CFRP Composites

The histograms and tables show significant variation in the characteristics of the specimens tested. Of particular concern are the modulus and strength values below the design modulus of 64.95 GPa (9.42 msi) and design strength of 0.887 GPa (128.66 ksi), since locations with mechanical properties less than the design value indicates

manufacturing and materials processing inferior to the expected performance of the deck rehabilitation.

Figure 8.12, Figure 8.13, and Figure 8.14 show average values and ranges for thickness, tensile modulus, and tensile strength. Comparing the one, two, and three layer CFRP measure results graphically provides indications about the quality of the manufacturing process.
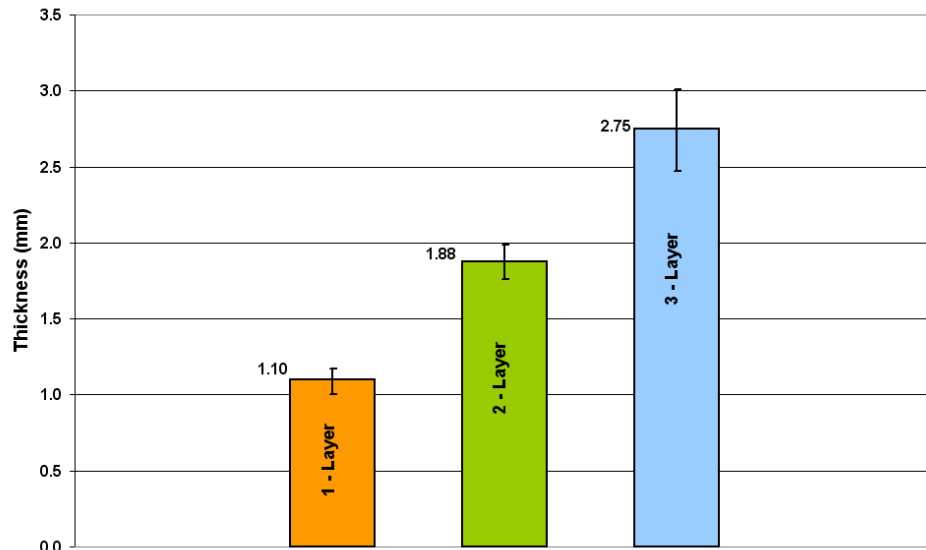
Figure 8.12. Thickness Scatter of Wet Lay-up CFRP Composites

The nominal thickness of a single ply of carbon fabric is 1.016 mm (0.040 in). An average thickness of 1.10 mm (0.043 in) is measured from a one-layer CFRP composite, where the thickness increase compared to the nominal thickness is attributed to the impregnation of resin.

Nominal thickness for two layers of carbon fabric is 2.032 mm (0.080 in), while the measured average thickness of the two-layer CFRP composite specimens is 1.88 mm (0.074 in). The difference in nominal and measured thicknesses indicates that compaction of the fibers is taking place during the manufacturing process.

An average thickness of 2.75 mm (0.108 in) is measured for the three-layer CFRP composite. The measured thickness is less than the nominal thickness of 3.048 mm (0.120 in) for three layers of carbon fabric, indicating the effect of compaction.
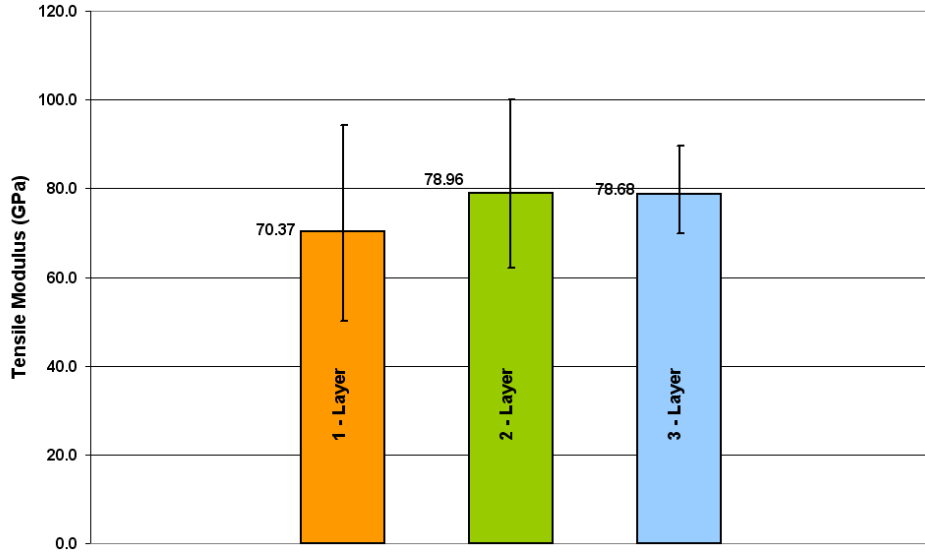
Figure 8.13. Tensile Modulus Scatter of Wet Lay-up CFRP Composites

A comparison of the average tensile modulus between the one, two, and three layer CFRP composites shows that tensile modulus increases by 12.21% from 70.37 GPa (10.21 msi) to 78.96 GPa (11.45 msi) between the one and two layer CFRP composites, while remaining steady for the three layer composite at 78.68 GPa (11.41 msi).
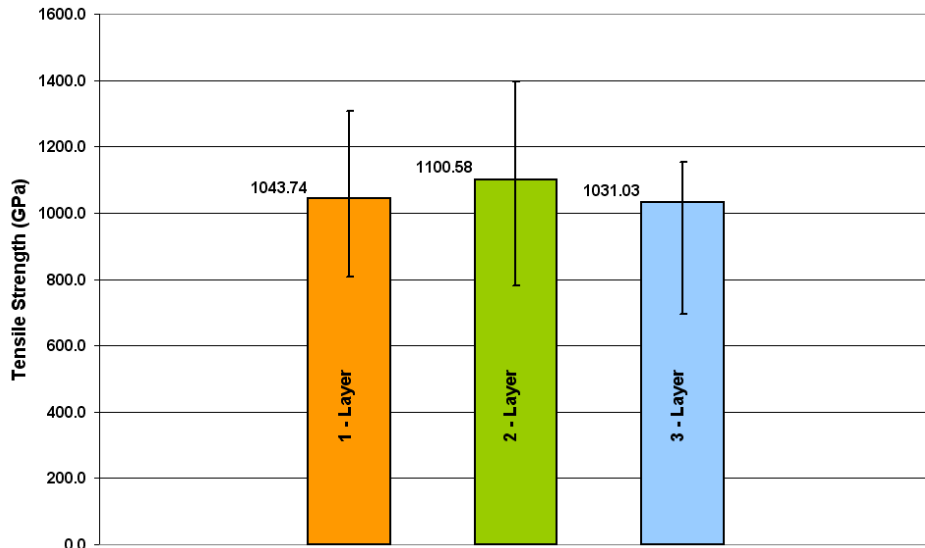
Figure 8.14. Tensile Strength Scatter of Wet Lay-up CFRP Composites

The variation in tensile strength between the one, two, and three layer CFRP shows a trend where the tensile strength of the CFRP composite increases by 5.45% from 1.04 GPa (151.38 ksi) for the one layer composite to 1.10 GPa (159.63 ksi) or the two layer composites.

8.4.2 Mechanical Properties by Location

In each location, two sets of panels (5 test specimens per panel) are examined in order to evaluate the manufacturing and application per bay. The statistical results presented in Table 8-7, Table 8-8, and Table 8-9 for the wet lay-up CFRP composite rehabilitation locations of the Watson Wash Bridge are based on results of the test specimen populations. Presentation of results by location indicates the quality of manufacturing at the different bays and identifies the material properties and their variation for specific CFRP design applications. The maximum average tensile modulus and average tensile strength values of the bays are highlighted in yellow.

Table 8-7. One Layer CFRP Properties by Location

Location		Thickness mm (in)	Tensile Modulus GPa (ksi)	Tensile Strength MPa (ksi)
Span 9, Bay 3	Average	1.12 (0.0443)	70.53 (10229.75)	956.58 (138.74)
	St. Dev.	0.0308 (0.0012)	9.57 (1387.59)	107.19 (15.55)
	COV	0.0274	0.1356	0.1121
	Maximum	1.17 (0.0462)	90.68 (13152.20)	1148.23 (166.54)
	Minimum	1.08 (0.0427)	50.24 (7286.37)	806.04 (116.91)
Span 8, Bay 3	Average	1.07 (0.0422)	71.16 (10320.96)	1070.59 (155.28)
	St. Dev.	0.0182 (0.0007)	10.58 (1533.77)	76.21 (11.05)
	COV	0.0170	0.1486	0.0712
	Maximum	1.10 (0.0432)	89.29 (12949.71)	1212.71 (175.89)
	Minimum	1.05 (0.0413)	59.61 (8645.91)	945.99 (137.20)
Span 8, Bay 5	Average	1.10 (0.0434)	66.72 (9676.94)	1122.42 (162.79)
	St. Dev.	0.0445 (0.0018)	2.83 (410.08)	54.23 (7.86)
	COV	0.0403	0.0424	0.0483
	Maximum	1.16 (0.0455)	71.12 (10315.29)	1207.62 (175.15)
	Minimum	1.03 (0.0405)	63.13 (9155.64)	1049.49 (152.22)
Span 9, Bay 5	Average	1.08 (0.0426)	73.16 (10611.42)	1120.17 (162.47)
	St. Dev.	0.0807 (0.0032)	12.51 (1815.11)	154.59 (22.42)
	COV	0.0747	0.1711	0.1380
	Maximum	1.17 (0.0462)	94.18 (13659.23)	1308.48 (189.78)
	Minimum	1.00 (0.0395)	53.70 (7788.14)	911.07 (132.14)

Table 8-8. Two Layer CFRP Properties by Location

Location		Thickness mm (in)	Tensile Modulus GPa (ksi)	Tensile Strength MPa (ksi)
Span 9, Bay 3	Average	1.88 (0.0742)	79.12 (11475.26)	1148.80 (166.62)
	St. Dev.	0.0186 (0.0007)	8.10 (1174.42)	80.26 (11.64)
	COV	0.0099	0.1023	0.0699
	Maximum	1.92 (0.0756)	96.64 (14016.44)	1293.35 (187.58)
	Minimum	1.85 (0.0728)	62.02 (8995.46)	972.07 (140.99)
Span 8, Bay 3	Average	1.84 (0.0724)	78.86 (11437.13)	1191.10 (172.75)
	St. Dev.	0.0654 (0.0026)	4.43 (642.53)	99.79 (14.47)
	COV	0.0356	0.0562	0.0838
	Maximum	1.92 (0.0755)	85.35 (12379.54)	1396.69 (202.57)
	Minimum	1.76 (0.0693)	72.88 (10570.28)	1059.73 (153.70)
Span 8, Bay 5	Average	1.91 (0.0752)	78.77 (11425.25)	1094.01 (158.67)
	St. Dev.	0.0242 (0.0010)	5.76 (836.09)	122.04 (17.70)
	COV	0.0127	0.0732	0.1116
	Maximum	1.94 (0.0765)	88.81 (12880.83)	1288.41 (186.87)
	Minimum	1.85 (0.0693)	69.01 (10008.67)	864.47 (125.38)
Span 9, Bay 5	Average	1.86 (0.0733)	78.92 (11446.71)	920.19 (133.46)
	St. Dev.	0.0922 (0.0036)	9.55 (1384.44)	92.92 (13.48)
	COV	0.0495	0.1209	0.1010
	Maximum	1.99 (0.0782)	100.09 (14516.45)	1054.55 (152.95)
	Minimum	1.77 (0.0697)	68.28 (9903.40)	782.05 (113.43)

Table 8-9. Three Layer CFRP Properties by Location

Location		Thickness mm (in)	Tensile Modulus GPa (ksi)	Tensile Strength MPa (ksi)
Span 8, Bay 5	Average	2.84 (0.1120)	79.41 (11517.76)	1056.75 (153.27)
	St. Dev.	0.0640 (0.0025)	5.47 (793.16)	56.39 (8.18)
	COV	0.0225	0.0689	0.0534
	Maximum	3.01 (0.1183)	89.71 (13010.62)	1134.08 (164.48)
	Minimum	2.79 (0.1097)	70.29 (10194.58)	963.26 (139.71)
Span 9, Bay 5	Average	2.64 (0.1038)	77.77 (11279.21)	998.88 (144.87)
	St. Dev.	0.0810 (0.0032)	5.52 (800.77)	177.68 (25.77)
	COV	0.0307	0.0710	0.1779
	Maximum	2.71 (0.1065)	85.18 (12354.42)	1153.56 (167.31)
	Minimum	2.47 (0.0973)	69.96 (10147.21)	696.34 (101.00)

Figure 8.15 and Figure 8.16 illustrate the average tensile strength and average tensile modulus obtained by pooling of data from the wet lay-up specimens. The average tensile strength and average tensile modulus results exceed the assumed design values of 0.89 GPa (128.66 ksi) and 64.92 GPa (9.42 msi), respectively.
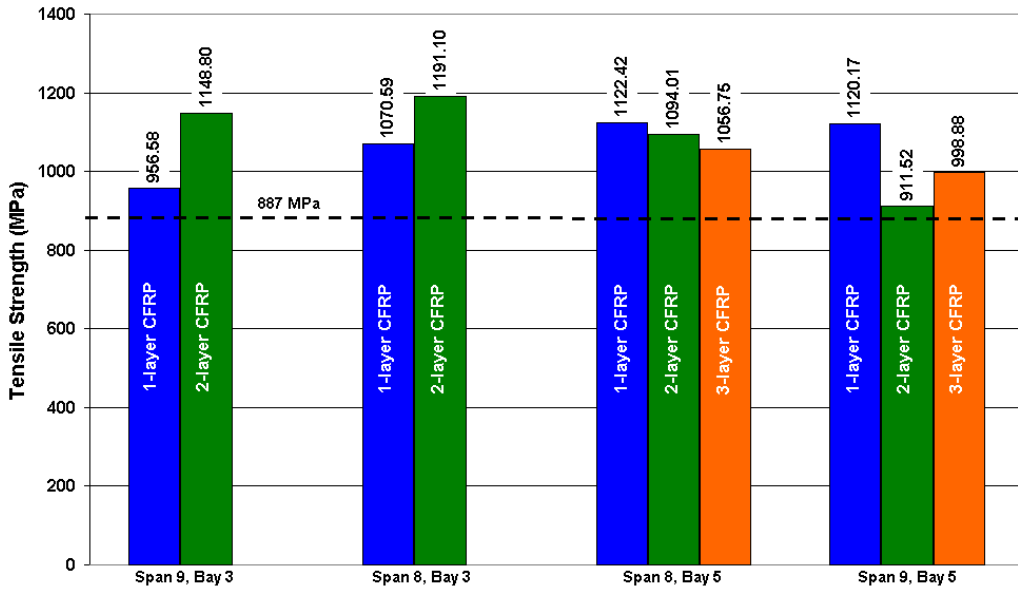
Figure 8.15. Tensile Strength of CFRP Composites by Location
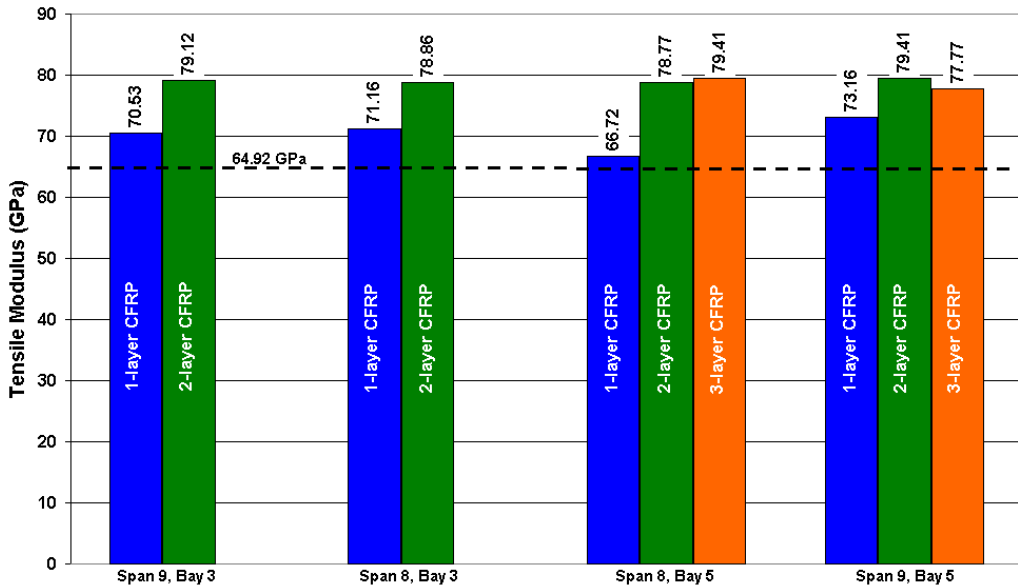
Figure 8.16. Tensile Modulus of CFRP Composites by Location

8.5 Epoxy Adhesives and Resin

The impregnating resin and adhesives are critical components of the rehabilitation procedure and thus it is essential that their performance characteristics are assessed as well.

8.5.1 Mechanical Properties of Epoxy Adhesives

The mechanical properties of the System 1 and System 2 epoxy adhesives are characterized in accordance with ASTM D638. Dog bone shaped specimens of 177.8 mm (7 inches) length and 25.4 mm (1-inch) width at the ends. The specimens are tapered to a width of 12.7 mm (0.5 inches) and have a tapered gauge length of 57.2 mm (2.25 inches). Results for mechanical properties of the System 1 and System 2 epoxy adhesives used to bond the prefabricated CFRP strips to the soffit of the bridge deck are listed in Table 8-10 and Table 8-11

Table 8-10. Mechanical Properties of System 1 Epoxy Adhesive

	Thickness mm (in)	Modulus GPa (ksi)	Strength MPa (ksi)
Average	5.19 (0.204)	5.44 (789.11)	30.15 (4.37)
St. Dev.	0.702 (0.028)	0.825 (119.66)	7.183 (1.041)
COV	13.52%	15.16%	23.83%
Maximum	6.26 (0.2465)	7.27 (1054.34)	47.80 (6.93)
Minimum	4.55 (0.1791)	4.85 (703.14)	24.64 (3.57)
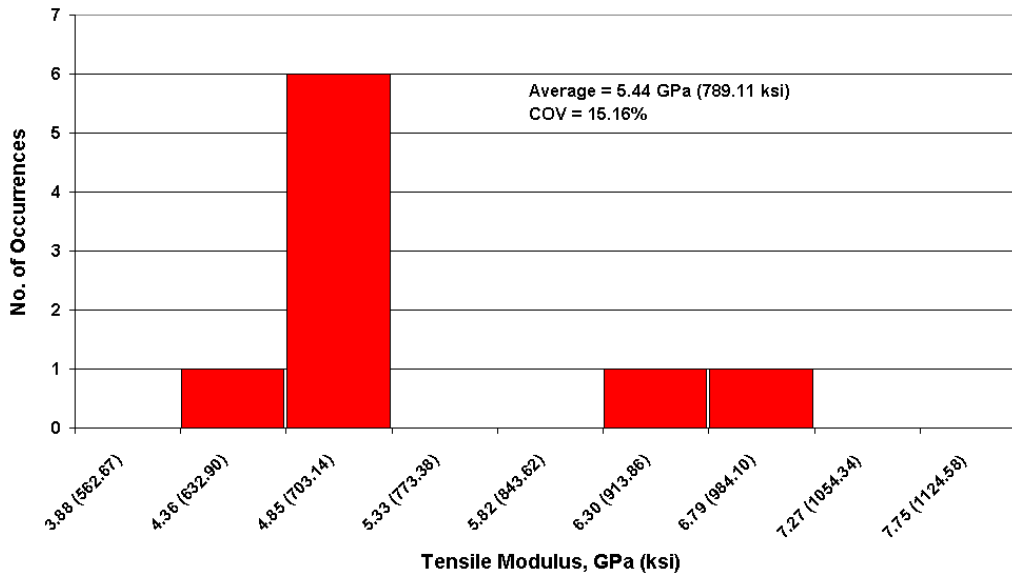
Figure 8.17. Histogram of Tensile Modulus Distribution for System 1 Adhesive
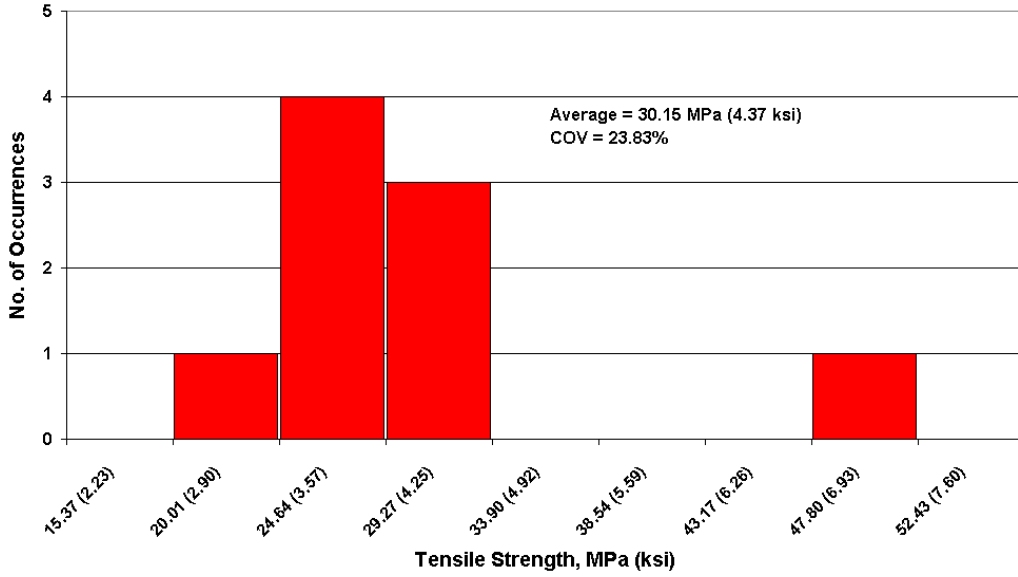
Figure 8.18. Histogram of Tensile Strength Distribution for System 1 Adhesive

Table 8-11. Mechanical Properties of System 2 Adhesive

	Thickness mm (in)	Modulus GPa (ksi)	Strength MPa (ksi)
Average	7.27 (0.286)	6.54 (949.18)	26.55 (3.85)
St. Dev.	0.688 (0.0271)	0.829 (120.20)	1.887 (0.274)
COV	9.46%	12.66%	7.11%
Maximum	8.50 (0.335)	7.80 (1130.89)	28.80 (4.18)
Minimum	6.34 (0.250)	5.49 (796.49)	22.67 (3.29)
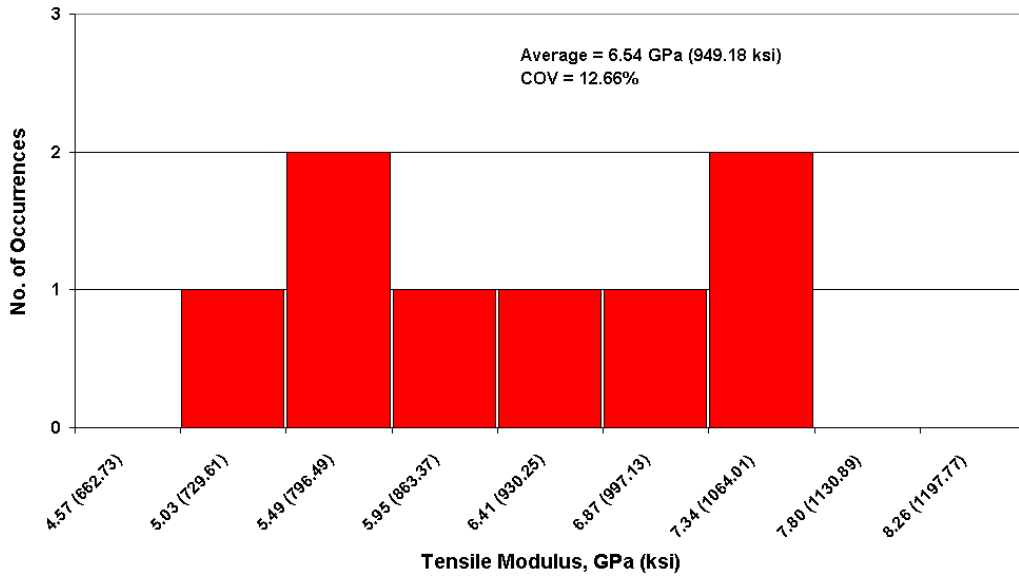
Figure 8.19. Histogram of Tensile Modulus Distribution for System 2 Adhesive
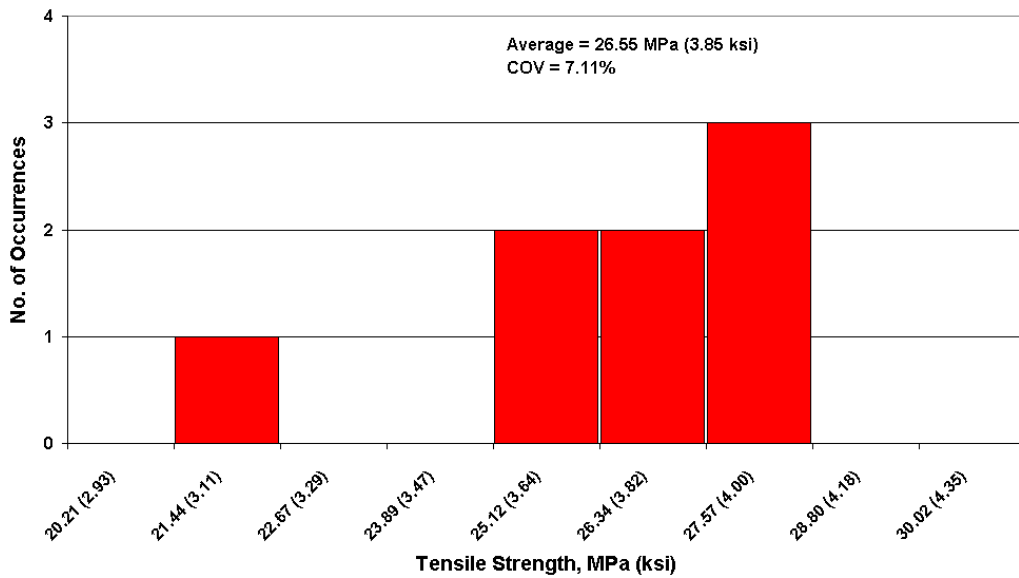
Figure 8.20. Histogram of Tensile Strength Distribution for System 2 Adhesive

8.5.1.1 Discussion of Epoxy Adhesive Results

A comparison with manufacturer specified properties provides a means to ascertain the quality of these materials and to verify that the epoxy adhesive performs as intended in the field. Manufacturer specified properties for System 1 and System 2 epoxy adhesives is shown in the following table.

Table 8-12. Manufactured Specified Adhesive Mechanical Properties

Epoxy Adhesive	Tensile Modulus GPa (msi)	Tensile Strength MPa (ksi)
System 1	Not Available	41.37 (6.0)
System 2	4.48 (0.65)	24.8 (3.6)

The measured System 2 adhesive modulus and strength properties are 45.9% and 6.7% greater than the manufacturer specified modulus and strengths of 4.48 GPa and 24.8 MPa, respectively. Here, large margins between the measured and specified modulus are observed, which indicate that the epoxy adhesive in the field is performing above manufacturer specifications.

As for the System 1 adhesive the measured strength value of 30.15 MPa (4.37 ksi) is approximately 27% less than the manufacturer specified strength of 41.37 MPa. However, compared to the System 2 specified strength, the System 1 epoxy adhesive displays a strength that is approximately 21% greater. The manufacturer does not provide modulus results from ASTM D638 tests for System 1 adhesive. However, as a reference the tested System 1 epoxy adhesive modulus of 5.44 GPa (0.79 msi) is approximately 21% greater than the System 2 epoxy specification of 4.48 GPa (0.65 msi).

8.5.2   Epoxy Resin

During the wet lay-up application of the Watson Wash Bridge, epoxy resin is used to impregnate carbon fabric and bond the composite to the deck soffit. Dog bone shaped specimens of 177.8 mm (7 inches) length and 25.4 mm (1-inch) width at the ends. The specimens are tapered to a width of 12.7 mm (0.5 inches) and have a tapered gauge length of 57.2 mm (2.25 inches). Mechanical properties are listed in Table 8-13.

Table 8-13. Mechanical Properties of Epoxy Resin

	Thickness mm (in)	Tensile Modulus GPa (ksi)	Tensile Strength MPa (ksi)
Average	4.73 (0.186)	3.15 (456.25)	52.33 (7.59)
St. Dev.	0.233 (0.009)	0.535 (77.53)	12.068 (1.75)
COV	0.0492	0.1699	0.2306
Maximum	5.068 (0.1995)	4.58 (664.26)	68.56 (9.94)
Minimum	4.188 (0.1649)	2.59 (375.92)	40.06 (5.81)
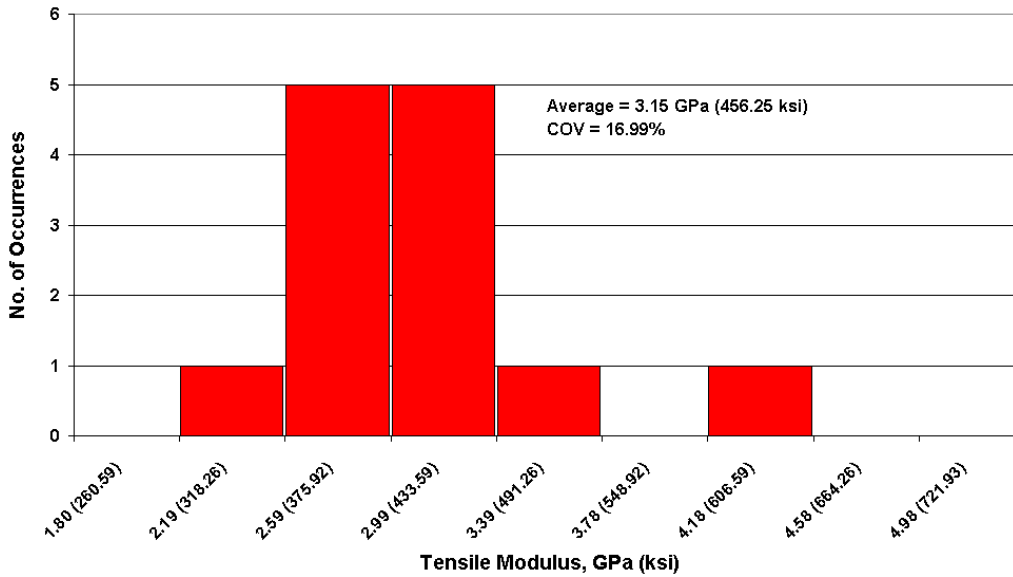
Figure 8.21. Histogram of Tensile Modulus Distribution for Epoxy Resin
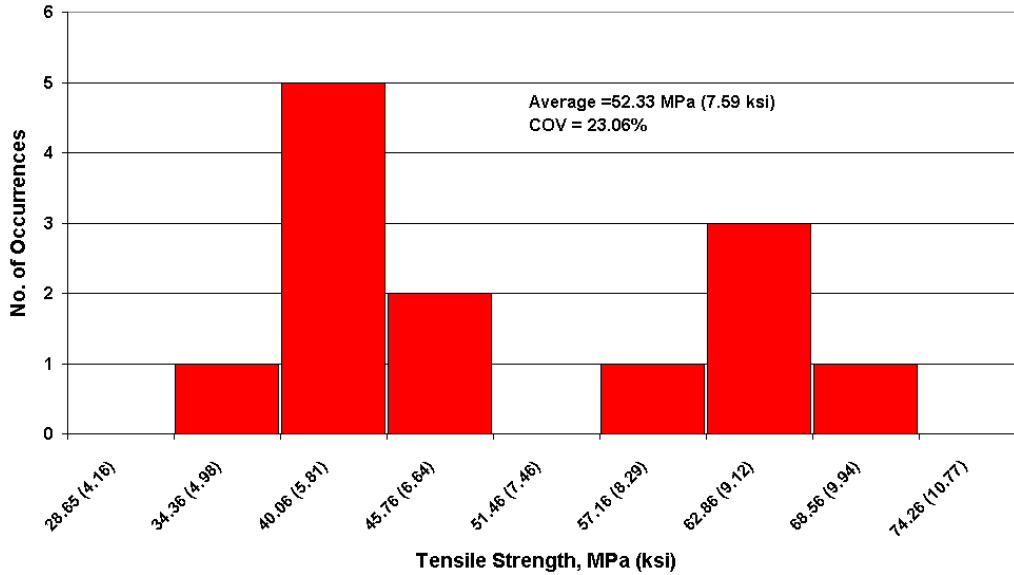
Figure 8.22. Histogram of Tensile Strength Distribution for Epoxy Resin

8.5.2.1 Discussion of Epoxy Resin Results

The manufacturer specifications indicate tensile strength of 41 MPa (17.57 ksi). The measured strength is 27.6% greater than the manufacturer specified product. The manufacturer does not specify the modulus of the resin; however, the measured modulus of 3.15 GPa (0.46 msi) lies within a standard range for epoxy tensile modulus values of 2.6-3.8 GPa (0.38-0.55 msi) (Astrom 1997).

8.6 Analysis of Margin of Safety

The measured mechanical properties from the tested CFRP composite samples suggests that while the pooled average values may meet or exceed a property used for design, the variation in the measured values may potentially lead to locally unsafe structures. In order to take into account the variation that occurs in a material parameter and ensure safety in a FRP rehabilitation design exists, current design guidelines such as ACI 440, fib-CEP, TR No. 55, use a characteristic value that is a result of subtracting a multiple of the standard deviation from the mean, i.e. mean – number x S.D.; furthermore, partial safety factors act as knockdown factors to account for material type, manufacturing process, and environmental exposure in design. The purpose of utilizing characteristic values and applied safety factors is to take into account variation of material parameters and the expected degradation in FRP composite.

8.6.1 Margins Compared to Design Material Properties

Comparing the design tensile modulus and tensile strength versus the average, maximum, and minimum values measured during tension tests provides a means to compare any safety factors made available versus design property values. Table 8-14 and Table 8-15 show the ratios for tensile modulus and tensile strength, respectively, for average,

maximum, and minimum values in sections 8.3 and 8.4. A margin greater than one indicates that a safety margin exists for the material properties.

Table 8-14. Margins between Measured and Design Modulus

Material ID	Design Value GPa (msi)	Safety Margins		
		Ave/Design	Max/Design	Min/Design
System 1	141.34	0.988	1.266	0.874
System 2	141.34	1.176	1.391	1.067
1-Layer Wet Lay-up	64.92	1.084	1.451	0.774
2-Layer Wet Lay-up	64.92	1.216	1.542	0.955
3-Layer Wet Lay-up	64.92	1.212	1.382	1.078

The margins in Table 8-14 for tensile modulus shows that the average and minimum measured tensile modulus of System 1 and the minimum of the 2-layer wet lay-up fail to provide a measure of safety relative to their respective design values.

Table 8-15. Margins between Measured and Design Strength

Material ID	Design Value MPa (ksi)	Safety Margins		
		Ave/Design	Max/Design	Min/Design
System 1	2100	1.192	1.362	0.887
System 2	2100	1.201	1.381	0.944
1-Layer Wet Lay-up	887	1.177	1.475	0.909
2-Layer Wet Lay-up	887	1.241	1.575	0.882
3-Layer Wet Lay-up	887	1.162	1.301	0.785

The margins in Table 8-15, show that all minimum measured tensile strengths implying that a local regions of the composite rehabilitation fail to meet the design tensile strength.

8.6.2 *Material Safety Factor Analysis*

8.6.2.1 Procedures Pursuant to ACI 440.2 (ACI 2002)

The ACI guidelines (ACI 2002) suggest that the design ultimate strength, f_{fu}, be determined by modifying the reported strength, f_{fu}^*, by an environmental reduction factor, C_E, such that,

$$f_{fu} = C_E f_{fu}^*$$
Eqn. 8.1

where

$$f_{fu}^* = \overline{f}_{fu} - 3\sigma \qquad \textbf{Eqn. 8.2}$$

where $\overline{f}_{fu}$, is the mean ultimate strength and σ, is the standard deviation of the test population. For cased of exterior exposure and aggressive environments the ACI guidelines (ACI 2002) suggest that $C_E = 0.85$, for CFRP. The design tensile modulus, E_f, of FRP is taken as the mean value of the test population.

Table 8-16 shows design tensile strength and tensile modulus using the environmental reduction factor and characteristic properties as recommended by ACI guidelines (ACI 2002). Design tensile strength and design tensile modulus are shown for System 1, System 2, one layer wet lay-up (1-layer), two layer wet lay-up (2-layer), and three layer wet lay-up (3-layer) CFRP composites.

Table 8-16. Design Tensile Properties Per ACI 440.2

Material ID	Tensile Strength				Tensile Modulus
	$\overline{f}_{fu}$ MPa (ksi)	σ MPa (ksi)	f_{fu}^* MPa (ksi)	$f_{fu} = C_E f_{fu}^*$ MPa (ksi)	E_f GPa (ksi)
System 1	2503.46 (363.10)	289.74 (42.02)	1634.26 (237.03)	1389.12 (201.47)	139.71 (20263.79)
System 2	2522.03 (365.79)	273.70 (39.70)	1700.91 (246.70)	1445.78 (209.69)	166.18 (24102.46)
1-Layer	1043.74 (151.38)	125.98 (18.27)	665.79 (96.56)	565.92 (82.08)	70.37 (10205.65)
2-Layer	1100.58 (159.63)	133.86 (19.42)	698.99 (101.38)	594.14 (86.17)	78.96 (11451.92)
3-Layer	1031.03 (149.54)	124.73 (18.09)	656.83 (95.26)	558.30 (80.97)	78.68 (11411.74)

A comparison of these values with assumed design values determined in Chapter 5, indicates that if the ACI procedures are used intrinsically the design tensile strengths of all systems and design tensile modulus of System 1 are more conservative.

8.6.2.2 Procedures Pursuant to CEB-FIP Task Group 9.3 (*fib* 2001)

The CEB-FIP guidelines suggest that the design tensile strength, f_{fd}, be taken as

$$f_{fd} = \frac{f_{fk}}{\gamma_f} \cdot \frac{\varepsilon_{fue}}{\varepsilon_{fum}} \qquad \textbf{Eqn. 8.3}$$

where

$$f_{fk} = \overline{f}_f - 1.65\sigma \qquad \textbf{Eqn. 8.4}$$

where, $\overline{f}_f$ is the mean measured tensile strength and σ is the standard deviation. For a CFRP composite constructed by wet lay-up, $\gamma_f = 1.35$; whereas, a CFRP composite is prefabricated, i.e. a pultruded CFRP composite, $\gamma_f = 1.2$. The ratio of effective and mean ultimate strains is approximately 1 i.e., $\varepsilon_{fue}/\varepsilon_{fum} \approx 1$. The design tensile modulus, E_{fd}, is not taken less than its characteristic value E_{fk}.

$$E_{fk} = \overline{E}_f - 1.65\sigma \qquad\qquad \textbf{Eqn. 8.5}$$

where $\overline{E}_f$ is the mean measured modulus of elasticity.

Table 8-17 shows the design properties for the measured tensile strength and tensile modulus of specimens from the Watson Wash Bridge rehabilitation in accordance with procedures for the CEB-FIP code for externally bonded FRP composites. Materials are identified as in Table 8-16.

Table 8-17. Design Tensile Properties Per CEB-FIP Code

Material ID	Tensile Strength				Tensile Modulus		
	$\overline{f}_f$ MPa (ksi)	σ MPa (ksi)	f_{fk} MPa (ksi)	f_{fd} MPa (ksi)	$\overline{E}_f$ GPa (ksi)	σ GPa (ksi)	E_{fk} GPa (ksi)
System 1	2503.46 (363.10)	289.74 (42.02)	2025.40 (293.76)	1687.83 (244.80)	139.71 (20263.79)	12.86 (1864.48)	118.50 (17187.40)
System 2	2522.03 (365.79)	273.70 (39.70)	2070.42 (300.29)	1725.35 (250.24)	166.18 (24102.46)	12.33 (1787.90)	145.84 (21152.43)
1-Layer	1043.74 (151.38)	125.98 (18.27)	835.87 (121.23)	619.16 (89.80)	70.37 (10205.65)	9.44 (1369.66)	54.78 (7945.70)
2-Layer	1100.58 (159.63)	133.86 (19.42)	879.71 (127.59)	651.64 (94.51)	78.96 (11451.92)	7.20 (1044.75)	67.07 (9728.08)
3-Layer	1031.03 (149.54)	124.73 (18.09)	825.22 (119.69)	611.27 (88.66)	78.68 (11411.74)	5.39 (782.29)	69.78 (10120.96)

A comparison of these values with the earlier assumed design values of Chapter 5, indicates that if the CEB-FIP procedures are used intrinsically than the CEB-FIP recommended design tensile strength and design tensile modulus are more conservative except for the System 2 tensile modulus.

8.6.2.3   Procedures Pursuant to The Concrete Society (TR No. 55 2000)

The design guidance for FRP composite strengthening, Technical Report No. 55 (TR No. 55 2000) suggests a design values for tensile strength, f_{fd}, and tensile modulus E_{fd}, with partial safety factors for fiber type, γ_{mf}, for manufacturing process, γ_{mm}, and for tensile modulus at ultimate, γ_{mE}, such that,

$$f_{fd} = \frac{f_{fk}}{\gamma_{mf}\gamma_{mm}}$$ **Eqn. 8.6**

$$E_{fd} = \frac{E_{fk}}{\gamma_{mE}}$$ **Eqn. 8.7**

where,

$$f_{fk} = f_{fm} - 2\sigma$$ **Eqn. 8.8**

$$E_{fk} = E_{fm} - 2\sigma$$ **Eqn. 8.9**

where f_{fm}, is the mean tensile strength of FRP; σ, is the standard deviation; E_{fm} is the mean tensile modulus of FRP composite.

For pultruded CFRP composites, $\gamma_{mm} = 1.1$ and $\gamma_{mf} = 1.4$. For wet lay-up CFRP composites, $\gamma_{mm} = 1.4$ and $\gamma_{mf} = 1.4$. $\gamma_{mE} = 1.1$ for CFRP composites.

Table 8-18 shows the design properties for the measured tensile strength and tensile modulus of specimens from the Watson Wash Bridge rehabilitation in accordance with procedures in TR No. 55 design guidelines for externally bonded FRP composites. Materials are identified as in Table 8-16.

Table 8-18. Design Tensile Properties Per TR No. 55

Material ID	Tensile Strength				Tensile Modulus			
	f_{fm} MPa (ksi)	σ MPa (ksi)	f_{fk} MPa (ksi)	f_{fd} MPa (ksi)	E_{fm} GPa (ksi)	σ GPa (ksi)	E_{fk} GPa (ksi)	E_{fd} GPa (ksi)
System 1	2503.46 (363.10)	289.74 (42.02)	1923.99 (279.05)	1249.35 (181.20)	139.71 (20263.79)	12.86 (1864.48)	114.00 (16534.84)	103.64 (15031.67)
System 2	2522.03 (365.79)	273.70 (39.70)	1974.62 (286.39)	1282.22 (185.97)	166.18 (24102.46)	12.33 (1787.90)	141.53 (20526.67)	128.66 (18660.61)
1-Layer	1043.74 (151.38)	125.98 (18.27)	791.77 (114.84)	403.97 (58.59)	70.37 (10205.65)	9.44 (1369.66)	51.48 (7466.32)	46.80 (6787.56)
2-Layer	1100.58 (159.63)	133.86 (19.42)	832.86 (120.80)	424.93 (61.63)	78.96 (11451.92)	7.20 (1044.75)	64.55 (9362.42)	58.68 (8511.29)
3-Layer	1031.03 (149.54)	124.73 (18.09)	781.56 (113.36)	398.75 (57.83)	78.68 (11411.74)	5.39 (782.29)	67.89 (9847.16)	61.72 (8951.97)

A comparison of these values with the earlier assumed design values of Chapter 5, indicates that if the TR No. 55 procedures are used intrinsically than the TR No. 55 recommended design tensile strengths and design tensile moduli are more conservative.

8.6.2.4 Procedures Pursuant to Design Guidelines (Tajlsten 2002)

Design guidelines by Tajlsten (2002) suggest the use of design FRP composite tensile modulus and tensile strength with safety factors that account for systematic differences between laboratory and field environments, η_T, safety class of the structure, γ_n, and material characteristics, γ_m,

$$f_d = \frac{f_k}{\eta_T \gamma_m \gamma_n} \qquad \qquad \textbf{Eqn. 8.10}$$

where,

$$f_k = \bar{f}_f - 1.65\sigma \qquad \qquad \textbf{Eqn. 8.11}$$

$\bar{f}_f$ is average material strength; σ, is the corresponding standard deviation. For cases of exterior exposure and aggressive environments at serious safety level structures, $\eta_T = 1.1$, $\gamma_n = 1.1$, and γ_m ranges from 1.54 to 2.03 for pultruded CFRP composites and 1.68 to 2.35 for wet lay-up CFRP composites.

Tajlsten suggests that for the design tensile modulus the safety factor $\eta_T \gamma_m = 1.20$. The design tensile modulus, E_d is determined utilizing the recommended safety factor $\eta_T \gamma_m = 1.20$.

$$E_d = \frac{E_k}{\eta_T \gamma_m \gamma_n} = \frac{\bar{E}_f - 1.65\sigma}{\eta_T \gamma_m \gamma_n} \qquad \qquad \textbf{Eqn. 8.12}$$

where, E_k, is the characteristic value; $\bar{E}_f$, is the average measured tensile modulus of the FRP composites; all other variables are defined previously. Table 8-19 shows values of the design tensile properties according to the design guidelines by Tajlsten (2002).

Table 8-19. Design Properties Per Tajlsten

Material ID	Ultimate Tensile Strength					Modulus of Elasticity			
	$\overline{f}_f$ MPa (ksi)	σ MPa (ksi)	f_k MPa (ksi)	f_{dUPPER} MPa (ksi)	f_{dLOWER} MPa (ksi)	$\overline{E}_f$ GPa (ksi)	σ GPa (ksi)	E_k GPa (ksi)	E_d GPa (ksi)
System 1	2503.46 (363.10)	289.74 (42.02)	2025.40 (293.76)	1089.66 (158.04)	823.01 (119.37)	139.71 (20263.79)	12.86 (1864.48)	118.50 (17187.40)	89.77 (13020.76)
System 2	2522.03 (365.79)	273.70 (39.70)	2070.42 (300.29)	1113.88 (161.55)	841.30 (122.02)	166.18 (24102.46)	12.33 (1787.90)	145.84 (21152.43)	110.49 (16024.57)
1-Layer	1043.74 (151.38)	125.98 (18.27)	835.87 (121.23)	412.22 (59.79)	294.36 (42.69)	70.37 (10205.65)	9.44 (1369.66)	54.78 (7945.70)	41.50 (6019.47)
2-Layer	1100.58 (159.63)	133.86 (19.42)	879.71 (127.59)	433.84 (62.92)	309.80 (44.93)	78.96 (11451.92)	7.20 (1044.75)	67.07 (9728.08)	50.81 (7369.76)
3-Layer	1031.03 (149.54)	124.73 (18.09)	825.22 (119.69)	406.97 (59.03)	290.61 (42.15)	78.68 (11411.74)	5.39 (782.29)	69.78 (10120.96)	52.86 (7667.40)

A comparison of these values with the earlier assumed design values of Chapter 5, indicates that if design procedures by Tajlsten (2002) are used intrinsically than the recommended design tensile strengths and design tensile moduli are more conservative.

8.7   Discussion

The variation in tensile strength and tensile modulus results in variation in levels of safety for a FRP rehabilitated structure. From existing design codes safety factors range from 1.46 to 3.05 for pultruded CFRP tensile strength and 1.69 to 3.55 for wet lay-up CFRP tensile strength. For tensile modulus safety factors range from 1.0 to 1.56 for pultruded CFRP and 1.0 to 1.7 for wet lay-up tensile modulus. Design procedures utilize techniques that result in knockdown factors due to uncertainty with durability, design, and construction of FRP composites for rehabilitation.

8.8   Summary

While the global NDE investigates at the systems level of the rehabilitated structure, which includes the bridge deck and applied FRP composite, characterization of the state of the materials is critical to evaluate material quality and manufacturer ability to meet specified design properties. The pultrusion manufacturing technique is an efficient and uniform manufacturing technique producing composites of high quality in terms of uniform mechanical properties throughout the composite area; therefore, a minimal sampling of pultruded composite are necessary to determine the variation of modulus and strength in the pultruded CFRP composites strips applied to the deck soffit. The wet lay-up manufacturing process is subject to defects in alignments and placement of fibers due to the manual nature of the technique, as well as exposure to changing environmental conditions including changes in temperature during manufacture and cure. Therefore, characterization of field manufactured or wet lay-up manufactured CFRP composites

requires a more critical analysis of mechanical property measurements besides a large quantity of material samples in order to qualify the applied CFRP composites manufactured at the Watson Wash Bridge.

The average moduli and strength values of both wet lay-up and pultruded CFRP composites are generally greater than or equal to the design moduli of 9.42 and 20.5 msi for wet lay-up and pultruded processes, respectively, and are greater than design strength values of 128.66 ksi and 305 ksi for wet lay-up and pultruded processes, respectively. Variation of properties, however, remains a concern since the scatter in the data for modulus may result in specific CFRP composite locations with CFRP composite properties being below design values.

Evaluating mechanical properties determines the difference between the manufactured and applied composite verse the mechanical properties used to design the quantity of composite necessary. The impact of the variation and margins in mechanical properties to the structure remain unknown, except in extreme cases where measure properties are all greater than or all less than design values. Similarly, measurement of stiffness changes in the system by the vibration based global NDE methodology does not fully character the altered performance of the structure following FRP composite rehabilitation.

In the upcoming chapters, a reliability-based approach is developed and employed to evaluate the impact of FRP composite rehabilitation on reinforced concrete bridge decks. The performance indicator is reliability or probability of failure of the bridge deck. The probability-based approach is considered because it incorporates the variation in measured mechanical properties of materials. The measure of reliability for the rehabilitated bridge deck is able to incorporate measured stiffness changes from the global NDE procedure. Although not specifically addressed in this chapter, the reliability measure of performance integrates FRP composite durability data to estimate the remaining service life of a FRP composite rehabilitated bridge deck. Full characterization of the effectiveness and integrity of a FRP composite rehabilitated bridge deck is possible with a reliability based approach, which combines variability in material properties, global NDE measurements of the physical structure, and durability data of FRP composites to estimate remaining service life of the FRP rehabilitated structure.

9 ESTIMATION OF SERVICE LIFE

9.1 Introduction

In the previous chapter, the CFRP composite materials applied to the deck soffit of the Watson Wash Bridge were characterized. The evaluation of FRP mechanical properties directly addressed the composite materials used during the rehabilitation, while the global NDE evaluated the system of the reinforced concrete bridge deck and bonded CFRP composites. The materials characterization identified the modulus and strength of the applied CFRP and compared them to the design values. Although, the average values for strength and modulus of the bonded CFRP composite materials was greater than or equal to the design properties, the properties of the existing CFRP composite are not deterministic and the effect of material variation on the performance of the strengthened bridge deck remains unclear.

The quality and performance of the FRP rehabilitated bridge deck is designed first to prevent the occurrence of punching shear and, if applicable, provide sufficient strength to support the permit truck wheel load. Variation in material parameters of the applied CFRP composite and degradation of material parameters over time leaves uncertain the ability of the structure to perform as intended. Design safety margins are directly affected by variation in material properties (Plevris, et al., 1995), while issues related to durability and aging of materials in a FRP strengthened structure limits its service life.

Determining the functionality and service life of the rehabilitated deck in Spans 8 and 9 of the Watson Wash Bridge requires a methodology that incorporates the variation in properties of the rehabilitated bridge deck and durability characterization of the bonded composite materials. The generalized reliability index, β, a measure of the probability of failure, is applied as a measure of performance to understand the effect of variation and durability in terms of remaining service life of the CFRP rehabilitated bridge deck. This chapter investigates the changes in the reliability index of the bridge deck before and after CFRP rehabilitation and the impact of material degradation on the performance of the rehabilitated decks slabs of the Watson Wash Bridge. Failure in the reliability analysis is defined as yield of flexural steel reinforcement, tensile strain of 0.002; the punching shear criterion, discussed in chapters 5 and 6, establishes a limit on the tensile strain developed in the bonded CFRP composite to retain aggregate interlock in the deck. The reliability analysis involves a section analysis at each instant of time where degradation occurs and thus provides strain information for concrete and FRP composite; if concrete crush, a compressive strain limit of 0.3%, or the punching shear criterion, tensile strain limit of 0.75%, are violated before steel yield, the limit criteria for the section analysis is modified to match either concrete crush or punching shear strain limit criteria and a change in failure mode is noted. It is important to note that for the FRP composite rehabilitation analysis in the deck slab of the Watson Wash Bridge, in all cases and time periods steel yield occurs first. Following the service life estimation with the effect of material degradation, design recommendations are made for FRP composite rehabilitation.

9.2 Structural Reliability

A measure of performance evaluates the likelihood a structural component is able to resist a level of demand. For example the resistance of a RC beam section is defined by its moment capacity, while demands are anticipated moment loads on the structure.

The reliability of a structure or component is defined as its probability of survival, p_{sur}, which is relate to the probability of failure, p_f, by (Cheung and Kyle, 1996):

$$p_{sur} = 1 - p_f \qquad \textbf{Eqn. 9.1}$$

Considering the possible variation of a structural component or system, the reliability index provides a quantitative measure of the ability of a structure to perform its intended function. Failure of a structural member is defined as physical failure or exceeding a predefined serviceability limit.

9.2.1 Overview of the Basic Reliability Problem

The basic structural reliability problem considers a load effect defined by S, resisted by resistance, R. These are described by a probability distribution function $f_S(\ )$ and $f_R(\ )$, respectively. In general R is a function of material properties and geometry, while S is a function of applied loads, Q, material densities, and geometry of the structure (Melchers, 1999). The probability of failure of a structural component or member is defined as the probability that the demand on the structure is greater than or equal to its resistance.

$$p_f = P(R \leq S) \qquad \textbf{Eqn. 9.2}$$

$$p_f = P(R - S \leq 0) \qquad \textbf{Eqn. 9.3}$$

$$p_f = P(g(R,S) \leq 0) \qquad \textbf{Eqn. 9.4}$$

where, $g(R,S)$ is defined as the performance function; the probability of failure, p_f, is the probability that the performance function is less than or equal to zero. Evaluation of the probability of failure utilizes measures of marginal probability density functions f_R and f_S for R and S, respectively and joint probability density function $f_{RS}(r,s)$. Definitions and explanations for density functions and joint density functions are available in standard texts for probability theory (Rosenkrantz, 1997). The failure probability of the performance function is defined as follows (Melchers, 1999),

$$p_f = P(R - S \leq 0) = \iint\limits_{R-S \leq 0} f_{RS}(r,s)\,drds \qquad \textbf{Eqn. 9.5}$$

Figure 9.1 illustrates the calculation for the probability of failure (Melchers, 1999),
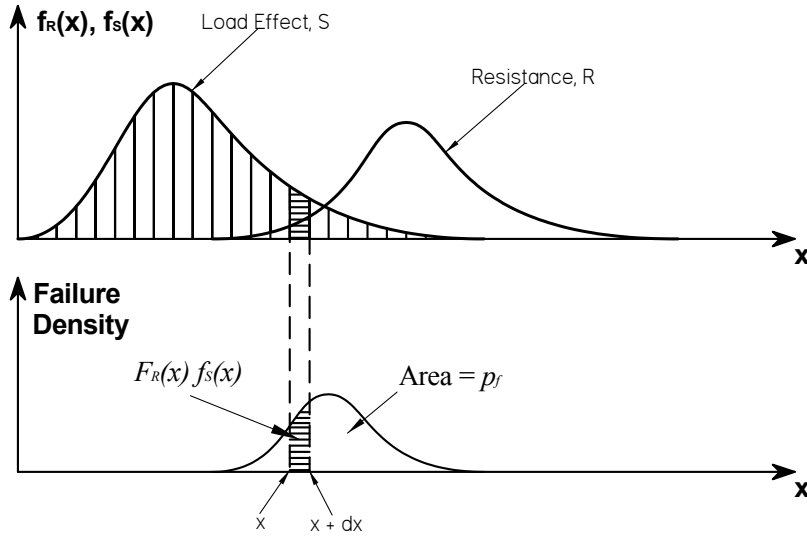
Figure 9.1. Illustration of the Basic Reliability Problem

9.3 Generalized Reliability Problem

In general, the resistance, R is a function of random variables, X_i, which may represent material properties and dimensions,

$$R(X_i) \text{ for } i = 1,..., n \text{ number of random variables} \qquad \textbf{Eqn. 9.6}$$

Similarly, the load, S, on a structure is a function of random variables, X_i, which may represent applied loads, material densities, and possibly geometry of the structure.

$$S(X_i) \text{ for } i = 1,..., n \text{ number of random variables} \qquad \textbf{Eqn. 9.7}$$

The performance function of the reliability problem is then conveniently expressed as a function of all relevant basic variables,

$$z = g(R,S) = g(X_1,...,X_n) = g(\vec{\mathbf{X}}) \qquad \textbf{Eqn. 9.8}$$

where $\vec{\mathbf{X}}$ is the vector of random variables with probability distributions, $f_{\vec{\mathbf{X}}}(\ )$. With the performance function or limit state function in terms of n random variable, the calculation for the probability of failure is formulated as

$$p_f = P\left[g(\vec{\mathbf{X}}) \leq 0 \right] = \int ... \int\limits_{g(\vec{\mathbf{X}}) \leq 0} f_{\vec{\mathbf{X}}}(\vec{\mathbf{x}}) d\vec{\mathbf{x}} \qquad \textbf{Eqn. 9.9}$$

where, $f_{\vec{\mathbf{X}}}(\vec{x})$, is the joint probability density function for the n-dimensional vector $\vec{\mathbf{X}}$ of random variables in the performance function. As in the basic reliability formulation, the region of integration $g(\vec{\mathbf{X}}) \leq 0$ defines the failure domain or "unsafe" region and $g(\vec{\mathbf{X}}) > 0$ is the "safe" region. Typically the solution for the above integral is determined via numerical simulation techniques such as Monte Carlo simulation or by avoiding the

- 212 -

integration problem with a transformation of the density function, $f_{\bar{X}}(\bar{x})$ to a multi-normal probability density function and using its unique characteristics to approximate the probability of failure. Methods that incorporate the latter include first order second moment method, first order reliability methods (FORM), and second order reliability methods (SORM).

9.4   Normal Random Variables

In the case where resistance, R, and load, S, are normally distributed random variables, an analytical solution of the convolution integral for the probability of failure is available in the basic reliability problem. If R and S are normal random variables, their distributions are described by their means, μ_R and μ_S, respectively and variances, σ_R^2 and σ_S^2, respectively. The mean and variance of the performance function are determined according to rules of addition and subtraction for normal variables, available in standard statistics texts. The relationship between performance function, $Z = g(R,S)$ and variables for resistance and load is shown below,

$$Z = R - S \qquad\qquad \textbf{Eqn. 9.10}$$

$$\mu_z = \mu_R - \mu_S \qquad\qquad \textbf{Eqn. 9.11}$$

$$\sigma_z^2 = \sigma_R^2 + \sigma_S^2 \qquad\qquad \textbf{Eqn. 9.12}$$

where, z, is the performance function or limit state function; μ_z and σ_z^2 are the mean and variance of the performance function, respectively. The probability of failure is available in the following form,

$$p_f = P(R - S \leq 0) = P(Z \leq 0) = \Phi\left(\frac{0 - \mu_z}{\sigma_z}\right) \qquad \textbf{Eqn. 9.13}$$

where, $\Phi(\ )$ denotes the standard normal distribution. Figure 9.2 illustrates the probability of failure measurement for the basic reliability problem with performance function $z = R - S$, where random variables are normally distributed (Melchers, 1999).
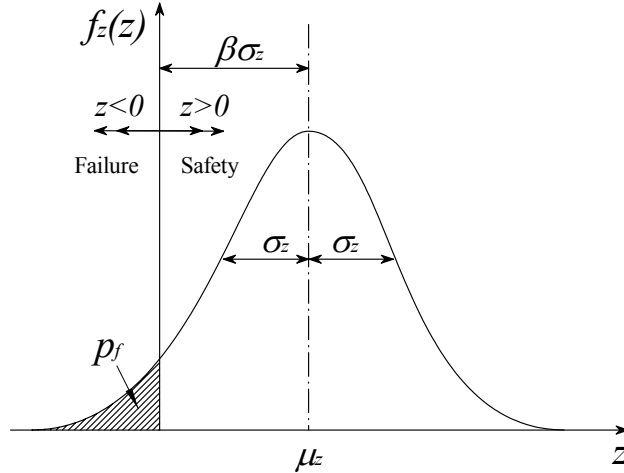
Figure 9.2. Distribution of Safety Margin, *Z = R-S*

Combining equations 9.14, 9.15 and 9.16, the probability of failure, p_f, is defined,

$$p_f = \Phi\left(\frac{-\left(\mu_R - \mu_S\right)}{\left(\sigma_R^2 + \sigma_S^2\right)^{\frac{1}{2}}}\right) = \Phi\left(-\beta\right)$$ **Eqn. 9.14**

where, $\beta = \mu_z / \sigma_z$ and is called the reliability index or "safety" index. A closer look at the relationship in equation 9.14 shows that an increasing variance causes the reliability index, β to decrease, thus the probability of failure increases. In the case where maintenance action for a structure is intended to increase the reliability index, variations inherent in the construction and design process may negate the benefits expected from the maintenance action.

9.5   Methodology for Service Life Estimation

The service life estimation methodology uses a mean value, first order, second moment formulation of the reliability index where random variables are described by their respective means and variances (Melchers, 1999). Formulation of the reliability analysis for service life estimation requires the following steps:

1.   Identification of random variables with means and variances

2.   Determination of mean μ_z and variation σ_z of the performance function, z

3.   Evaluation of time-dependent reliability for service life assessment

Each of the steps requires knowledge of the material composition of the structure, the load conditions and failure mechanisms of a structure. A performance function and its definition for failure are also necessary. In the current situation (the rehabilitated deck), for a single instance of time the standard second moment equation is used for calculations of the reliability index, β, of the deck slab.

$$\beta = \frac{\mu_z}{\sigma_z} = \frac{(\mu_R - \mu_S)}{(\sigma_R^2 + \sigma_S^2)^{\frac{1}{2}}}$$ **Eqn. 9.15**

$$p_f = \Phi(-\beta)$$ **Eqn. 9.16**

where quantities are defined previously. The standard normal distribution, $\Phi(\ )$, is then used to compute the corresponding probability of failure. Utilizing the reliability index assists in evaluating the effect of variation in material properties of the applied FRP composite and existing steel reinforcement and concrete. In addition, use of the mean value first order second moment reliability index provides a method to include the effects of material degradation and thus allows for determination of a time-dependent measure of reliability.

Although easily implemented, the standard second moment equation is not without its constraints. One of the primary assumptions in using the mean value, first order, second moment measure of the reliability is that random variables are described only by their means and variances and all random variables in the reliability analysis are assumed normally distributed. A second constraint is a result of the lack of invariance of the reliability index with change in the form of the performance function (Melchers, 1999). However, this constraint is resolved by using the same form of the performance function for all analyses, i.e. $Z = R - S$.

In the following subsections, the method for service life estimation is described in conjunction with analyses of the CFRP rehabilitated RC deck slab of the Watson Wash Bridge. One of the primary concerns is the prevention of punching shear failure in the deck slab of the Watson Wash Bridge. The prevention of punching shear failure requires limiting the widths of cracks to 1 mm; this results in a maximum allowable strain in the CFRP of 0.75%. A linear performance function or limit state function for the moment capacity of a representative beam of the deck slab is applied, where failure in the reliability analysis is defined as yield of flexural steel for both FRP rehabilitated and un-rehabilitated RC decks; consideration for punching shear failure is provided in the section analyses where if the strain in the bonded CFRP composite exceeds 0.75% before steel yield or concrete crush, the change in failure mode is noted and the section analysis has to be conducted with the rupture strain of the FRP composite. The methodology for service life estimation, including a time-dependent reliability index measure, is described in this section to evaluate the effect of FRP composite degradation on rehabilitated structural components.

For the Watson Wash Bridge RC deck analyses, beam sections 30.48 cm (12 inches) wide are used to represent the deck slabs of the Watson Wash Bridge in the longitudinal and transverse slab directions. Utilizing 30.48 cm (12 inches) wide strips of the deck slab is analogous to the design procedure for decks slabs of reinforced concrete T-girder bridges in accordance with the Caltrans Bridge Design Specifications (Caltrans BDS, 2004). Geometries of longitudinal and transverse beam sections representative of the deck slab are shown in Figure 9.3.
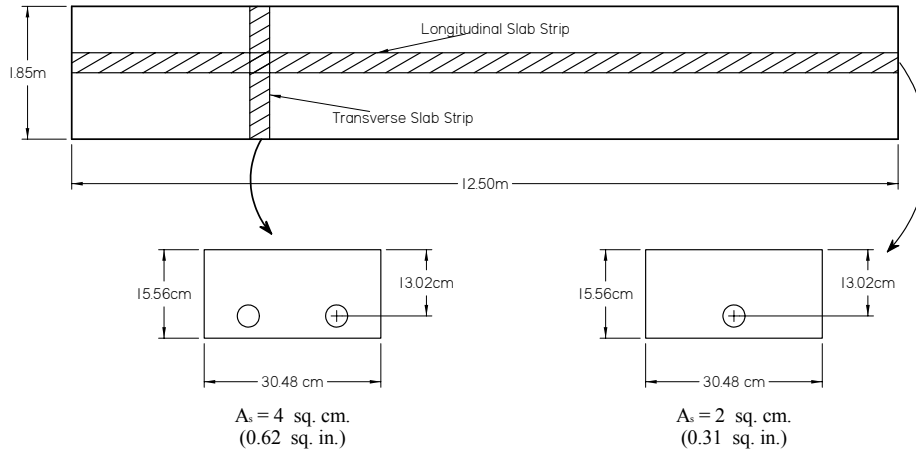
Figure 9.3. Representative Beam Sections for Deck Slab Analysis

The flexural reinforcement consists of two No. 5 rebar in a single transverse beam width and one No. 5 rebar in a single longitudinal beam width. The area of transverse and longitudinal steel reinforcement areas per beam width are 4 cm^2 (0.62 in^2) and 2 cm^2 (0.31 in^2).

9.5.1 Random Variables

For a FRP rehabilitated structure, such as the deck slabs of the Watson Wash Bridge, random variables are separated into those, which contribute to the moment capacity or resistance and those that contribute to the applied loading or demands on the deck slab.

9.5.1.1 Resistance Variables

An example of resistance for a beam structure is the nominal moment capacity at steel yield. Material parameters having a direct impact on the moment capacity of a CFRP rehabilitated structure are concrete compressive strength, f_c', yield strength of steel, f_y, and CFRP composite modulus of elasticity and ultimate strength. Each parameter is described by its respective mean and coefficient of variation, COV. For mean values of steel yield strength and concrete compressive strength, bias factors are available in Barker and Puckett (1997). The following table summarizes the means and COV's for steel yield strength and concrete compressive strength used in the analysis of the Watson Wash Bridge.

Table 9-1. Statistical Descriptors for Steel and Concrete Strengths

Variable	Design Value MPa (ksi)	Bias Factor	Mean Value MPa (ksi)	COV %
f_y	413.69 (60.0)	1.1	455.05 (66.0)	10
f_c'	24.82 (3.60)	1.14	25.55 (3.71)	15

For the statistical descriptors of CFRP composite, the mean value and COVs of as-built composite samples manufactured during the deck rehabilitation are applied for tensile modulus and strength. The following tables summarize mean values and COVs for tensile modulus and tensile strength of the bonded CFRP composite by location and direction of reinforcement.

Table 9-2. Longitudinal CFRP Composite Parameters

Location	Thickness mm (inch)	A_{frp}, FRP Area per slab length mm^2 / m (in^2 / ft)	E_{frp}, Mean Tensile Modulus GPa (msi)	Tensile Modulus COV %	f_{frp}, Mean Tensile Strength GPa (ksi)	Strength COV %
S8, B1	1.27 (0.050)	139.17 (0.066)	139.71 (20.26)	9.20	2.50 (363.10)	11.57
S8, B2	1.27 (0.050)	173.98 (0.082)	139.71 (20.26)	9.20	2.50 (363.10)	11.57
S8, B3	1.07 (0.042)	352.40 (0.167)	71.16 (10.32)	14.86	1.071 (155.28)	7.12
S8, B4	N/A	N/A	N/A	N/A	N/A	N/A
S8, B5	1.91 (0.075)	627.97 (0.297)	78.77 (11.43)	7.32	1.094 (158.67)	11.16
S9, B1	1.27 (0.050)	139.17 (0.066)	139.71 (20.26)	9.20	2.50 (363.10)	11.57
S9, B2	1.27 (0.050)	173.98 (0.082)	139.71 (20.26)	9.20	2.50 (363.10)	11.57
S9, B3	1.13 (0.044)	366.66 (0.175)	70.53 (10.23)	13.56	0.957 (138.74)	11.21
S9, B4	1.30 (0.051)	141.96 (0.067)	166.18 (24.10)	7.42	2.52 (365.79)	10.85
S9, B5	1.86 (0.073)	612.10 (0.289)	78.92 (11.45)	12.09	0.920 (133.46)	10.10

Table 9-3. Transverse CFRP Composite Parameters

Location	Thickness mm (inch)	A_{frp}, FRP Area per slab length mm^2 / m (in^2 / ft)	E_{frp}, Mean Modulus GPa (msi)	Modulus COV %	f_{frp}, Mean Strength GPa (ksi)	Strength COV %
S8, B1	1.27 (0.050)	108.41 (0.051)	139.71 (20.26)	9.20	2.50 (363.10)	11.57
S8, B2	1.27 (0.050)	299.42 (0.142)	139.71 (20.26)	9.20	2.50 (363.10)	11.57
S8, B3	1.84 (0.072)	627.93 (0.297)	78.86 (11.44)	5.62	1.191 (172.75)	8.38
S8, B4	N/A	N/A	N/A	N/A	N/A	0
S8, B5	2.84 (0.112)	728.55 (0.344)	79.41 (11.52)	6.89	1.057 (153.27)	5.3
S9, B1	1.27 (0.050)	108.41 (0.051)	139.71 (20.26)	9.20	2.50 (363.10)	11.57
S9, B2	1.27 (0.050)	299.42 (0.142)	139.71 (20.26)	9.20	2.50 (363.10)	11.57
S9, B3	1.88 (0.074)	643.55 (0.304)	79.12 (11.48)	10.23	1.149 (166.62)	6.99
S9, B4	1.31 (0.052)	112.74 (0.053)	166.18 (24.10)	7.42	2.52 (365.79)	10.85
S9, B5	2.64 (0.104)	675.21 (0.319)	77.77 (11.28)	7.10	0.999 (144.87)	17.79

Since the effect of material degradation on the performance of the deck slab is sought, only characteristic material properties for the three major components of the CFRP rehabilitated bridge deck are applied, namely steel, concrete, and CFRP composite. All geometric parameters are considered deterministic.

9.5.1.2   Demand Variables

Dead load moment is calculated by modeling a transverse segment of the slab as a simply supported beam with a continuity factor of 0.8 per Caltrans BDS section 3.24.3.1 (Caltrans 2004). A dead load moment bias factor of 1.05 is included for cast-in-place concrete bridges, with coefficient of variance (COV) of 10% (Nowak 1999). The bias factor and COV of the surface overlay are assumed negligible in this analysis since an overall bias factor and COV are applied to the total dead load moment.

$$M_{DL} = \lambda_{DL} 0.8 \cdot \frac{w_{DL} \cdot L_{slab}^2}{2} \qquad \textbf{Eqn. 9.17}$$

$$w_{\mathrm{DL}} = t_s \cdot w_c + surface \qquad \textbf{Eqn. 9.18}$$

where, M_{DL}, is the dead load moment; λ_{DL}, is the dead load moment bias factor, 1.05; L_{slab}, is the clear span of the slab, 1.854 m (73 inches); w_{DL}, is the distributed dead load; t_s, thickness of the slab, 15.56 cm (6.125 inches); w_c, is the density of normal weight concrete, 2402.77 kg/m³ (150 pcf); *surface*, is the wearing surface on the top of the deck, 364.85 N/m (25 lb/ft). The resulting dead load moment is 0.535 kN-m per 30.48 cm of slab, or 1.76 kN-m/m.

Consideration for live load moment demands on the deck slab of the structure includes two load levels, i.e. HS20 and Permit wheel loads. The first is the original design load for the bridge structure, the HS20 wheel load of 71.2 kN (16 kips). The second wheel load is the Permit Truck wheel load of 106.76 kN (24 kips). A live load bias factor of 1.2 is applied to HS20 live load moment demands, while the COV of 18% is specified for both HS20 and Permit Truck live load moments (Nowak 1999). In addition, the dynamic load factor of 1.3 is applied to both live load moments (Caltrans 2004). A live load moment reduction factor of 0.85 is conservatively specified for a two-lane highway bridge according to NCHRP Report 368 (Nowak 1999) instead of the 0.8 continuity factor indicated in the Caltrans BDS. Live load moment demands are calculated per equation 3-15 in the Caltrans BDS (Caltrans 2004). Equation 9.19 is specified for the FPS unit system. The resulting live load moment is converted to SI units following the calculation.

$$M_{LL} = \lambda_{LL} \lambda_{dyn} 0.85 \left(\frac{L_{slab} + 2}{32} \right) \cdot P \qquad \textbf{Eqn. 9.19}$$

where M_{LL}, is the live load moment demand; λ_{dyn}, is the dynamic load factor, 1.3; λ_{LL}, is the live load bias factor, 1.2 applied only for the HS20 wheel load; L_{slab}, is the clear span of the slab, 1.85 m; P, is the design truck wheel load, equal to 71.2 kN (16 kips) for the HS20 design load and 106.76 kN (24 kips) for the Permit Truck wheel load. The resulting live load moment is 7.27 kN-m per 30.48 cm of slab or 23.84 kN-m/m for the HS20 design load and 8.22 kN-m per 30.48 cm of slab or 26.97 KN-m/m with a COV of 18%. A summary of dead and live load moments is given in Table 9-4.

Table 9-4. Summary of Demand Moments

Moment Type	Unfactored Moment kN-m/m (kip-ft/ft)	Live Load Moment Reduction Factor	Dynamic Amplification Factor	Bias Factor	Mean Value kN-m/m (kip-ft/ft)	COV %
Dead Load	2.09 (0.47)	0.8	N/A	1.05	1.756 (0.40)	10
Live - HS20	17.98 (4.04)	0.85	1.3	1.2	23.84 (5.36)	18
Live - Permit	26.97 (6.06)	0.85	1.3	1	29.80 (6.70)	18

9.5.2 *Performance Function*

The performance function translates the limit of the structure to a quantitative measure of the reliability index; the reliability index quantifies the probability that a violation of the selected criteria occurs. In the case of the Watson Wash Bridge deck slabs, this criterion is the yield strain of steel, equal to 0.002, in the deck slab in both the longitudinal and transverse directions. The cracking pattern of the deck slab indicates that the moment demands on the deck slab are approximately the same in the longitudinal and transverse slabs; first, transverse cracking occurs in the deck slab since insufficient longitudinal steel reinforcement exists to accommodate the design moment demands followed by longitudinal cracking. The basic performance function, its mean, and its variance are shown in equations 9.10, 9.11, and 9.12.

The equation for moment resistance of the section is taken about the axis of zero strain, c, such that moment contributions from steel, concrete, and FRP are considered in the moment resistance formulation.

$$\mu_R = \mu[M_R] = \mu[M_C] + \mu[M_{steel}] + \mu[M_{frp}] \qquad \textbf{Eqn. 9.20}$$

$$M_C = C_C \cdot \left(c_1 - \frac{a}{2}\right) = 0.85 f_c' \beta_1 c_1 b \cdot \left(c_1 - \frac{\beta_1 c_1}{2}\right) \qquad \textbf{Eqn. 9.21}$$

$$M_{steel} = T_S \cdot (d - c_1) = A_S f_y \cdot (d - c_1) \qquad \textbf{Eqn. 9.22}$$

$$M_{frp} = T_{frp} \cdot (h - c_1) = A_{frp} E_{frp} \varepsilon_{frp} \cdot (h - c_1) \qquad \textbf{Eqn. 9.23}$$

where μ denotes mean value; M_R is the moment resistance of the reinforced concrete section about the axis of zero strain, or the sum of the moment contributions from concrete, M_C, steel reinforcement, M_{steel}, and FRP composite, M_{frp}; C_c is the force acting in the concrete; f_c', is the compressive strength of concrete; β_1, rectangular compressive stress block factor equal to 0.85; c_1, denotes the axis of zero strain from the extreme compression fiber; b, is the representative beam width; T_s, force in steel reinforcement; A_s, area of steel reinforcement; f_y, yield strength of steel; d, is the depth to steel reinforcement from the extreme compression fiber of the section; T_{frp}, force in CFRP composite; A_{frp}, area of FRP composite; E_{frp}, modulus of FRP composite; ε_{frp}, strain in FRP composite; h, is the height of the section. M_R, represents the mean value of the resistance with random variables, f_y, f_c' and E_{frp}.

A standard section analysis for reinforced concrete is conducted to determine the depth of the axis of zero strain, such that if the force in the FRP exceeds its ultimate strength the section analysis is conducted with the corresponding ultimate FRP strain or 0.75% used in design for punching shear as the limiting criteria. Similarly if concrete crush occurs, i.e. strain in concrete, ε_c, exceeds 0.003, the section analysis is conducted with concrete strain at crush as the limiting criteria.

Determination of the variation in resistance utilizes standard rules for probability. Given the moment resistance equation and coefficient of variation *COV* of the independent

random variables f_y, f_c' and E_{frp}, the coefficients of variation, *COV,* for the moment contributions are the same as their respective random variable.

$$COV_{M_{f_{c'}}} = \frac{\sigma_{M_{f_{c'}}}}{\mu_{M_{f_{c'}}}} = COV_{f_c'}$$ **Eqn. 9.24**

$$COV_{M_{steel}} = \frac{\sigma_{M_{steel}}}{\mu_{M_{steel}}} = COV_{f_y}$$ **Eqn. 9.25**

$$COV_{M_{f_{c'}}} = \frac{\sigma_{M_{f_{c'}}}}{\mu_{M_{f_{c'}}}} = COV_{f_c'}$$ **Eqn. 9.26**

$$\sigma_R^2 = \sigma_{M_R}^2 = \sigma_{M_{f_{c'}}}^2 + \sigma_{M_{steel}}^2 + \sigma_{M_{frp}}^2$$ **Eqn. 9.27**

where, μ denotes mean value of the subscript variable; σ^2, is the variance of the material noted in its subscript; COV is the coefficient of variation of the subscript variable.

The mean value for the demand component of the performance function, *S,* is the sum of the mean dead load and mean live load moments. The total moment demand and variance are determined as in the resistance evaluation.

$$\mu_S = \mu[M_S] = \mu[M_{LL}] + \mu[M_{DL}]$$ **Eqn. 9.28**

$$\sigma_S^2 = \sigma_{M_S}^2 = \sigma_{M_{LL}}^2 + \sigma_{M_{DL}}^2$$ **Eqn. 9.29**

$$\sigma^2 = (COV \cdot \mu)^2$$ **Eqn. 9.30**

where, μ, denotes the mean value of the variable in brackets [ ]; σ^2, is the variance of the variable in brackets [ ]. Unlike the resistance formulation it is assumed that the demand does not change with respect to location and time. Total demands on the structure for the HS20 and Permit Truck wheel loads are shown in Table 9-5.

Table 9-5. Total Moment Demands

Total Moment Demands, M_S	Total Mean Value, μ_S kN-m/m (kip-ft/ft)	Standard Deviation, σ_S kN-m/m (kip-ft/ft)	COVs %
HS20	25.60 (5.76)	4.294 (0.966)	16.8
Permit Truck	31.556 (7.10)	5.366 (1.21)	17.0

Substituting for appropriate terms in the performance function, for resistance and demand moments, the mean and variation of the performance function are determined as given by equations 9.11 and 9.12, respectively. The reliability index and probability of failure are determined for a single set of material parameters at a single instance of time with the relationships in equations 9.15 and 9.16, and results are reported 9.6.1.

9.5.3 *Time Dependent Reliability*

The previous mean value first order second moment reliability index computes an instantaneous reliability of a structure and does not incorporate the change in reliability with respect to time. Combining a prediction for the change in reliability as a function of time with an acceptable limit of the probability of failure effectively provides an estimate for the available service life of a structure or component. Specifically, the effect of material degradation on the performance of the structure is made available.

Time-dependent reliability, $\beta(t)$, is developed by introducing time-dependent variables within the second moment reliability equation (Sarja and Vesikari 1996):

$$\beta(t) = \frac{\mu_z}{\sigma_z} = \frac{\mu_R(t) - \mu_S}{\left(\sigma_R^2(t) + \sigma_S^2\right)^{\frac{1}{2}}} \qquad \textbf{Eqn. 9.31}$$

where, μ, denotes the mean value; σ^2 is the variance; R is resistance; S is demand; t is time. Specifically, time may be introduced from predictions for degradation of material parameters such as loss in steel area under corrosion or, in the case of the Watson Wash Bridge deck, potential degradation in CFRP mechanical properties due to environmental exposure.

Means and variance of moment demands on the deck slab are assumed to remain unchanged over time. COV of the random variables, f_y, f_c' and E_{frp} are assumed to remain constant with respect to time, while changes in the mean moment are a function of the time dependent material parameters. The time dependent moment resistance and variance are provided for a beam component with externally bonded FRP composite.

$$\mu_R(t) = \mu[M_R] = \mu[M_C(t)] + \mu[M_{steel}(t)] + \mu[M_{frp}(t)] \qquad \textbf{Eqn. 9.32}$$

$$M_C = C_C(t) \cdot \left(c_1(t) - \frac{a}{2}\right) = 0.85 f_c' \beta_1 c_1(t) b \cdot \left(c_1(t) - \frac{\beta_1 c_1(t)}{2}\right) \qquad \textbf{Eqn. 9.33}$$

$$M_{steel} = T_S \cdot \left(d - c_1(t)\right) = A_S f_y \cdot \left(d - c_1(t)\right) \qquad \textbf{Eqn. 9.34}$$

$$M_{frp}(t) = T_{frp} \cdot \left(h - c_1(t)\right) = A_{frp} E(t) \varepsilon_{frp} \cdot \left(h - c_1(t)\right) \qquad \textbf{Eqn. 9.35}$$

$$\sigma_R^2(t) = \sigma_{M_R}^2(t) = \sigma_{M_{f_c'}}^2(t) + \sigma_{M_{steel}}^2(t) + \sigma_{M_{frp}}^2(t) \qquad \textbf{Eqn. 9.36}$$

where, t, denotes time; $E(t)$, is the time dependent modulus of the FRP composite; all other variables are previously defined. Substitution of equations 9.32 and 9.36 into equation 9.31 yields an estimate of the reliability as a function of time.

$$\beta(t) = \frac{\mu_z}{\sigma_z} = \frac{\mu\left[M_C(t)\right] + \mu\left[M_{steel}(t)\right] + \mu\left[M_{frp}(t)\right] - \mu_S}{\left(\sigma^2_{M_{f'c}}(t) + \sigma^2_{M_{steel}}(t) + \sigma^2_{M_{frp}}(t) + \sigma^2_S\right)^{\frac{1}{2}}}$$

<div align="right">**Eqn. 9.37**</div>

where, variables are described previously. Note, μ_S is the mean moment demand and σ^2_S is the variance of the moment demand.

Equations 9.32 thru 9.37 are a time dependent form of the instantaneous reliability. Although, only the FRP composite is assumed to degrade, the steel and moment contributions change with respect to time due to change in depth of the axis of zero strain, $c_1(t)$. Accordingly, a section analysis is required to determine the resultant change following a change in material parameters. The section analysis also serves to validate the pattern of failure and detect changes in the failure pattern as components for the force equilibrium changes over time. More importantly, the section analysis provides information about the changing strain levels in the FRP composite as a function of time to determine if FRP rupture occurs, if the punching shear criterion is violated, or if concrete crush occurs prior to steel yield. It is also observed that variance is a function of the moment contributions and thus the variance of the mean resistance also changes with respect to time. The general solution procedure for the time-dependent reliability estimation for a specific time range is shown in Figure 9.4.

Define Time Range
For t = 0,...,years

Material Degradation Model
$E(t) = E_0\, y(t)$

RC Section Analysis
c(t)

Mean Moment Resistance
$\mu\left[M_R(t)\right]$

Variance of Resistance
$\sigma^2_R(t) = \sigma^2_{M_R}(t)$

Estimate Reliability Index
$\beta(t) = \mu_z/\sigma_z$
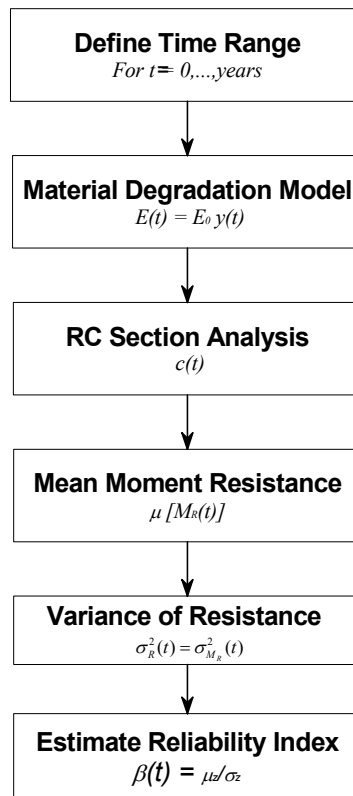
Figure 9.4. Solution Procedure for Time-Dependent Reliability

For a given time period, the material degradation model provides an estimate of the FRP modulus, from which the solution procedure is followed with a section analysis and calculations for the mean moment resistance and its variance. The reliability of the structure at time, t, is given by the second moment reliability index. An essential component of the time-dependent reliability assessment is the material degradation model selected. In this study of time-dependent reliability, the effect of CFRP degradation on the performance of the FRP rehabilitated deck slab is the primary focus.

9.5.3.1 Material Degradation Models

For the purposes of the current investigation durability of FRP composites is characterized by the use of accelerated aging procedures. Predictions for CFRP composite tensile modulus and tensile strength are modeled with an Arrhenius rate relationship (ARR) for 2-layer wet lay-up CFRP composites immersed in deionized water at 23°C for approximately two years (Abanilla 2004). The percent retention of tensile modulus and tensile strength for the 2 layer CFRP composite are,

$$y_m(t) = -0.4182 \cdot \ln(t \cdot 365 \tfrac{days}{year}) + 106.07\% \qquad \textbf{Eqn. 9.38}$$

$$y_s(t) = -3.366 \cdot \ln(t \cdot 365 \tfrac{days}{year}) + 106.07\% \qquad \textbf{Eqn. 9.39}$$

where, $y_m(t)$, is the percent retention of tensile modulus; $y_s(t)$, is the percent retention of tensile strength; t, is time in years.

Both modulus and strength are included in the time-dependent reliability formulation to account for the condition where predicted CFRP composite modulus multiplied by the strain in the composite is greater than the predicted CFRP composite strength.

The ARR is based on the Arrhenius reaction rate, which is a function of the speed of the reaction, activation energy, and temperature to predict changes in material parameters as a function of time. The ARR predictions for tensile strength and tensile modulus assume that the composite is fully immersed in deionized water at 23°C; therefore, the prediction is conservative for CFRP composites not fully immersed in deionized water at 23°C

In addition to the ARR predictions it is possible to model the material degradation of a CFRP composite with an exponential curve fit of durability data. This approximation yields a severely conservative model in addition to conservatism provided by environmental condition. Exponential curve fit for 2-layer CFRP composites in 23°C deionized water are given in percent retention.

$$y_m(t) = e^{-0.0572 \cdot t}, \textbf{2 Layer Modulus} \qquad \textbf{Eqn. 9.40}$$

$$y_s(t) = e^{-0.0312 \cdot t}, \textbf{2 Layer Strength} \qquad \textbf{Eqn. 9.41}$$

where, $y_m(t)$, is the percent retention of tensile modulus; $y_s(t)$, is the percent retention of tensile strength; t, is time in years. The percent retention material properties with respect to time are determined for tensile strength and tensile modulus with,

$$E(t) = E_{frp} \cdot y_m(t) \qquad \textbf{Eqn. 9.42}$$

$$f(t) = f_{frp} \cdot y_s(t) \qquad \textbf{Eqn. 9.43}$$

where E_{frp} and f_{frp} are initial tensile modulus and tensile strength values, $E(t)$ and $f(t)$ are time dependent FRP composite tensile modulus and tensile strength. Substituting equation 9.46 into equation 9.37 provides the necessary information to complete the time-dependent reliability analysis. If the tensile strength of the composite is exceeded, the section analysis is conducted with the strength degradation model of the CFRP at time, t. Table 9-6 summarizes the material degradation models for ARR and exponential curve fit (ECF) used in the following analysis.

Table 9-6. CFRP Composite Deterioration Models

Model Description	Tensile Modulus	Tensile Strength
2 – Layer ARR	$y_m(t) = -0.4182 \cdot \ln(t \cdot 365 \tfrac{days}{year}) + 100\%$	$y_s(t) = -3.366 \cdot \ln(t \cdot 365 \tfrac{days}{year}) + 100\%$
2 – Layer ECF	$y_m(t) = \exp(-0.0572 \cdot t)$	$y_s(t) = \exp(-0.0312 \cdot t)$

9.6 Results and Discussion

Post rehabilitation and service life results using the reliability index are shown with respect to deck slab location, rehabilitation type, load condition, and direction of reinforcement, i.e. longitudinal or transverse directions of the slab. The reliability index results quantify the likelihood that steel yield occurs in the deck slabs of the Watson Wash Bridge structure, i.e. an increase in the reliability index indicates a decrease in the probability that steel yield occurs. The definition of failure of the deck components is yield of steel flexural reinforcement.

9.6.1 Pre- and Post-Rehabilitation Reliability Index

Before application of CFRP composite, every bay of the bridge structure is assumed to be in the same condition and have the same distribution of steel reinforcement and concrete compressive strength. Although the deck slabs of the Watson Wash Bridge are designed as one-way slabs, the deck slab behaves as a two-way slab as indicated by the development of transverse flexural cracks followed by longitudinal flexural cracks as shown in Chapter 4. The initial transverse cracking indicates moment demands on the structure also act in the longitudinal direction of the slab, where insufficient reinforcement exists. Accordingly, the transverse moment demands in Table 9-5 are applied in both the longitudinal and transverse slab directions in this analysis. Two load conditions are considered; they are moment demand due to the HS20 wheel load (71.2 kN or 16 kips) and the Permit Truck wheel load (106.8 kN or 24 kips).

Reliabilities of sections with and without CFRP composite are computed using equations in section 9.5.2. The pre-rehabilitation reliabilities for all locations are shown in the following table.

Table 9-7. Pre-Rehabilitation Reliability Index Values for Deck Slabs

Direction	HS20		Permit Truck	
	β	P_f	β	P_f
Longitudinal	2.07	0.0192	0.854	0.1964
Transverse	5.92	1.61E-09	4.72	1.18E-06

As reference values for the reliability index results, consider that a value of 3.5 is used in the calibration of the *AASHTO LRFD Bridge Design Specifications* for girder bridges (Nowak, 1999). The LRFD design manual for steel implies a different level of β of approximately 2.6 for flexural members and 4.0 for connections for braced compact beams in flexure and tension (AISC 1998). The reliability index values for the non-rehabilitated deck slab show deck slabs having relatively high reliabilities 5.92 and 4.72 in the transverse slab directions for both the HS20 and Permit Truck wheel load moment demands, respectively. However, in the longitudinal slab directions, reliabilities of 2.07 and 0.854 for the HS20 and permit load moment demands, respectively, which shows that the deck slab is susceptible to failure in longitudinal slab direction and does not satisfy any of reference reliability levels of 3.5 or 2.6.

Three categories of FRP composite rehabilitation are considered and identified here as prevention, strengthened, and factored designs for the purposes of this chapter:

Prevention Design: in locations Span 8 Bay 1 (S8 B1), S9 B1, and S9 B4, pultruded CFRP composites are used to prevent the occurrence of punching shear failures in the deck slab by maintaining crack widths within 1 mm or a strain limit on CFRP of 0.75% for aggregate interlock to resist shear loads; this design does not provide for added flexural capacity to the deck slab.

Strengthened Design: in locations S8 B2, S8 B3, S9 B2, and S9 B3, pultruded and wet lay-up manufactured CFRP composites are applied to prevent the occurrence of punching shear failure and increase capacity of the deck slabs to accommodate the Permit Truck demands. The CFRP composite rehabilitation is designed to match the reinforcement distribution requirements of the Caltrans BDS in longitudinal and transverse slab directions such that a greater stiffness increase is expected in the transverse slab direction as opposed to the longitudinal slab direction.

Factored Design: in locations 8-5 and 9-5, the intent is to prevent punching shear failure and increase the capacity of the deck slab to support the Permit Truck design load; in addition, nominal safety factors of 1.2 and 1.56 are applied in the transverse and longitudinal CFRP composite designs, respectively.

The following tables provide the reliability indices for all locations of the deck slab before and after FRP composite rehabilitation. Span 8, Bay 4 (S8, B4) is an un-rehabilitated bay of the deck slab and thus the reliability index for that location remains constant in all tables. Discussion of the pre- and post-FRP rehabilitation reliabilities focuses on the level of change from the un-rehabilitated deck slab with respect to the design type and material characteristics within each FRP composite rehabilitation

location. From a design perspective the largest reliabilities are expected in *factored* design slabs, then *strengthened* design slabs followed by *prevention* design slabs.

9.6.1.1 Transverse Reinforcement

Table 9-8 and Table 9-9 show reliability indices for HS20 and Permit Truck demand moments, respectively, in the transverse slab directions for rehabilitated spans 8 and 9 of the Watson Wash Bridge structure.

Table 9-8. Permit Truck Demand Transverse Reinforcement

Location	Design Type	PRE – Rehabilitation		POST - Rehabilitation	
Span (S), Bay (B)		β	P_f	β	P_f
S8, B1	*Prevention*	4.72	1.17×10^{-6}	5.34	4.56×10^{-8}
S8, B2	*Strengthened*	4.72	1.17×10^{-6}	6.39	8.55×10^{-11}
S8, B3	*Strengthened*	4.72	1.17×10^{-6}	6.73	8.52×10^{-12}
S8, B4	*None*	4.72	1.17×10^{-6}	4.72	1.17×10^{-06}
S8, B5	*Factored*	4.72	1.17×10^{-6}	7.03	1.07×10^{-12}
S9, B1	*Prevention*	4.72	1.17×10^{-6}	5.34	4.56×10^{-08}
S9, B2	*Strengthened*	4.72	1.17×10^{-6}	6.39	8.55×10^{-11}
S9, B3	*Strengthened*	4.72	1.17×10^{-6}	6.70	1.07×10^{-11}
S9, B4	*Prevention*	4.72	1.17×10^{-6}	5.49	2.02×10^{-08}
S9, B5	*Factored*	4.72	1.17×10^{-6}	6.82	4.52×10^{-12}

Table 9-9. HS20 Demand Transverse Reinforcement

Location	Design Type	PRE – Rehabilitation		POST - Rehabilitation	
Span (S), Bay (B)		β	P_f	β	P_f
S8, B1	*Prevention*	5.92	1.60×10^{-9}	6.61	2.00×10^{-11}
S8, B2	*Strengthened*	5.92	1.60×10^{-9}	7.73	5.33×10^{-15}
S8, B3	*Strengthened*	5.92	1.60×10^{-9}	8.12	2.22×10^{-16}
S8, B4	*None*	5.92	1.60×10^{-9}	5.92	1.60×10^{-9}
S8, B5	*Factored*	5.92	1.60×10^{-9}	8.43	1.72×10^{-18}
S9, B1	*Prevention*	5.92	1.60×10^{-9}	6.61	2.00×10^{-11}
S9, B2	*Strengthened*	5.92	1.60×10^{-9}	7.73	5.33×10^{-15}
S9, B3	*Strengthened*	5.92	1.60×10^{-9}	8.05	4.44×10^{-16}
S9, B4	*Prevention*	5.92	1.60×10^{-9}	6.77	6.69×10^{-12}
S9, B5	*Factored*	5.92	1.60×10^{-9}	8.21	1.11×10^{-16}

In general, the application of the FRP composite rehabilitation to the deck, as seen in Table 9-8 and Table 9-9, shows the same pattern of change amongst the post-rehabilitated reliability index results where the highest reliability result occurs in S8, B5 for factored design with a reliability of 7.03 (Permit Load) and 8.43 (HS20 Load). The lowest reliability of the rehabilitated spans occurs in S8B1 and S9B1 with reliabilities of 5.34 (Permit Load) and 6.61 (HS20 Load). The unrehabilitated reliability of the deck slab is 4.72 (Permit Load) and 5.92 (HS20) and thus the likelihood of steel yield is low without FRP rehabilitation.

For a given RC section with steel reinforcement ratio, ρ_s, a nondimensional design ratio of FRP-to-steel reinforcement is used to show a relationship between design and reliability of FRP composite rehabilitations.

$$\eta = \frac{E_{frp}\rho_{frp}}{E_s\rho_s} = \frac{E_{frp}\frac{A_{frp}}{bh}}{E_s\frac{A_s}{bd}} = \frac{E_{frp}A_{frp}}{E_sA_s} \cdot \frac{d}{h} \qquad\qquad \textbf{Eqn. 9.44}$$

where, η is the nondimensional design ratio that is a function of tensile modulus of FRP composite and steel reinforcement and their respective reinforcement ratios, ρ_f and ρ_s. Table 9-10 shows values of the design ratio and the reliability index following FRP composite rehabilitation. Note, in S8B4 no FRP rehabilitation is conductd and thus the reliability index does not change between pre and post FRP rehabilitation.

Figure 9.5 shows a plot of the post rehabilitation reliability index versus the nondimensional design ratio, η, for the HS20 and Permit load conditions. As η increases the reliability of the FRP rehabilitated structural component increases. A linear relationship is observed between the constructed FRP composite rehabilitation design and the post rehabilitation reliability index.

Table 9-10. Transverse CFRP Design Ratios

Location	E_f GPa (msi)	A_f mm²/m (in²/ft)	$\eta = \dfrac{E_{frp}\rho_{frp}}{E_s\rho_s}$	Reliability Index	
				HS20	Permit
S8, B1	139.71 (20.26)	108.41 (0.051)	0.058	6.61	5.34
S8, B2	139.71 (20.26)	299.42 (0.142)	0.159	7.73	6.39
S8, B3	78.86 (11.44)	627.93 (0.297)	0.189	8.12	6.73
S8, B4	N/A	N/A	N/A	5.92	4.72
S8, B5	79.41 (11.52)	728.55 (0.344)	0.220	8.43	7.03
S9, B1	139.71 (20.26)	108.41 (0.051)	0.058	6.61	5.34
S9, B2	139.71 (20.26)	299.42 (0.142)	0.159	7.73	6.39
S9, B3	79.12 (11.48)	643.55 (0.304)	0.194	8.05	6.7
S9, B4	166.18 (24.10)	112.74 (0.053)	0.071	6.77	5.49
S9, B5	77.77 (11.28)	675.21 (0.319)	0.200	8.21	6.82
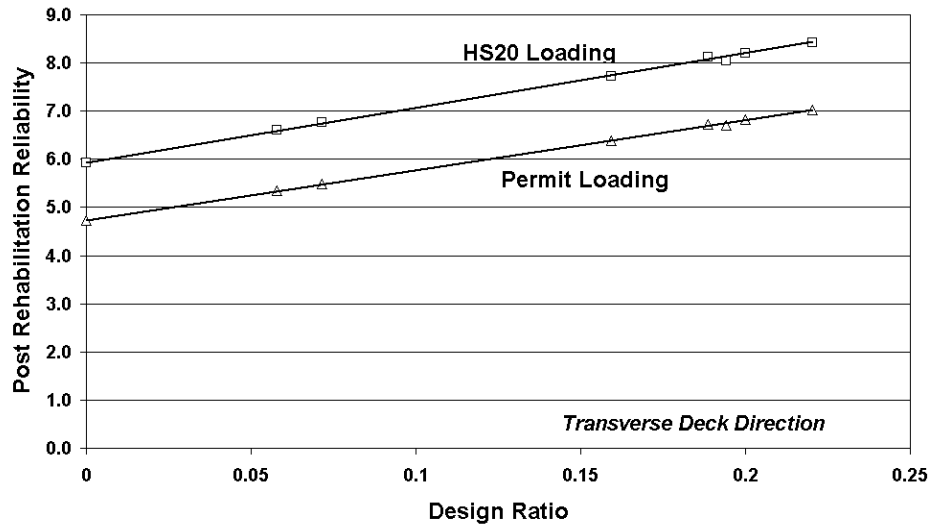
Figure 9.5. Reliability Index vs. Transverse Design Ratio

In Figure 9.5, a FRP composite rehabilitation design and the resulting reliability index of the rehabilitated transverse RC section is described by a linear function as shown in equations 9.49 and 9.50.

$$\beta_{post} = 11.392 \cdot \eta + 5.92; \text{ HS20 wheel load} \qquad \textbf{Eqn. 9.45}$$

$$\beta_{post} = 10.476 \cdot \eta + 4.72; \text{ Permit wheel load} \qquad \textbf{Eqn. 9.46}$$

where β_{post}, is the reliability index of the deck slab after rehabilitation or the post rehabilitation reliability index. These linear relationships can be used to determine a FRP rehabilitation design that achieves a desired reliability level for a structural component under a given load. For instance, to achieve a β_{post} of 6.0 in the transverse direction under a permit wheel load, an η of 0.122 would be required for the FRP composite rehabilitation design.

9.6.1.2   Longitudinal Reinforcement

Table 9-11 and Table 9-12 show reliability indices for HS20 and Permit Truck demand moments, respectively, for longitudinal CFRP rehabilitation designs in spans 8 and 9 of the Watson Wash Bridge structure. While the transverse slab directions show high reliability levels before FRP composite construction, the longitudinal slab directions are subject to pre-rehabilitation failure probabilities of 20.4% and 2.06% in the presence of full HS20 and Permit Truck load demands, respectively.

Table 9-11. Permit Truck Demand Longitudinal Reinforcement

Location	Design	PRE – Rehabilitation		POST - Rehabilitation	
Span (S), Bay (B)	Type	β	P_f	β	P_f
S8, B1	*Prevention*	0.854	1.96×10^{-1}	1.91	2.79×10^{-2}
S8, B2	*Strengthened*	0.854	1.96×10^{-1}	2.17	1.49×10^{-2}
S8, B3	*Strengthened*	0.854	1.96×10^{-1}	2.19	1.43×10^{-2}
S8, B4	*None*	0.854	1.96×10^{-1}	0.85	1.96×10^{-1}
S8, B5	*Factored*	0.854	1.96×10^{-1}	3.51	2.26×10^{-4}
S9, B1	*Prevention*	0.854	1.96×10^{-1}	1.91	2.79×10^{-2}
S9, B2	*Strengthened*	0.854	1.96×10^{-1}	2.17	1.49×10^{-2}
S9, B3	*Strengthened*	0.854	1.96×10^{-1}	2.25	1.23×10^{-2}
S9, B4	*Prevention*	0.854	1.96×10^{-1}	2.14	1.62×10^{-2}
S9, B5	*Factored*	0.854	1.96×10^{-1}	3.35	4.01×10^{-4}

Table 9-12. HS20 Demand Longitudinal Reinforcement

Location	Design	PRE – Rehabilitation		POST - Rehabilitation	
Span (S), Bay (B)	Type	β	P_f	β	P_f
S8, B1	*Prevention*	2.07	1.93×10^{-2}	3.29	4.95×10^{-4}
S8, B2	*Strengthened*	2.07	1.93×10^{-2}	3.59	1.64×10^{-4}
S8, B3	*Strengthened*	2.07	1.93×10^{-2}	3.58	1.71×10^{-4}
S8, B4	*None*	2.07	1.93×10^{-2}	2.07	1.93×10^{-2}
S8, B5	*Factored*	2.07	1.93×10^{-2}	5.12	1.56×10^{-7}
S9, B1	*Prevention*	2.07	1.93×10^{-2}	3.29	4.95×10^{-4}
S9, B2	*Strengthened*	2.07	1.93×10^{-2}	3.59	1.64×10^{-4}
S9, B3	*Strengthened*	2.07	1.93×10^{-2}	3.65	1.29×10^{-4}
S9, B4	*Prevention*	2.07	1.93×10^{-2}	3.56	1.86×10^{-4}
S9, B5	*Factored*	2.07	1.93×10^{-2}	4.86	5.73×10^{-7}

In order to assess the design characteristics of the FRP rehabilitation and the resulting reliability index, the design ratio, η, is calculated for the longitudinal slab directions. Table 9-13 shows the resulting reliability index and the associated design ratio. Figure 9.6 shows a linear relationship between the design ratio and the post FRP rehabilitation reliability index in the longitudinal slab direction, which is useful in determining the design necessary to achieve a desired level of reliability.

Table 9-13. Longitudinal CFRP Design Ratios

| Location	E_f GPa (msi)	A_f mm^2/m (in^2/ft)	$\eta = \dfrac{E_{frp}\rho_{frp}}{E_s\rho_s}$	Reliability Index	
				HS20	Permit
S8, B1	139.71 (20.26)	139.17 (0.066)	0.124	3.29	1.91
S8, B2	139.71 (20.26)	173.98 (0.082)	0.155	3.59	2.17
S8, B3	71.16 (10.32)	352.4 (0.167)	0.160	3.58	2.19
S8, B4	N/A	N/A	N/A	2.07	0.85
S8, B5	78.77 (11.43)	627.97 (0.297)	0.316	5.12	3.51
S9, B1	139.71 (20.26)	139.17 (0.066)	0.124	3.29	1.91
S9, B2	139.71 (20.26)	173.98 (0.082)	0.155	3.59	2.17
S9, B3	70.53 (10.23)	366.66 (0.175)	0.165	3.65	2.25
S9, B4	166.18 (24.10)	141.96 (0.067)	0.150	3.56	2.14
S9, B5	78.92 (11.45)	612.1 (0.289)	0.308	4.86	3.35
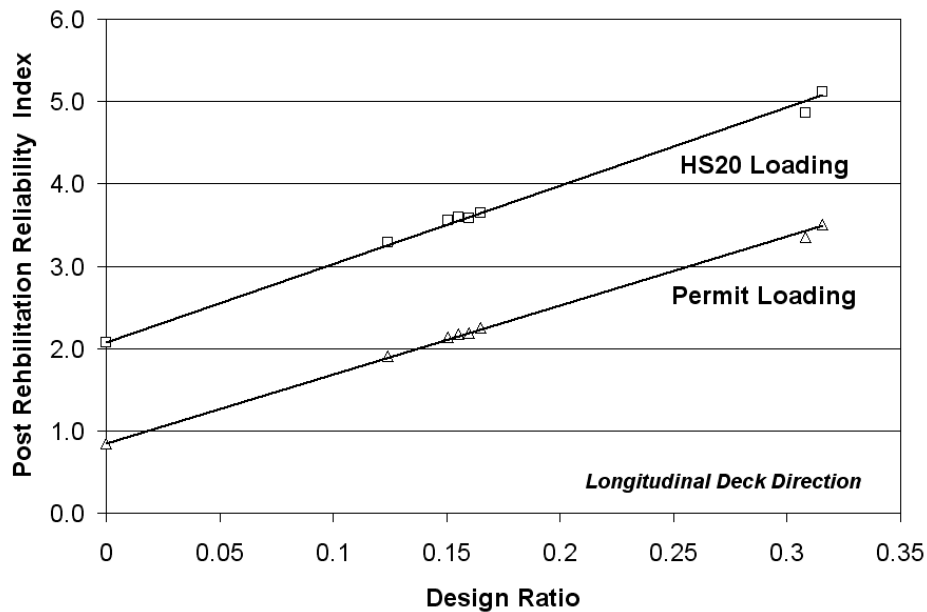
Figure 9.6. Reliability Index vs. Longitudinal Design Ratio

In Figure 9.6, a FRP composite rehabilitation design and the resulting reliability index of the rehabilitated longitudinal RC section is described by a linear function as shown in equations 9.51 and 9.52

$$\beta_{post} = 9.523 \cdot \eta + 2.07; \text{ HS20 wheel load} \qquad \textbf{Eqn. 9.47}$$

$$\beta_{post} = 8.377 \cdot \eta + 0.85; \text{ Permit wheel load} \qquad \textbf{Eqn. 9.48}$$

where β_{post}, is the reliability index of the deck slab after rehabilitation or the post rehabilitation reliability index. This linear relationship can be used to determine a FRP rehabilitation design necessary to achieve a desired reliability level for a structural component. For instance, to achieve a β_{post} of 4.0 in the longitudinal slab direction under a HS20 wheel load, an η of 0.203 would be required for the FRP composite rehabilitation design.

9.6.2 Effect of Material Degradation

One of the advantages of the reliability index evaluation is the ability to quantify the effect of FRP composite rehabilitation based solely on the variation in mechanical properties of the as-built structure and the area of composite applied to a reinforced concrete section for flexural failure. As the modulus of the CFRP composite degrades with respect to time, the reliabilities can approach the un-rehabilitated reliability index of the deck slab for both the HS20 and Permit load demands. Inclusion of the degradation model shows the rate of change of reliability with respect to time.

The effects of material degradation on performance of the FRP rehabilitated spans are shown for the 2 layer ARR and ECF material prediction models in the following sections. It is assumed that the applied models are applicable to all CFRP composite types used in the rehabilitation. The un-rehabilitated reliability index values for bay 4 of span 8 (S8B4) are shown in all figures as a reference.

9.6.2.1 2-Layer ARR Material Model

9.6.2.1.1 Longitudinal Reinforcement Direction

Figure 9.7 and Figure 9.8 show the change in reliability versus time for the HS20 wheel load in the longitudinal slab direction, when incorporating the 2-layer ARR CFRP material predictions for tensile strength and tensile modulus.

Figure 9.7. Performance, Longitudinal CFRP, HS20, 2 Layer ARR
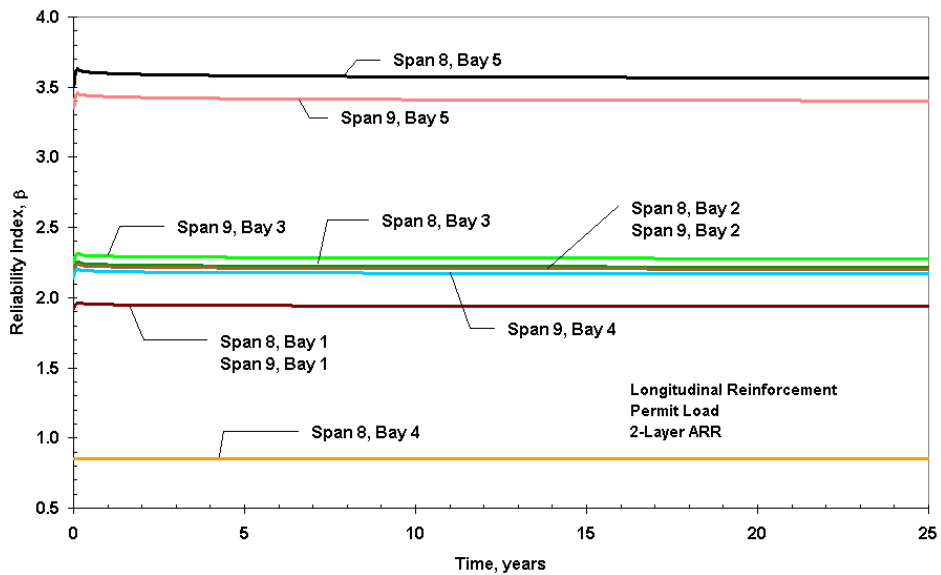
Figure 9.8. Performance, Longitudinal CFRP, Permit, 2 Layer ARR

For a minimum allowable reliability of 3.5, as specified by Nowak (1999), the service life estimate for each location of the rehabilitated components can be determined with respect to the design ratio as shown in Table 9-14.

Table 9-14. Service Life Estimates in Longitudinal Direction for 2 Layer ARR

Location	$\eta = \dfrac{E_{frp}\rho_{frp}}{E_s\rho_s}$	Estimated Service Life $\beta_{allowable} = 3.5$		β at 25 years	
		HS20	Permit	HS20	Permit
S8, B1	0.124	0	0	3.32	1.94
S8, B2	0.155	> 25 yrs	0	3.62	2.20
S8, B3	0.160	> 25 yrs	0	3.61	2.22
S8, B4	N/A	0	0	2.07	0.85
S8, B5	0.316	> 25 yrs	> 25 yrs	5.18	3.56
S9, B1	0.124	0	0	3.32	1.94
S9, B2	0.155	> 25 yrs	0	3.62	2.20
S9, B3	0.165	> 25 yrs	0	3.69	2.28
S9, B4	0.150	> 25 yrs	0	3.59	2.17
S9, B5	0.308	> 25 yrs	0	4.92	3.40

Figure 9.7 and Figure 9.8 show that if the post rehabilitation reliability index is 3.5 or greater the 2-layer ARR durability predictions for CFRP composite does not violate the minimum allowable reliability level due to post cure effects and a service life estimate greater than 25 years results. Only location S8B5 with a η of 0.316 is able to provide a reliability index of 3.5 or greater for both the HS20 and permit wheel loads and thus an estimated service life greater than 25 years.

For the 2-layer ARR durability model and HS20 load in the longitudinal slab direction, a design ratio, η, greater than or equal to 0.15 provides a reliability level of 3.5 for a period greater than 25 years. For a 2-layer ARR durability model and permit loading a η of 0.316 is recommended to achieve a post rehabilitation reliability index of 3.5 and a service life greater than 25 years.

9.6.2.1.2 Transverse Reinforcement Direction

Figure 9.9 and Figure 9.10 show the change in reliability in the transverse slab direction with the 2-layer ARR CFRP material predictions. For a minimum allowable reliability index of 3.5, all locations satisfy the criteria for a period greater than 25 years since the reliability index level prior to rehabilitation is 5.92 and 4.72 for the HS20 and permit wheel loads, respectively. CFRP composite rehabilitation is needed in the transverse slab direction to prevent the occurrence of punching shear failure, which are 21 CFRP composite strips spaced at 60.96 cm (24 inches) on center, as determined in Chapter 5.

Figure 9.9. Performance, Transverse CFRP, HS20, 2 Layer ARR
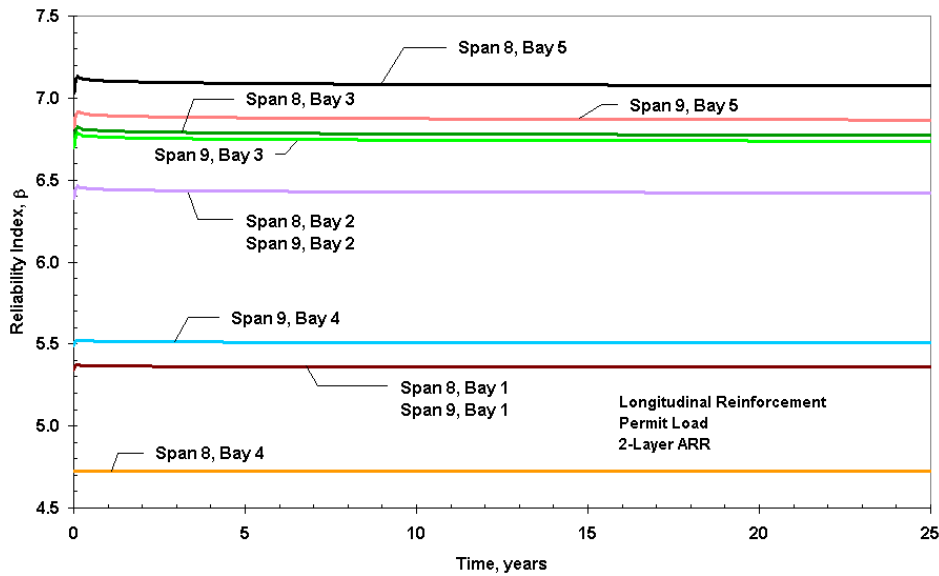
Figure 9.10. Performance, Transverse CFRP, Permit, 2 Layer ARR

The 2-layer ARR model presents a conservative estimate of the degradation in material properties of 2-layer, wet lay-up manufactured CFRP composites, since the model assumes the material is fully immersed in deionized water at 23°C. Deterioration in the CFRP composite is minimal over the life of the rehabilitated structural component implying that the bonded CFRP composites are able to extend the life of a structural component.

9.6.2.2 2-Layer ECF Material Model

In order to illustrate a condition of continuous deterioration in FRP composite materials that is severely aggressive, the exponential curve fit model is applied to the time dependent reliability formulation.

9.6.2.2.1 Longitudinal Reinforcement Direction

Figure 9.11 and Figure 9.12 show the change in reliability with respect to the longitudinal slab direction for the HS20 and permit loads, respectively. A continuous decrease in reliability is observed in all locations as opposed to the asymptotic behavior when the material parameter deterioration is described by the 2-layer ARR prediction.
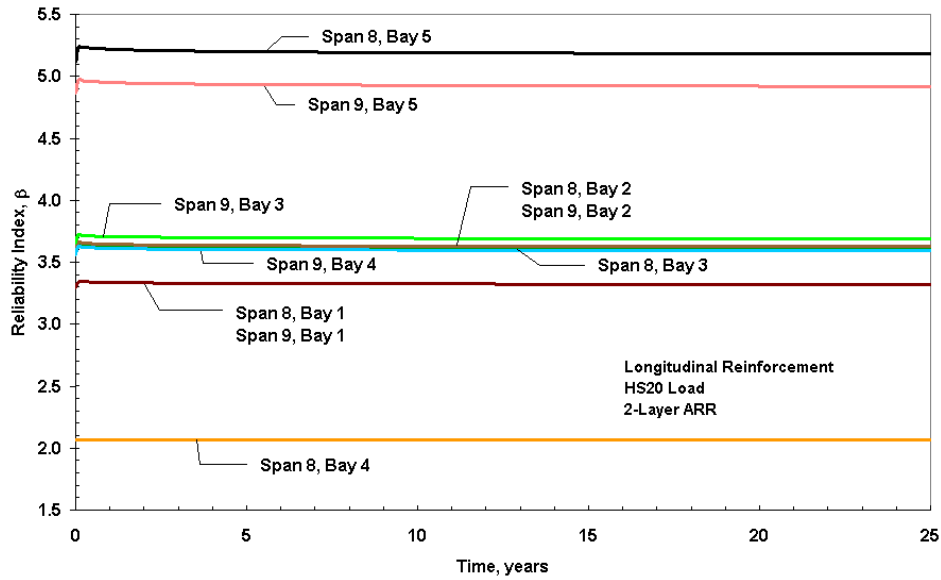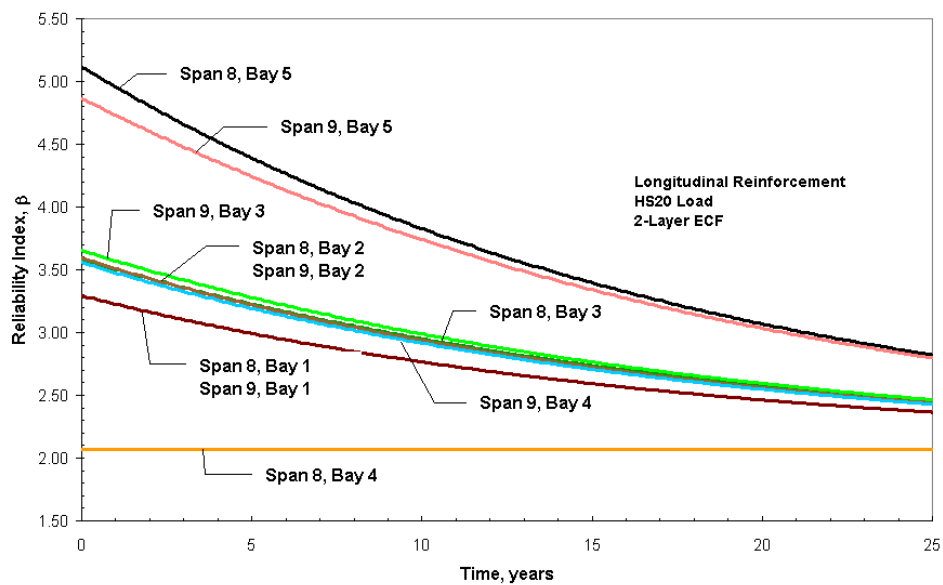

Figure 9.11. Performance, Longitudinal CFRP, HS20, 2 Layer ECF
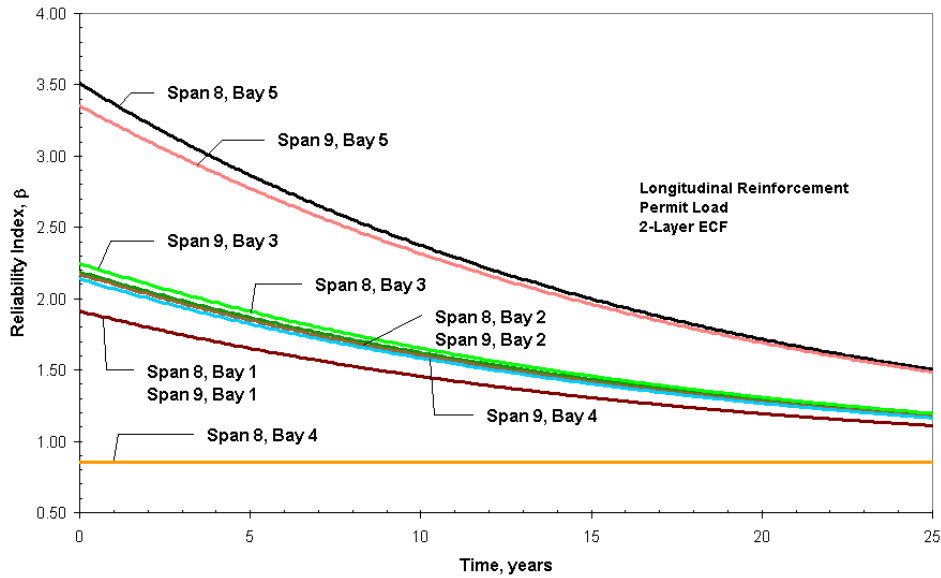
Figure 9.12. Performance, Longitudinal CFRP, Permit, 2 Layer ECF

For a minimum allowable reliability index of 3.5, the service life estimate for each location of the rehabilitated decks slabs can be determined with respect to the design ratio as shown in Table 9-15.

Table 9-15. Service Life Estimates in Longitudinal Direction with 2 Layer ECF

Location	$\eta = \dfrac{E_{frp}\rho_{frp}}{E_s\rho_s}$	Estimated Service Life $\beta_{allowable} = 3.5$		β at 25 years	
		HS20	**Permit**	**HS20**	**Permit**
S8, B1	0.124	0	0	3.32	1.94
S8, B2	0.155	1.1 yrs	0	3.62	2.20
S8, B3	0.160	1.1 yrs	0	3.61	2.22
S8, B4	N/A	0	0	2.07	0.85
S8, B5	0.316	13.7 yrs	0.1 yrs	5.18	3.56
S9, B1	0.124	0	0	3.32	1.94
S9, B2	0.155	1.1 yrs	0	3.62	2.20
S9, B3	0.165	1.9 yrs	0	3.69	2.28
S9, B4	0.150	0.7 yrs	0	3.59	2.17
S9, B5	0.308	12.8 yrs	0	4.92	3.40

For an HS20 load and an allowable reliability index of 3.5, locations S8B5 and S9B5 provide a service life estimate of 13.7 and 12.8 years, respectively, and are the only appreciable extensions to service life with rehabilitation. For the permit load condition,

none of the rehabilitation designs for CFRP composite rehabilitation are able to provide an increase in the estimate of the service life.

9.6.2.2.2 Transverse Reinforcement Direction

Figure 9.13 and Figure 9.14 show the reliability index versus time in the transverse deck direction with the 2-layer ECF material prediction. The reliability indices tend towards the unrehabilitated RC deck component reliability as the CFRP composite deteriorates. For an allowable reliability limit of 3.5, all locations provide service lives greater than 25 years, since the limit is not violated with CFRP composite deterioration. CFRP composite rehabilitation is needed in the transverse slab direction to prevent the occurrence of punching shear failure, which are 21 CFRP composite strips spaced at 60.96 cm (24 inches) on center, as determined in Chapter 5.
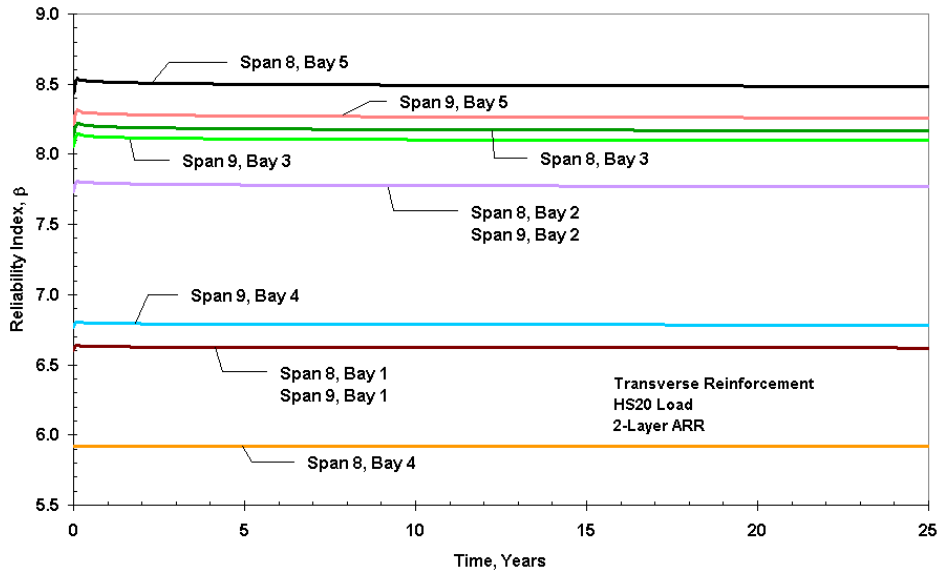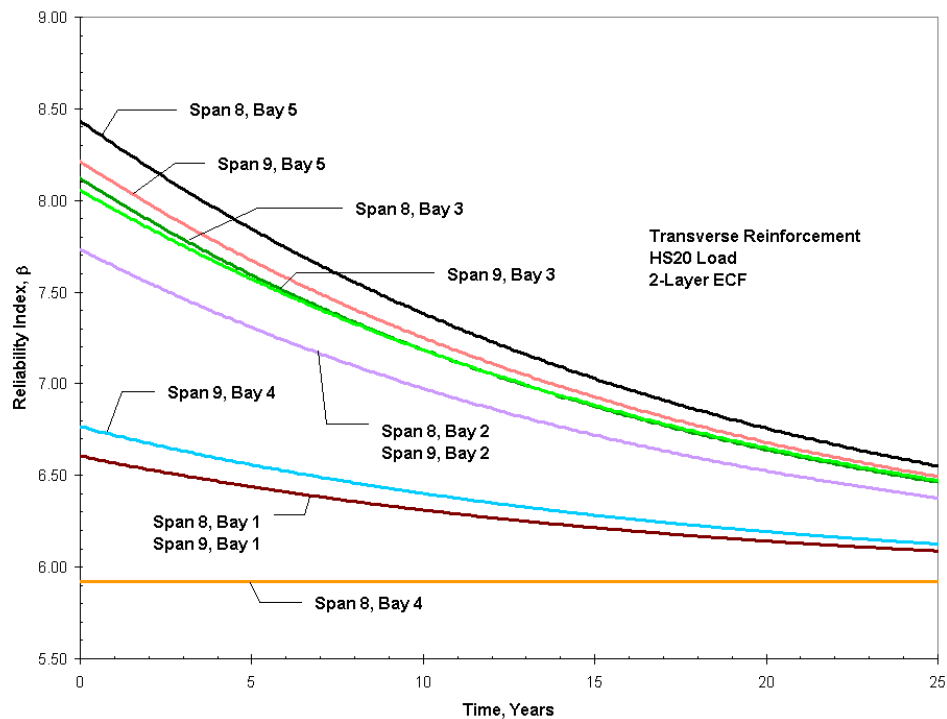

Figure 9.13. Performance, Transverse CFRP, HS20, 2 Layer ECF
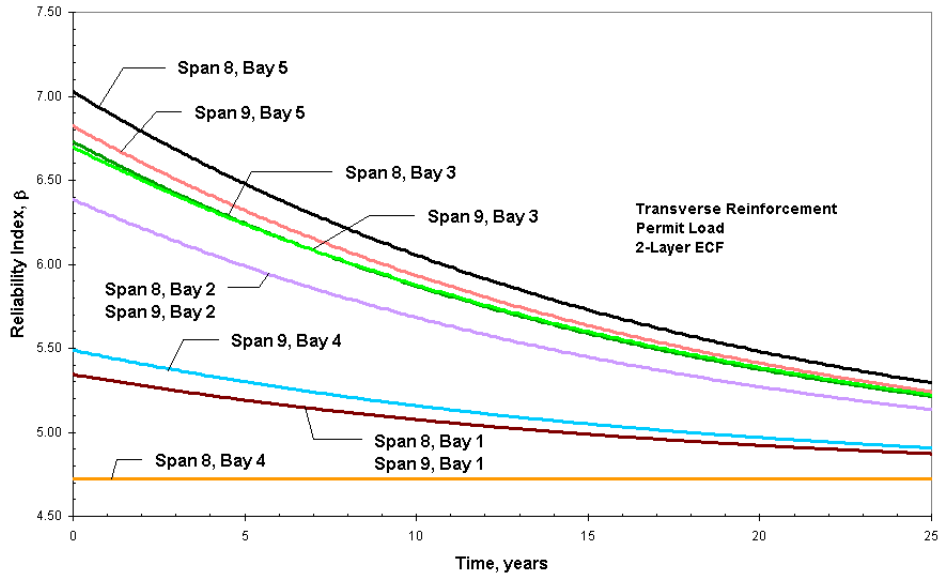
Figure 9.14. Performance, Transverse CFRP, Permit, 2 Layer ECF

9.7 Discussion

It is important to note that the application of the ECF is used to illustrate a very severe deterioration of CFRP composite properties and the use of an ARR durability model is also conservative since the model is derived from CFRP composites that are fully immersed in 23°C deionized water.

For an estimate of service life greater than 25 years, design requirements were established for the longitudinal and transverse slab directions assuming deterioration occurs only in CFRP composite in section 9.6.2.1 and are summarized in Table 9-16.

Table 9-16. Design Requirements for Watson Wash Bridge Decks

Reinforcement Direction	Design Requirement	
	HS20 Load	**Permit Load**
Longitudinal	$\eta \geq 0.15$	$\eta \geq 0.316$
Transverse	21 CFRP Strips	21 CFRP Strips

For a prefabricated CFRP composite system with tensile properties and variation identical to the System 2 composites as shown in Chapter 8, the number of strips and spacing are determined for the Watson Wash Bridge deck slab.

Table 9-17. Pultruded CFRP Requirements for Watson Wash Bridge Decks

Reinforcement Direction	Design Requirement	
	HS20 Load	Permit Load
Longitudinal	5 strips @ 28 cm on center	5 pairs (10 strips) @ 28 cm on center
Transverse	21 strips @ 61 cm on center	21 strips @ 61 cm on center

For a wet lay-up manufactured CFRP composite with tensile properties and variation as measured in location S8B5 as shown in Chapter 8, the number of strips and spacing are determined for the Watson Wash Bridge deck slab.

Table 9-18. Wet Lay-up CFRP Requirements for Watson Wash Bridge Decks

Reinforcement Direction	Design Requirement	
	HS20 Load	Permit Load
Longitudinal	4-1 layer @ 23 cm on center	4-2 layer @ 28 cm on center
Transverse	21-2 layer @ 61 cm on center	21-2 layer @ 61 cm on center

9.8 Summary

The use of probabilistic methods in the form of the reliability index presents a means to assess the performance of a FRP rehabilitated structure. The methodology is useful in two aspects: first, the variation in material properties affecting resistance demand of the structure is quantified in terms of probability of failure. Second, a procedure to assess the impact of material degradation on the reliability of the structure as a function of time is readily available.

The effect of material degradation is observed in the changing rate of reliability from initial reliability measures of all FRP rehabilitated locations of the deck slab. Using both the time-dependent reliability measures and independently established limit reliabilities, it is possible to determine the effect of CFRP composite rehabilitation and the impact of material degradation in terms of service life.

Application of material degradation models to the reliability index gives the change in reliability as material degrades for the conservative case of full immersion in deionized water. This change in reliability with respect to time with CFRP material degradation provides a conservative estimate, since the degradation model assumes the CFRP composite is fully immersed in deionized water at 23°C for an extended period of time. A design methodology is suggested in Appendix A, that utilizes the time dependent

reliability relationship to develop design charts such that a rehabilitation design can be determine based on a desired service life extension and required limit reliability level.

The following chapter seeks to combine the material degradation procedure and measures of stiffness change via the reliability index. Results of the global NDE procedure are used to provide a measure of the state of the structure in an instant of time. The material degradation model follows to provide a measure of the rate of change in reliability with respect to time. The methodology is applied experimentally by means of progressive damage testing, where a sequence of damage is introduced to the deck slabs of the Watson Wash Bridge and the corresponding stiffness losses are used to measure the performance or reliability of the structure at a single instance of time. Measured stiffness changes from the deck of the Watson Wash Bridge and laboratory material durability data are used to provide a lower bound estimate of the remaining service life of the CFRP rehabilitated deck components.

10 PROGRESSIVE DAMAGE

10.1 Introduction

In Chapter 9 of this report, the probabilistic assessment of the FRP composite rehabilitation was conducted by means of the reliability index. The reliability index was used as a performance indicator to evaluate the effect of the variation of mechanical properties of as-built CFRP composites. A time-dependent reliability formulation was also developed to assess the effect of CFRP composite modulus degradation and variation of the mechanical properties of the structure. Using limit reliabilities, relationships between the CFRP rehabilitation design, post-rehabilitation reliability, and service life were established. The previous chapter evaluated the change in reliability due to CFRP composite degradation and variation of mechanical properties, but did not consider the changes in the reinforced concrete deck of the Watson Wash Bridge from global NDE measurements.

In Chapter 10 the effect of deterioration in a RC deck and degradation in CFRP composite are combined to estimate remaining service life of a FRP rehabilitated structure using the time dependent reliability formulation in Chapter 9. First, an experimental procedure involving a sequence of damage to the FRP rehabilitation is used to simulate deterioration in the Watson Wash Bridge Deck. Modal parameters are measured and stiffness losses are calculated with the damage index method (Stubbs et al. 2000). Second, using both the measured stiffness losses and the rate of change of reliability due to CFRP composite degradation, predictions for the remaining service life are made..

10.2 Dynamic Testing with Progressive Damage

The demolition of the Watson Wash Bridge in June of 2003 presented an opportunity to implement a destructive testing sequence, which simulates the degradation of a RC bridge deck slab rehabilitated with CFRP composite or progressive damage. Results from the progressive damage experiment are used to combine structural health monitoring data with an estimate of the remaining life of a structure. The objectives of the field work are to validate the application of the service life estimation methodology proposed through simulation of actual damage.

The damage scenario involves the removal of CFRP composite rehabilitation in an order, which reflects the development of punching shear failures in the deck of the bridge. Namely, the development of transverse cracks initiates debonding in a longitudinal CFRP strip within a bay. Subsequent longitudinal cracks cause disbond of transverse CFRP strips, after which a punching shear failure is probable at the intersection of the removed strips. Therefore, one longitudinal CFRP composite strip is removed from a location, then four transverse CFRP composite strips, followed by punch-out of the RC bridge deck.

Damage scenarios were applied to two locations of the structure, one of which was rehabilitated using pultruded CFRP strips in Span 8, Bay 1 (S8B1), which is the northernmost bay of Span 8 and is a design intended to prevent the occurrence of punching shear failure, which in effect is a minimum deck rehabilitation using CFRP

composites. The other inflicted damage location was Span 9, Bay 5 rehabilitated with wet lay-up manufactured CFRP strips. Progressive damage locations are identified in red in Figure 10.1.
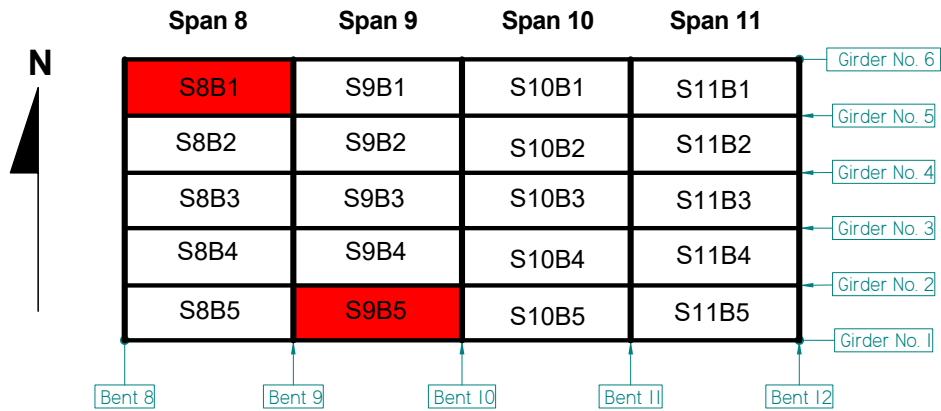
Figure 10.1. Locations for Progressive Damage Testing

Following each sequence of damage, a dynamic test was conducted to determine modal parameters and to characterize changes in response. The sequence of activities at each location, S8B1 and S9B5, are described in the following sections.

10.2.1 Progressive Damage Scenario Details

The investigations related to progressive damage were initiated with a baseline modal test which provided parameters that could be used as the intial state characteristics of the structure. In the case of the pultruded strip rehabilitation in Span 8 Bay 1 (S8B1), the first damage state was represented by the removal of a single longitudinal strip (Figure 10.2). Care was taken to ensure that the removal did not result in damage to concrete beyond the level anticipated through debonding and transverse crack opening. Once modal data were obtained for this state, 4 adjoining transverse strips were removed from the central span region (Figure 10.3). Again modal data was obtained and then a punching shear failure was simulated through impact loading on the top surface of the deck. This resulted in a damage area of about 46 cm by 25 cm, which is representative of punch through under normal service conditions (Figure 10.4), after which modal characterization was again repeated.

A similar procedure was followed in S9B5 which had been rehabilitated using the wet lay-up procedure. The sequence of damage is illustrated in Figure 10.5, Figure 10.6, and Figure 10.7.

Figure 10.2. Removal of Longitudinal CFRP Strip in Location S8B1
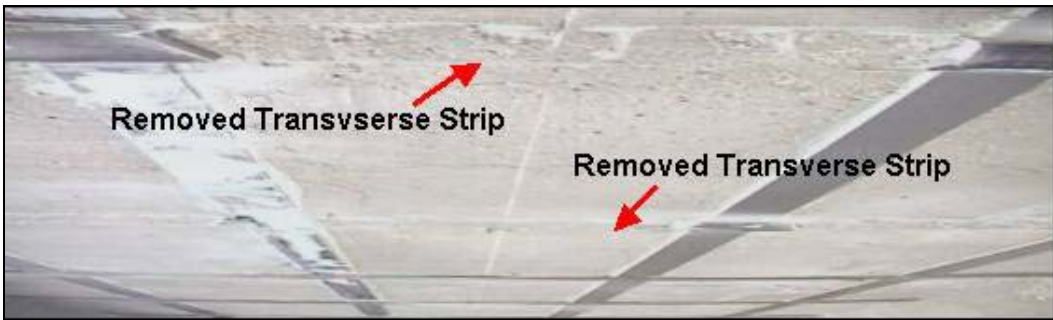
Figure 10.3. Removal of Four Transverse Strips in Location S8B1
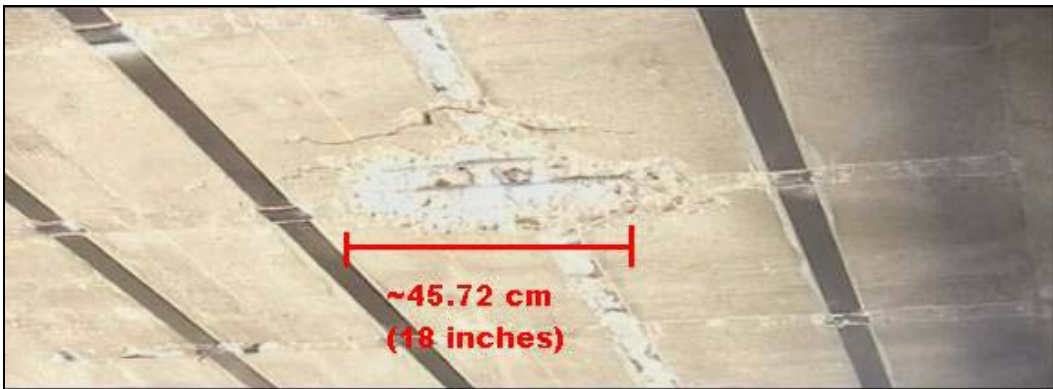
Figure 10.4. Punch Out of Bridge Deck in S8B1

Figure 10.5. Removal of Longitudinal CFRP Strip in Location S9B5
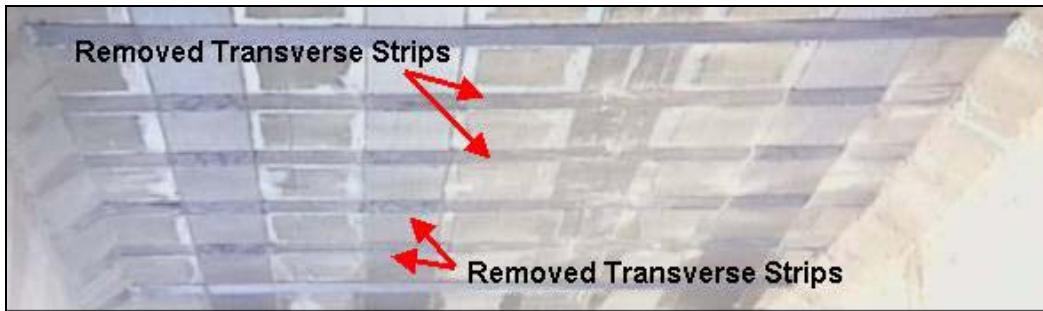
Figure 10.6. Removal of Four Transverse CFRP Strips in Location S9B5

Figure 10.7. Punch Out of Bridge Deck in S9B5

10.3 Destructive Testing Results

Modal characterization was conducted following the approach developed in Chapter 3 and used for SHM in Chapter 4. In each case stiffness losses are determined relative to the prior damage state (assuming the intial undamaged state to be the base line. Thus the changes in stiffness are representative of a single damage event, for clarity rather than a cumulative set.

10.3.1 Measured Stiffness Changes

Table 10-1 lists fractional stiffness losses associated with each damage case applied. Longitudinal strip removal, transverse strip removal, and punchout are identified as damage cases B1, B2, and B3, respectively, for location S8B1. Similarly in location S9B5, damage cases are denoted C1, C2, and C3.

Table 10-1. Relative Fractional Stiffness Loss

Fractional Stiffness Loss Per Damage Case					
Pultruded CFRP, S8B1			Wet Lay-up CFRP, S9B5		
B1	B2	B3	C1	C2	C3
-7.0%	-4.0%	-6.0%	-8.0%	N.A.	-9.0%

As shown in Table 10-1 removal of the single pultruded longitudinal strip in location S8B1 resulted in a stiffness loss of 7%, followed by a stiffness loss of 4% with the removal of transverse strips in damage case B2. The punch out in damage case B3 shows a 6% stiffness loss after the punch out at the intersection of the strips.

In location 9-5, removal of a single wet lay-up manufactured CFRP strip resulted in an 8% stiffness loss of the structure. Since the stiffness loss measured for damage case C2 is unavailable, the measured stiffness loss of 9% following damage case C3 represents the combined effect of removing 4 transverse strips (damage C2) and punch-out of the RC deck (damage C3).

10.3.1.1 <u>Cumulative Damage Severity.</u>

Damage severity estimates as determined above merely provide an approximation of effects through a relative comparison of stiffness. In order to assess true cumulative stiffness loss a method for combining stiffness changes in the structure from test to test has to be developed.

Consider a structural element, j, at time, t_i, with stiffness, $k_{i,j}$. For $t_{i+1} > t_i$, the stiffness of element, j, is defined as:

$$k_{i+1,j} = \left(1 + \alpha_{i,j}\right)k_{i,j} \qquad \textbf{Eqn. 10.1}$$

where $\alpha_{i,j}$ is the fractional change in stiffness of element, j, from t_i to t_{i+1}; for $0 > \alpha_{i,j} \geq -1$, a loss of stiffness has occurred, where $\alpha_{i,j} = -1$ is a complete loss of stiffness in the element and $\alpha_{i,j} > 0$ indicates an increase in stiffness of the structure. Consider time t_i with element stiffness $k_{i,j}$. At another time $t_{i+1} > t_i$, the stiffness of element, j, is defined by the following relationship:

$$k_{i+1,j} = \left(1 + \alpha_{i,j}\right)k_{i,j} \qquad \textbf{Eqn. 10.2}$$

At subsequent time intervals, the stiffness of the element is defined similarly:

$$\begin{aligned}
t_{i+2} &\rightarrow k_{i+2,j} = (1 + \alpha_{i+1,j})k_{i+1,j} \\
t_{i+3} &\rightarrow k_{i+3,j} = (1 + \alpha_{i+2,j})k_{i+2,j} \\
\vdots \quad &\quad \vdots \qquad \vdots \qquad \vdots \\
t_n &\rightarrow k_{n,j} = (1 + \alpha_{n-1,j})k_{n-1,j}
\end{aligned} \qquad \textbf{Eqn. 10.3}$$

By substitution of prior stiffness definitions in to the current stiffness definition under consideration, a relationship between the final stiffness of the structure and the initial stiffness of the structure can be developed,

$$k_{n,j} = \left(1 + \alpha_{n-1,j}\right)\ldots\left(1 + \alpha_{i+2,j}\right)\left(1 + \alpha_{i+1,j}\right)\left(1 + \alpha_{i,j}\right)k_{i,j} \qquad \textbf{Eqn. 10.4}$$

Thus, the cumulative fractional stiffness change $\alpha_{c,j}$ for element j between time t_i and t_n is defined in equation 10.5.

$$1+\alpha_{c,j} = \left(1+\alpha_{n-1,j}\right)\ldots\left(1+\alpha_{i+2,j}\right)\left(1+\alpha_{i+1,j}\right)\left(1+\alpha_{i,j}\right)$$

$$\alpha_{c,j} = \left(1+\alpha_{n-1,j}\right)\ldots\left(1+\alpha_{i+2,j}\right)\left(1+\alpha_{i+1,j}\right)\left(1+\alpha_{i,j}\right)-1 \qquad \textbf{Eqn. 10.5}$$

The cumulative fractional stiffness losses in Span 8, Bay 1 (S8B1) relative to the baseline modal test of the Watson Wash Bridge is shown in Table 10-2 for damage cases B1, B2, and B3 while, the cumulative stiffness change in location Span 9, Bay 5 (S9B5) is defined relative to the modal test conducted for damage case B3.

Table 10-2. Cumulative Stiffness Loss Results in S8B1 and S9B5

Damage Scenario					
Pultruded CFRP, S8B1			Wet Lay-up CFRP, S9B5		
B1	B2	B3	C1	C2	C3
-7.0%	-11.0%	-16.0%	-8.0%	N/A	-16%

The cumulative stiffness loss in locations S8B1 and S9B5 is 16% following the removal of a longitudinal CFRP strip, four transverse CFRP strips, and a punch out of the concrete deck.

10.3.2 Applying Stiffness Changes to Reliability Assessment

Utilizing measured stiffness changes, the reliability of the structure following each damage scenario can be determined using a simple beam relationship with time dependence, as

$$M_y(t) = EI(1+\alpha_c)\cdot\phi_y(t) \qquad \textbf{Eqn. 10.6}$$

where $M_y(t)$, is the time dependent moment resistance of the system, E is the stiffness of the rehabilitated deck component, I is the moment of inertia of the component which is assumed constant with respect to time, $\phi_y(t)$ is the time dependent yield curvature of a beam, and α_c, is the cumulative fractional stiffness change.

Each damage scenario applied can be considered as an isolated instant in time. The measured percentage stiffness change is applied directly to the flexural stiffness in equation 10.6 to acquire an updated resistance measure of the resistance of the system and ultimately a reliability estimate can be made through equation 10.7. It is assumed, that yield curvature changes negligibly with damage and deterioration in the system.

$$\beta(t) = \frac{\mu_z}{\sigma_z} = \frac{\mu_R(t)-\mu_S}{\left(\sigma_R^2(t)+\sigma_S^2\right)^{\frac{1}{2}}} \qquad \textbf{Eqn. 10.7}$$

where, μ, denotes the mean value; σ^2 is the variance; R is resistance; S is demand; t is time. The analytical procedure used follows the details described in Chapter 9 for estimation of service life. The performance function of the reliability analysis evaluates the probability of the occurrence of steel yield.

10.4 Service Life Estimation

The post-rehabilitation reliabilities are measured from means and variances of concrete, steel, and CFRP composite material properties. In S8B1, post-rehabilitation reliabilities are 3.29 and 6.61 in the longitudinal and transverse slab directions, respectively, for HS20 load demands. In Span 9, Bay 5, the post rehabilitation reliabilities are 4.86 and 8.21 in the longitudinal and transverse slab directions, respectively, for HS20 load demands.

For service life assessment of the CFRP composite rehabilitation, allowable target reliabilities are selected examples independent of the initial reliabilities of the deck slab before and after rehabilitation. Three allowable reliabilities are selected. The first limit reliability is 3.5, corresponding to a 0.02% probability of failure, corresponding to the AASHTO LRFD code calibration (Nowak, 1999). The second limit reliability is 2.6, 0.47% failure probability, from the AISC LRFD steel design manual (AISC, 1998). The final limit reliability is 2.33 corresponding to a failure probability of 1%.

The HS20 and Permit level loads are considered for evaluation of the remaining service life of FRP rehabilitated decks taking into account the potential deterioration of the RC structure and the FRP composite materials. As a demonstration of the approach, potential CFRP composite deterioration (described in Chapter 9) is modeled with an exponential curve fit. The measured tensile modulus and tensile strength of 2-layer wet lay-up CFRP composites immersed in a 23°C deionized water environment is used as a representative example. Tensile modulus and tensile strength can be described as,

$$E(t) = E_{2frp} \cdot e^{-0.0572 \cdot t} \qquad \textbf{Eqn. 10.8}$$

$$f(t) = f_{2frp} \cdot e^{-0.0312 \cdot t} \qquad \textbf{Eqn. 10.9}$$

where, E_{2frp} is the initial tensile modulus of the 2 layer FRP composite; $E(t)$ is the time dependent FRP composite tensile modulus; f_{2frp}, is the initial tensile strength of FRP composite; $f(t)$ is the time dependent FRP composite tensile strength; t is time in years. The reliability index measures the likelihood of steel yield; however, if the strain in the concrete exceeds 0.3% prior to steel yield, or if the FRP composite ruptures prior, or if strain in composite exceeds 0.75% to maintain crack widths for punching shear failure, the change in failure mode is noted and the section analysis is revisited with the appropriate limiting strain value. Remaining service life is determined for progressive damage locations.

10.4.1 Service Life Estimate of Span 8, Bay 1

Location Span 8, Bay 1 is designed for prevention of punching shear failure and is not intended to increase the load carrying capacity of the slab in either direction. For damage cases B1 (removal of longitudinal strip), B2 (removal of 4 transverse strips, and B3 (punchout), remaining service life is calculated with respect to HS20 and Permit truck wheel loads for both longitudinal and transverse truck loads.

10.4.1.1 <u>HS20 Loading</u>

The reliability of the longitudinal and transverse reinforcement following rehabilitation and each measured stiffness loss in the deck slab is summarized in the following table.

Table 10-3. Span 8, Bay 1, Reliability Index Values, HS20 Loading

Direction	Pre Rehabilitation	Post Rehabilitation	Damage Case		
			B1	B2	B3
Longitudinal	2.07	3.29	2.81	2.53	2.15
Transverse	5.92	6.61	6.19	5.94	5.59

Prior to rehabilitation the reliability indices of the deck slab are 2.07 and 5.92 in the longitudinal and transverse slab directions, respectively. The reliability index of span 8, bay 1 increases to 3.29 with rehabilitation and decreases to 2.81, 2.53, and 2.15 corresponding to damage cases B1, B2, and B3, respectively in the longitudinal direction. The reliability index in the transverse direction increases to 6.61 with rehabilitation then decreases to 6.19, 5.94, and 5.59, respectively for damage cases B1, B2, and B3. The inclusion of these instantaneous measurements for the reliability of the deck slab into the time-dependent reliability formulation provides an estimate of the remaining service life of a structure. A time based superposition of the reliability index assuming degradation in CFRP composites following damage provides the change in reliability with respect to time as shown in Figure 10.8.
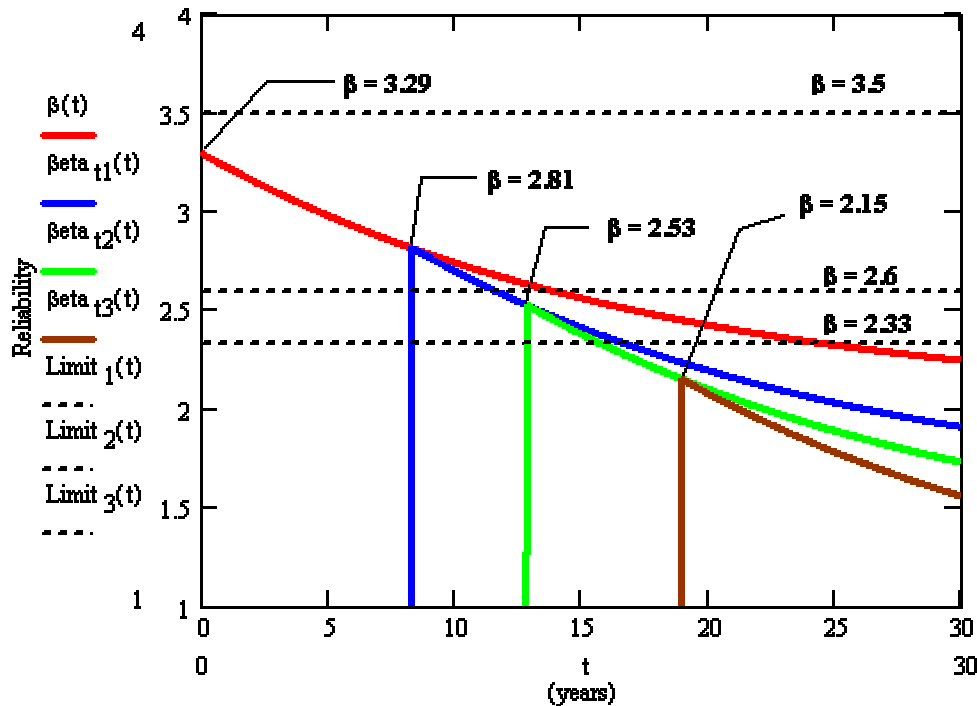
Figure 10.8. Span 8, Bay 1, Longitudinal, HS20

For the HS20 load demand level, the CFRP composite rehabilitation in location S8B1 is predicted to provide a service life of 11.54 years and 15.7 years corresponding to the limit reliabilities of 2.6 and 2.33, respectively.
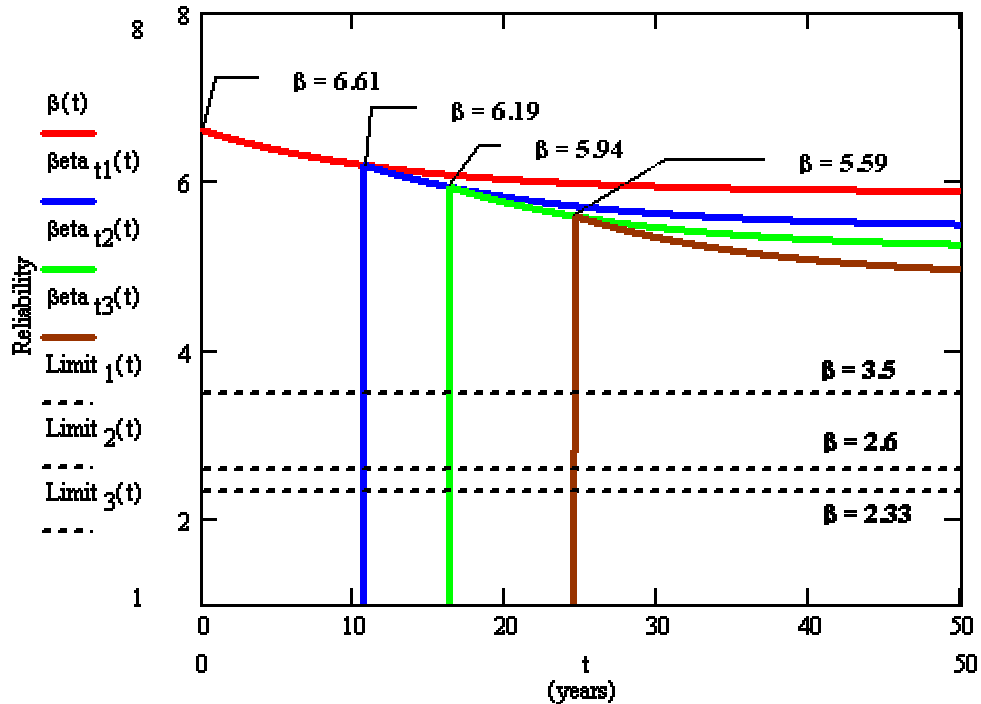
Figure 10.9. Span 8, Bay 1, Transverse, HS20

The change in reliability index versus time is shown for the transverse direction in Figure 10.9 for location S8B1 for the HS20 wheel load. Transverse CFRP rehabilitation continues to sustain a reliability index greater than 3.5 following successive damage to the deck slab and degradation of the CFRP composite.

10.4.1.2 Permit Load Demand

The reliability indices in the longitudinal and transverse directions following FRP rehabilitation and each damage case are summarized in Table 10-4 for the permit load condition.

Table 10-4. Span 8, Bay 1, Reliability Index Values, Permit Loading

Direction	Pre Rehabilitation	Post Rehabilitation	Damage Case		
			B1	B2	B3
Longitudinal	0.854	1.91	1.46	1.20	0.86
Transverse	4.72	5.34	4.89	4.61	4.24

The initial reliability indices of the deck slab prior to FRP rehabilitation are 0.854 and 4.72 in the longitudinal and transverse slab directions, respectively. Following

rehabilitation, the reliability indices of the deck slab increases to 1.90 in the longitudinal direction and 5.32 for the transverse slab direction. Following the damage cases of B1, B2, and B3, the reliabilities are determined to be 1.45, 1.79, and 0.84 in the longitudinal slab direction and 4.86, 4.58, and 4.20, in the transverse slab direction. Figure 10.10 illustrates the deterioration in the deck slab with time superposition of each successive damage case.

From Figure 10.10, the longitudinal CFRP rehabilitation design does not provide a service life extension for the permit load condition. A FRP rehabilitation design must provide a post rehabilitation reliability index greater than the allowable reliability level in order to provide a service life extension.
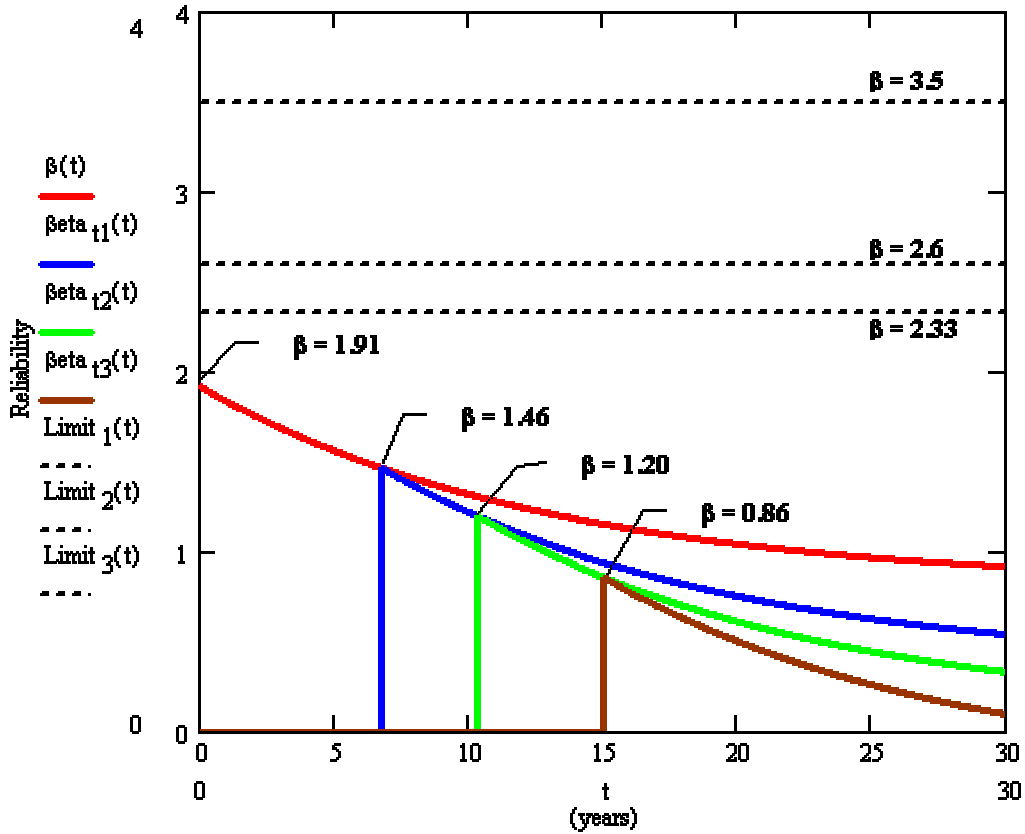
Figure 10.10. Span 8, Bay 1, Longitudinal, Permit

The change in reliability index as a function of time is shown for the transverse direction in Figure 10.11 for location S8B1 for the permit wheel load. Transverse CFRP rehabilitation continues to sustain a reliability index above 3.5 following successive damage to the deck slab and degradation of FRP composite parameters.
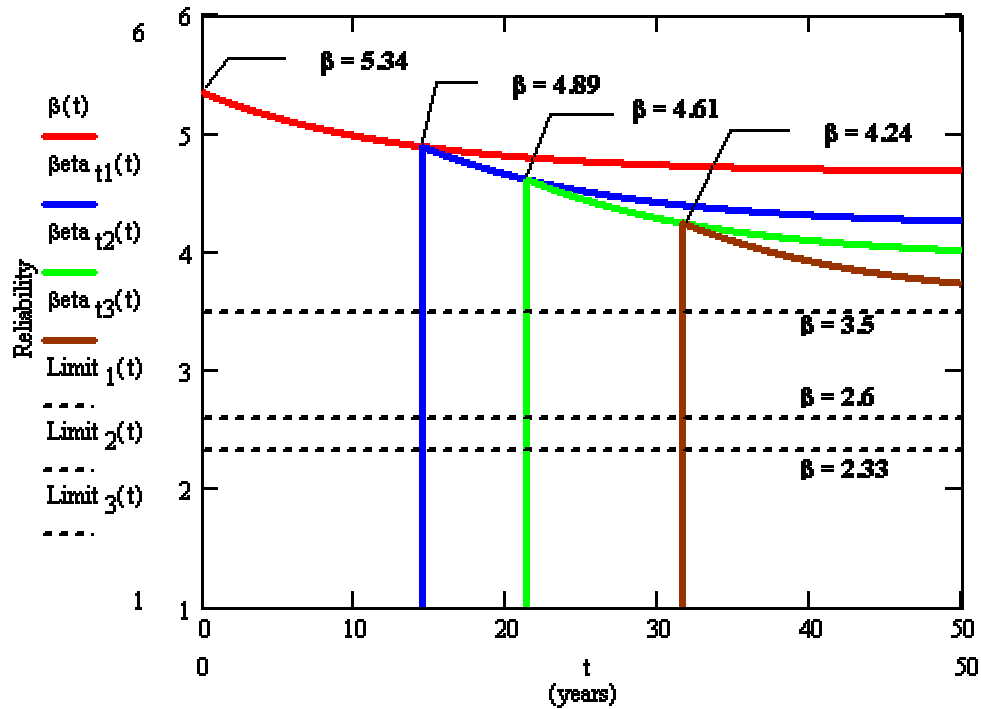
Figure 10.11. Span 8, Bay 1, Transverse, Permit

10.4.2 Span 9, Bay 5

Location Span 9, Bay 5 is designed to increase the load carrying capacity of the deck slab in both directions. For damage cases C1 (removal of a longitudinal strip), C2 (removal of 4 transverse strips), and C3 (punchout), remaining service life is calculated with respect to HS20 and Permit load level for both longitudinal and transverse directions..

10.4.2.1 HS20 Loading

The reliability indices in the longitudinal and transverse directions following rehabilitation and each measured stiffness loss in the deck slab are summarized in the following table.

Table 10-5. Span 9, Bay 5, Reliability Index Values, HS20

Direction	Pre Rehabilitation	Post Rehabilitation	Damage Case		
			C1	C2	C3
Longitudinal	2.07	4.86	4.27	N/A	3.63
Transverse	5.92	8.21	7.69	N/A	7.10

Prior to rehabilitation the reliability indices of the deck slab are 2.07 and 5.92 in the longitudinal and transverse slab directions respectively. After rehabilitation with wet lay-

up CFRP composites the reliability index increases to 4.86, then decreases to 4.27 and 3.63 corresponding to damage cases C1 and the combined damage case of C2 and C3, respectively for the longitudinal direction. In the transverse direction, the reliability index increases to 8.21 after rehabilitation, then decreases to 7.69 and 7.10 for damage cases C1 and the combined damage case of C2 and C3, respectively. The inclusion of these instantaneous measurements of the reliability index into the time-dependent reliability measure provides an estimate of the remaining service life. A time based superposition is used on the reliability index assuming degradation in CFRP composites following damage provides the change in reliability with respect to time as shown in Figure 10.12.
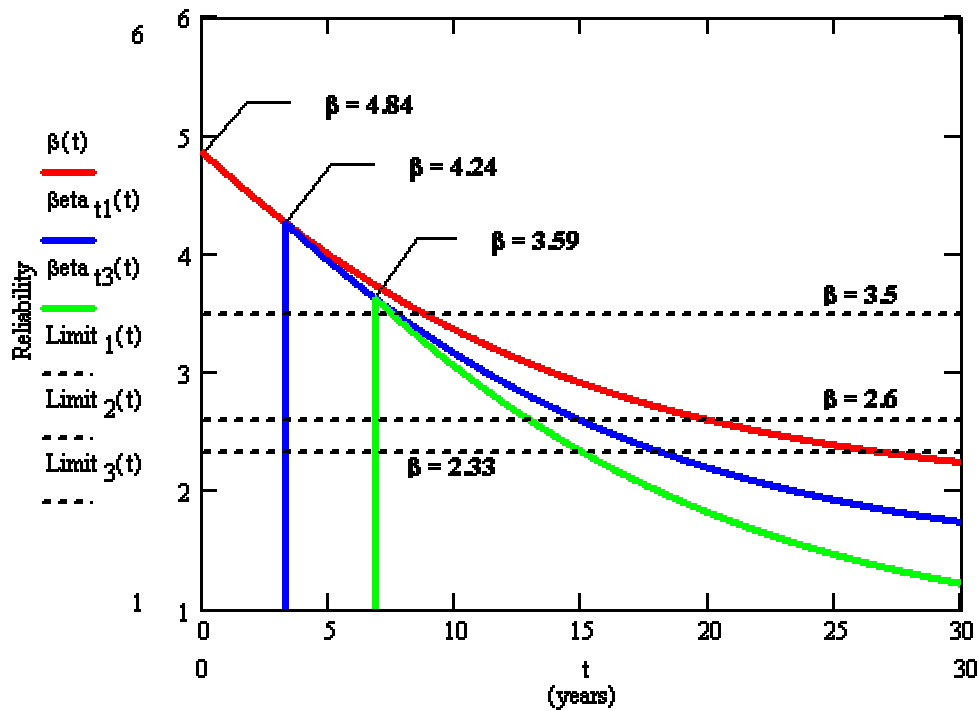
Figure 10.12. Span 9, Bay 5, Longitudinal, HS20

Figure 10.12 shows the change in reliability index as a function of time for location S9B5 in the longitudinal slab direction with the HS20 load condition. For the HS20 load demand level, the CFRP composite rehabilitation in location S9B5 is predicted to provide a service life of 7.5 years, 12.9 years, and 15.0 years for limit reliabilities of 3.5, 2.6, and 2.33.
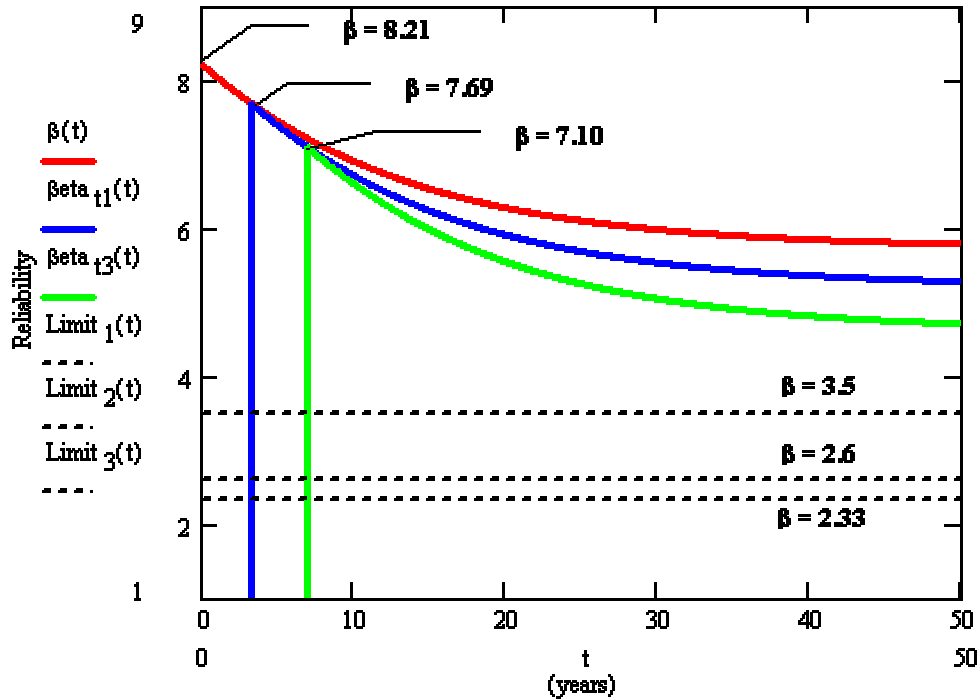
Figure 10.13. Span 9, Bay 5, Transverse, HS20

As in the transverse reinforcement in location S8B1, the application of CFRP composites assists in sustaining a level of reliability above 3.5 for following successive damage to the deck slab and degradation of the CFRP composite.

10.4.2.2 Permit Loading

The reliability of the longitudinal and transverse reinforcement following rehabilitation and each damage case is summarized in Table 10-6.

Table 10-6. Span 9, Bay 5, Reliability Index Values, Permit Loading

Direction	Pre Rehabilitation	Post Rehabilitation	Damage Case		
			C1	C2	C3
Longitudinal	0.854	3.32	2.74	N/A	2.13
Transverse	4.72	6.34	5.84	N/A	5.28

Prior to rehabilitation, the reliability indices of the deck slab are 0.854 and 4.72 in the longitudinal and transverse directions, respectively, for the permit load condition. After the rehabilitation the reliability index increases to 3.32, then decreases to 2.74 and 2.13 corresponding to damage cases C1 and the combination of C2 and C3, respectively for the longitudinal direction. In the transverse direction the reliability index of the deck slab increases to 6.34 with rehabilitation, then decrease to 5.84, and 5.28, respectively for damage cases C1 and combined C2 and C3.
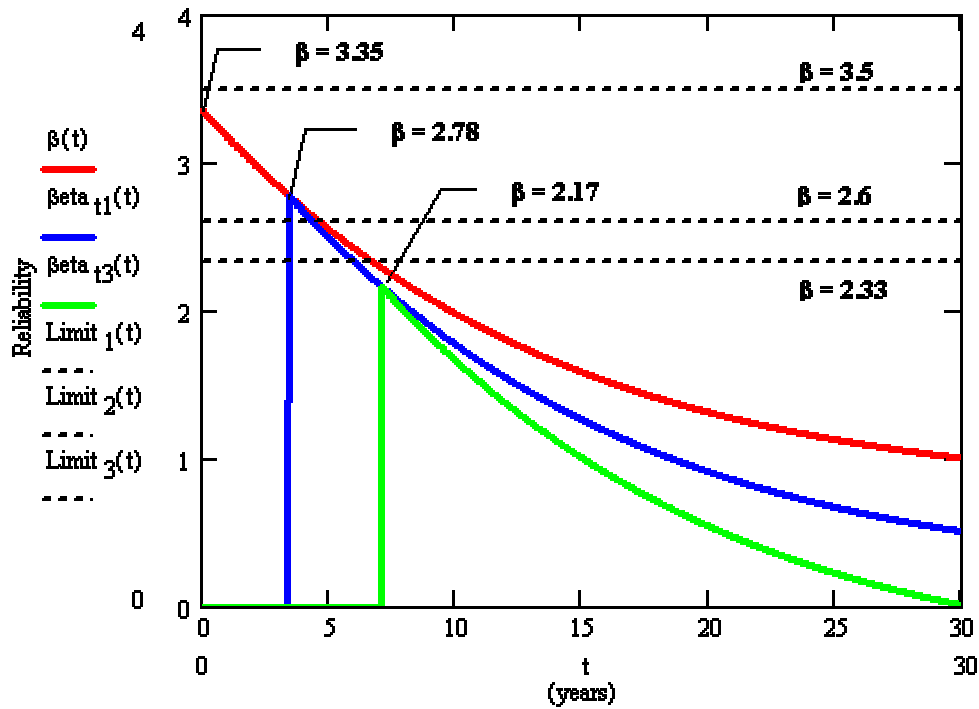
Figure 10.14. Span 9, Bay 5, Longitudinal, Permit

The change in reliability index as a function of time is shown for the longitudinal direction in Figure 10.14. For the Permit load level in S9B5, the CFRP composite rehabilitation provides a service life of 4.4 years and 6.0 years for the limits of 2.6 and 2.33, respectively.
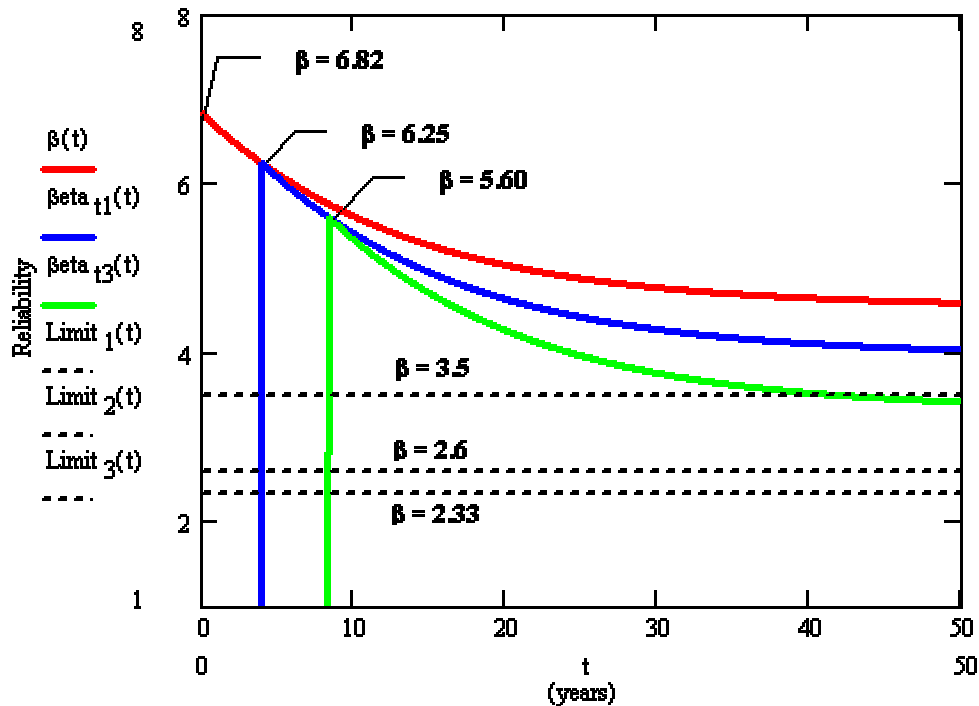
Figure 10.15. Span 9, Bay 5, Transverse, Permit

For the transverse slab direction in location S9B5 for the permit load level, a service life of 41.5 years for a limit of 3.5. The reliability index does not violate the limits of 2.6 and 2.33 with the successive damage cases and assumed material parameter predictions.

10.5 Discussion

Consideration of the reliability index provides a value method of assessment of the effectiveness of the rehabilitation independent of the design procedure followed to determine the quantity of composite necessary to rehabilitate a structure. For example the FRP rehabilitation design in location 9-5 fails to meet an allowable reliability index of 3.5 for the permit load condition, while for HS20 load levels, the design is able to exceed the allowable index of 3.5 and provide a service life extension of approximately 7.5 years. It is important to note that these service life predictions are severely conservative due to the use of the exponential curve fit durability model applied. However, the approach enables illustrates the ability for designs to be evaluated based on level of reliability and service life required thereby allowing for ease of comparison of various alternatives.

10.6 Summary

The estimation of the remaining service lives in locations 8-1 and 9-5 are evaluated using experimental procedures at the Watson Wash Bridge and laboratory characterization of durability of CFRP composites. A simulation of progressive damage is applied to locations S8B1 and S9B5, with the removal of CFRP composite rehabilitation strips and punch out of the concrete deck. The measured stiffness losses represent degradation in a FRP rehabilitated reinforced concrete section at points of time in the life of the component. By combining field measured data of the bridge structure and laboratory characterization of CFRP composite modulus fully immersed in deionized water at 23°C, estimates of the service life of the structure are obtained for progressive damage locations.

The results of the analysis indicate that the reliabilities of existing composite areas and modulus in the transverse slab direction are able to sustain a limit reliability of 3.5 (failure probability of 0.02%) for periods of time greater than 50 years in bay 5 for the HS20 load. In the presence of the Permit Loads, the transverse slabs provide a lower bound estimate of approximately 40years. It is important to note that these predictions for CFRP composite material deterioration are severely conservative with the use of an exponential curve fit of two layer CFRP deterioration data.

For the longitudinal slab direction, it is observed that only bays 5 of span 9 provides an appreciable time of no less than 7.5 years to reach the limit reliability of 3.5 in the presence of HS20 load demands, progressive reinforced concrete stiffness loss, and severely conservative estimates of CFRP deterioration. Considering permit loads, the longitudinal CFRP composite does not provide a reliability greater than 3.5 and does not provide an extended time to reach the limit reliability of 3.5.

It is concluded that the rehabilitation design in chapter 9 sufficiently provides service life extension of no less than 10 years at a reliability level greater than 3.5, since the CFRP composite applied to the soffit of the bridge deck of the Watson Wash bridge is not fully immersed in water, and the degradation of the CFRP does not reinitiate.

While prior chapters focused on the aspects of the FRP composite rehabilitation related to design, construction, and performance assessment in terms of structural reliability, the cost effectiveness of FRP composite rehabilitation for bridge decks remains unknown. The following chapter compares the cost required to rehabilitate the bays of the Watson Wash Bridge to State of California Bridge costs. The focus of the following chapter is to determine if the use of CFRP composites for bridge deck rehabilitation, while structurally effective, is financially feasible.

11 COST EVALUATION

11.1 Introduction

In prior chapters, the structural performance of CFRP composite rehabilitation was evaluated with consideration for the variation in as-built mechanical properties, degradation of FRP composites, and including measured stiffness losses from global NDE examination of the structure. The reliability index was used to combine these measurements and provide an estimate of the service life available in a CFRP composite rehabilitated bridge deck for a set of limit reliabilities. However, the cost effectiveness of CFRP composite rehabilitated bridge decks remain unknown.

In the following chapter, a cost analysis is conducted on the recommended design to provide a service life of 10 years with a reliability greater than 3.5. The cost of rehabilitation for a bay is calculated for prefabricated and wet lay-up manufactured CFRP composites for HS20 load demands and for Permit load demands. The calculation per bay is then extended to determine the cost of rehabilitation of an entire bridge structure with the same design. As a demonstration, the cost to rehabilitate the parallel structure at the Watson Wash Bridge, specifically the westbound structure, is determined. The analysis is conducted to determine the cost of FRP composite rehabilitation versus bridge replacement.

11.2 Cost of CFRP rehabiltiation

The cost of CFRP composite rehabilitation is estimated for the following designs, which provide for 10 years of service life for a reinforced concrete deck structure with a reliability greater than 3.5 per the AASHTO LRFD Bridge Design Specifications.

Table 11-1. Recommended Design for HS20 Loading

	Longitudinal	Transverse
Wet Lay-up	4-1 Layer Strips	21-2 layer strips
Pultruded	5 strips	21 strips

Table 11-1 describes the CFRP composite rehabilitation designs to retain a reliability index greater than 3.5 for a period greater than 25 years in both slab directions for HS20 load demands, with a 2-layer ARR material parameter prediction as described in Chapter 9 of this report.

Table 11-2. Recommended Design for Permit Loading

	Longitudinal	Transverse
Wet Lay-up	4-2 layer strips	21- 2 layer strips
Pultruded	5 pairs (10 strips)	21 strips

Table 11-2 describes the CFRP composite rehabilitation designs for wet lay-up and pultruded CFRP to retain a reliability index greater than 3.5 for a period greater than 25 years in both slab directions for permit load demands, with a 2 layer ARR material parameter predication as described in Chapter 9 of this report.

In the following sections the costs for materials and labor for the CFRP composite rehabilitation designs shown in the Table 11-1 and Table 11-2 are determined per square meter of bridge area, including the cost required to rehabilitate all bays and spans of the parallel Watson Wash Bridge structure which has a total length of 226 m (741 ft) and span width of 12.5 m (41 ft).

11.3 Materials Cost

In order to estimate the cost of bridge rehabilitation with CFRP composites, the cost of labor and materials are established first. The cost of materials includes estimated market prices as follows:

MATERIALS:

Prefabricated CFRP strips $40/m ($12/ft)

      (includes: prefabricated CFRP, epoxy adhesive, primer, coating)

Carbon fabric/epoxy resin $15/m ($5/ft)

      (includes: fabric, epoxy resin, primer, coating)

For purposes of estimation, a typical bay of the Watson Wash Bridge is considered, where the length of longitudinal strips applied in a bay are 12.5 m (41 ft) and the length of transverse strips is 1.65 m (5.42 ft). The total bridge deck area of a bay is the product of the effective width of a bay at 1.85 m (6.1 ft) and the length of a bay is the span length of 12.8 m (42 ft). The total deck area of the parallel Watson Wash Bridge is used to determine the material cost to rehabilitated an entire bridge structure.

Table 11-3. Estimated Material Costs for HS20 Load Design[1]

Material	Total length of material/bay meters	Material Cost per bay SI Units	Cost per Area of Bridge per m^2	Material Cost for Entire Bridge Structure Bridge Area = 2830 m^2
Wet Lay-up	119.3	$1790	$60/m^2	$170,000
Pultruded	97.2	$3890	$125/m^2	$350,000

The estimated material cost to extend the bridge life for HS20 load demands for the parallel Watson Wash Bridge Structure with CFRP composite rehabilitation is $170,000 for wet lay-up manufactured CFRP and $350,000 for pultruded CFRP composite.

Table 11-4 shows material costs for Permit load demands on the following page.

Table 11-4. Estimated Material Costs for Permit Load Design[2]

Material	Total length of material/bay meters	Material Cost per bay SI Units	Cost per Area of Bridge per m^2	Material Cost for Entire Bridge Structure Bridge Area = 2830 m^2
Wet Lay-up	169.3	$2540	$80/m^2	$230,000
Pultruded	159.6	$6390	$200/m^2	$570,000

---

[1] Table 2-3. Material Costs for HS20 Load Design in FPS Units System.

Material	Total length of material/bay ft	Material Cost per bay FPS	Cost per Area of Bridge per ft^2	Material Cost for Entire Bridge Structure Bridge Area = 30381 ft^2
Wet Lay-up	391.5	$1790	$6/ft^2	$180,000
Pultruded	318.5	$3890	$12/ft^2	$370,000

[2] Table 2-4. Material Costs for Permit Design in FPS Units System.

Material	Total length of material/bay ft	Material Cost per bay FPS	Cost per Area of Bridge per ft^2	Material Cost for Entire Bridge Structure Bridge Area = 30381 ft^2
Wet Lay-up	555.5	$2780	$8/ft^2	$250,000
Pultruded	523.8	$6290	$19/ft^2	$580,000

The estimated material cost to extend the bridge life for Permit load demands for the parallel Watson Wash Bridge Structure with CFRP composite rehabilitation is $230,000 for wet lay-up manufactured CFRP and $570,000 for pultruded CFRP composite.

11.4 Labor Cost

For a wet lay-up rehabilitation on the Watson Wash Bridge, total time for setup, surface preparation, movable scaffolding, and manufacturing and application occurred over a period of 2.5 days per bay at approximately 12 hrs/day, with three men on the job. For purposes of this cost estimation the total number of days is taken as 3 days.

In the case of the pultruded CFRP composites, the total time for set up, surface preparation movable scaffolding, and bonding of strips occurred over a period of 1.5 days per bay at approximately 12 hrs/day, with three men on the job. For purposes of this cost estimation the total number of days is taken as two.

The price per hour per man of work is estimated at $25/hour/man with a factor of 3 for margins and conservatism; therefore, the cost per hour per man is $75/hour/man.

The total labor costs for pultruded and wet lay-up CFRP composites is provided per bay, per area of bridge and for an entire bridge structure in the following table.

Table 11-5. Estimated Labor Costs for FRP Bridge Rehabilitation[3]

	Days /bay	Hours /day	Men /hour	Cost /hour /man	Cost /bay	Cost per Area of Bridge per m^2	Labor Cost for Entire Bridge Structure Bridge Area = 2830 m^2
Wet Lay-up	3	12	3	75	$8100	$255/$m^2$	$720,000
Pultruded	2	12	3	75	$5400	$170/$m^2$	$480,000

11.5 .Total Cost for Bridge Rehabilitation

Here the estimated total cost for CFRP composite rehabilitation of a bridge structure to extend the life of the structure 10 years, at a limit reliability index of 3.5 is summarized in the following table. The table shows the amounts required to rehabilitate the entire parallel Watson Wash Bridge Structure (westbound), since the east bound structure has been replaced as described in Chapter 10 of this report. The parallel Watson Wash Bridge structure has a length of 226 m (741 ft) and span width of 12.5 m (41 ft).

---

[3] Table 2-5. Labor Costs for FRP Bridge Rehabilitation with FPS Units

	Days /bay	Hours /day	Men /hour	Cost /hour /man	Cost /bay	Cost per Area of Bridge per ft^2	Labor Cost for Entire Bridge Structure Bridge Area = 30381 ft^2
Wet Lay-up	3	12	3	75	$8100	25/ft^2	$760,000
Pultruded	2	12	3	75	$5400	16/ft^2	$490,000

The following table shows the cost to rehabilitate the entire parallel Watson Wash Bridge structure for HS20 load demands.

Table 11-6. Total Estimated Cost of Bridge Rehabilitation for HS20 Loads[4]

Material	Material Cost for Entire Bridge Structure Bridge Area = 2830 m^2	Labor Cost for Entire Bridge Structure Bridge Area = 2830 m^2	Total Cost for Entire Bridge Structure Bridge Area = 2830 m^2
Wet Lay-up	$170,000	$720,000	$890,000
Pultruded	$350,000	$480,000	$830,000

The conservative cost estimate for FRP composite rehabilitation for the HS20 load demands is approximately $1 million US dollars with wet lay-up fabricated CFRP composites or pultruded CFRP composites.

The following table shows the cost to rehabilitate the entire parallel Watson Wash Bridge structure for Permit load demands in the longitudinal and transverse slab directions.

---

[4] Table 2-6. Total Estimate Cost of Bridge Rehabilitation for HS20 Loads with FPS Units

Material	Material Cost for Entire Bridge Structure Bridge Area = 30381 ft^2	Labor Cost for Entire Bridge Structure Bridge Area = 30381 ft^2	Total Cost for Entire Bridge Structure Bridge Area = 30381 ft^2
Wet Lay-up	$180,000	$760,000	$940,000
Pultruded	$370,000	$490,000	$860,000

Table 11-7. Total Estimated Cost of Bridge Rehabilitation for Permit Loads[5]

Material	Material Cost for Entire Bridge Structure Bridge Area = 2830 m^2	Labor Cost for Entire Bridge Structure Bridge Area = 2830 m^2	Total Cost for Entire Bridge Structure Bridge Area = 2830 m^2
Wet Lay-up	$230,000	$720,000	$950,000
Pultruded	$570,000	$480,000	$1,050,000

To rehabilitate the entire parallel Watson Bridge structure for permit loads will also cost an estimated $1 million US dollars for wet lay-up CFRP composites and $1.1 million US dollars for pultruded CFRP composites.

11.6 Rehabilitation Versus Bridge Replacement Costs

The following section provides a comparison between the costs to replace a bridge structure versus FRP composite rehabilitation. From the Caltrans Construction statistics data of 2003, "Comparative Bridge Costs, January 2004", the estimated cost to replace a RC T-beam, skewed bridge in a remote location, such as the Watson Wash Bridge structure located in the Mojave desert, is approximately $1,450/m^2 ($130/ft^2). These bridge construction costs do not include costs for bridge removal, approach slabs, slope paving, or retaining walls.

The total cost of bridge construction is calculated as follows for a bridge length of 226 m (741 ft.) and span width of 12.5 m (41ft).

$$\text{Total Cost} = (\text{Cost /Area}) \times \text{Bridge Area}$$

$$\textbf{Total Cost} = \textbf{(1450/m}^2\textbf{)} \times \textbf{2830 m}^2 = \textbf{\$ 4.1 million}$$

$$\text{Total Cost} = (130/\text{ft}^2) \times 30381 \text{ ft}^2 = \$ 4 \text{ million}$$

---

[5] Table 2-7. Total Estimated Cost of Bridge Rehabilitation for Permit Loads in FPS Units

Material	Material Cost for Entire Bridge Structure Bridge Area = 30381 ft^2	Labor Cost for Entire Bridge Structure Bridge Area = 30381 ft^2	Total Cost for Entire Bridge Structure Bridge Area = 30381 ft^2
Wet Lay-up	$250,000	$760,000	$1,010,000
Pultruded	$580,000	$490,000	$1,070,000

The following tables provide a comparison between the bridge construction cost and the FRP composite rehabilitation design for HS20 load and Permit loads using wet lay-up CFRP composite and pultruded CFRP composite.

Table 11-8. Comparison of HS20 Design for Life Extension vs. Bridge Costs[6]

Material Type	Total Cost of FRP Rehabilitation for HS20 Loads $\$_{FRP}$ Bridge Area = 2830 m^2	Cost of New Bridge Construction $\$_{NEW}$ Bridge Area = 2830 m^2	% Savings with FRP Rehab vs. New Bridge $\left(\dfrac{\$_{NEW}-\$_{FRP}}{\$_{NEW}}\right)\times100$ Bridge Area = 2830 m^2
Wet Lay-up	$890,000	$4,100,000	78.29%
Pultruded	$830,000	$4,100,000	79.76%

Opting for FRP rehabilitation with wet lay-up or pultruded CFRP composites provides a savings of approximately 80% compared to bridge construction costs. The following table provides a comparison between permit load FRP design and bridge replacement.

---

[6] Table 3-1. Comparsion of HS20 Design for Life Extension vs. Bridge Costs with FPS Units

Material Type	Total Cost of FRP Rehabilitation for HS20 Loads $\$_{FRP}$ Bridge Area = 30381 ft^2	Cost of New Bridge Construction $\$_{NEW}$ Bridge Area = 30381 ft^2	% Savings with FRP Rehab vs. New Bridge $\left(\dfrac{\$_{NEW}-\$_{FRP}}{\$_{NEW}}\right)\times100$ Bridge Area = 30381 ft^2
Wet Lay-up	$940,000	$4,000,000	76.50%
Pultruded	$860,000	$4,000,000	78.50%

Table 11-9. Comparison of Permit Design for Life Extension vs. Bridge Costs[7]

Material Type	Total Cost of FRP Rehabilitation for Permit Loads $\$_{FRP}$ Bridge Area = 2830 m²	Cost of New Bridge Construction $\$_{NEW}$ Bridge Area = 2830 m²	% Savings with FRP Rehab vs. New Bridge $\left(\dfrac{\$_{NEW}-\$_{FRP}}{\$_{NEW}}\right)\times100$ Bridge Area = 2830 m²
Wet Lay-up	$950,000	$4,100,000	76.83%
Pultruded	$1,050,000	$4,100,000	74.39%

For the permit load designs, the option of FRP composite rehabilitation provides an approximate savings of 75% versus the cost of constructing a new bridge structure such as the Watson Wash Bridge.

11.7 Summary

The costs of bridge rehabilitation, using wet lay-up and pultruded CFRP composites is evaluated for a design which extends the service life of a structure for a period greater than 25 years with a reliability limit of 3.5 based on CFRP composite material deterioration.

The total cost of FRP rehabilitation for an entire bridge structure, such as the parallel structure, for west bound traffic on Interstate 40, of the Watson Wash Bridge is estimated and compared to the cost of new bridge construction. Considering HS20 loads, a cost savings of approximately 80% is observed when opting for FRP composites versus new bridge construction. To extend the life of the structure for permit load demands, a savings of approximately 75% is observed compared to new bridge construction costs.

---

[7] Table 3-2. Comparison of Permit Design for Life Extension vs. Bridge Costs with FPS Units

Material Type	Total Cost of FRP Rehabilitation for Permit Loads $\$_{FRP}$ Bridge Area = 30381 ft²	Cost of New Bridge Construction $\$_{NEW}$ Bridge Area = 30381 ft²	% Savings with FRP Rehab vs. New Bridge $\left(\dfrac{\$_{NEW}-\$_{FRP}}{\$_{NEW}}\right)\times100$ Bridge Area = 30381 ft²
Wet Lay-up	$1,010,000	$4,000,000	74.75%
Pultruded	$1,070,000	$4,000,000	73.25%

12 CONCLUSIONS

12.1 Introduction

The objective of this research was to develop methodologies to evaluate the effectiveness and integrity of RC bridge structures rehabilitated with FRP composites. This dissertation implemented a methodology for structural health monitoring of FRP rehabilitated structures to evaluate the effectiveness of rehabilitations in the field. A reliability-based approach was formulated to characterize the performance of a FRP rehabilitation that included the effects of material variation. A methodology for estimation of service life of FRP rehabilitated structures was developed using a time dependent reliability formulation to include both the effects of material variation and material deterioration. The methodology for estimation of service life was extended to include measurements from structural health monitoring data and validated through a series of unique progressive damage experiments in the field. A service life based approach for design of FRP composite rehabilitations was then developed such that the quantity of FRP composite can be determined based upon needs of service life and performance level of the structure.

Table 12-1 provides comparisons of the research aspects for FRP rehabilitation, its current state, and the advancements made through this research.

Table 12-1 Advances Through Research

Aspect	Current State-of-the-Art	Advances through This Research
Effectiveness of Composite Rehabilitation	▪ Load Test on Bridge Structure ▪ Guess Based on Design	▪ Incorporation of material variation and measured field data for estimation of service life
Assessment of Damage	▪ Global Evaluation on Load and Stiffness Only	▪ Localize stiffness changes in rehabilitated structure ▪ Estimation of position of damage and stiffness losses ▪ Assessment and Testing of time dependent load reduction and damage
Reliability	▪ Based on initial design value of β (not verifiable)	▪ Verifiable Reliability Assessment through Progressive Damage Testing ▪ Time Dependent Reliability Formulation for FRP rehabilitation to include field data and material deterioration data

12.2 Service Life Extension

The deck slab of the west bound structure of the Watson Wash Bridge showed signs of deterioration in the form of longitudinal and transverse cracking in the deck slabs. The longitudinal and transverse cracking patterns of the deck slab created the potential for punching shear failure in the deck slab. In order to prevent the occurrence of punching shear failure and increase the capacity of the deck slab CFRP composites were bonded to the deck soffit of the deck slab. The CFRP composite rehabilitation in the deck slab was intended to increase the life of the bridge structure.

In order to validate the service life extension approach it was necessary to develop a performance measure of the FRP rehabilitated deck in the presence of variation in properties and material degradation of applied CFRP composites. The reliability index suffices in providing a measure of the performance of the FRP rehabilitated deck slab and is able to incorporate the effect of material degradation. The application of a time-dependent reliability procedure allows for an estimation of the remaining service life of a structure following FRP composite degradation and progressive damage in the reinforced concrete (RC) section. In order to establish the service life estimation an allowable limit reliability must be included. In this report, a limit reliability of 3.5 is used since it is the calibration level of the AASHTO LRFD bridge design specifications (Nowak, 1999). An important aspect of the reliability index as a performance measure is that the likelihood of failure of the CFRP composite is measured independent of the design and based on a standard such as the criteria for steel yield in the section.

A cost evaluation of the FRP rehabilitation designs was also conducted to determine if the use of CFRP composite for rehabilitation of aging RC bridge decks is cost-effective. Specifically, the cost to rehabilitate, using CFRP composites, the entire deck area of the parallel Watson Wash Bridge structure is calculated versus the cost of replacing a skewed bridge structure such as the parallel Watson Wash Bridge Structure, which also shows deterioration characterized by the formation of longitudinal and transverse cracks. It is found that the cost of FRP rehabilitation is approximately 20% of the cost of new bridge construction. The cost to sustain permit loads is approximately 25% of the cost of new bridge construction.

12.3 Monitoring of Bridge Structure

In order to achieve the monitoring objective, global NDE by means of vibration based damage detection, materials characterization, and visual inspection of the CFRP composites was conducted.

It is shown that the use of the global NDE procedure by Stubbs et al. (2000) is effective in evaluating the changes in stiffness in the deck slab following rehabilitation with CFRP composite materials. The purpose of the global NDE procedure was to localize stiffness changes in the deck of the T-girder bridge following FRP composite rehabilitation. The use of material sampling and materials characterization of CFRP composites from the CFRP rehabilitation reflects the mechanical properties of FRP composite applied to the deck soffit of the bridge.

Furthermore, the deck of the bridge was visually inspected to identify any potential defects and flaws in the manufacturer rehabilitation. Defects and their locations were noted for continuous monitoring.

Finally, as part of the validation and monitoring of FRP composite rehabilitation, a sequence of progressive damage was applied to two bays of the Watson Wash Bridge. Using the vibration based damage detection procedure to determine stiffness losses following each damage case, results of a global NDE methodology and results of laboratory predictions for CFRP degradation were combined to assess the performance of the rehabilitated structure with respect to time.

12.4 Findings

Investigation of the integrity of FRP composite rehabilitation on the Watson Wash Bridge Structure resulted in the following findings and developments:

- FRP composites are capable of extending the service life of RC bridge structures

- Global NDE using modal parameters is able to validate and assess the FRP rehabilitation

- The effect of material degradation and material parameter variation is incorporated via structural reliability theory

- Service life estimation of FRP strengthened structures is determined using a time-dependent reliability formulation, incorporating durability information of FRP composite, material parameter variation, and measured stiffness changes from the structure.

- A linear relationship is observed between the area of CFRP applied and the initial reliability index of the structure; furthermore, for the CFRP composite.

12.5 Recommendations

The current report exemplifies the ability to evaluate and estimate the service life extension and effectiveness of CFRP composite bonded to the decks of RC bridge structures. The use of the reliability index as a performance measure based upon section analysis of the CFRP rehabilitated section allows the incorporation of material variation, CFRP composite degradation, and field measured stiffness changes of the deck slab. In this report, a recommendation for design of the CFRP composite rehabilitation of a bridge deck slab is made to provide a service life greater than 25 years at reliability greater than 3.5 (0.02% failure probability) considering laboratory characterized FRP composite durability. Additional investigations are necessary to apply the findings of this report to various classes of RC bridge structures. In addition, the CFRP composite rehabilitation is only applied to two spans of the Watson Wash Bridge with various application procedures and extrapolation to the entire bridge structure assumes a weakest-link system to assess the reliability of the entire bridge deck.

Based upon the findings of this report the following recommendations are made for future work and application of methodologies for service life extension and monitoring developed in this report:

- Monitor the existing westbound Watson Wash Bridge structure to improve durability.

- Apply durability characterization of CFRP composite materials from exposure to other environments such as immersion in saltwater solution, alkali solution) to the performance of a FRP rehabilitated beam structure.

- Application of service life estimation procedure in available on-line monitoring approaches to provide a basis for decisions of repair, replacement, or no action

- Incorporation of service life estimates and durability models in design of FRP composite rehabilitation as suggested in Appendix A of this report.

APPENDIX A: SERVICE LIFE BASED DESIGN

A.1   Introduction

In Appendix A, a service-life based design methodology is developed which employs a framework for service life estimation; the time-dependent reliability-based procedure is used since it provides a means to relate the variability and deterioration models of material parameters to the performance of the entire structure.

A.2   Methodology

A service life based design methodology requires the development of design curves that relate a potential FRP rehabilitation design to an estimate of service life.   In order to include the variation of material properties and material deterioration, the time dependent reliability formulation in Chapter 9 is applied for estimation.   The first order second moment time-dependent reliability formulation is shown below:

$$\beta(t) = \frac{\mu_z(t)}{\sigma_z(t)} = \frac{\left(\mu_R(t) - \mu_S(t)\right)}{\left(\sigma_R^2(t) + \sigma_S^2(t)\right)^{\frac{1}{2}}} \qquad \textbf{Eqn. A.1}$$

where $\beta(t)$ is the reliability of the structure as a function of time, t; μ, denotes the mean value of its respective subscript; σ^2 is the variance of its respective subscript; subscripts R and S, denote resistance and demand, respectively; the subscript Z denotes the performance function.   The service life estimation procedure, where deterioration is assumed to only occur in materials (i.e. concrete, steel, FRP composite), requires the following preliminary components: (a) establishment of acceptable performance level or minimum allowable reliability; (b) material deterioration models; (c) development of a time dependent performance function

The remaining service life of a component is then determined by solving for time, t, to reach an allowable reliability level.   The service life estimation model is available as a design tool for FRP composite rehabilitation by establishing a desired time of service life extension and calculating a required quantity of FRP composite to satisfy the minimum allowable reliability over the desired extension in service life.   In addition the service life estimation procedure can be used to develop design charts for varying FRP composite rehabilitation designs of a structure to develop a relationship for the FRP rehabilitation design as a function of the service life extension provided to the structure.   Figure A.1 shows a schematic of the service life design procedure.
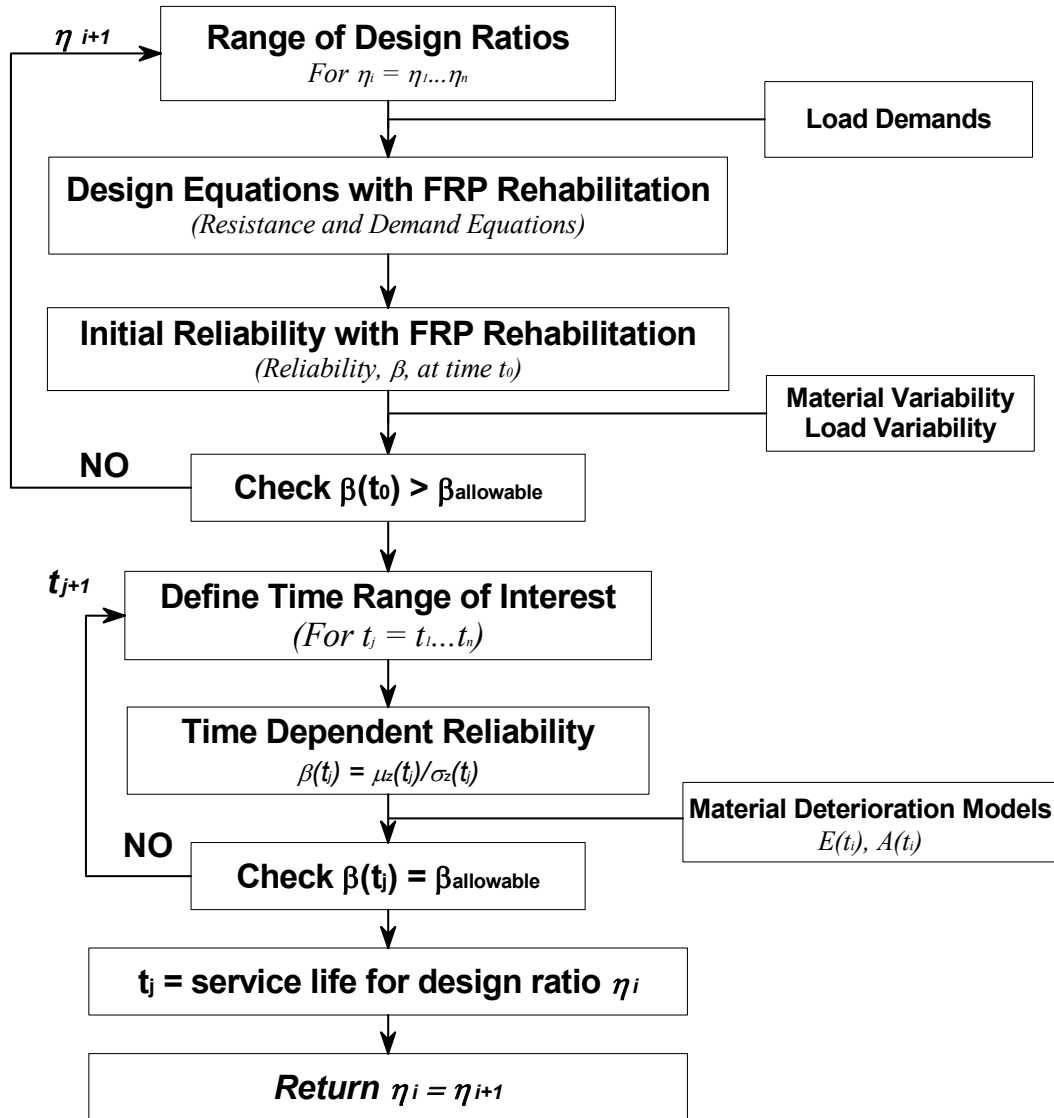
Figure A.1. Developmental Procedure for Service Life Design Charts

A.2.1 *Identification of Structural Deficiency*

Prior to determining the design of a FRP composite rehabilitation, the deficiency in the structure or structural component must be determined so as to apply the appropriate design equations and justify the use of FRP composites. The cause of structural deficiencies include, but are not limited to, changes in demands, code requirements, or in structural behavior. Regardless of the root cause of a structure's deficiency, the use of FRP composites for structural strengthening must be deemed appropriate. For example in ACI 440 Guidelines (2002), strengthening of an interior RC beam which experiences a 50% increase in live load demand is used to illustrate a case for FRP composite flexural rehabilitation.

A.2.2 Design Ratios

Assuming the need for rehabilitation and the use of FRP composites is well-established, a range of design ratios is selected which is an initial estimation for the quantity of FRP composite needed to rehabilitate the structure or component. A non-dimensional design ratio for a RC beam is the ratio of FRP composite modulus multiplied by an FRP reinforcement ratio over the steel reinforcement modulus multiplied by the steel reinforcement ratio for a RC beam structure. The aforementioned design relationship is shown below.

$$\eta_i = \frac{E_{frp}\rho_{frp}}{E_s\rho_s} = \frac{E_{frp}\dfrac{A_{frp}}{bh}}{E_s\dfrac{A_s}{bd}} \qquad \textbf{Eqn. A. 2}$$

where, η_i is the ith FRP rehabilitation design ratio; E_{frp} is the mean FRP composite modulus, ρ_{frp} is the FRP composite reinforcement ratio; E_s is the mean steel modulus; A_{frp} is the area of FRP composite in the RC section; A_s, is the area of steel reinforcement in the RC section; b, h, and d, are the width, height, and depth-to-steel reinforcement in the RC section, respectively.

For a given design ratio, the initial FRP rehabilitation design is used to determine the reliability of the structure with FRP composites using the first order second moment reliability relationship in equation 11.1 at time $t=0$. A check is conducted to determine if the reliability level with FRP rehabilitation is greater than a minimum performance level or allowable reliability, $\beta_{allowable}$, since degradation in the FRP composite decreases the reliability of the structure and the time to decrease from the initial reliability to the $\beta_{allowable}$ is the remaining service life of the structure.

A.2.3 Service Life Estimation

If the reliability of the structure for a given FRP rehabilitation design ratio at time $t=0$ is greater than the allowable reliability level, $\beta_{allowable}$, the time required to reach $\beta_{allowable}$ is determined. Here, the material deterioration models are incorporated to characterize the change in performance of the structure with respect to time and design ratio. In addition to the performance function and statistical descriptors of random variables, the remaining service life is influenced by, (1) minimum acceptable performance level, or allowable reliability, $\beta_{allowable}$ and (2) selected material degradation models.

A.2.3.1 Minimum Acceptable Performance Level

The selection of an acceptable reliability level is critical in the design process since it is the basic performance requirement of the structure. A low allowable reliability results in a longer available service life extension with the acceptance of a greater likelihood of failure. On the other hand, a higher allowable reliability level may require an overly conservative design, which may be an unrealistic criteria for the FRP rehabilitated structure and may negate the practicality of using FRP composites all together. As an example of limit reliabilities, the load and resistance factored design codes are calibrated according to various levels of reliability depending on the criticality of structures and the

variation of loads and material parameters used in design. For instance, a value of 3.5 is used in the calibration of the *AASHTO LRFD Bridge Design Specifications* for bridges (Nowak, 1999). The LRFD design manual for steel implies a reliability of approximately 2.6 for the member and 4.0 for connections for braced compact beams in flexure and tension (AISC, 1998). Table A - 1 provides a comparison of limit reliabilities and their corresponding failure probabilities.

Table A - 1. Reliability Levels and Associated Failure Probabilities

Reliability, β	Percent Probability of Failure
2.33	1%
2.6	0.47%
3.0	0.13%
3.5	0.023%
4.0	0.0032%

A.2.3.2 *Material Degradation Models*

The selection of a potential material degradation model to predict the time dependent behavior of material or geometric parameters impacts the service life estimation. Durability of FRP composites is characterized by the use of accelerated aging experiments, whereby composite samples are exposed to environments varying in solution and temperatures. Accelerated aging experiments are used to extrapolate long-term data from short-term data obtained from the laboratory where a stimulus, such as temperature, is applied to accelerate failure. At specified time intervals, samples are characterized. Using measured material properties (i.e. tensile modulus, ultimate strength, glass transition temperature), acceleration models are developed based on the physics or chemistry of a failure mechanism of the composite. Examples of these material prediction models include time-temperature superposition (Liao et al. 1998), Arrhenius rate relationship, Phani and Bose methods (Phani and Bose 1997), or an exponential curve fit of measured laboratory data. The accuracy of these durability models is directly correlated to the conservatism or non-conservatism of the service life prediction and consequently the FRP rehabilitation design.

A.3   Application of Service Life Based Design

The service life based design methodology is applied to a beam structure from design example 14.3 of ACI 440, the flexural strengthening of a simply supported RC beam which is to undergo a 50% increase in live-load demands. The RC beam has sufficient shear strength to resist the new required shear demand and meets the deflection and crack control service requirements. Its flexural strength, however, is deemed inadequate to carry the increased live load. The geometry and reinforcement details of the beam structure are summarized in Table A - 2. Table A - 3. shows the unfactored and factored load demands the beam structure is to resist for the existing loads and the anticipated increase in live load. The factors used are 1.4 for dead load and 1.7 for live load, in accordance with ACI 318 (2002).

Table A - 2. RC Section Geometry and Material Properties

Dimension or Property	Value
Length of beam, l	7.31 m (24 ft)
Width of beam, b	30.48 cm (12 in)
d	54.61 cm (21.5 in)
h	60.96 cm (24 in)
f'_c	34 N/mm^2 (5 ksi)
f_y	414 N/mm^2 (60 ksi)
Reinforcement	3 ϕ 28 bars (No. 9)

Table A - 3. Load Demands on Beam Structure

Moment Demand	Existing Load	Anticipated Load
Unfactored Dead Load	96.2 kN-m (72 k-ft)	96.2 kN-m (72 k-ft)
Unfactored Live Load	114.9 kN-m (86 k-ft)	173.6 kN-m (130 k-ft)
Total Factored Moment	331.3 kN-m (248 k-ft)	428.8 kN-m (321 k-ft)

A.3.1 FRP Composite Properties

The FRP composite properties used in this design application are from wet lay-up manufactured carbon/epoxy composites from the Watson Wash Bridge. Mechanical properties from an actual field application are used to obtain a realistic measure of variation in FRP composites manufactured by wet lay-up. Table A - 4 summarizes mechanical properties of a field manufactured two-layer carbon/epoxy composite having plies of nominal thickness equal to 1.016 mm.

Table A - 4. Wet Lay-up CFRP Composite Properties

Ultimate Tensile Stress			Average Modulus GPa (ksi)	Rupture Strain cm/cm (=in/in)	Ply Thickness mm (in)
Mean MPa (ksi)	Std. Dev MPa (ksi)	Mean – 3SD MPa (ksi)			
1100.61 (159.63)	133.83 (19.41)	699.12 (101.4)	78.96 (11451)	0.00886	1.02 (0.040)

ACI 440 recommends the design value for strength and rupture strain of a FRP composite be taken as the mean strength minus three times the standard deviation. However, no specification is provided for the design modulus of a FRP composite other than to measure chord modulus in accordance with ASTM D3039 and calculate chord modulus between 0.003 and 0.006 strain (ACI 440, 2002).

The modulus coefficient of variation (COV) for the carbon/epoxy composite is measured at 5.2%; however, in the reliability evaluations to follow, a standard COV of 10% is conservatively assumed for CFRP composites.

A.3.2 ACI 440 Design

The procedures of ACI 440 for strengthening concrete structures requires the use of knockdown factors on material parameters as a means to account for environmental

surroundings and fiber/resin system used. For an interior RC beam strengthened with a carbon/epoxy composite system, an environmental factor, C_E, of 0.95 is used. The ACI 440 design procedure with material parameters given in Table A - 4 are detailed in (Atadero et al. 2004); the final FRP rehabilitation design for an interior beam with a 50% increase in live load moment demands is a two-layer, 17.78 cm (7 inches) wide and 2.04 mm (0.080 inch) thick carbon/epoxy composite. The cross-sectional area of the CFRP composite required by the ACI 440 design procedure is 362.71 mm^2 (0.562 in^2). The resulting ACI 440 design ratio is computed per equation 11.2, as follows:

$$\eta_{ACI} = \frac{E_{frp} \dfrac{A_{frp}}{bh}}{E_s \dfrac{A_s}{bd}} = \frac{78.96 \text{ GPa} \left(\dfrac{3.62 \text{ cm}^2}{30.48 \text{ cm} \cdot 60.96 \text{ cm}} \right)}{413.69 \text{ GPa} \left(\dfrac{19.355 \text{ cm}^2}{30.48 \text{ cm} \cdot 54.61 \text{ cm}} \right)} = 0.032 \qquad \textbf{Eqn. A. 3}$$

It is important to note, ACI 440 assumes that modulus of elasticity is typically unaffected by environmental conditions (ACI 440 2002). While the ACI 440 design guidelines provides a knockdown factor for environmental exposure, a design methodology is necessary which directly incorporates predictions of material parameters over time.

A.3.3 Reliability Analysis

The reliability analysis of the interior RC beam structure uses a mean value, first order, second moment (MVFOSM) reliability formulation where random variables are described by their respective means and variances. A linear performance function or limit state function for the moment capacity of the beam structure is applied, where failure is defined as the likely of steel reinforcement yield. Formulation of the reliability analysis of the beam structure involves the following components prior to calculation of the reliability index: (1) Identification of random variables with corresponding means and variances; (2) Determination of mean, μ_z, and variation, σ_z, of the performance function, Z.

A.3.3.1 Resistance Variables

The measure of resistance in this analysis is the nominal moment capacity of the RC beam at steel yield. Material parameters having a direct impact on the moment capacity of the deck slab are the concrete compressive strength, f_c', yield strength of steel, f_y, and tensile modulus and tensile strength of composite. For mean values of steel yield strength and concrete compressive strength, bias factors are applied in accordance with NCHRP Report 368 (Nowak, 1999). Table A - 5. summarizes the means and COV's for steel yield strength and concrete compressive strength. CFRP composite properties are provided in Table A - 4.

Table A - 5. Statistical Descriptors for Steel and Concrete Strengths

Variable	Design Value MPa (ksi)	Bias Factor	Mean Value MPa (ksi)	COV %
f_y	413.7 (60.0)	1.1	455.1 (66.0)	10
f_c'	34.5 (5.0)	1.14	39.33 (5.7)	15

A.3.3.2 Demand Variables

The total demand on the RC beam is the sum of dead and live loads. Dead load is modeled as a normally distributed variable with bias factor 1.05 and coefficient of variation 10% (Atadero et al. 2004). The bias factor on the live load is taken as 1 while the coefficient of variation is taken as 25% (Atadero et al., 2004).

A.3.3.3 Performance Function

The performance function translates the limiting condition of the structure (i.e. yield of steel reinforcement) to a quantitative measure of the reliability index; the reliability index quantifies the probability that a violation of the selected criteria occurs. In the case of the beam structure, this criterion is the yield strain of steel, equal to 0.002. The basic performance function, Z, or limit state function, in the reliability analysis is as follows.

$$Z = g(R, S) = R - S \qquad \textbf{Eqn. A. 4}$$

$$\mu_z(t) = \mu_R(t) - \mu_S(t) \qquad \textbf{Eqn. A. 5}$$

$$\sigma_z^2(t) = \sigma_R^2(t) + \sigma_S^2(t) \qquad \textbf{Eqn. A. 6}$$

where, R, is resistance and S, denotes demand; μ, indicates mean value of its respective subscript; σ^2, denotes variance of its respective subscript, and t is time. For evaluation of the example beam section, the resistance and demand for the structure are expressed in terms of moment resistance and moment demand.

$$\mu_R(t) = \mu[M_R] = \mu[M_C(t)] + \mu[M_{steel}(t)] + \mu[M_{frp}(t)] \qquad \textbf{Eqn. A. 7}$$

$$M_C(t) = C_C(t) \cdot \left(c_1(t) - \frac{a}{2} \right) = 0.85 f_c' \beta_1 c_1(t) b \cdot \left(c_1(t) - \frac{\beta_1 c_1(t)}{2} \right) \qquad \textbf{Eqn. A. 8}$$

$$M_{steel}(t) = T_S \cdot (d - c_1(t)) = A_S(t) f_y \cdot (d - c_1(t)) \qquad \textbf{Eqn. A. 9}$$

$$M_{frp}(t) = T_{frp} \cdot (h - c_1(t)) = A_{frp} E(t) \varepsilon_{frp} \cdot (h - c_1(t)) \qquad \textbf{Eqn. A. 10}$$

where μ denotes mean value of its respective subscript; M_R is the moment resistance about the axis of zero strain and is equal to the sum of the moment contributions from concrete, M_C, steel reinforcement, M_{steel}, and FRP composite, M_{frp}; C_c is the force acting in the concrete; f_c', is the compressive strength of concrete; β_1, rectangular compressive stress block factor equal to 0.85; c_1, denotes the axis of zero strain from the extreme compression fiber; b, is the representative beam width; T_s, force in steel reinforcement;

$A_s(t)$, area of steel reinforcement with respect to time, t; f_y, yield strength of steel; d, is the depth to steel reinforcement from the extreme compression fiber of the section; T_{frp}, force in CFRP composite; A_{frp}, area of FRP composite; $E(t)$, modulus of FRP composite as a function of time, t; ε_{frp}, strain in FRP composite; h, is the height of the section. M_R, represents the mean value of the resistance with random variables, f_y, f'_c and E_{frp}. The dependence on time allows for the incorporation of material degradation models to estimate the remaining service life of a structure.

A standard section analysis for reinforced concrete is conducted to determine the depth of the axis of zero strain; if the force in the FRP composite exceeds its predicted ultimate strength the section analysis is conducted with the corresponding ultimate FRP strain set as the limiting criteria. Similarly if concrete crush occurs, i.e. strain in concrete, ε_c, exceeds 0.003, the section analysis is revisited with concrete strain at crush as the limiting criteria.

Determination of the variation in resistance utilizes standard rules for probability. The coefficient of variation, *COV*, for the moment contributions are the same as the corresponding material component. The time dependent variation in resistance is shown below.

$$\sigma_R^2(t) = \sigma_{M_R}^2(t) = \sigma_{M_{f'c}}^2(t) + \sigma_{M_{steel}}^2(t) + \sigma_{M_{frp}}^2(t) \quad \textbf{Eqn. A. 11}$$

where,; σ^2, is the variance of the variable in subscript as a function of time, t. The mean value for the demand is the sum of the mean dead load and live load moments. The total moment demand and variance are determined similar to the resistance evaluation.

$$\mu_S = \mu[M_S] = \mu[M_{LL}] + \mu[M_{DL}] \qquad \textbf{Eqn. A. 12}$$

$$\sigma_S^2 = \sigma_{M_S}^2 = \sigma_{M_{LL}}^2 + \sigma_{M_{DL}}^2 \qquad \textbf{Eqn. A. 13}$$

where, μ, denotes the mean value of the variable in brackets; σ^2, is the variance of the variable in brackets. Unlike the resistance formulation it is assumed that the demand does not change with respect to time.

Substituting for appropriate terms in the performance function, for resistance and demand moments, the reliability index is determined for a single set of material parameters as a function of time with substitution into equation 11.1.

$$\beta(t) = \frac{\mu_z}{\sigma_z} = \frac{\mu\left[M_C(t)\right] + \mu\left[M_{steel}(t)\right] + \mu\left[M_{frp}(t)\right] - \mu_S}{\left(\sigma_{M_{f'c}}^2(t) + \sigma_{M_{steel}}^2(t) + \sigma_{M_{frp}}^2(t) + \sigma_S^2\right)^{\frac{1}{2}}} \qquad \textbf{Eqn. A. 14}$$

where, variables are described previously. Accordingly, a section analysis is required to determine the resultant change following a change in material parameters. The section analysis also serves detect changes in the initiating failure mechanism and provides information about the changing strain levels in the FRP composite to determine if the rupture strain of FRP is reached or if concrete crush occurs prior to steel yield.

A.3.4 Instantaneous Reliabilities without FRP Rehabilitation

Using the reliability formulation in equation 11.14, at a single instance of time, the reliability of the interior RC beam prior to the increase in live load demands is 4.365, corresponding to a probability of failure of 6.353 x 10⁻⁶. With the increase in live load demands on the RC beam structure, the reliability index of the beam is 2.721, corresponding to a probability of failure of 0.0033.

With the increase in live load demands, a significant decrease in the reliability of the beam structure is observed. Depending on the allowable reliability index and the material degradation model used an appropriate CFRP composite rehabilitation design can be determined following design procedure outlined in Figure A.1.

A.4 Results of Service Life Based Design Approach Example

The predictions for CFRP composite material parameters are taken from tensile modulus and tensile strength of 2-layer and 6-layer wet lay-up CFRP composites immersed in deionized water at 23°C, 40°C, and 60°C. The ARR for tensile modulus and tensile strength are measured in terms of percent retention with respect to time.

$$y_m(t) = -0.4182 \cdot \ln(t \cdot 365 \tfrac{days}{year}) + 106.07\% \qquad \textbf{Eqn. A. 15}$$

$$y_s(t) = -3.366 \cdot \ln(t \cdot 365 \tfrac{days}{year}) + 106.07\% \qquad \textbf{Eqn. A. 16}$$

where, $y_m(t)$, is the percent retention of tensile modulus; $y_s(t)$, is the percent retention of tensile strength; t, is time in years. Similarly for the 6 layer CFRP composite the ARR for tensile modulus and tensile strength are,

$$y_m(t) = -2.9626 \cdot \ln(t \cdot 365 \tfrac{days}{year}) + 106.07\% \qquad \textbf{Eqn. A. 17}$$

$$y_s(t) = -5.2543 \cdot \ln(t \cdot 365 \tfrac{days}{year}) + 106.07\% \qquad \textbf{Eqn. A. 18}$$

The 2 and 6 layer CFRP ARR used to predict long-term behavior exemplify the possible variations in thickness of as-built composites that may occur during construction. The predictions for percent modulus and strength retention are incorporated into the performance function with the definition of a time-dependent modulus and strength, shown below.

$$E(t) = E_{frp} \cdot y_m(t) \qquad \textbf{Eqn. A. 19}$$

$$f(t) = f_{frp} \cdot y_s(t) \qquad \textbf{Eqn. A. 20}$$

where, $E(t)$, represents the time dependent FRP composite modulus, $f(t)$ is the time dependent FRP composite strength; f_{frp} is the ultimate strength of the composite; all other variables were previously defined.

The moment resistance corresponding to the deteriorating tensile strength and tensile modulus parameters is given by the following relationship, having previously defined variables.

$$M_R(t) = \begin{cases} A_{frp} \cdot E(t) \cdot \varepsilon_{frp} \cdot (h-d) + 0.85 \cdot f_c' \cdot \beta_1 \cdot c_1(t) \cdot b \cdot (d - \frac{\beta_1 \cdot c_1(t)}{2}) & \text{for } E(t) \cdot \varepsilon_{frp} \leq f(t) \\ A_{frp} \cdot E(t) \cdot \varepsilon_{frp} \cdot (h-d) + 0.85 \cdot f_c' \cdot \beta_1 \cdot c_1(t) \cdot b \cdot (d - \frac{\beta_1 \cdot c_1(t)}{2}) & \text{for } f(t) \leq E(t) \cdot \varepsilon_{frp} \end{cases}$$ **Eqn. A. 21**

Applying the material degradation models into the service life design procedure yields a relationship between design ratio, η, versus the service life extension provided by bonding CFRP composites to the soffit of the RC beam. In the following sections the effect of minimum acceptable reliability levels and variation of FRP composite properties on the service life design are investigated.

A.4.1 Effect of Allowable Reliabilities

The selection of a minimum allowable reliability is dependent on the criticality of the structure or component or the safety required. Consequently, a high value of the minimum allowable reliability index may negate the ability of FRP composites to sustain load for an extended period of time. The use of the service life based design approach allows for the investigation of the effect of varying performance requirement on the design and service life of FRP rehabilitated structures.

Figure A.2 shows design ratio versus the service life extension provided by FRP composite rehabilitation to the example FRP strengthening problem. Allowable reliabilities of 3.0, 3.5, and 4.0 are presented for the CFRP degradation models with a COV of 10% on FRP modulus.
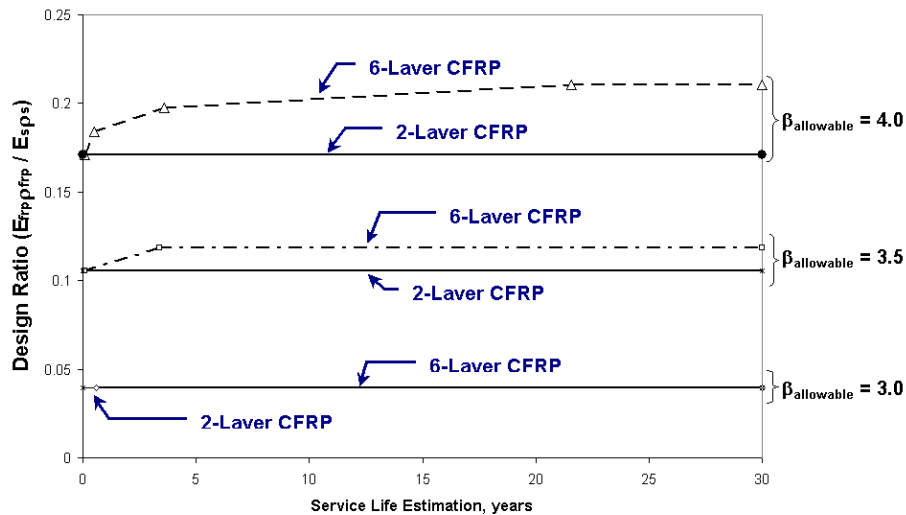

Figure A.2. Design Ratio vs. Service Life for Varying $\beta_{allowable}$

An allowable reliability index of 3.0 indicates that a CFRP rehabilitation design for the beam with design ratio greater than 0.04 will not violate the allowable reliability level as a result of material deterioration for both the 2 and 6 layer ARR models. A horizontal line indicates that the asymptotic effect from the ARR prediction is such that if a FRP rehabilitation design reaches a specific reliability level, the reliability of the FRP rehabilitated beam component will not decrease below the minimum acceptable performance level.

For an allowable reliability index of 3.5, a CFRP design ratio for the beam greater than 0.118 provides sufficient reinforcement to sustain the increased live load demands without decreasing below the minimum allowable reliability. The required design ratio for an allowable reliability of 3.5 is approximately three times greater than the design ratio requirement with allowable reliability of 3.0. For the 2-layer ARR model, a FRP rehabilitation design ratio greater than 0.105 allows for sufficient FRP reinforcement to sustain the additional live load demand without violating the minimum acceptable reliability.

With an allowable reliability index value of 4.0, the 6-layer ARR prediction shows a logarithmic relationship between design ratio and service life as a result of the degradation procedure. In order to increase the service life of the beam structure for 10 years, a design ratio of 0.21 is necessary. For the 2-layer ARR, a design ratio greater than 0.121 does not intersect the minimum allowable reliability level for the applicable duration of the material prediction.

It is important to note that the ACI design methodology results in a design ratio of 0.032, which fails to meet any of the allowable reliability index levels and thus would not be able to sustain the increased live load for any duration of service in the presence of FRP material deterioration.

A.5   Influence of CFRP COV on Service Life Design Example

For FRP strengthening of RC structures, the composite manufacturing process is typically wet lay-up or pultrusion. While pultrusion is a highly controlled manufacturing process with consistent mechanical and thermal properties present in the composite, wet lay-up is a manual process, which may result in large variation of mechanical and thermal properties of the composite due to defects from material preparation (i.e. improper mixing of resins), misalignment of fibers, damage during placement, operator, and environmental conditions during manufacture. Therefore, a study is conducted on the potential variation present in FRP material properties and the influence on the service life based design of the FRP composite rehabilitation. COV values of 0, 10, and 20 percent are considered for the CFRP modulus used to strengthen the beam structure for an increase in live load. The resulting design chart considering an allowable reliability index of 3.5 is shown in Figure A.3 for the 2-layer and 6-layer ARR predictions.
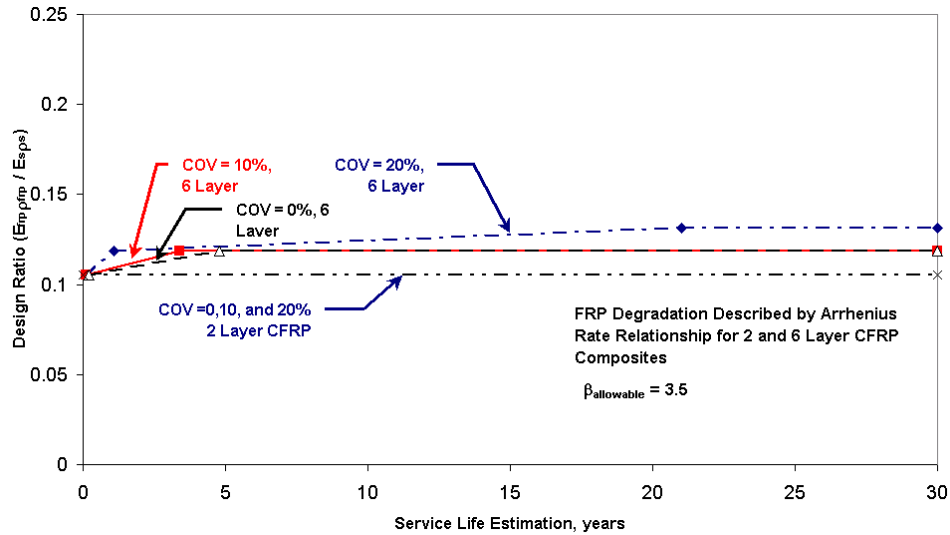
Figure A.3. Effect of COV on Design Ratio vs. Service Life Estimation

For the 2-layer ARR model, the changing COV does not affect the design result for the example beam structure. The 2-layer ARR model does not result in significant deterioration of the CFRP composite properties, in fact applying the ARR deterioration model provides benefits from post cure of carbon/epoxy coupons. Comparatively, the percent retention of initial FRP modulus from the 2-layer ARR model is 102.182% at 30 years; whereas, the 6-layer ARR model provides a 78.51% retention of CFRP modulus at the same time. The increasing COV is not sufficient to cause significant decreases in the reliability performance of the beam structure in the presence of post cure effects.

The 6-layer ARR model for CFRP composites shows that increases in variability of the mechanical properties results in corresponding changes or increases in design ratio for a given amount of time. A more significant change in design requirements is observed from an increase in COV from 10% to 20% as opposed to 0 to 10%. For instance, for a service life design requirement of 20 years, the required design ratio for COV's of 0% and 10% is the same at 0.12, while the required design ratio for a FRP modulus COV of 20% is 0.13. Therefore, such information may be applied to classify variation between 0 and 10% of FRP modulus as "excellent", COV's between 10% and 20% as "standard", and COV's greater than 20% as "poor."

A.6   Corrosion Affected Structure

The service life based design procedure is capable of including and combining the effects of other time dependent parameters such as reductions in concrete compressive strength or losses in steel reinforcement area as a result of corrosion.

Termination of the service life of concrete bridge decks is conventionally associated with the accumulation of irreversible damage resulting from corrosion of reinforcement, freeze thaw cycles, traffic loading in addition to the initial damage resulting from poor design and/or construction and inadequate inspection and maintenance practices (Lounis 2000).

Corrosion induced reduction in steel cross-sectional area is included in the service life based design procedure with the following relationship (Cheung and Kyle 1996).

$$A_s(t) = \frac{n\pi}{4}\left(D_0 - 2C_r t\right)^2$$

where, $A_s(t)$, denotes the time dependent cross-sectional area of steel reinforcement; n, is the number of steel rebar in the section; D_0, is the initial diameter of a single rebar; C_r, is the rate of reinforcing corrosion per year in mm/year; t, is time in years. The rate of reinforcing corrosion is derived for a moderate corrosion rate of 1 μA/cm^2, which results in a loss of cross-sectional radius of approximately 0.0115 mm/year (Andrade and Alonso 2001; Liang and Yang 2005). Incorporating this corrosion rate and relationship for steel cross-sectional area into the service life design procedure provides a means to determine the quantity of CFRP composite necessary to rehabilitate a RC beam structure for an increase in live load demand and steel reinforcement corrosion.
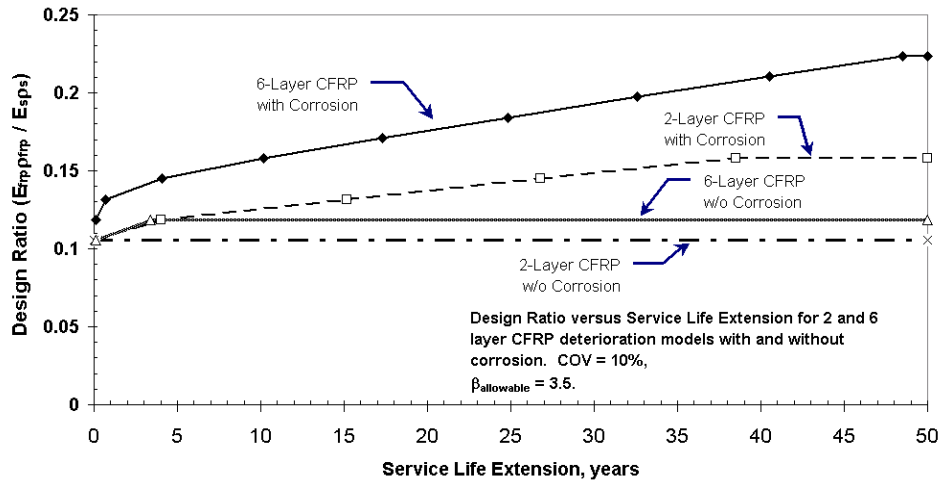

Figure A.4. Design Chart with Corrosion and CFRP Degradation

Figure A.4 shows a comparison of design ratio versus service life extension with and without steel reinforcement corrosion for the 2-layer and 6-layer ARR long-term durability predictions for FRP composite tensile properties. The design ratios for the 6-layer and 2-layer CFRP composites with corrosion show a steady increase in quantity of FRP required to maintain a reliability greater than 3.5 as the service life requirement increases. This is as expected, since the contribution of CFRP composite as tensile reinforcement increases as steel area reinforcement decreases. A closer observation between design curves with and without corrosion, shows that that the combined effect of steel reinforcement corrosion and FRP material degradation results in greater separation in design ration between 2 and 6 layer ARR models versus the difference between the design ratio of the 2 and 6 layer ARR models without corrosion. In the presence of corrosion and an increased load demand, in order to sustain a reliability of 3.5 for 20 years with FRP rehabilitation, design ratios of 0.136 and 0.177 are required for 2 layer and 6 layer ARR predictions, respectively. These values are approximately 29% and 47% greater than their design requirements without corrosion.

A.7 Discussion

A.7.1 Perspectives of Service Life Based Design of FRP Rehabilitations

The development of design charts from the service life based design procedure allows for a designer to select a design ratio, η, based on an allowable reliability level and desired service life extension. For example, for a 6-layer CFRP composite deterioration model, according to Figure A.2, if a designer requires a service life of 10years with an allowable reliability index of 3.5, then a design ratio of 0.118 is required. For an allowable reliability index of 3.0, a design ratio of 0.04 will provide a rehabilitation design that does not decrease below 3.0 in the presence of FRP composite material deterioration, i.e. the durability of FRP composites is not a factor in service life termination of the structural component.

While the design example in this chapter utilized the same parameters of the design example 14.3 of ACI 440 guidelines (2002), the service life design procedure evaluates the end result of the design (i.e. the area of FRP composite and material characteristics of the composite does not require the use of partial safety factors on manufacturing procedure, fiber type, etc.) Therefore, the result of any rehabilitation procedure can be assessed using the developed design procedure for FRP rehabilitation of RC structures. The service life based design approach extends beyond the need for characteristic values and safety factors as in TR No. 55, fib-CEP, ACI 440, and design guidelines by Tajlsten (2002) since the variation in FRP composite properties and material parameter predictions are included directly and the performance of the structure is represented by a likelihood of failure (i.e. the reliability index, β) for given demands.

The service life design procedure to develop design charts, illustrated in Figure A.1, is applicable to other failure mechanisms and rehabilitation types (i.e. shear and torsional rehabilitation), provided that a performance function can be defined for a limiting criteria (i.e. steel yield) and material durability predictions are available as input into the methodology.

A.7.2 Integration with Structural Health Monitoring

The service life based design approach can be integrated with results of structural health monitoring data as shown in Figure A.5.
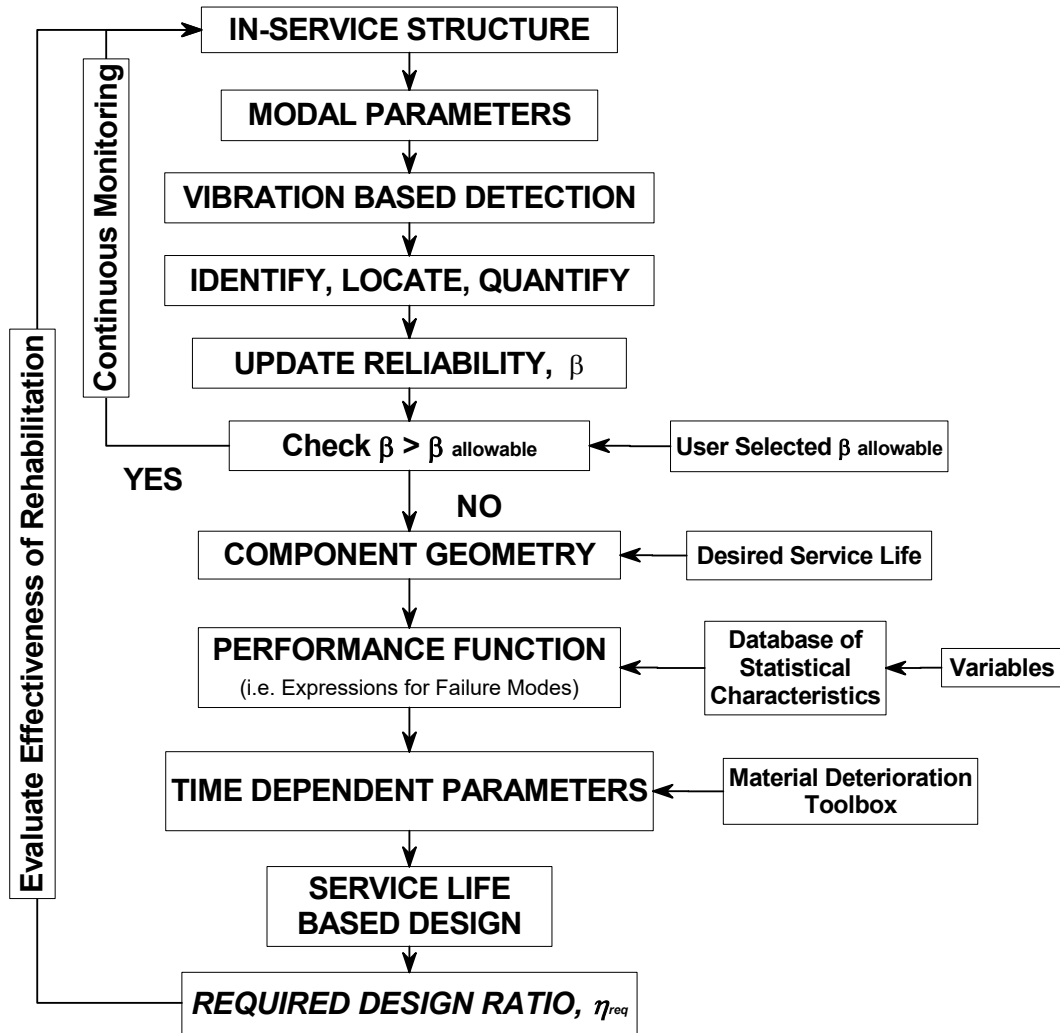
Figure A.5. Flowchart of Monitoring with Service Life Based Design

Figure A.5. is explained as a possible application to the Watson Wash Bridge structure. For the Watson Wash Bridge structure, the service life based design integrated with SHM can be conducted as follows. First structural health monitoring is initiated to evaluate the condition of the structure relative to its original state, i.e. undamaged state of the structure. Based upon identified stiffness losses on locations of the bridge, (i.e., bays of the bridge with varying severities of damage as identified in Chapter 7), the reliability index of a structural element such as a bay of the Watson Wash Bridge is updated as shown in Chapter 10 with the implementation of progressive damage. If the reliability of the structural component is greater than a user selected allowable reliability, continuous monitoring is conducted. However, if the updated reliability index is less than the allowable reliability, parameters for the service life based design approach are identified (i.e., desired service, allowable reliability, material deterioration models, performance function) and the required design ratio, η is determined.

If FRP composite rehabilitation of the component is conducted, then monitoring is implemented to assess the effectiveness of the rehabilitation and provide a continuous update of the state and remaining service life of the structure.

LIST OF REFERENCES

AASHTO, American Association of State Highway and Transportation Officials (1993). "*AASHTO Guide for Design of Pavement Structures*", Washington, DC.

ACI, American Concrete Institute. (2002). "Guide for the Design and Construction of Externally Bonded FRP Systems for Strengthening Concrete Structures." *ACI 440.2R-02, Emerging Technology Series*, Reported by ACI Committee 440, October, First Printing.

AISC, American Institute of Steel Construction. (1998). "Commentary on the Load and Resistance Factor Design Specification for Structural Steel Building." *Manual of Steel Construction, Load and Resistance Factor Design*, Third Edition, p.16.1-175-16.1-176.

ASCE, American Society of Civil Engineers. (2003). "2003 Progress Report – An Update to the 2001 Report Card." Published by ASCE, available on the world wide web, http://www.asce.org/reportcard/index.cfm

Abanilla, M.A.D. (2004). "Physio-Mechanical Characterization of T700 based Carbon Epoxy Systems for Infrastructure Rehabilitation." M.S. Thesis, Department of Structural Engineering, University of California, San Diego, 259 pages.

Abdalla, M.O., Grigoriadis, K.M., and Zimmerman, D.C. (1998). "Enhanced Structural Damage Detection Using Alternating Projection Methods." *AIAA Journal*, 46(7), 1305-1311.

Abdo, M.A.B. and Hori, M. (2002). "A Numerical Study of Structural Damage Detection Using Changes in the Rotation of Mode Shapes." *J. Sound and Vibration*, 251(2), 227-239.

Adams, R.D., Cawley, P., Pye, C.J., and Stone, B.J. (1978). "A Vibration Technique for Non-destructively Assessing the Integrity of Structures." *J. Mechanical Engineering Science*, 20, 93-100.

Adeli, H. and Hung, S. (1995). *Machine Learning – Neural Networks, Genetic Algorithms, and Fuzzy Systems*. John Wiley & Sons.

Adeli, H. (2001). "Neural Networks in Civil Engineering: 1989-2000." *Computer-Aided Civil and Infrastructure Engineering*, 16, 126-142.

Aktan, A.E., Farhey, D.N., Helmicki, A.J., Brown, D.L., Hunt, V.J., Lee, K-L. and Levi, A. (1997). "Structural Identification for Condition Assessment: Experimental Arts." *J. Structural Engineering*, 123(12), 1674-1684.

Aktan, E., Catbas, N., Turer, A, and Zhang, Z. (1998). "Structural Identification: Analytical Aspects." *J. Structural Engineering*, 124(7), 817-829.

Aktan, A.E., Catbas, F.N., Grimmelsman, K.A., and Tsikos, C.J. (2000). "Issues in Infrastructure Health Monitoring for Management." *J. Eng. Mech.*, 126(7), 711-724.

Alampalli, S., Fu, G., and Dillon, E.W. (1997). "Signal Versus Noise in Damage Detection by Experimental Modal Analysis." *J. Structural Engineering*, 123(2), 237-245.

Alkhrdaji, T., Nanni, A., Chen, G., and Barker, M. (1999). "Upgrading the Transportation Infrastructure: Solid RC Decks Strengthened with FRP." *Concrete International*, 21(10), 37-41.

Almusallam, T.H. and Al-Salloum, Y.A. (2001). "Ultimate Strength Prediction for RC Beams Externally Strengthened by Composite Materials." *Composites: Part B*, 32, 609-619.

Andrade, C. and Alonso, C. (2001). "On-site Measurements of Corrosion Rates of Reinforcements." *Construction and Building Materials*, 15(2-3), 141-145.

Arduini, M., Nanni, A., and Romagnolo, M. (2004). "Performance of One-Way Reinforced Concrete Slabs with Externally Bonded Fiber-Reinforced Polymer Strengthening." *ACI Structural Journal*, 101(2), 193-201.

Arya, C., Clarke, J.L., Kay, E.A., and O'Regan, P.D. (2002). "TR55: Design Guidance for Strengthening Concrete Structures Using Fibre Composite Materials: A Review." Engineering Structures, 24: 889-900.

Ascione, L. and Feo, L. (2000). "Modeling of Composite/Concrete Interface of RC Beams Strengthened with Composite Laminates." *Composites: Part B*, 31: 535-540.

Astrom, B.T. (1997). *Manufacturing of Polymer Composites*. Chapman & Hall, First Edition.

Atadero, R.A., Lee, L.S., and Karbhari, V.M. (2004). "Effect of Variability of Composite Properties on Wet Layup Based Rehabilitation of Concrete Structures." *ASC-ASTM D30 Joint 19th Annual Technical Conference*, Atlanta, Georgia, October 17-20, 2004.

Atkinson, A.C. and Donev, A.N. (1992). *Optimal Experimental Designs*. Oxford Science Series Vol. 8. Oxford: Clarendon Press.

Bakis, C.E., Bank, L.C., Brown, V.L., Cosenza, E., Davalos, J.F., Lesko, J.J., Machida, A., Rizkalla, S.H., and Triantafillou, T.C. (2002) "Fiber-Reinforced Polymer Composites for Construction – State-of-the-Art Review." *J. Composites for Construction*, 6(2), 73-87.

Bannister, M. (2001). "Challenges for Composites into the Next Millenium – A Reinforcement Perspective." *Composites: Part A.*, 32, 901-910.

Barai, S.V. and Pandey, P.C. (1995). "Performance of the Generalized Delta Rule in Structural Damage Detection." *Engineering Applications of Artificial Intelligence*, 8(2), 211-221.

Barai, S.V. and Pandey, P.C. (1997). "Time-delay Neural Networks in Damage Detection of Railway Bridges." *Advances in Engineering Software*, 28, 1-10.

Barker, R.M. and Puckett, J.A. (1997). *Design of Highway Bridges*. John Wiley & Sons, Inc.

Barroso, L.R. and Rodriguez, R. (2004). "Damage Detection Utilizing the Damage Index Method to A Benchmark Structure." *J. Engineering Mechanics*, 130(2), 142-151.

Baruch, M. and Bar-Itzhack, I.Y. (1978). "Optimal Weighted Orthogonalization of Measured Modes." *AIAA Journal*, 16(4), 346-351.

Bicanic, N and Chen, H. (1997) "Damage Identification in Framed Structures Using Natural Frequencies." *International Journal for Numerical Methods in Engineering,* 40, 4451-4468.

Bolton, R, Stubbs, N., Sikorsky, C., and Choi, S., (2001a) "A Comparison of Modal Properties Derived from Forced And Output-Only Measurements for a Reinforced Concrete Highway Bridge." *Proceedings of the 19th International Modal Analysis Conference (IMAC), Kissimmee, Florida*, 1, 857-863.

Bolton, R., Stubbs, N., Park, S. and Sikorsky, C. (2001b). "Documentation of Changes in Modal Properties of a Concrete Box Girder Bridge Due to Environmental and Internal Conditions." *Computer-Aided Civil and Infrastructure Engineering*, 16(1), 42-57.

Bonacci, J.F. and Maalej, M. (2000). "Externally Bonded FRP for Service Life-Extension of RC Infrastructure." *J. Infrastructure Systems*, 6(1), 41-51.

Bonacci, J.F. and Maalej, M. (2001). "Behavioral Trends of RC Beams Strengthened with Externally Bonded FRP." *J. Composites for Construction*, 5(2), 102-113.

Brincker, R., Zhang, L. & Andersen, P. (2000) "Modal Identification from ambient responses using frequency domain decomposition." Proceedings of the 18th International Modal Analysis Conference (IMAC). San Antonio, Texas, 5-8 February 2000.

Catbas, F.N. and Aktan, A.E. (2002). "Condition and Damage Assessment: Issues and Some Promising Indices." *J. Struct. Eng.*, 128(8), 1026-1036.

Caltrans, California Department of Transportation. (2004). *Bride Design Specifications*. September 2004.

Cheung, M.S. and Kyle, B.R. (1996). "Service Life Prediction of Concrete Structures." *Construction and Building Materials*, 10(1), 45-55.

Chong, K.P., Carino, N.J., and Washer, G. (2003). "Health Monitoring of Civil Infrastructures." *Smart Mater. Struct.*, 12, 483-493.

Chopra, A. K. (1995). *Dynamics of Structures: Theory and Applications to Earthquake Engineering.* Prentice Hall, Inc.

Chou, J.-H. and Ghaboussi, J. (2001). "Genetic Algorithm in Structural Damage Detection." *Computers and Structures*, 79(14), 1335-1353.

Clough, R. W. and Penzien, J. (1975) *Dynamics of Structures*. McGraw-Hill Book Company.

Contursi, T., Messina, A., and Williams, E.J. (1998). "A Multiple Damage Location Assurance Criterion Based on Natural Frequency Changes." *J. Vibration Control*, 4(5), 619-633.

Cornwell, P., Doebling, S.W., and Farrar, C.R. (1999). "Application of the Strain Energy Damage Detection Method to Plate-like Structures." *J. Sound and Vibration*, 224(2), 359-374.

Crasto, A.S., Kim, R.Y., and Mistretta, J.P. (2001). "The Application of Composites for the Rehabilitation of Concrete Bridge Infrastructure." *Adv. Composite Materials*, 10(2,3): 147-157.

De Lorenzis, L. and Nanni, A. (2002). "Bond Between Near Surface Mounted FRP Rods and Concrete in Structural Strengthening." *ACI Structural Journal*, 99(2), 123-133.

Doebling, S.W., Farrar, C.R., Prime, M.B., and Shevit, D.W. (1996). "Damage Identification and Health Monitoring of Structural and Mechanical Systems from Changes in Their Vibration Characteristics: A Literature Review." Los Alamos National Laboratory (LANL) Report No. LA-13070-MS.

Erki, M.A. and Meier, U. (1999). "Impact Loading of Concrete Beams Externally Strengthened with CFRP Laminates." *J. Composites for Construction*, 3(3), 117-124.

Escobar, J.A., Sosa, J.J., and Gomez, R. (2001). "Damage Detection in Framed Buildings." *Canadian Journal of Civil Engineering*, 28(1), 35-47.

Ewins, D. J. (2000). *Modal Testing: Theory, Practice and Application.* Research Studies Press, Ltd. Second Edition.

fib, International Federation for Structural Concrete. (2001). "Externally Bonded FRP Reinforcement for RC Structures." *Technical Report, Bulletin 14,* Task Group 9.3.

Farrar, C.R. and James III, G.H. (1997). "System Identification from Ambient Vibration Measurements on a Bridge." *J. Sound and Vibration*, 205(1), 1-18.

Farrar, C.R. and Jauregui, D.A. (1998a). "Comparative Study of Damage Identification Algorithms Applied to Bridge: Part I. Experiment." *Smart Materials & Structures*, 7, 704-719.

Farrar, C.R. and Jauregui, D.A. (1998b). "Comparative Study of Damage Identification Algorithms Applied to Bridge: Part II. Numerical Study." *Smart Materials & Structures*, 7, 720-731.

Farrar, C.R., Duffey, T. A., Cornwell, P. J. and Doebling, S. W. (1999) "Excitation Methods for Bridge Structures." *Proceedings of the 17th International Modal Analysis Conference, Kissimmee, Florida.* 1, 1063-1068..

Farrar, C.R., Duffey, T.A., Doebling, S.W., and Nix, D.A. (1999). "A Statistical Pattern Recognition Paradigm for Vibration-Based Structural Health Monitoring." *Proceedings of the 2nd International Workshop on Structural Health Monitoring, Stanford, CA. Sept. 8-10, 1999,* 764-773.

Farrar, C.R. and Sohn, H. (2001). "Condition/Damage Monitoring Methodologies." Invited Talk, *The Consortium of Organizations for Strong Motion Observation Systems (COSMOS) Workshop, Emeryville, CA, November 14-15, 2001.*

Farrar, C.R., Doebling, S.W., and Nix, D.A. (2001). "Vibration-based Structural Damage Identification." *Philosophical Transactions: Mathematical, Physical, & Engineering Sciences*, 359(1778), 131-149.

Farrar, C.R. and Doebling, S.W. (1997) "An Overview of Modal-based Damage Identification Methods." Los Alamos National Laboratory (LANL) Report No. LA-UR-97-2468.

Ferreira, A.J.M., Marques, A.T, and Cesar de Sa, J. (2000). "Analysis of Reinforced Concrete with External Composite Strengthening." *Composites: Part B*, 31: 527-534.

fib, International Federation for Structural Concrete. (2001). "Externally Bonded FRP Reinforcement for RC Structures." *Technical Report, Bulletin 14,* Task Group 9.3.

Fleming, C.J. and King, G.E.M. (1967). "The Development of Structural Adhesives for th Three Original Uses in South Africa." *Rilem International Symposium, Synthetic Resins in Building Construction, Paris*, 75-92.

Fugate, M.L., Sohn, H., and Farrar, C.R. (2001) "Vibration-Based Damage Detection Using Statistical Process Control." *Mechanical Systems and Signal Processing*, 15(4), 707-721.

Gay, D., Hoa, S.V., and Tsai, S.W. (2003). *Composite Materials – Design and Applications*. CRC Press, LLC.

Graybeal, B.A., Phares, B.M., Rolander, D.D., Moore, M., and Washer, G. (2002). "Visual Inspection of Highway Bridges." *J. Nondestructive Evaluation*, 21(3), 67-83.

Green, M. F. (1995) "Modal Test Methods For Bridges: A Review." *Proceedings of the 13th International Modal Analysis Conference, Nashville, Tennessee,* 1, 552-558.

Grossman, S. I. (1995). *Multivariable Calculus, Linear Algebra, and Differential Equations*. Third Edition. Saunders College Publishing.

Hag-Elsafi, O., Alampalli, S., and Kunin, J. (2001). "Application of FRP Laminates for Strengthening of a Reinforced Concrete T-beam Bridge Structure." *Composite Structures*, 52: 453-466.

Hao, H. and Xia, Y. (2002). "Vibration-based Damage Detection of Structures by Genetic Algorithm." *J. Computing in Civil Engineering*, 16(3), 222-229.

Hassiotis, S. and Jeong, J.D. (1995). "Identification of Stiffness Reductions Using Natural Frequencies." *J. Engineering Mechanics*, 121(10), 1106-1113.

Hassiotis, S. (2000). "Identification of Damage Using Natural Frequencies and Markov Parameters." *Computers and Structures*, 74, 365-373.

Heo, G., Wang, M.L., and Satpathi, D. (1997). "Optimal Transducer Placement for Health Monitoring of Long Span Bridge." *Soil Dynamics and Earthquake Engineering*, 16, 495-502.

Hermans, L. and Van der Auweraer, H. (1999). "Modal Testing and Analysis of Structures Under Operational Conditions: Industrial Applications." *Mechanical Systems and Signal Processing*, 13(2), 193-216.

Huang, C.S., Yang, Y.B., Lu, L.Y., and Chen, C.H. (1999). "Dynamic Testing and System Identification of a Multi-Span Highway Bridge." *Earthquake Engineering and Structural Dynamics,* 28, 857-878.

Hung, S-L. and Kao, C.Y. (2002). "Structural Damage Detection Using the Optimal Weights of the Approximating Artificial Neural Networks." *Earthquake Engineering and Structural Dynamics*, 31, 217-234.

Hunter, N. F. (2001). "Vibration Testing: Reviewing the State of the Art – Prospects and Challenges." *Structural Dynamics @ 2000: current status and future directions*, Research Studies Press Ltd, 175-192.

Jensen, E.A. and Hansen W. (2003). "A New Model for Predicting Aggregate Interlock Shear Transfer in Jointed Concrete Pavements." *Proc. 16th ASCE Engineering Mechanics Conference*, University of Washington, Seattle, July 16-18, 2003.

Johnson, E.A., Lam, H.F., Katafygiotis, L.S., and Beck, J.L. (2004). "Phase I IASC-ASCE Structural Health Monitoring Benchmark Problem Using Simulated Data." *J. Eng. Mech.,* 130(1), 3-15.

Karbhari, V.M., Chin, J.W., Hunston, D., Benmokrane, B., Juska, T., Morgan, R., Lesko, J.J., Sorathia, U., and Reynaud, D. (2003). "Durability Gap Analysis for Fiber-Reinforced Polymer Composites in Civil Infrastructure." *J. Composites for Construction*, 7(3), 238-247.

Karbhari, V.M. (2000). "Determination of Materials Design Values for The Use of Fibre-Reinforced Polymer Composites in Civil Infrastructure." *Proc Instn Mech Engrs*, 214, Part L, 163-171.

Karbhari, V.M. and Seible, F. (2000). "Fiber Reinforced Composites - Advanced Materials for the Renewal of Civil Infrastructure." *Applied Composite Materials*, 7, 95-124.

Karbhari, V.M. and Zhao, L. (2000). "Use of Composites for 21st Century Civil Infrastructure." *Comput. Methods Appl. Mech. Engrg.*, 135, 433-454.

Kim, B-H. (2002). "Local Damage Detection Using Modal Flexibility." PhD Dissertation, Civil Engineering, Texas A&M University.

Kim, J-T., Ryu, Y-S., Cho, H-M., and Stubbs, N. (2003). "Damage Identification in Beam Type Structures: Frequency-Based Method vs. Mode-Shape-Based Method." *Engineering Structures*, 25, 57-67.

Kim, J.T. and Stubbs, N. (2002). "Improved Damage Identification Method Based on Modal Information." *J. Sound and Vibration*, 252(2), 223-238.

Lamanna, A.J., Bank, L.C., and Scott, D.W. (2004). "Flexural Strengthening of Reinforced Concrete Beams by Mechanically Attaching Fiber-Reinforced Polymer Strips." *J. Composites for Construction*, 8(3), 203-210.

Lathi, B.P. (2002). *Linear Signals and Systems*. Oxford University Press, Inc., New York.

Lau, K. and Zhou, L. (2001). "Mechanical Performance of Composite-Strengthened Concrete Structures." *Composites: Part B*, 32: 21-31.

Law, S.S., Shi, Z.Y., and Zhang, L.M. (1998). "Structural Damage Detection From Incomplete and Noisy Modal Test Data." *J. Engineering Mechanics*, 124(11), 1280-1288.

Liao, K., C.R. Schltheisz, D.L. Hunston, and L.C. Brinson. (1998). "Long-term Durability of Fiber- Reinforced Polymer Matrix Composite Materials for Civil Infrastructure Applications: A Review." *J. Advanced Materials*, 30(4), 3-40.

Limam, O, Foret, G, and Ehrlacher, A. (2003). "RC Two-way Slabs Strengthened with CFRP Strips: Experimental Study and A Limit Analysis Approach." *Composite Structures*, 60, 467-471.

Maia, N. M. M. and Silva, J. M. M. editors. (1997). *Theoretical and Experimental Modal Analysis*. Research Studies Press, Ltd.

Malek, A.M. and Patel, K. (2003). "Flexural Strengthening of Reinforced Concrete Flange Beams with Composite Laminates." *J. Composites for Construction*, 6(2), 97-103.

Mares, C. and Surace, C. (1996). "An Application of Genetic Algorithms to Identify Damage in Elastic Structures." *J. Sound and Vibration*, 195(2), 195-215.

Melhem, H.G. and Nagaraja, S. (1996). "Machine Learning and Its Application to Civil Engineering Systems." *Civil Engineering Systems*, 13, 259-279.

McConnell, K.G. (2001). "Modal Testing." *Philosophical Transactions of the Royal Society of London Series A-Mathematical, Physical, and Engineering Sciences*, 359 (1778), 11-28.

Meier, U. (1995). "Strengthening of Structures Using Carbon Fibre/Epoxy Composites." *Construction and Building Materials*, 9(6), 341-351.

Meier, U. (2000). "Composite Materials in Bridge Repair." *Applied Composite Materials*, 7, 75-94.

Melchers, R. (1999). *Structural Reliability Analysis and Prediction*. John Wiley & Sons.

Messina, A., Contursi, T., and Williams, E.J. (1997). "Multiple Damage Evaluation Using Natural Frequency Changes." *Proceedings of the 15th International Modal Analysis Conference, Orlando, Florida*, 1, 652-657.

Messina, A, Williams, E.J., and Contursi, T. (1998). "Structural Damage Detection by a Sensitivity and Statistical-Based Method." *J. Sound and Vibration*, 216(5), 791-808.

Mosallam, A.S. and Mosalam K.M. (2003). "Strengthening of Two-way Concrete Slabs with FRP Composite Laminates." *Construction and Building Materials*, 17, 43-54.

Nanni, A. (2003). "North American Design Guidelines for Concrete Reinforcement and Strengthening Using FRP: Principles, Applications, and Unresolved Issues." *Construction and Building Material*, 17, 439-446.

Nowak, A.S., (1999). *NCHRP Report 368, Calibration of LRFD Bridge Design Code*. National Academy Press, Washington D.C.

Oh, H. and Sim, J. (2004). "Punching Shear Strength of Strengthened Deck Panels with Externally Bonded Plates." *Composites: Part B*, 35: 313-321.

Pandey, A. K., Biswas, M., and Samman, M.M. (1991). "Damage Detection from Changes in Curvature Mode Shapes." *J. Sound and Vibration*, 145(2), 321-332.

Park, K.C. and Reich, G.W. (1998). "Structural Damage Detection Using Localized Flexibilities." *J. Intelligent Material Systems and Structures*, 9, 911-919.

Park, K.C. and Felippa, C.A. (1998). "A Variational Framework for Solution Method Developments in Structural Mechanics." *J. Applied Mechanics*, 65(1), 242-249.

Park, S., Stubbs, N., Bolton, R., and Choi, S. (2001). "Field verification of Damage Index Method in a Concrete Box Girder Bridge via Visual Inspection." *Computer Aided Civil and Infrastructure Engineering*, 16, 58-70.

Park, S., Stubbs, N., and Sikorsky, C. (1997). "Linkage of Nondestructive Damage Evaluation to Structural System Reliability." *Smart Structures and Materials 1997: Smart Systems for Bridges, Structures, and Highways, Proceedings of the SPIE,* 3043, 234-245.

Phani, K.K. and Bose, N.R. (1997). "Temperature Dependence of Hygrothermal Ageing of CSM Laminates During Water Immersion." *Composites Science and Technology*, 29, 79-87.

Pickrel, C. R. (1999). "A Practical Approach to Modal Pretest Design." *Mechanical Systems and Signal Processing*, 13(2), 271-295.

Plevris, N., Triantafillou, T. C. and Veneziano, D. (1995). "Reliability of RC Members Strengthened with CFRP Laminates." *J. Structural Engineering*, 121(7), 1037-1044

Pothisiri, T. and Hjelmstad, K.D. (2004). "Structural Damage Detection and Assessment from Modal Response." *J. Eng. Mech.*, 129(2), 135-145.

Rao, S. S. (1995). *Mechanical Vibrations*. Third Edition. Addison-Wesley.

Ray, L.R. and Tian, L. (1999). "Damage Detection in Smart Structures Through Sensitivity Enhancing Feedback Control." *J. Sound and Vibration*, 227(5), 987-1002.

Reed, C.E. and Peterman, R.J. (2004). "Evaluation of Prestressed Concrete Girders Strengthened with Carbon Fiber Reinforced Polymer Sheets." *J. Bridge Engineering*, 9(2), 185-192.

Reich, G.W. and Park, K.C. (2000). "Experimental Application of a Structural Health Monitoring Methodology." *Proc. 2000 Smart Structures and Materials Conference: Smart Systems for Bridges, Structures, and Highways,* Newport Beach, CA, March 6-9, 2000.

Reynolds, P. and Pavic, A. (2000). "Impulse Hammer vs. Shaker Excitation for the Modal Testing of Building Floors." *Experimental Techniques. Structural Testing Series: Part 7,* 39-44.

Rosenkrantz, W.A. (1997). *Introduction to Probability and Statistics for Scientists and Engineers*. McGraw-Hill.

Rytter, A. (1993). "Vibration based inspection of civil engineering structures." Ph.D. Thesis, Department of Building Technology and Structural Engineering, Aalborg University, Denmark.

Salawu, O.S. (1995). "Non-Destructive Assessment of Structures Using the Integrity Index Method Applied to a Concrete Highway Bridge." *Insight*, 37(11), 875-878.

Salawu, O.S. and Williams, C. (1995). "Review of Full-Scale Dynamic Testing of Bridge Structures." *Engineering Structures,* 17(2), 113-121.

Salawu, O.S. (1997a) "Assessment of Bridges: Use of Dynamic Testing." *Canadian Journal of Civil Engineering*, 24, 218-228.

Salawu, O.S. (1997b). "Detection of Structural Damage Through Changes in Frequency: A Review." *Engineering Structures*, 19(9), 718-723.

Salawu, O.S. (1997c). "An Integrity Index Method for Structural Assessment of Engineering Structures Using Modal Testing." *Insight*, 39(1), 33-37.

Sampaio, R.P.C., Maia, N.M.M., and Silva, J.M. M. (1999). "Damage Detection Using the FRF Curvature Method." *J. Sound and Vibration*, 226(5), 1029-1042.

Sanayei, M., Wadia-Fascetti, S., Arya, B., and Santini, E.M. (2001). "Significance of Modeling Error in Structural Parameter Estimation." *Computer-Aided Civil and Infrastructure Engineering*, 16(1), 12-27.

Sarja, A. and E. Vesikari. (1996). *Durability Design of Concrete Structures*, *Report of RILEM Technical Committee 130-CSL*. E&FN Spon, London.

Sato, Y. and Vecchio, F.J. (2003). "Tension Stiffening and Crack Formation in Reinforced Concrete Members with Fiber-Reinforced Polymer Sheets." *J. Structural Engineering*, 129(6), 717-724.

Seim, W., Horman, M., Karbhari, V., and Seible, F. (2001). "External FRP Poststrengthening of Scaled Concrete Slabs." *J. Composites for Construction*, 5(2): 67-75.

Seim, W., Vasques, A., Karbhari, V., and Seible, F. (2003). "Poststrengthening of Concrete Slabs: Full-Scale Testing and Design Recommendations." *J. Structural Engineering*, 129(6), 743-752.

Shahawy, M.A., Beitelman, T., Arockiasamy, M., and Sowrirajan, R. (1996). "Experimental Investigation on Structural Repair and Strengthening of Damaged Prestressed Concrete Slabs Utilizing Externally Bonded Carbon Laminates," *Composites: Part B*, 27B, 217-224.

Shahrooz, B.M. and Boy, S. (2004). "Retrofit of a Three-Span Slab Bridge with Fiber Reinforced Polymer Systems – Testing and Rating." *J. Composites for Construction*, 8(3), 241-247.

Sherwood, E.G. and Soudki, K.A. (2000). "Rehabilitation of Corrosion Damaged Concrete Beams with CFRP laminates – a Pilot Study." *Composites: Part B*, 31, 453-459.

Shi, Z.Y., Law, S.S., and Zhang, L.M. (1998). "Structural Damage Localization From Modal Strain Energy Change." *J. Sound and Vibration*, 218(5), 825-844.

Shi, Z.Y., Law, S.S., and Zhang, L.M. (2000). "Structural Damage Detection From Modal Strain Energy Change." *J. Engineering Mechanics*, 126(12), 1216-1223.

Sivico, J. V., Rao, V. S., and Koval, L. R. (1997) "Health monitoring of bridge like structures using state variable models." *The International Society of Optical Engineering, SPIE Proceedings*, 3043, 156-168.

Sikorsky, C. (1999). "Development of a Health Monitoring System for Civil Structures Using a Level IV Non-Destructive Damage Evaluation Method." *Proc., the 2nd International Workshop on Structural Health Monitoring*, 68-81.

Sikorsky, C., Stubbs, N., Bolton, R., and Karbhari, V. (2002). "The Application of Structural Health Monitoring to Evaluate Bridge Strength." *Proc. of the First International Workshop on Structural Health Monitoring of Innovative Civil Engineering Structures*, September 19-20, 2002, Winnipeg, Manitoba, Canada.

Sikorsky, C., Stubbs, N., Bolton, R.W., and Karbhari, V., (2002) "Non-Destructive Evaluation of FRP Composite Strengthening – Byron Road Bridge," State of California, Department of Water Resources, Sacramento, CA, #28C-0121.

Stallings, J.M., Tedesco, J.W., El-Mihilmy, M. and McCauley, M. (2000). "Field Perfromance of FRP Bridge Repairs." *J. Bridge Engineering*, 5(2), 107-113.

Stanbridge, A.B. and Ewins, D.J. (1999) "Modal Testing Using a Scanning Laser Doppler Vibrometer." *Mechanical Systems and Signal Processing*, 13(2), 255-270.

Strang, G. (1988). *Linear Algebra and Its Applications*. Third Edition. Saunders College Publishers, Harcourt Brace Jovanovich College Publishers.

Stubbs, N. and Kim, J-T. (1996). "Damage Localization in Structures without Baseline Modal Parameters." *AIAA Journal*, 34(8), 1644-1649.

Stubbs, N. and Park, S. (1996). "Optimization of Sensor Placement for Mode Shapes Via Shannon's Sampling Theorem." *Microcomputers in Civil Engineering*, 11, 411-419.

Stubbs, N., Choi, S., Bolton, R.W., Park, S., and Sikorsky, C. (2001). "Nondestructive Evaluation of District 08 Bridges Using Modal Parameters," State of California, Department of Transportation, Sacramento, CA, TEES Project 32525-58520CE.

Stubbs, N., Park, S., Sikorsky, C., and Choi, S. (2000) "A Global Non-destructive Damage Assessment Methodology for Civil Engineering Structures." *Intl. J. Systems Science*, 31(11), 1361-1373.

Stubbs, N. and Bolton, R.W. (2002). "Condition Assessment of Frame 3 of the Watson Wash Bridge Between July 2001 and November 2002." Texas A&M University, College Station, Texas, Submitted to Vistasp Karbhari, University of California San Diego, P.O. #10214634.

Swamidas, A.S.J and Chen Y. (1995). "Monitoring Crack Growth Through Change of Modal Parameters." *J. Sound and Vibration*, 186, 325-343.

Tajlsten, B. (2002). *FRP Strengthening of Existing Concrete Structures – Design Guidelines*. Lulea University Printing Office, Lulea, Sweden.

Teng, J.G., Chen, J.F., Smith, S.T., and Lam, L. (2003). "Behavior and Strength of FRP-Strengthened RC structures: A State-of-the-Art Review." *Structures & Buildings*, 156(1), 51-62.

Triantafillou, T.C. and Plevris, N. (1991). "Post-Strengthening of R/C Beams with Epoxy-Bonded Fiber Composite Materials." *Proceedings of the Specialty Conference on Advanced Composites Materials in Civil Engineering Structures. Las Vegas, Nevada, January 31 thru February 1, 1991*, 245-256.

TR No. 55, The Concrete Society (2000). "Design Guidance for Strengthening Concrete Structures Using Fibre Composite Materials." Report of a Concrete Society Committee, Technical Report No. 55.

Van Den Einde, L., Zhao, L., and Seible, F. (2003). "Use of FRP Composites in Civil Structural Applications." *Construction and Building Materials*, 17, 389-403.

Wang, M.L., Xu, F.L., and Lloyd, G.M. (2000). "A Systematic Numerical Analysis of the Damage Index Method used for Bridge Diagnostics." *Smart Structures and Materials 2000: Smart Systems for Bridges, Structures, and Highways, Proceedings of SPIE*, 3988, 154-164.

Williams, E.J., Messina, A, and Payne, B.S. (1997). "A Frequency-Change Correlation Approach to Damage Detection." *Proceedings of the 15th International Modal Analysis Conference, Orlando, Florida*, 1, 652-657.

Yuen, K-V., Au, S.K., and Beck, J.L. (2004). "Two Stage Structural Health Monitoring Approach for Phase I Benchmark Studies." *J. Eng. Mech.*, 130(1), 16-33.

Zang, C. and Imregun, M. (2001). "Structural Damage Detection Using Artificial Neural Networks and Measured FRF Data Reduced Via Principal Component Projection." *J. Sound and Vibration*, 242(5), 813-827.

Zang, C. and Imregun, M. (2001). "Combined Neural Network and Reduced FRF Techniques for Slight Damage Detection Using Measured Response Data." *Archive of Applied Mechanics*, 71, 525-536.